On-line Dynamic Security Assessment in Power Systems.

Weckesser, Johannes Tilman Gabriel; Jóhannsson, Hjörtur; Østergaard, Jacob

Publication date:
2014

Document Version
Publisher's PDF, also known as Version of record

Technical University of Denmark

J. Tilman G. Weckesser

On-line Dynamic Security Assessment in Power Systems

PhD thesis, October 2014

DTU Electrical Engineering
Department of Electrical Engineering

J. Tilman G. Weckesser

On-line Dynamic Security Assessment in Power Systems

PhD thesis, October 2014

On-line Dynamic Security Assessment in Power Systems,

This report was prepared by
J. Tilman G. Weckesser

Supervisors
Hjörtur Jóhannsson
Jacob Østergaard

Release date:	September 7, 2015
Category:	1 (public)
Edition:	First
Comments:	This report is part of the requirements to achieve the Doctor of Philosophy (PhD) at the Technical University of Denmark. This report represents 120 ECTS points.

Department of Electrical Engineering
Centre for Electric Power and Energy (CEE)
Technical University of Denmark
Elektrovej building 325
DK-2800 Kgs. Lyngby
Denmark

www.elektro.dtu.dk/cet
Tel: (+45) 45 25 35 00
Fax: (+45) 45 88 61 11
E-mail: cet@elektro.dtu.dk

Abstract

The thesis concerns the development of tools and methods for on-line dynamic security assessment (DSA). In a future power system with low-dependence or even independence of fossil fuels, generation will be based to a large extent on non-controllable renewable energy sources (RES), such as wind and solar radiation. Moreover, ongoing research suggests that demand response will be introduced to maintain power balance between generation and consumption at all times. Due to these changes, the operating point of the power system will be less predictable. Consequently, today's stability and security assessment tools, which are generally dependent on extensive off-line studies, may no longer be feasible in their current development state.

A core component of an efficient on-line dynamic security assessment is a fast and reliable contingency screening. As part of this thesis a contingency screening method is developed and its performance is assessed utilizing a set of test cases. The developed method reliably assesses first-swing transient angular stability of a power system in its current state with respect to a given set of contingencies. In order to ensure fast performance of the screening method, first a review of existing transient stability assessment (TSA) methods was carried out and their computational complexity was investigated. This allowed to identify the single machine equivalent (SIME) method as the potentially fastest assessment method and, hence, well suited for on-line DSA. Means for further performance improvement of the SIME method are investigated such as the reduction of the degree of system model detail used in time-domain simulation. This results in a recommendation for the required model detail for synchronous generator. A challenging task when using the SIME method is to early and reliably determine the critical machine cluster, which is the group of generators likely to lose synchronism. Therefore, a novel approach to identify the critical machine cluster is proposed in the thesis. This approach uses a new coupling coefficient, which is a measure of the coupling strength of pairs of generators, and a simple clustering algorithm to identify the critical group of generators.

In order to determine a system to be transient secure, it is not sufficient to solely assess if all synchronous generators remain in synchronism, it is also required that the bus voltages remain within acceptable limits. A transient disturbance and the following angular divergence of a group of generators can cause critical voltage sags at certain buses in the system. In this thesis assessment of such voltage sags is proposed using two types of sensitivities, which are derived from the algebraic

network equations. These sensitivities are derived after an in-depth study of the mechanism causing the voltage sags. The first sensitivity type is called load voltage sensitivity and allows identifying which bus voltages are affected by a change in rotor angle of a particular generator. The second proposed type is called generator power sensitivity, which provides information on the effect of load variation on the generator's power injection. It is shown that the derived sensitivities can give valuable information to identify critical generator-load pairs as well as locations for applying preventive or remedial control measures. Furthermore, the development of a method for early prediction of critical voltage sags is described. The method's performance is compared to other prediction approaches. The results show that the proposed method succeeds in early, accurately and consistently predicting critically low voltage sags.

An efficient on-line DSA not only identifies unstable or insecure operation, but also proposes preventive or remedial control actions to restore stability and security in the system. In this thesis a further development of a method for determining real-time remedial action against aperiodic small signal rotor angle instability is described. A real-time aperiodic small signal rotor angle stability assessment method is employed to monitor the respective stability boundary and to compute the respective stability margin of each generator in the system. In case that the stability margin of a particular generator falls below a pre-defined security threshold, the proposed method analytically determines power generation re-dispatch solutions, which restore stable and secure operation in the system. The effectiveness of the method is presented on two test cases in two different test systems.

Resumé

Denne afhandling omhandler udvikling af metoder for online dynamisk sikkerhedsvurdering (DSA). I fremtidens elsystem med lav afhængighed eller sågar uafhængighed af fossile brændstoffer vil en høj andel af elproduktion være baseret på ikke-regulerbare energikilder (RES) såsom vind og sol. Desuden indikerer forskning løbende at fleksibelt elforbrug vil indføres for at holde balancen mellem elproduktion og elforbrug til alle tider. På grund af disse forandringer vil driftstilstanden af elsystemet være mindre forudsigelig, og nuværende metoder til stabilitets- og sikkerhedsvurdering, som generelt er baseret på omfattende offline undersøgelser, vil måske ikke længere være tilstrækkelige.

En central komponent i en effektiv online dynamisk sikkerhedsvurdering er en hurtig og pålidelig fejl-screening. Som del af denne afhandling er en metode til fejlscreening udviklet, og dens resultater er vurderet på et sæt af testcases. Den udviklede metode vurderer pålideligt første-svings rotorvinkel transient stabilitet af et elsystems aktuelle driftstilstand med hensyn til et givent sæt af fejl. For at sikre at screeningsmetoden kan udføres hurtigt, bliver en undersøgelse først udført af eksisterende metoder til vurdering af transient stabilitet og deres beregningsmæssige kompleksitet blev undersøgt. Dette gjorde det muligt at identificere single machine equivalent (SIME) metoden som den potentielt hurtigste vurderingsmetode og er dermed velegnet til online DSA. Muligheder for yderligere præstationsforbedring af SIME metoden undersøges for eksempel reducering af modeldetaljen brugt i tidsdomæne simulation. Undersøgelsen resulterede i en anbefaling af den nødvendige modeldetalje brugt i repræsentation af synkrongeneratorer. En udfordrende opgave. når SIME-metoden er brugt, er at bestemme den kritiske maskingruppe tidligt og pålideligt. Den gruppe vil sandsynligvis gå ud af synkronisme. Derfor er en ny tilgang til at identificere den kritiske maskingruppe foreslået i afhandlingen. Denne tilgang bruger en ny koblingskoefficient, som er et mål for koblingsstyrken mellem et par generatorer og en simpel klyngealgoritme for at identificere den kritiske gruppe af generatorer.

For at bestemme om et elsystem er transientsikkert er det ikke nok at vurdere, om alle synkrongeneratorer forbliver i synkronisme. Det kræves også, at busspændinger forbliver indenfor acceptable grænser. En transientforstyrrelse og den efterfølgende vinkeldivergens af en gruppe af generatorer kan medføre kritisk spændingssænkning på visse busser i elsystemet. I afhandlingen foreslås at to sensitiviteter, som afledes fra algebraiske netværksligninger, bruges til vurdering af disse spændingssænkninger. Disse sensitiviteter blev fundet efter dybdeborende

undersøgelse af mekanismen, som forårsager spændingssænkninger. Den første sensitivitet kaldes last-spændingssensitivitet (load voltage sensitivity). Den gør det muligt at identificere, hvilke busspændinger der påvirkes af en forandring i rotorvinklen af en bestemt generator. Den anden sensitvitet kaldes generatoreffekt sensitivitet (generator power sensitivity). Den giver informationer om virkningen af en belastningsændring på generatorens effekt. Det vises, at de afledte sensitiviteter kan give værdifulde informationer for at identificere kritiske generator-belastningspar og steder for anvendelse af et præventiv eller afhjælpende regulering. Yderligere beskrives udviklingen af en metode til tidlig forudsigelse af kritiske spændingssænkninger. Metodens ydeevne sammenlignes med andre forudsigelsesmetoder, og resultaterne viser, at den foreslåede metode succesfuldt forudsiger kritiske spændingssænkninger tidligt, akkurat og konsistent.

En effektiv online DSA identificerer ikke kun ustabil eller usikker drift, men foreslår også en præventiv eller afhjælpende regulering for at genoprette stabilitet og sikkerhed i systemet. I afhandlingen beskrives en videreudvikling af en metode for at beregne afhjælpende regulering (remedial action) mod aperiodisk småsignal rotorvinkel ustabilitet i realtid. En vurderingsmetode for aperiodisk småsignal rotorvinkel ustabilitet bruges i realtid til at overvåge den tilhørende stabilitetsgrænse og at beregne den tilhørende stabilitetsmargin af hver generator i systemet. I tilfælde af at en generators stabilitetsmargin er lavere end en fastlagt grænseværdi, beregner metoden analytisk løsninger for genfordeling af effekten, der genopretter stabil og sikker systemdrift. Brugbarheden af metoden vises på to testcases i to forskellige testsystemer.

Acknowledgement

First of all, I would like to thank my supervisors Hjörtur Jóhannsson and Jacob Østergaard for their consistent support and advice throughout the project.

I would like to thank my colleagues and friends at CEE for the good collaboration throughout my PhD.

In particular, I would also like to thank Prof. Thierry Van Cutsem from the University of Liège for his supervision during my external stay, which made it professional very rewarding. Furthermore, I would like to thank Prof. Van Cutsem for providing me access to their simulation tool RAMSES. The colleagues and friends at the University of Liège I would like to thank for their support before and during my external stay.

Finally, I would like to thank my family and friends for their support, especially my parents who have always been very supportive.

Contents

List of publications

The following is a list of publications, which have been prepared as part of the PhD project.

The publications A to H present the main results of the PhD project. The method described in H resulted in a patent, which is listed as publication I. Publication E was one of the papers from the 18^{th} PSCC selected to be published as an extended version in a special issue of the International Journal of Electrical Power and Energy Systems (IJEPES), which is listed below as publication F. The publication J only contains minor contributions of the author.

A Weckesser, T., Jóhannsson, H., Sommer, S., & Østergaard, J. (2012). Investigation of the Adaptability of Transient Stability Assessment Methods to Real-Time Operation. In IEEE Proc., *Innovative Smart Grid Technologies (ISGT Europe 2012)*. Berlin, Germany.

B Weckesser, T., Jóhannsson, H., & Østergaard, J. (2013). Impact of Model Detail of Synchronous Machines on Real-time Transient Stability Assessment. In *2013 IREP Symposium Bulk Power System Dynamics and Control - IX Optimization, Security and Control of the Emerging Power Grid*. Rethymnon, Greece.

C Weckesser, T., Jóhannsson, H., and Østergaard, J., On-line Contingency Screening using Wide-Area Measurements, *IET Generation, Transmission & Distribution*, Submitted.

D Weckesser, T., Jóhannsson, H., and Østergaard, J., Critical Machine Cluster Identification using the Equal Area Criterion, Accepted for presentation at *IEEE PES General Meeting (IEEE PES GM'15)*. Denver, Colorado, USA.

E Weckesser, T., Jóhannsson, H., Østergaard, J., & Van Cutsem, T. (2014). Sensitivity based Assessment of Transient Voltage Sags caused by Rotor Swings. In Proceedings of 18^{th} *Power System Computation Conference 2014 (PSCC'14)*. Wroclaw, Poland.

F Weckesser, T., Jóhannsson, H., Østergaard, J., & Van Cutsem, T. (2015). Derivation and Application of Sensitivities to Assess Transient Voltage Sags caused by Rotor Swings. *International Journal of Electrical Power and Energy Systems* - Special Issue. In Press.

G Weckesser, T., Jóhannsson, H., & Van Cutsem, T. (2014). Early Prediction of Transient Voltage Sags cause by Rotor Swings. In Proceedings of *IEEE*

PES General Meeting (IEEE PES GM'14). Washington DC, USA.

H Weckesser, T., Jóhannsson, H., and Østergaard, J. (2015). Real-Time Remedial Action Against Aperiodic Small Signal Rotor Angle Instability, *IEEE Transaction on Power Systems*, In Press.

I Weckesser, T., Jóhannsson, H., (2011), Method of determining remedial control actions for a power system in an insecure state, Patent No. WO2013098184, IPC No. G05D5/00; H02J3/24; H02J3/46.

J Heussen, K., Weckesser, T., & Kullmann, (2013), Pattern-based Automatic Translation of Structured Power System Data to Functional Models for Decision Support Applications. In Proceedings of *IEEE International Workshop on Intelligent Energy Systems (IWIES 2013)*. IEEE.

Chapter 1

Introduction

1.1 Background

1.1.1 Problem and motivation

Modern society is very dependent on the availability of energy and the consumption is increasing. From 2004 to 2011 the per capita energy consumption increased by almost 8 % worldwide and the electricity consumption per capita even grew by approximately 18 % in the same period [1]. This increase shows that society's dependency on a reliable and secure electric power supply is growing and it is not expected to change in the future, in particularly with regards to the introduction and the growing number of electric vehicles.

Due to the high dependency on the availability of electricity, a breakdown of the supply, such as the 2003 blackout in the northeast of the United States of America and in Ontario, Canada, has a large economic impact. The blackout, which affected approximately 50 million people and lasted up to 4 days, is estimated to have caused a loss of $4 billion to $10 billion (U.S. dollars) [1]. After the blackout a task force was appointed to investigate the blackout, their findings were documented in [1]. They concluded that one of the principal causes of the blackout was the lack of situational awareness, which was due to inadequate reliability tools. Therefore, it was recommended to evaluate the real-time operating tools, which are required for reliable and secure operation.

The growing size and complexity of the power systems on the one hand and on the other hand the political induced paradigm shift in electric power generation from conventional to renewable energy sources (RES) in several parts of the world, e.g. documented in [2], pose great challenges with respect to secure and reliable operation of the electric grid. The power generation based on RES, such as solar radiation and wind, is dependent on forecasting accuracies. In order to account for forecasting inaccuracies and to match power generation with consumption at all times, research is carried out in the area of energy storage, demand response and

[1] http://data.worldbank.org

other intelligent systems such as virtual power plants. Given that these projects succeed and provide tools to balance consumption and generation at all times, the generation and consumption pattern in the system will change frequently, which may lead to a heavily fluctuating operating point of the power system.

Today's tools and methods to determine and monitor stability as well as security of the system are based on extensive off-line studies and are performed in advanced e.g. day-ahead. This approach is feasible in a system, where power generation is based on conventional energy sources and, therefore, can be planed ahead easily. However, in a system with fluctuating energy sources and a consumption pattern which is frequently adjusted to match the generation, these stability and security assessment methods may no longer be sufficient. In [3] it is stated that in a future smart transmission grid on-line stability assessment methods, e.g. for voltage and transient angular stability, should be available, in order to ensure stable and secure system operation. Furthermore, the authors suggest using measurements from phasor measurement units (PMUs) for monitoring and visualization instead of system snapshots from today's state estimator, since state estimators require additional runtime and are less robust. In fact, the phasor measurement technology [4, 5, 6] is considered to be the enabling technology for the development of real-time wide-area monitoring and control applications [7, 8].

Recent publications have presented methods which are utilizing synchronized wide-area measurement to carry out on-line stability assessment. In [9] an entirely new approach was developed for real-time aperiodic small signal rotor angle stability assessment of power systems. The authors of [10] and [11] adopted an existing off-line voltage stability method to real-time operation.

1.1.2 On-line dynamic security assessment

In order to improve situation awareness of the system operator, it is of great importance to know stability of the power system in its current condition with respect to a number of credible contingencies. Dynamic security assessment (DSA) tools are addressing this need. DSA is defined in [12] as follows:

> "DSA refers to the analysis required to determine whether or not a power system can meet specified reliability and security criteria in both transient and steady-state time frames for all credible contingencies."

In systems with conventional generation, power system operators depended heavily on the security assessment results from off-line operation analysis to guarantee a secure and reliable day-to-day operation. Today's power systems are more complex, due to open markets and integration of more renewable energies. Hence, the predictability of power system operation is reduced and relying solely on off-line DSA results is impractical or may even be infeasible. Therefore, the use of and the demand for on-line DSA is growing worldwide [13].

In [14, Chap. 6] a structure for an on-line DSA was proposed as shown in Fig. 1.1.

In the following a short description of the different components of an on-line DSA will be presented based on [14, Chap. 6].

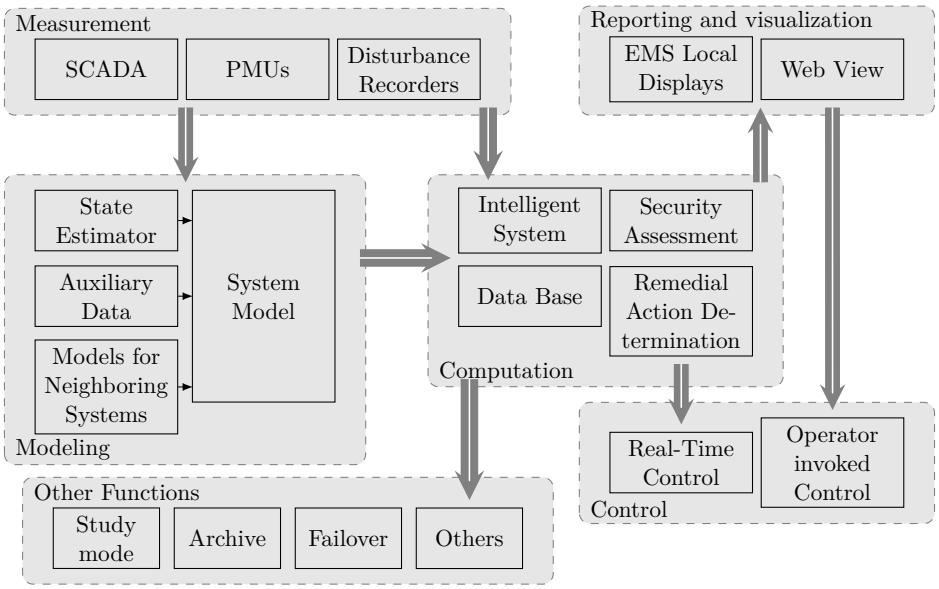

Figure 1.1: Components of an DSA and their interaction [14]

Measurement: Measurements can be obtained, e.g. from SCADA systems or PMUs. The choice is depending on the measurement requirements such as accuracy, sampling rate, and so on. The measurements are then used as input to a state estimator or may directly be used in the security assessment tools.

Modeling: Accurate modeling of the power system and its components may be the most important and critical part of an on-line DSA. Firstly, since the trend is towards larger and larger interconnected systems, it is a challenge to determine the required size of the used model and the adequate representation of external systems. Secondly, another critical issue is to identify, the needed detail of the model representation, e.g. model representation of distribution grids. Thirdly, in order to carry out dynamic assessments and simulations, the system components have to be represented by dynamic models suitable for the chosen time frame. Finally, the models need to be validated with e.g. measurements, field tests or comparison of simulations with recorded measurements of events.

Computation: In order to determine security of the system, a wide range of methods has been developed, which may be split into two extreme groups.

- *Deterministic evaluation using analytical solutions:* Most complex; requires detailed models; techniques such as detailed time-domain simulation
- *Direct inference from measurements:* Simplest approach; security inferred directly from measurements (e.g. comparison of phasor angles)

Many of the currently used methods are somewhere in between the two extreme groups or are even hybrid methods, which are combining detailed time-domain simulation with for example a direct approach.

In order to operate the system securely, the assessment methods have to answer the following questions at all times to the operator:

1. How secure is the current state?
2. How secure is the operation in a different state?
3. What remedial actions can be performed to improve stability?

Consequently, the challenge of DSA is to determine the stability condition and margin of the current state as well as the secure region. The security criteria defining the secure region are as follows: thermal overloading, steady state voltage and frequency excursion, transient voltage dip/rise, transient stability, small signal stability, voltage stability frequency stability, etc. The assessment of these criteria are carried out using either a full simulation approach (e.g. time-domain simulation, Eigenvalue analysis and power-flow solution of P-V curves) or an approximated approach (e.g. sensitivity based methods or direct energy methods).

Despite the considerable improvement of the processor speed of computers, DSA and its computation still pose a great challenge. Consequently, the combination of utilizing direct methods together with detailed simulation seems to be a promising approach. Direct methods may be used to carry out a quick contingency screening of the current system state and detailed time-domain simulation is only conducted for critical contingencies and cases. Another approach to reduce the computation time may be parallelization of the tasks.

Moreover, it is desirable that the DSA is highly automated with only little interference of the human operator. Consequently, it needs to be equipped with some intelligence to determine the right remedial action, which considers all security margins. This automatized system needs to be very reliable and, therefore, redundancy and self-healing may be important features of an on-line DSA.

Reporting and Visualization: In order to maneuver the system within the secure region determined by the DSA, it is important that the results are displayed simple as well as meaningful and that the key findings (e.g. critical contingencies, potential criteria violations, security margins, etc.) are clearly displayed.

Control: In case that a contingency leading to insecure operation was identified, the DSA should determine and present the required remedial action, which may be preventive or corrective. Furthermore, the included intelligence should determine, if the remedial action is automatically applied or if it is solely presented to the operator.

1.1.3 Focus of the presented work

The aim of the PhD project was to contribute and advance the development of as well as the research on on-line DSA systems. Since it is expected that the generation and consumption pattern in the system become less predictable and dependent on forecasting accuracies, it is expected that methods based on off-line databases are going to be challenged by the vast amount of possible operating conditions. Moreover, blackouts are occurring in extreme situations, which may be extreme weather conditions or $N - x$ contingency scenarios. It is likely that these very unpredictable situations are not part of the database and may even deviate significantly from the scenarios in the database. Hence, methods, which are trained on them and provide a certain degree of generalization, may not always be capable of correctly determining security and stability. For these reasons, the

ambition of the PhD project was to develop on-line stability and security assessment methods, which are independent of off-line case databases and simulations, and, hence, approaches that are using data mining, decision trees or other machine learning approaches were not considered to be an option. The chosen approach was to develop or use methods, which are or were derived from in-depth studies of the respective instability mechanism.

In this PhD project, it was investigated, how the availability of synchronized wide-area measurements, e.g. provided by PMUs, can be used for on-line DSA. In this work focus was on contingency screening, which was in [13] identified as a main element of an efficient on-line DSA, and on-line transient stability assessment (TSA) of the system. As defined in [15] TSA ...

> "...is concerned with the ability of the power system to maintain synchronism when subjected to a severe disturbance, such as a short circuit on a transmission line. The resulting system response involves large excursions of generator rotor angles and is influenced by the nonlinear power-angle relationship."

As discussed in [16], TSA is not necessarily only concerned with loss of synchronism of generators since in very stressed conditions other parameters may have a large impact on the system dynamics, e.g. the transient voltage response. The angular separation of generators caused by a large disturbance may lead to transient voltage dips at certain buses in the system. Hence, in this work TSA is treated under consideration of angular stability and transient voltage sags caused by rotor angle swings.

Since DSA is not only concerned with transient stability, but also steady state stability, the PhD project investigated means to restore secure operation with respect to aperiodic small signal rotor angle stability (ASSRAS), which is a quasi steady state stability phenomena.

1.2 State-of-the-art

1.2.1 Installations of on-line dynamic security assessment

In 2007 Working Group Cigré C4.601 published an extensive review of on-line dynamic security assessment tools and techniques [13]. The report covers state-of-the-art on-line DSA and on-going research in the field. Table 1.1 shows a list of a selected number of on-line DSA installations worldwide.

The table provides information on the assessment methods, which are part of the DSA, where TSA stands for transient security assessment, VSA for voltage security assessment, SSA for small signal security assessment and FSA for frequency security assessment. Moreover, the last column informs on the current status of the installation, where I/S refers to "in service", O/S to "tested but out-of-service" and U/D to "under development".

Since the focus in this work is particular on transient stability/security assessment,

Table 1.1: State-of-the-art dynamic security assessment installation [13]

Country	Location/Company/Proj.	SCOPE				Status
		TSA	VSA	SSSA	FSA	
Australia	NEMMCO	×		× (MB)	×	I/S
Bosnia	NOS	×	×			I/S
Brazil	ONS	×	×	×	×	I/S
Canada	BCTC	×	×			U/D
Canada	Hydro-Quebec	×	×			I/S
China	Beijing Elect. Power Corp	×				I/S
China	CEPRI	×				I/S
China	Guangxi Elect. Power Co.	×		×	×	I/S
Finland	Fingrid		×	× (MB)		I/S
Greece	Hellenic Power System		×			I/S
Ireland	ESB	×	×			I/S
Italy & Greece	Omases Project	×	×			O/S
Japan	TEPCO	×	×			I/S
Malaysia	Tenaga Nasional Berhad	×	×			I/S
New Zealand	Transpower	×	×		×	I/S
Panama	ETESA	×	×			I/S
Romania	Transelectrica	×	×			I/S
Russia	Unif. Elect. Power System	×	×			I/S
Saudi Arabia	SEC	×	×			U/D
South Africa	ESKOM	×	×			U/D
USA	PJM	×	×	×		I/S
USA	Southern Company	×				I/S
USA	Northern States Power	×				I/S
USA	MidWest ISO		×			I/S
USA	Entergy		×			I/S
USA	ERCOT	×	×			I/S
USA	FirstEnergy		×			U/D
USA	BPA		×			I/S
USA	PG&E		×			U/D
USA	Southern Cal Edison		×			U/D

MB: Measurement based

Table 1.2 provides more information on the TSA systems employed in the DSA installations listed in Tab. 1.1.

The table shows that in all installations time-domain simulations (TDS) are used and often are extended with approaches using direct methods. The direct methods are used to allow an early determination of stability and/or termination of the TDS or estimation and computation of stability margins.

In the following, the on-line DSA with particular focus on transient security assessment of three different approaches is briefly discussed on basis of three installations described in [13].

1. *Detailed time-domain simulation:* Operating limits derived from extensive time-domain simulation such as the one in Australia – NEMMCO.
2. *Stability indicators derived from steady state data:* The on-line DSA uses for example a security margin for dynamic stability evaluation, which is deter-

Table 1.2: State-of-the-art transient security assessment approaches used in the installations described in [13]

Country – Company/Proj.	Type	Description
Australia – NEMMCO	TDS	Extensive off-line studies to determine operating limits
Bosnia – NOS	SSSL TDS	Max. power transfer margin using Dimo's method security margin: large enough to ensure TSA
Brazil – ONS	TDS DM	Simulation in combination with SIME method
Canada – Hydro-Quebec	TDS	Power transfer limits are determined off-line and are employed during on-line operation.
China – CEPRI	TDS	Extensive time-domain simulation utilizing parallel processing
China – Guangxi Elect. Power Co.	TDS	Simulation of a limited selection of contingencies.
Italy & Greece – Omases Project	TDS DM	Simulation in combination with SIME method
Japan – TEPCO	TDS DM	Simulation in combination with TEPCO-BCU method and BCU classifiers
Malaysia – Tenaga Nasional Berhad	TDS	Simulations of a set of contingencies
New Zealand – Transpower	TDS	Operating limits are determined from off-line studies
Panama – ETESA	SSSL TDS	Dimo's method to determine max. loading Off-line TDS to determine necessary security margin
Romania – Transelectrica	SSSL TDS	Dimo's method to determine max. loading Off-line TDS to determine necessary security margin
USA – PJM	TDS DM	TDS to compute non-linear system response TSA margin determined using SIME based approach
USA – Southern Company	TDS DM	TDS to compute non-linear system response TSA margin determined using SIME based approach

TDS: time-domain simulation; SSSL: steady state stability limit; DM: direct method; SIME: single machine equivalent; BCU: boundary of stability region based controlling unstable equilibrium point;

mined from a steady state stability limit, e.g. in Bosnia and Herzegovina – NOS

3. *Combination of TDS with direct method:* The on-line DSA combines both approaches to speed up the assessment, e.g. in Brazil – ONS TDS is combined with the SIME method

For a discussion of the remaining assessment methods, the reader is referred to the full report of the Cigré working group [13].

Australia – NEMMCO: TSA is of particular interest in the system, due to its network structure. The desired performance of the on-line DSA is $10-15$ minutes, which is due to the requirement that the system needs to be maneuvered back into a secure state within 30 minutes after it had entered an insecure post-contingency state. The TSA heavily utilizes results from off-line studies, which provide system operating limits. NEMMCO applies those as constraints in the power dispatch process of the electricity market. The limits are determined by extensive time-domain simulations using PSS/E. NEMMCO also developed and employs a real-time security assessment tool. The tool receives the current system snapshot from the state estimator and forwards it to a time-domain simulation engine, which monitors transient security in real-time for a number of credible contingencies. The current implementation usually considers 55 as credible classified contingencies. The considered system model consists of approximately 2100 buses, 300 generators and 700 dynamic models. The DSA server is capable of evaluating the stability of all contingencies in less than ten minutes including five second PSS/E simulations per contingency.

In conclusion, the TSA of NEMMCO is based on detailed time-domain simulation and the on-line assessment is enabled by choosing a small number of credible contingencies.

Bosnia and Herzegovina – NOS: The installed on-line DSA consists of a state estimator and a Fast Maximum Transfer Capability Analyzer (FMTCA). It works seamlessly with the off-line power flow and transient stability program used in operations planning. The on-line DSA is not using detailed time-domain simulation but FMTCA, which employs a method developed by Paul Dimo to assess the maximum transfer capability of the power system [14, Chap. 2]. The method receives a load-flow solution from the state estimator and it is claimed that it determines the following in less than *one* second:

- Maximum loadability of each area including a user-defined security margin,
- The generators likely to cause instability as well as impact of machines and tie-lines on system stability,
- And the stability indices for system buses.

Here, *security margin* is defined as a steady state stability reserve that is sufficient large, in order that the system can withstand any set of credible contingency. It is not described, how the security margin is determined. In [14, Chap. 2] it is stated that the security margin may be chosen as a fixed percentage (e.g. $8 - 15\%$) of the steady state stability limit, which corresponds to the maximum power transfer limit. Moreover, the authors propose an algorithm to heuristically determine the security margin in terms of steady state stability reserve. The approach utilizes a load-flow solution at peak load conditions and runs extensive transient stability simulation of a set of credible contingencies. The security margin corresponds to the loading level or rather steady state stability reserve, where all contingencies are stable and an increasing of the loading level leads to at least one contingency becoming unstable.

The determination of a static heuristically computed security margin poses a large computational burden and requires knowing generation as well as consumption patterns well in advanced. Therefore, in a future system with large share of RES the approach may be insufficient. Moreover, the usage of a static security margin could be very conservative.

Brazil – ONS: The on-line DSA comprises six security assessment methods, which are as follows: operating point steady state contingency analysis, operating point dynamic contingency analysis, import-export steady state transfer limit between two-generation areas, import-export dynamic transfer limit between two-generation areas, steady state security region computation and dynamic security region computation. Moreover, the DSA system can provide information on preventive or remedial action, such as generation active power re-dispatch to avoid rotor angle instability. For the assessment of dynamic security, ONS utilizes detailed time-domain simulation as well as hybrid or direct methods based on the equal area criterion or numerical energy functions, which are mainly used for stability margin computation.

The approach and the implementation described by ONS seems to be promising and it is stated that the performance targets, e.g. dynamic security assessment of 100 contingencies in a test system with 3000 buses and 700 generators in less than

30 s, was achieved. However, the next steps are integration into the main control center to evaluate real world performance.

1.2.2 Research on on-line dynamic security assessment

In the following, the results of on-going research efforts in the area of on-line dynamic security assessment are presented.

In [17, Chapter 6] the authors describe the further developed functions of the on-line DSA system used in Brazil – ONS. As mentioned earlier the DSA system uses a combination of detailed time-domain simulation and direct methods. The assessment of stability using solely time-domain simulation requires visual inspection of the results. The authors replace the need for inspection by employing numerical energy functions and a modified version of the SIME method to compute stability margins, detect instability and enable early termination of the simulations. The further development of the DSA functions is mainly concerning the transient stability assessment approach, where the original SIME method was modified. The modified version of SIME improves the speed and the accuracy of the computation of stability margins for stable cases. The central idea was to estimate the $P_e - \delta$ characteristic of the single machine equivalent or rather the one machine infinite bus system (OMIB) by the following equation.

$$P_e(\delta) = \frac{E_m(\delta)E_\infty}{X_e} \sin\delta + P_0 \tag{1.1}$$

This equation expresses the electric power of the OMIB as a function of the equivalent machine voltage behind the transient reactance E_m , the voltage at the infinite bus E_∞, the equivalent machine rotor angle δ and a local power P_0, which is determined to fit a particular operating point. The authors suggest computing the parameters $E_m(\delta)$ and E_∞ as the average of the generators' voltages behind the synchronous reactance in the critical and non-critical generator group. Moreover, X_e is determined as the weighted average of the external impedance seen by each generator in the critical group. The $P_e - \delta$ characteristic of the OMIB can then be used to determine the stability margin of a case as soon as the maximum kinetic energy is known.

The recent achievements in research on on-line DSA systems using the transient energy function are presented in [18]. The authors present an update on the on-line DSA system implemented at TEPCO in Japan. The presented DSA system exists of two major blocks. The first block carries out a dynamic contingency screening given a system state and a list of contingencies. The contingencies are classified and the definitely stable cases are filtered out. The unstable and/or undecided cases are forwarded to the second block, which carries out detailed time-domain analysis. In order to efficiently filter and classify all given contingencies, the authors propose an improved version of the BCU classifiers, which were proposed in [19]. Each of the seven classifiers is designed to filter out contingencies with a certain characteristic, e.g. contingencies causing islanding. The second block carries out BCU-guided time domain simulation for each unstable and/or undecided case, which is described in detail in [20]. In this approach detailed time-domain simulation is carried out and the simulation output is used to determine stability as well as the stability margin

with the BCU method. Depending on the case it may be necessary to run several simulations with varying clearing time for one contingency.

The authors of [21] propose a new approach for on-line dynamic security assessment, which uses phasor measurement units and off-line created decision trees. The method receives on-line data for the next 24 hours consisting of a series of operating conditions corresponding to load profile and unit commitment-based generation patterns. These data are used for exhaustive detailed time-domain simulations of $N-1$ and credible $N-k$ contingencies. The simulation results are stored in a database, which is used to train a decision tree (DT). Critical attributes (CAs), which characterize the system's dynamic performance, are determined using the DT. Moreover, thresholds for the CAs are identified on basis of the simulation database and the DT. Contrary to the traditional terminal-node based DT method, the authors propose a path based DT method. In that approach, insecurity scores are computed for each path of the DT and acceptability limits for this score are defined. During on-line operation PMU measurements are used to measure or compute the critical attributes and the values are used to identify related paths in the DT. If any insecurity score exceeds the pre-defined limit and the related contingency has a high probability, then preventive measures can be determined and executed.

In [22] the authors propose another decision tree based approach for on-line DSA and preventive control. For that purpose, two DTs are trained daily using a database of power system simulations and prediction data for a 24-h horizon. One DT uses measurable variables to monitor the system condition and identify potential security issues, which is called the observation DT (ODT). The second DT of controllable variables is used to provide on-line decision support for preventive controls and is called the preventive DT (PDT). During on-line operation, real-time measurements are utilized and compared to thresholds in the ODT. If a threshold is violated, the data are forwarded to the PDT, where the most efficient preventive control in terms of generation shift is determined. The security of the system is determined with simple security indices such as transient security indices based on the maximum angular separation of generators.

A third approach using decision trees was described in [23]. Here, particular focus was on reducing the impact of missing PMU measurements. Multiple small DTs are trained off-line and then re-checked with new cases in near real-time. In real-time operation, the method utilizes wide-area PMU measurements, where some measurements may be missing; a boosting algorithm is used to weight viable small DTs before assembly.

The authors of [24] propose a linear approach for a risk based DSA. For that purpose, an indicator representing the total system risk is proposed. The indicator is computed as the sum of the risks of each considered contingency. The risk associated to a certain contingency is computed as the product of the probability of its occurrence, the probability of its stability margin and its severity. The severity of a contingency is described by a linear function and dependent on the ratio of the critical fault clearing time to the actual fault clearing time. The probability of the stability margin originates from uncertainties for example introduced by the prediction of power consumption. The presented results show that the linear method is considerably faster than other risk assessment approaches, which for example use the Monte Carlo method.

1.2.3 Identified research challenges

The prior mentioned Cigré report presented an overview of on-line DSA installations from all around the world and showed that a variety of techniques are used e.g. detailed simulation, direct methods and simplified methods. This was followed by an overview of on-going research in the field and will be concluded with a list of identified research challenges for on-line DSA systems.

- *Speed of analysis:* Further performance improvements are required, which is for example due to the increasing size of power system models.
- *Robustness of analysis:* The used stability/security assessment and screening methods have to generate robust and reliable assessment results. Therefore, a further development and improvement of the methods is needed.
- *Solution robustness:* State estimators have to be reliable also under stressed system conditions, since their output is used and needs to be matched with the dynamic system model. For that reason, system wide monitoring with PMUs is very attractive.
- *Load modeling:* Need for methods which provide correct models of aggregated loads, which correctly represent the important load characteristics.
- *System modeling:* Since SCADA only can cover a limited geographical area, adequate model approximations of the external systems have to be made, and development of wide-are state estimators needs to be promoted.
- *Risk based security assessment:* Development of risk-based DSA solutions, which take into account the probability of the occurrence of a fault as well as its severity.
- *Optimal remedial measures:* Development of highly robust and reliable closed-loop preventive or remedial control methods.

In the thesis in each chapter more specific state-of-the-art sections can be found, which address a particular part of dynamic security assessment.

1.3 Contributions

In the following, the main contributions of the presented work are listed:

- *Investigation of the adaptability of transient stability assessment methods to real-time operation:* A review of the existing transient stability assessment methods was carried out and their development was traced back. The computational complexity of individual methods was then evaluated under consideration of the respective assessment algorithms. This allowed investigating the performance of the methods in large power systems and future power systems, where the system composition may be changed. Finally, it allowed identifying the method best suited for real-time transient stability assessment in future power systems.
- *Impact of model detail of synchronous machine on real-time transient stability assessment:* With an heuristic approach it was shown how detailed the model of a synchronous machine needs to be to correctly display the instability mechanism in power system simulations and to allow correct as well as early stability assessment with a hybrid transient stability assessment method.

- *A method for fast contingency screening and on-line transient stability assessment:* The method carries out on-line transient stability assessment in a power system with respect to a set of contingencies. The contingencies are then corresponding to their severity divided in six different categories. Furthermore, the run-time of the method was assessed to show the superior performance in direct comparison to pure time-domain simulation, due to an early simulation stop. The run-time assessment also allowed identifying means for future improvements of the method.
- *A method for early and reliable identification of the critical machine cluster:* The method aims at early and reliably identifying the critical group of machines. For that purpose, a novel coupling coefficient was derived, which is a measure of the coupling strength between a pair of generators. After fault clearance, these coupling coefficients are utilized to identify the group of generators, which is likely to lose synchronism. This information can then be used to early and reliably determine transient stability of the system.
- *Sensitivities were derived to investigate voltage sags caused by rotor swings:* Two types of sensitivities were derived from the algebraic network equations. The first sensitivity allows identifying critical generator-load pairs, which means that a change in the generator's respective rotor angle greatly impacts the voltage at a particular load. For example these sensitivities can be used to determine the contributions of individual generators to observed voltage sags. The second sensitivity reveals the impact of a change in load consumption on the generators in the system. These sensitivities can provide valuable insight, when designing special protection schemes such as undervoltage load-shedding schemes.
- *A method to predict transient voltage sags caused by rotor swings:* The developed method uses post-fault measurements and a transient stability assessment method, which is based on the single machine equivalent approach, to predict crossing of a critical voltage level at the system buses as well as the minimum of the voltage sag. The method may be part of a closed-loop emergency control against voltage sags.
- *Further development of a remedial action method:* The method determines remedial action against aperiodic small signal rotor angle instability. It proposes re-dispatch solutions of active power generation, which lead to a stabilization of the imminent unstable generator and restores security in the system.

A list of the publications prepared throughout the project can be found on page xi.

1.4 Thesis structure

In this section the report structure is introduced to help the reader to easily find his way through the thesis. The project's main results are published in separate scientific papers, which are attached to this report in the appendix as paper A to H. Throughout the report there will be references to these papers, where it is needed. However, the papers may also be read independently of the report.

In the prior section the background of the project was briefly discussed and the state-of-the-art of on-line dynamic security assessment was presented. The introduction chapter was then concluded by a listing of the contributions made by the

PhD project and this description of the thesis structure. The following three chapters are then summarizing the work in the three main topics, which have been addressed in the PhD project.

The second chapter presents the results on contingency screening and transient angular stability assessment, where the following questions were addressed.

1. Which transient stability assessment methods have been developed? And how suitable are those for on-line stability assessment?
2. How can the computational performance of the methods be improved? And what model simplifications can be assumed?
3. How can the contingency screening method be implemented in an on-line environment? What is the performance and reliability of the method? How can the performance be further improved?

The third chapter concludes on the results achieved in the area of transient voltage sag assessment and prediction, where the following questions were investigated.

1. What mechanism causes transient voltage sags?
2. Which sensitivities can be used to assess voltage sags? And what can they be used for?
3. How can voltage sags be predicted? And what is the best prediction method?

Finally, in the third chapter the results from preventive and remedial control are summarized, which tried to answer the following question.

1. What can be done when aperiodic small signal rotor angle instability was detected with a real-time assessment method?

Chapter 2

Fast contingency screening and on-line transient stability assessment

This chapter describes the development of the contingency screening and on-line transient stability assessment method as well as it summarizes the main results. The chapter begins with a short description of the topic. Then an overview of the existing transient stability assessment methods is presented and their potential to be used as an on-line assessment tool is investigated. The details of the investigation can be found in paper A in the Appendix. In the next section, the needed model detail for generators is investigated and the detailed results are documented in paper B. The findings of the two prior papers enabled the development of a method for contingency screening and on-line transient stability assessment. The method itself is proposed and results are presented, all the details can be found in paper C. The last section of the chapter addresses the issue of identifying the critical cluster of machines after the occurrence of a fault. A new approach for identifying the cluster is presented. The detailed findings as well as the derivation of the approach can be found in paper D.

2.1 Motivation

A very important part of an extensive on-line dynamic security assessment toolbox is an efficient contingency screening method [13]. This method assesses periodically the capability of the power system in its current state to sustain a set of credible contingencies. Here, of particular interest is if the system can survive the dynamic system response to a fault and its clearance, which is governed by the highly non-linear differential and algebraic system equations.

One of the measures of surviving a contingency is that all synchronous machines in the system remain in synchronism after the fault is cleared. This stability mechanism is called transient stability and has been studied intensely. Assessing tran-

sient stability by numerically integrating the system of differential and algebraic equations poses a large computational burden and, hence, already since the 1930's research efforts have been conducted to develop direct methods to replace the use of extensive power system simulations e.g. the equal area criterion (EAC). The origin of EAC is not precisely documented [25], but it was one of the first times mentioned in [26]. Another widely studied direct method is based on Lyapunov's second method, where the power system and its dynamics are represented by the transient energy function, which is a possible Lyapunov function describing the dynamics of a power system [27].

However, neither of the aforementioned methods did succeed in replacing the use of time-domain simulations completely, since the direct methods have limitations, e.g. on how detailed the dynamic generator models can be represented. Hence, until now contingency screening approaches are carried out off-line using time-consuming power system simulations with detailed model representations of the power system components.

Due to the paradigm shift in today's power generation and, hence, in power system structure, as described in Sec. 1.1, a need for on-line DSA emerges and, hence, also for fast on-line contingency screening approaches.

2.2 State-of-the-art of contingency screening

A variety of methods for contingency screening have been developed. Generally these methods use three different approaches and combinations of them:

1. Detailed time-domain simulation
2. Direct transient stability assessment methods based on e.g. Lyapunov's second method or equal area criterion
3. Severity and stability indicators

A method for contingency ranking using a combination of detailed time-domain simulation and severity indices was described in [28]. A contingency is simulated until approximately 500 ms after the fault clearance and the derived severity indices are computed at the end of the simulation. For the purpose of measuring the severity of a contingency, the authors propose several indices, which are based on:

1. Coherency: Maximum relative change of rotor angle of a machine after fault clearance.
2. Transient energy conversion: Maximum deviation between kinetic and potential energy derived from the transient energy function (TEF) as described in [29].
3. Dot products of certain system states: E.g. dot product of rotor acceleration relative to the center of inertia (COI) and rotor speed with respect to COI.

Finally, the authors propose a composite index, which assigns different weights to the prior defined indexes and sums up their contributions.

The proposed indexes are tested on several test systems and test cases. The results show that to a certain extent the indexes may measure the severity of a contingency.

However, in particular in the test case with 161 generators the majority of the indexes do not obviously divide the contingencies into unstable and stable scenarios.

In [30] a screening method based on a direct method was proposed. The method utilizes the transient energy function and aims at filtering out the non-severe disturbances. The TEF has received a lot of attention and assessment methods based on it were continuously advanced. In [31, pp. 335], a recently developed on-line transient stability screening method based on TEF is presented. The approach uses the TEPCO-BCU method to determine stability [32]. Furthermore, seven BCU classifiers as discussed in [19] were improved and were employed to enable a fast screening of a given set of contingencies. Each of the classifiers is designed to screen out a particular category of contingencies, e.g. one classifier aims at filtering all highly stable cases. The method was tested on a large system with 14,500 buses. It was capable of capturing all unstable cases, $92 - 99.5$ % of the stable cases and needed approximately 1.356 s per contingency.

A contingency screening method utilizing the extended equal area criterion (EEAC) as described in [33] was presented in [34]. The EEAC is a further development of the equal area criterion (EAC) to allow an application of the criterion to multi-machine systems. The authors derived a set of rules to effectively filter out the stable cases from a set of credible contingencies. In order to identify and filter stable cases, just after fault clearance the stability margins determined from the static EEAC (SEEAC) and dynamic EEAC (DEEAC, as described [35, 36]) are computed. Then the aforementioned rules are employed to identify, if a case is stable and should be filtered out. The authors suggest that the remaining cases are then investigated using the integrating EEAC. The proposed method was tested on seven test systems and in total 1106 cases, where 859 cases were actually stable and 247 were unstable. The results showed that the method filters between $70 - 100$ % of the stable cases without any false positives.

In [25] the authors propose a contingency screening method, which is based on the single machine equivalent (SIME) method. The method carries out a contingency filtering, ranking and assessment. The method aims at first filtering out all the stable contingencies and then ranking of the remaining possible harmful contingencies. The ranking is carried out based on their estimated critical clearing times (CCTs). In order to filter and rank the contingencies, the method requires the results from up to two time-domain simulations for each contingency. In order to filter out most of the stable cases, a first relative long clearing time is chosen (CT_1) and all cases, which are assessed to be stable, are filtered out. The second simulation is carried out with a clearing time slightly higher than the protection setting ($CT_2 < CT_1$). If the case is assessed unstable, then the contingency is determined to be harmful and a CCT may be estimated as an extrapolation of CT_1, CT_2 and the respective computed stability margins. If the case is stable, a CCT is estimated from an interpolation of the two prior chosen clearing times and the respective stability margins in the two cases. Finally, if the estimated CCT is above a third clearing time threshold ($CT_2 < CT_3 < CT_1$), then the contingency is discarded as harmless, else it is classified as potentially harmful.

Another contingency screening method employing SIME was presented in [37]. A new index for grouping of the generators was proposed by the authors as well as a contingency classification based on the power-angle shape of the one machine

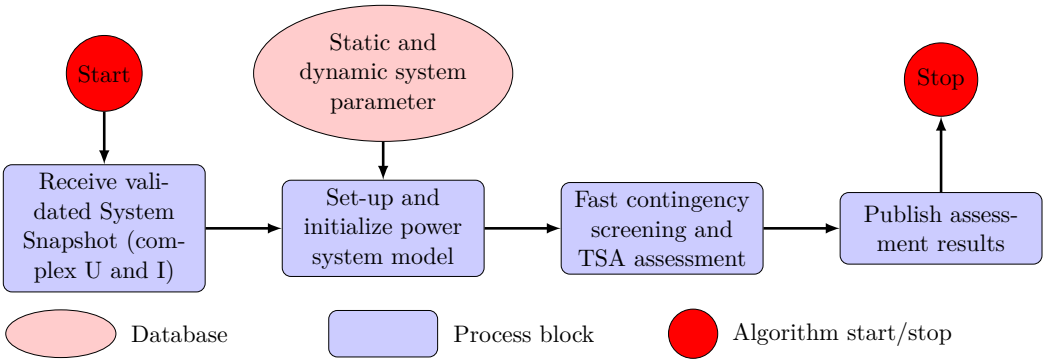

Figure 2.1: Block diagram of the proposed screening and assessment method integrated into a framework for online assessment

infinite bus system, which resulted from aggregation of the generators in the system. One to three detailed time-domain simulations per contingency are required to classify and rank the respective contingency.

2.3 Structure of the developed screening and assessment method

In this section the structure of the proposed screening and assessment method is briefly introduced and the assumptions are described. The method is described in detail in Sec. 2.6 and paper C. However, the method was developed based on the findings presented in Sec. 2.4 and 2.5.2 and, therefore, it is reasonable to introduce the frame of the method at this point.

The method was developed under the assumption that a validated system snapshot, e.g. from validated synchronized phasor measurements providing full system observability, is available and may be used to initialization a time-domain simulation. Furthermore, a database with static and dynamic system parameter is accessible, where each system component, e.g. synchronous generator, is represented with sufficient model detail, which is further discussed in Sec. 2.5.2. The structure of the developed method is shown in Fig. 2.1.

The method receives a validated system snapshot, which contains the complex bus voltages and complex branch currents of the system, as well as model parameter of the system components. These data are used to set-up and initialize a detailed power system model. This dynamic power system model is then input for the fast contingency screening and TSA method, whose derivation and development is the focus of this chapter. Finally, the screening and assessment results are forwarded to be available for other assessment, control and visualization methods, which may be part of the dynamic security assessment toolbox.

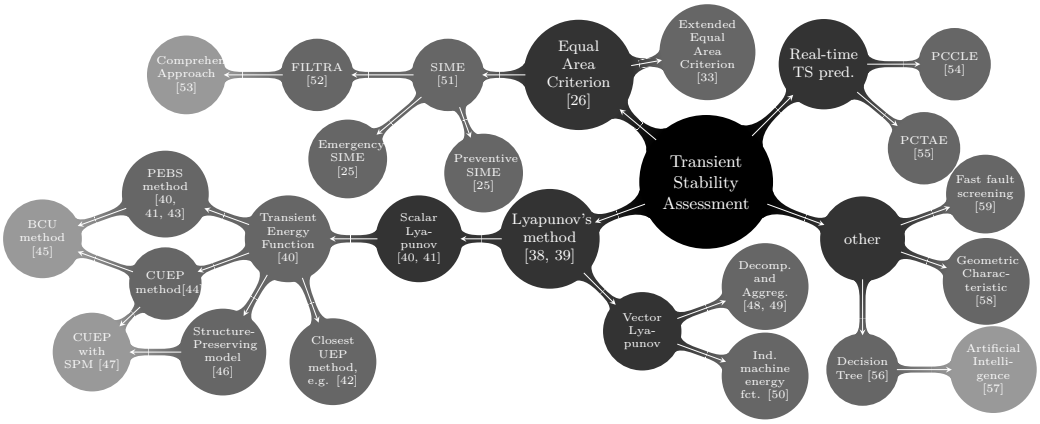

Figure 2.2: Available methods and their development steps (not intended to be exhaustive)

2.4 Review and investigation of existing transient stability assessment methods

The core of an efficient contingency screening method is a fast and accurate transient stability assessment method (TSA). Since research has been addressing the problem of TSA since the 1930s, a wide-range of assessment methods has already been developed and tested.

For fast assessment the aforementioned direct methods are appealing and, hence, a review of methods based on these was carried out. As part of the review, the performance of some of the methods was evaluated by investigating the computational complexity of the underlying algorithm.

2.4.1 Overview of existing methods

In Fig. 2.2 (adopted from paper A) the results of the investigation of existing methods and their development steps are shown. It should be noted that in particular the Equal Area Criterion as well as methods based on the Transient Energy Function have been developed extensively and show promising results. Therefore, it was chosen to investigate the complexity of those methods in more detail.

2.4.2 Runtime analysis through assessment of computational complexity

The computational complexity of a selection of methods was assessed through detailed analysis of the respective algorithms and was expressed in big O-notation, which is a common approach to evaluate the performance of algorithms in computer sciences [60].

For each of the methods the required computations were analyzed and their complexity was determined as a function of parameters of the power system such as number of buses n, branches b or generators m. This allows evaluating and as-

Table 2.1: Complexity estimation comparison, where b: number of branches; d: bandwidth of banded matrix; m: number of generators; n: number of buses

Method	Dominant Operation	Time
Closest UEP	Determine V	$O(m^4)$
BCU	Matrix Reduction	$O(dn^2)$
EEAC	Matrix Reduction	$O(dn^2)$
Preventive SIME	Time-domain Sim.†	x$O(d^2n)$

† : Explicit integration method (R-K method) with x time steps after fault clearance

sessing of the performance of the various methods with respect to the system size, e.g. number of generators or buses, and structure of the power system, e.g. ratio between number of generators and buses.

In comparison to runtime assessment using a particular test power system, the assessment of the algorithm has the great advantage that the results are valid for different power system structures, such as a future power system with large number of distributed energy generation.

As part of the investigation two methods based on the transient energy function and two based on the equal area criterion (EAC) were assessed. The transient energy function based methods are the closest unstable equilibrium point (UEP) method and the boundary of stability region based controlling unstable equilibrium point (BCU) method. The EAC based methods are the extended equal area criterion (EEAC) method and the preventive single machine equivalent (SIME) method. For each of these methods the complexity of each computational step was assessed and the dominant (most complex) computation was identified. Table 2.1 presents a comparison of the complexity of the prior mentioned methods.

The table shows the name of the respective method, a short description of the dominant operation and the associated runtime in big O-notation. The results suggest that the preventive SIME methods has the potential to be the fastest method, under the assumption that the number of required time-steps x as well as the bandwidth of the admittance matrix d are much less than the number of buses n in the system. The SIME method is a so-called hybrid method, since it combines the advantages of detailed time-domain simulation with the advantages of using a direct method in this case the EAC [25]. This combination allows to early determine transient stability of a case and, hence, an early stop of the time-domain simulation.

In this section only a short summary of the findings was presented and the reader is encouraged to read paper A, where the different assessment methods as well as the determination of the computational complexities are described in detail.

Update on runtime analysis: Further literature search and research has led to updated complexities, which are explained in the following.

Highly efficient algorithms have been developed to carry out LU-factorization of the very sparse admittance matrices in power systems a comparison can be found

Table 2.2: Complexity estimation processes shared by the two scalar Lyapunov methods

Function	Time	Freq.	
Y from PMU	$O(m+n+b)$	1	$O(m+n+b)$
Reduce Matrices$^{\diamond}$	$O(dn^2)$	1	$O(dn^2)$
Time domain simulation†	$O(n^{\alpha})$	x	$xO(n^{\alpha})$
Determine V_{cl}	$O(m^3)$	1	$O(m^3)$
Determine V_{crit}			Paper A III-B1 & Tab. 2.3
Compare V_{cl} and V_{crit}	1	1	1
TOTAL‡(one disturbance)			$O(dn^2)$

$^{\diamond}$: Matrix reduction by partitioning of the matrix, see [62, section 2.1]
† : Using an explicit integration method Runge-Kutta with x time steps with $\alpha \approx 1.2$
‡ : Runtime evaluation without determination of the critical energy

Table 2.3: Complexity estimation BCU

Function	Time	Freq.	
Lyapunov method frame$^{\diamond}$	$O(dn^2)$	1	$O(dn^2)$
Sim. until PEBS crossing †	$O(n^{\alpha})$	y	$yO(n^{\alpha})$
Sim. reduced system ‡	$O(n^{\alpha})$	z	$zO(n^{\alpha})$
Find CUEP	$O(m^3)$	1	$O(m^3)$
Determine V_{crit}	$O(m^2)$	1	$O(m^2)$
TOTAL(one disturbance)			$O(dn^2)$

$^{\diamond}$: see table 2.2
† : Time dom. sim. continued using R-K with y time steps with $\alpha \approx 1.2$
‡ : Time dom. sim. of red. system using R-K with z time steps with $\alpha \approx 1.2$

in [61]. The authors show experimentally that with very efficient factorization algorithms, such as KLU, the complexity of the factorization can be estimated as being quasi linear with complexity of $O(n^{\alpha})$ (where $\alpha \approx 1.2$). This is considerably faster as the estimation of $O(d^2n)$.

Furthermore, closer investigation of the computation of the differential equations of the generator rotor and stator as well as the associated algebraic equations has led to the conclusion that the complexity of the calculations is more appropriately estimated as being linear dependent on the number of generators. Hence, the associated complexity in O-notation is $O(m)$.

This leads to an alternation of the runtime assessment results. Therefore, the Tables II, V and VI from paper A are repeated with the updated values, where the new values are marked blue.

The updated complexity estimation results, which are affected by the update, are shown in Tables 2.2-2.4. It should be noted that the result of the complexity

Table 2.4: Complexity estimation SIME

Function	Time	Freq.	
PMU data	$O(m+n+b)$	1	$O(m+n+b)$
Time domain sim.†	$O(n^\alpha)$	x	$xO(n^\alpha)$
Rotor angle (pred.)	1	m	$O(m)$
Ident. critical mach.	$O(m \log m)$	1	$O(m \log m)$
Aggregate & form OMIB	$O(m)$	1	$O(m)$
$P-\delta$ approx.	1	1	1
Det. stability margin	1	1	1
TOTAL(one dist.)			$xO(n^\alpha)$

† : Explicit integration method (R-K method) with x time steps with $\alpha \approx 1.2$

Table 2.5: Updated complexity estimation comparison

Method	Dominant Operation	Time
Closest UEP	Determine V	$O(m^4)$
BCU	Matrix Reduction	$O(dn^2)$
EEAC	Matrix Reduction	$O(dn^2)$
Preventive SIME	Time-domain Sim.†	$xO(n^\alpha)$

† : Explicit integration method (R-K method) with x time steps after fault clearance

estimation of the Lyapunov method frame (see Table 2.2) and the BCU method (see Table 2.3) were not altered, since in both cases the step corresponding to the computation of the reduced matrix is dominant. In the estimation of the complexity of the SIME method (see Table 2.4), in spite of the updated complexities, the time-domain simulation remains to be dominant as long as the number of buses n is considerably larger than the number of generators in the system, e.g. $n > 2m$.

This as a consequence also leads to an updated table of the complexity comparison, which now shows the better performance of the preventive SIME method even clearer (see Table 2.5).

2.5 Investigation of speed-up possibilities of transient stability assessment

2.5.1 Motivation

The assessment of the existing transient stability assessment methods and their algorithm complexity presented in the previous section led to the conclusion that the hybrid method preventive SIME is potentially the fastest TSA method.

Since time-domain simulation was in the previous section identified as the operation

posing the largest computational burden. An attempt to speed up the simulation appears to be an efficient way to improve the overall performance of the method. There are various ways to speed up time-domain simulation amongst others:

- Improve algorithms to handle admittance matrix, e.g. LU-factorization.
- Reduction of the number of differential equations, which need to be solved.

As described in the previous section very efficient algorithms were developed for LU-factorization of the sparse admittance matrix. A simple reduction of the model detail of the components in the system, e.g. synchronous generators, and, hence, reducing the number of differential equations to be solved in each time step of the simulation could be an efficient way to speed up the simulation. For that purpose, it was investigated, how the model detail of synchronous generators impacts the transient stability assessment with preventive SIME.

2.5.2 Impact of model detail of synchronous machines on transient stability assessment

In this section the results are presented of the investigation on how detailed the model of synchronous generator needs to be to assess transient stability with the SIME method correctly. The method was prior identified as being a potentially fast assessment method. The idea is that a further speed-up of the assessment method can be achieved by reducing the detail of the models and, thereby, lowering the number of differential equations to be solved in each simulation step.

Hence, the task was to investigate, if it is possible to reduce the order of the synchronous machine model, while

- the instability mechanism is not altered
- and SIME correctly & early detects stability/instability

For that purpose, simulations and stability assessment results of two test systems, with synchronous machine models of four different degrees of detail, were conducted and compared. The considered synchronous machine models were the following:

Four Winding model (6^{th}-order): Two damper windings in the q-axis; one damper winding and the field winding in the d-axis; network and stator transients are neglected. Recommended in [63] for round-rotor generators with no dampers in the pole face region. Data supplied by manufacturer are usually based on this model.

Two-axis model (4^{th}-order): Damper winding dynamics ψ_{1d} and ψ_{2q} are neglected; E'_d and E'_q dynamics are maintained.

One-axis model (3^{rd}-order): Damper winding dynamics E'_d are neglected additionally.

Classical model (2^{nd}-order): Voltage behind transient reactance assumed to be constant.

The two test systems are listed below.

Western System Coordinating Council (WSCC) system: 9 buses, 3 generators; no governor model, excitation system and PSS (adopted from [64]).

New England & New York system: 68 buses, 16 generators; thermal/turbine governor, static exciters and PSS included (adopted from [65], see also Sec. I.1 in the Appendix).

For each of the test systems two test cases were set-up, a stable and an unstable case. In order to determine if a case is stable or unstable, the simulation with the highest order model (here: 6^{th}-order) was considered as a reference and the simulations with lower order models were compared against this reference.

Firstly, in order to assess if the instability mechanism is the same in the simulations with lower order model, the rotor angle trajectories were compared to the trajectory in the reference case. In the unstable case, the mechanism is considered to be equivalent, if the same generator or group of generators loses synchronism as in the reference case. In the stable case the critical generator or group of generators should show a similar rotor angle response as the reference. Secondly, in order to investigate if SIME correctly and early determines stability/instability, the stability margin trajectories are computed in the different simulations and compared to the respective stability margin of the reference simulation.

The study showed that SIME in all cases assessed stability correctly and in accordance to the rotor angle response of the critical generators. However, it was found that the stability/instability mechanism is only correctly exhibited, if the used synchronous machine model is of 4^{th}-order or higher. Figure 2.3 shows a result of the comparison of the different generator models. The rotor angle responses depicted in Fig. 2.3(a) reveal that only the simulations with 4^{th}-order exhibit the same instability mechanism as the reference case, which is the simulation with 6^{th}-order model. Hence, a representation of the generators with lower order models would not be sufficient. Figure 2.3(b) displays the stability margin computed with the SIME method over simulated time. It shows that the method in all cases determines the stability margin correctly. Correspondingly, the stability margin converges to a positive value for the simulations with 2^{nd}- & 3^{rd}-order and a negative value for 4^{th}- order and higher.

In this section a short summary of the findings was presented and the reader is referred to paper B in the Appendix to find the in-depth description of the investigation methodology as well as the detailed results.

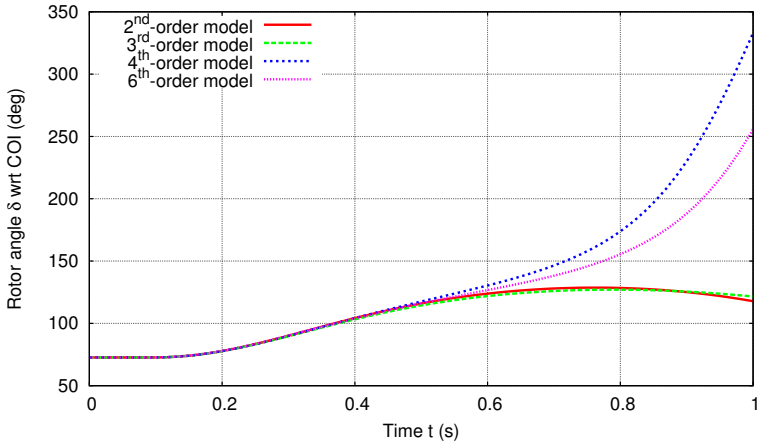

(a) Comparison of rotor angle responses

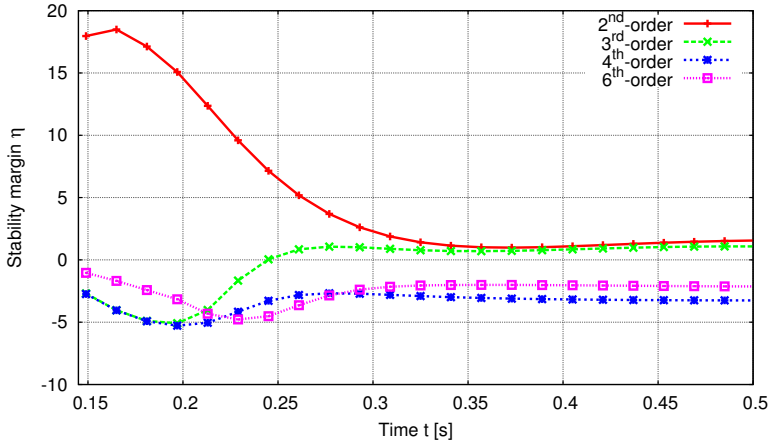

(b) Comparison of computed stability margins

Figure 2.3: Result comparison of the unstable case of the WSCC 14-bus system

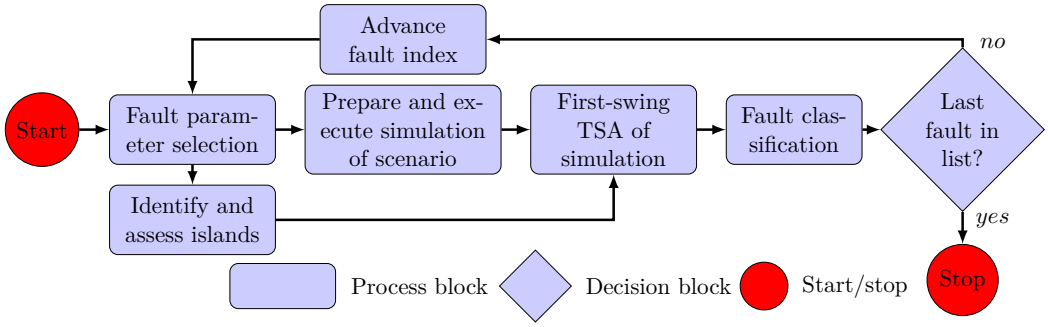

Figure 2.4: Block diagram of the fast contingency screening and TSA assessment algorithm

2.6 Fast contingency screening, ranking and on-line transient stability assessment

In order to ensure that the system is $N-1$ secure, a fast and reliable contingency screening method is essential. Moreover, to provide a more complete picture of the system state a ranking of each contingency is very valuable.

For that purpose in this section a method is introduced, which carries out a fast contingency screening, ranking and on-line transient stability assessment. The method was developed based on the findings of the prior sections (Sec. 2.4 & 2.5.2). Hence, the developed method uses the preventive SIME method to early and accurately determine stability of a particular case. In the following a short summary of the findings is described and the reader is encouraged to read paper C, where the method and the results are described in detail.

2.6.1 Contingency screening and ranking method

The framework for integration of the contingency screening and assessment method into an on-line assessment environment was briefly introduced in Sec. 2.3. In this section, the actual screening and assessment method is introduced. Fig. 2.4 shows the block diagram of the proposed method. As mentioned in Sec. 2.3 the input to the method is the initialized power system model.

Fault parameter selection: In the first call of the function a list of contingencies is set-up, then and in any subsequent call of the function the parameter (e.g. type of fault, fault location, protection relay settings, etc.) of the next fault on the list are extracted and used in the next simulation.

Prepare and execute simulation of scenario: The fault parameter and the detailed power system model are then used to initialize the time-domain simulation, which is then executed to determine the dynamic system response caused by the contingency and its clearance.

Identify and assess islands: At the same time the power system model and fault parameter are forwarded to a function, which checks if islands were created due to the fault clearance and determines if loads or generators are in the island. In order

Table 2.6: Classification of contingencies (where g: number of generators and l: number of loads)

Classifier	η	$\frac{dP_a}{d\delta}\big\vert_{\delta_r}$	ω	Number of gen. & loads	Explanation
Definitely Unstable (DU)	–	–	–	–	No intersection of $P(\delta)$-curve and P_m.
	–	–	–	$g \geq 1;\ l = 0$	Island contains generator, but no loads.
Unstable (U)	< 0	–	–	–	Preventive SIME returned a negative stability margin.
Not Classifiable (NC)	–	–	–	$g = 1;\ l \geq 1$	Only one generator in island and no synchronization reference available.
Marginal Stable (MS)	> 0	> 0	–	$g \geq 2;\ l \geq 1$	Return angle at point where $dP_a/d\delta > 0$
	–	> 0	< 0	$g \geq 2;\ l \geq 1$	and pos. margin or returning $\omega < 0$.
Stable (S)	> 0	< 0	–	$g \geq 2;\ l \geq 1$	Return angle at point where $dP_a/d\delta < 0$
	–	< 0	< 0	$g \geq 2;\ l \geq 1$	and pos. margin or returning $\omega < 0$.
Definitely Stable (DS)	–	–	$< \omega_{th}$	$g \geq 2;\ l \geq 1$	Barely accelerated during fault and rel. rotor speed less than a threshold ω_{th}.

to use the efficient algorithms from graph theory, the function to identify islands first converts the admittance matrix into an adjacency matrix and then uses an algorithm based on depth-first search to check for islands.

First-swing TSA of simulation results: The system trajectories, which describe the dynamic response of the system to the fault, and the island identification & assessment results are forwarded to the transient stability block. Here, preventive SIME is used to early determine stability or instability of the whole system or its respective islands.

Fault classification: After stability of the system or the islands was determined, some states and parameters of the computed single machine equivalent and island are utilized to classify the fault. Table 2.6 shows the classification categories and the characteristics used for categorization; namely the determined stability margin η, the gradient of the $P_a(\delta)$-curve $dP_a/d\delta|\delta_r$ at the return angle δ_r, the relative rotor speed ω as well as the number of generator g and loads l in an island.

After fault classification the assessment results are stored and the next fault on the contingency list is investigated. When the last contingency on the list was assessed, the contingency screening and ranking results are forwarded to the publication block (see Fig. 2.1).

2.6.2 Test results of the contingency screening and ranking method

The power system model used for test and evaluation of the method was the New England & New York test system, which was adopted from [65] (see also Sec. I.1 in the Appendix). The considered test cases were three-phase short circuits on either end of transmission lines and transformers, which resulted in a total number of 172 test cases. These test cases were then used to assess the method with respect to reliability and performance. Furthermore, the fault clearing time was varied between 50 to 500 ms, which resulted in three sets of fault scenarios and a total of 516 test cases.

Method reliability: In order to assess reliability, the stability assessment results were tested against a reference stability assessment. The reference assessment method solely considers the rotor angle trajectories extracted from detailed time-

Table 2.7: Performed tests, assessment results from time-domain simulation and reliability of proposed screening method

Test	Clearing time $[ms]$	Number of stable	Number of unstable	Identified stable cases	Identified unstable cases
Test I	50	168	40	94.64%	100.00%
Test II	200	137	71	93.43%	98.59%
Test III	500	55	153	90.91%	100.00%

domain simulation, where a case is determined to be unstable, if the rotor angles of at least two generators are more than 120° apart at the end of the simulation. This setting was chosen since it is a common setting for out-of-step protection of generators [27, p. 924]. Table 2.7 shows the number of cases identified as being stable and unstable in each set of contingencies.

Furthermore, the table shows how many of the unstable and stable cases the screening method correctly identifies. It should be noticed that the ratio of correctly identified stable cases is high with $90.91 - 94.64$ % and the share of correctly identified unstable cases is even higher with $98.59 - 100.00$ %.

Discussion of a particular case: The lower success rate for unstable cases in test II is due to the disagreement between the reference evaluation method and the proposed method in a particular case. The rotor angles and rotor speeds of the generators over time are shown in Fig. 2.5 for that case.

The graph shows that it is a marginal case. In the simulation the case is marginal stable, since a group of generator loses synchronism after the first swing, but resynchronizes after a pole slip. In reality, the protection system would detect loss of synchronism and protection relays, such as out-of-step protection would disconnect certain generators in the system, which would likely lead to a system collapse.

Corresponding, to the rotor angle deviation of two groups of generator, which is larger than 120°, the reference assessment method states that the case is unstable. The preventive SIME method predicts resynchronization of the generators, in accordance with the simulation results, and, consequently determines the case to be stable. This shows the importance of including and correctly modelling of the protection system in transient stability studies.

Performance of the method: In order to assess performance, the run time of the method and particular parts of the implementation were investigated. The application of preventive SIME allows to early stop simulations, when the assessment method has determined stability or instability. Therefore, the method needs to be seamlessly integrated into the simulator.

The time-domain simulation software RAMSES [66], which was used in this work, does not have a seamless integration of SIME. Hence, each case was simulated for a fixed time period and the system trajectories were analyzed afterwards. However, in order to show the effect of an integration of SIME into the simulation software, a second test was performed with variable simulation times, which were sufficient to determine stability with SIME and was extracted from the simulation with fixed simulation time. Table 2.8 shows the runtime results of the screening method for

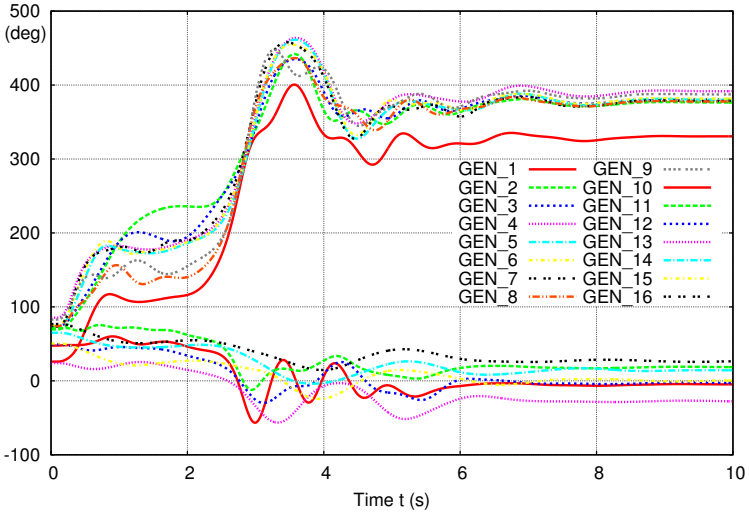

(a) Rotor angle over time

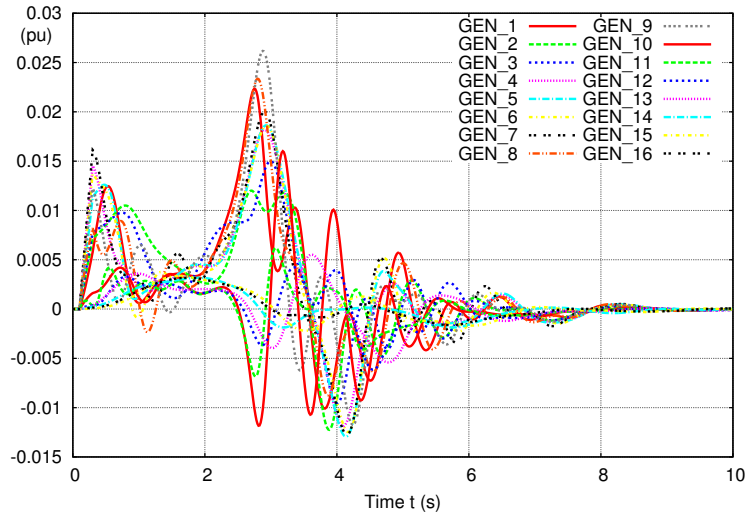

(b) Rotor speed over time

Figure 2.5: Rotor angle and rotor speed of the generators over time in a particular fault scenario with clearing time of 200 ms

Table 2.8: Performance of fast screening method with variable simulation time (and fixed simulation time in brackets)

Test	Runtime with simulation $[s]$		Runtime of assessment $[s]$	
	per cont.	total	per cont.	total
Test I	0.263 (0.449)	45.31 (77.30)	0.045 (0.057)	7.54 (9.78)
Test II	0.275 (0.536)	47.32 (92.17)	0.042 (0.055)	7.24 (9.53)
Test III	0.296 (0.636)	51.05 (109.36)	0.038 (0.051)	6.53 (8.85)

each set of contingencies with variable and fixed simulation time.

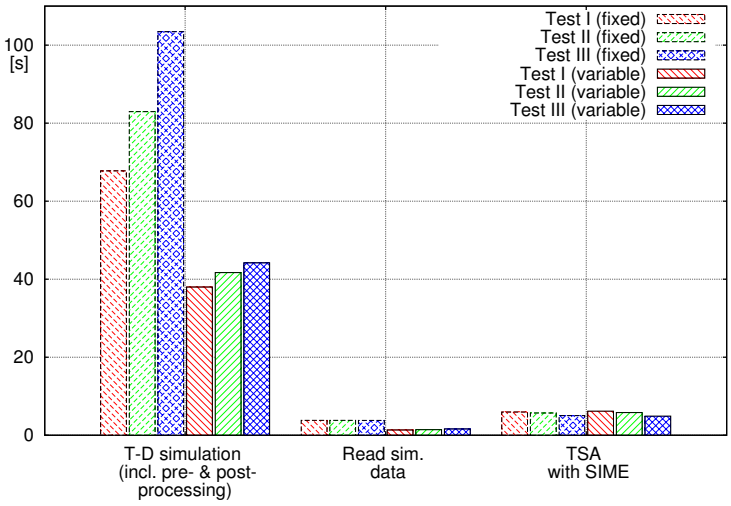

Figure 2.6: Comparison of the runtime of the major parts of the screening method with fixed and variable simulation time

It should be noted that in particular the runtime with included simulation is considerable reduced due to the variable and, hence, shorter simulation time. Furthermore, it can be observed that the runtime without simulation and only assessment is reduced. This originates from a lower amount of data, which needs to be read. This is confirmed by the bar graph shown in Fig. 2.6, which shows the runtime of different parts of the screening methods and compares the performance with fixed and flexible simulation time.

Classification of contingencies: In order to assess the proposed classification criteria, the critical clearing times (CCT) of the considered contingencies were determined and plotted against the assigned category of the respective fault. Figure 2.7 displays the result from all three tests.

The graph reveals that the CCT within a category vary greatly for stable cases. However, when considering the average CCT in each category a trend for increasing CCT can be observed from the category Definitely Unstable to Definitely Stable.

A more detailed discussion of the methodology and results can be found in paper C.

2.7 Identification of critical machine cluster

When employing the SIME method or other methods based on the equal area criterion for transient stability assessment, it is essential to correctly identify the critical machine cluster, which is the group of generators likely to lose synchronism. An early and accurate identification is the requirement to enable an early and accurate transient stability assessment.

In this section the development of a new approach for identification of the critical machine cluster is described. The detailed development was documented in

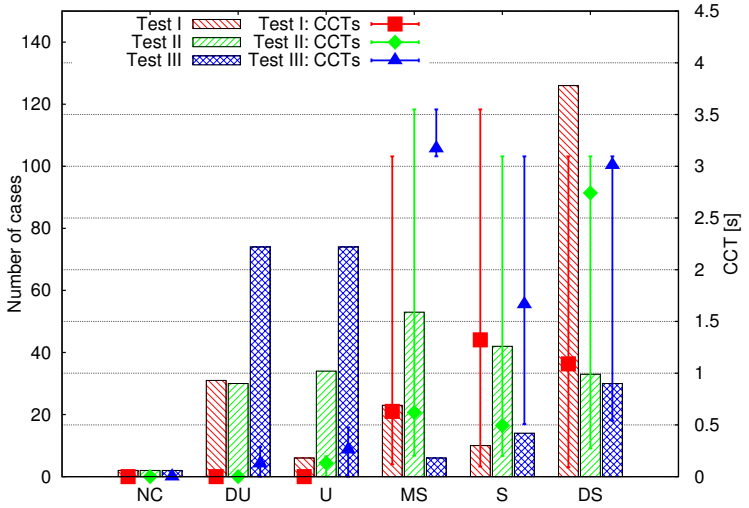

Figure 2.7: Fault ranking results: Bar graph (left y-axis) indicates number of cases in a particular category and test. The data points and error bars show average and range of CCTs in the corresponding category and test (right y-axis).

paper D. For the developed approach a new coupling coefficient for each pair of generators was derived and computed. A clustering algorithm then identifies the critical machine cluster in the system.

2.7.1 Coupling coefficient and coupling matrix

The coupling coefficient proposed in paper D is computed for each pair of generators i & j. It corresponds to the stability margin computed for a one-machine infinite bus system, when applying the equal area criterion. The stability margin is defined as the difference between the available dissipation energy $E_{dis,ij}$ and the kinetic energy $E_{kin,ij}$ of the equivalent machine.

$$\eta_{ij} = E_{dis,ij} - E_{kin,ij} \tag{2.1}$$

where

$$\begin{aligned} E_{dis,ij} &= -\int_{\phi_{c,ij}}^{\phi_{u,ij}} P_{m,ij} - P_{e,ij}(\phi_{ij}) d\phi_{ij} \\ E_{kin,ij} &= \frac{1}{2}\frac{M_{ij}}{\omega_0}\omega_{ij}^2 \end{aligned} \tag{2.2}$$

In these equations M_{ij} corresponds to the inertia coefficient of the equivalent machine, ω_0 corresponds to the synchronous speed, ω_{ij} to the rotor speed and ϕ_{ij} to the respective rotor angle, where $\phi_{c,ij}$ refers to the angle at fault clearance and $\phi_{u,ij}$ to the angle at the unstable equilibrium point. Furthermore, $P_{m,ij}$ is the equivalent mechanical power and $P_{e,ij}$ the electrical power.

In order to compute the coupling coefficient for each pair of generators, equations for the computation of a one-machine equivalent were derived. The rotor angle ϕ_{ij}, speed ω_{ij} and inertia coefficient M_{ij} of the equivalent machine were defined as follows.

$$\begin{aligned} \phi_{ij} &= \delta_i - \delta_j \\ \omega_{ij} &= \omega_i - \omega_j \end{aligned} \tag{2.3}$$

and

$$M_{ij} = \frac{M_i M_j}{M_T} \text{ with } M_T = M_i + M_j \tag{2.4}$$

where $\delta_{i/j}$ is the rotor angle, $\omega_{i/j}$ is the rotor speed and $M_{i/j}$ is the inertia coefficient of the i-th and j-th machine, respectively. Based on that, an equation for the equivalent mechanical power $P_{m,ij}$ and electrical power $P_{e,ij}$ was derived.

$$\begin{aligned} P_{m,ij} &= \frac{1}{M_T}\left(M_j P_{m,i} - M_i P_{m,j}\right) \\ P_{e,ij} &= \frac{1}{M_T}\left(M_j P_{e,i} - M_i P_{e,j}\right) \end{aligned} \tag{2.5}$$

where $P_{m,i/j}$ and $P_{e,i/j}$ are the individual mechanical or electrical power. It is shown in paper D that the electric power injection $P_{e,ij}$ of the one-machine equivalent can be reformulated as a function of ϕ_{ij}.

$$P_{e,ij} = P_{c,ij} + P_{max,ij}\sin(\phi_{ij} - \nu_{ij}) \tag{2.6}$$

where $P_{c,ij}$, $P_{max,ij}$ and ν_{ij} are independent of ϕ_{ij}, but functions of the reduced admittance matrix and the complex e.m.f.s of the machines in the system. Finally, the coupling coefficients determined for all pairs of machines can be assembled to the coupling matrix $\mathbf{H}$, which is an $m \times m$ matrix where m is equal to the number of generators in the system.

$$\mathbf{H} = \begin{pmatrix} \eta_{11} & \cdots & \eta_{1m} \\ \vdots & \ddots & \vdots \\ \eta_{m1} & \cdots & \eta_{mm} \end{pmatrix} \tag{2.7}$$

2.7.2 Method to identify the critical machine cluster

In order to identify the cluster of critical machines, the impact of the fault and its clearance on the coupling of the machines is important. For that purpose, the matrix $\mathbf{\Delta H}$ is proposed, which is defined as the difference of the coupling coefficients in the initial steady state and after fault clearance.

$$\mathbf{\Delta H} = \mathbf{H}(t_c^+) - \mathbf{H}^\circ \tag{2.8}$$

where $\mathbf{H}(t_c^+)$ is the coupling matrix determined at the time just after fault clearance t_c^+ and $\mathbf{H}^\circ$ is the coupling matrix determined before the fault occurs. $\mathbf{H}^\circ$ provides information on the initial coupling strength between individual generators and may allow identifying structural weak connected machines. By assessing the change in coupling for the individual pairs of machines, it allows to investigate the impact of the fault and its clearance on the coupling coefficients. These changes may be due to the dynamical response of the machines or structural changes in the system.

The method for identifying the critical cluster of machines was developed under the assumption that the coupling of the critical group of generators is considerably weakened because of the fault. The weakening may originate from an increase in kinetic energy during the fault or a degradation of the connectivity due to the fault clearance. Hence, the changes of the coupling coefficients may provide valuable information for identifying the critical machine cluster.

In the following a simple clustering algorithm to identify the critical machine cluster is described. A block diagram of the algorithm, which was proposed in paper D,

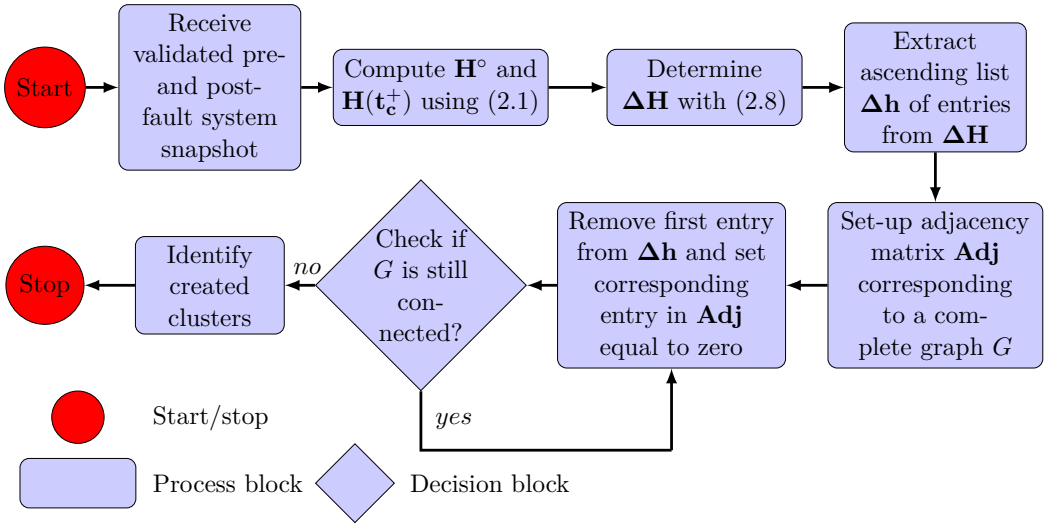

Figure 2.8: Block diagram of the critical machine cluster identification algorithm

is shown in Fig. 2.8. The diagram shows the sequence of operations carried out to identify the cluster. The different blocks are below described in more detail.

Receive system snapshots: The method receives a system snapshot of the pre- and post-fault condition. It is assumed, that these snapshots provide full observability of the system and contain the complex bus voltages as well as the transmission line and injection currents. Furthermore, it is assumed that the given data are sufficient to determine the system's admittance matrix in pre- and post-fault condition.

Compute pre- and post-fault cluster matrix: In this block the coupling matrix for the two conditions are computed. For that purpose and as described in detail in paper D, the Thévenin equivalent of the generators, the extended admittance matrix and, subsequently, the reduced admittance matrix are computed. These data are then utilized to determine the one-machine equivalent for each pair of machines and, finally, their coupling coefficients can be computed with (2.1).

Determine impact of fault on coupling coefficients $\mathbf{\Delta H}$: Corresponding to the assumption that the coupling coefficients of the critical group are strongly affected by the fault, the impact of the fault is computed as the difference of pre- and post-fault coupling with (2.8).

Set-up ascending list of changes in coupling coefficients $\mathbf{\Delta h}$: In this block a list $\mathbf{\Delta h}$ is created, which contains the sorted entries from $\mathbf{\Delta H}$. The entries are sorted ascending beginning with the lowest or rather most negative change in coupling. Moreover, two vectors $\mathbf{r}$ and $\mathbf{c}$ are built up which have the same size as $\mathbf{\Delta h}$ and contain the row and column numbers of the respective entries in $\mathbf{\Delta H}$.

Set-up adjacency matrix Adj: In order to use the efficient algorithms from graph theory to identify the critical machine cluster, a graph G is initialized corresponding to the matrix $\mathbf{\Delta H}$. The resulting graph G is a complete graph with m vertexes and with an adjacency matrix **Adj**.

Remove entry with lowest change in coupling: There are several algorithms in graph theory to identify clusters, e.g. minimum cut, which determines the cut set with the smallest sum of weights possible to split the graph into two disjoint subsets, or hierarchical clustering, which determines clusters according to the "distance" of the individual vertexes to each other. However, in this work individual connections one after another are removed according to the list in $\mathbf{\Delta h}$ and beginning with the lowest or rather most negative change in coupling. Therefore, the corresponding entries in $\mathbf{\Delta h}$, $\mathbf{r}$ and $\mathbf{c}$ are removed and the respective entry in $\mathbf{Adj}$ is set equal to zero.

Check if the graph is still connected: After a connection in the graph was removed, a depth-first search is executed to identify, if the resulting graph is still connected. If the graph is still connected, the next entry in $\mathbf{\Delta h}$, which corresponds to the next lowest change in coupling, is removed and the corresponding entry in $\mathbf{Adj}$ is set to zero. Then it is again checked, if the graph is still connected. This process is continued until the graph is split in two.

Identify created clusters: When the graph was split into two disjoint subsets, then the created clusters need to be identified. For this purpose, the graph is explored with multiple depth-first searches until all vertexes are associated with a cluster. The results are the identified clusters as well as the nodes belonging to each cluster.

New England & New York example case: In paper D two test cases were presented and the capability of the method to determine the critical machine cluster was demonstrated. The used test system was the New England & New York system, which is described in detail in Sec. I.1 in the Appendix. In both test cases a short circuit on a transmission line was applied and was cleared after 250 ms by opening of the breakers at both ends of the line.

Figure 2.9 shows the simulation results of the second case, where the disturbance led to the loss of synchronism of the generators GEN 2 and 3. Figure 2.9(a) shows the rotor angle response of a selection of generators, where time of fault clearance is indicated by t_c^+. At fault clearance, it may be difficult to identify the critical machine cluster solely based on the observed rotor angles, since at that time the selected generators in the range of GEN $4-9$ are relatively close to the unstable generators GEN 2 and 3. However, shortly after the rotor angles of the selected generators in the range of GEN $4-9$ split from the unstable generators.

In Fig. 2.9(b) the fault induced changes of the coupling coefficients is displayed, when $\mathbf{\Delta H}$ is computed at t_c^+. Visual inspection of the graph indicates three groups:

- Group I: GEN 2 and 3
- Group II: GEN 1 and $4-9$
- Group III: GEN $10-16$

This is in good agreement with the groups identified in Fig. 2.9(a). When the algorithm, which was shown in Fig. 2.8, is employed to identify the critical machine cluster, GEN 2 and 3 are determined to be the most critical ones, which is in good agreement with the prior discussed observations.

In conclusion, in the presented test case the proposed coupling coefficients or rather the change of the coefficients due to the fault indicated correctly which generators

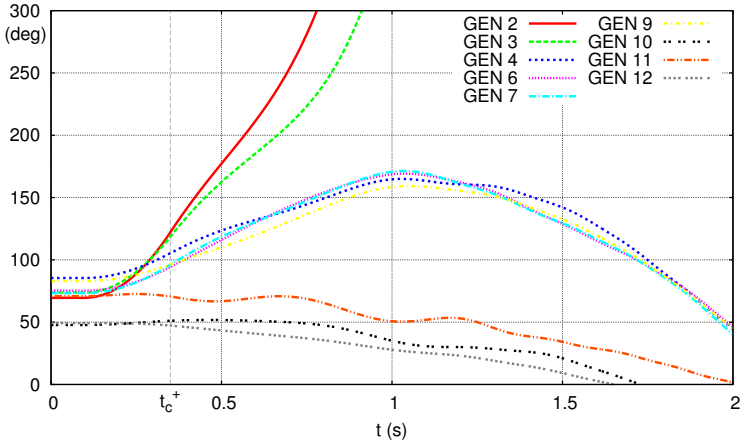

(a) Rotor angle over time of a selection of generators

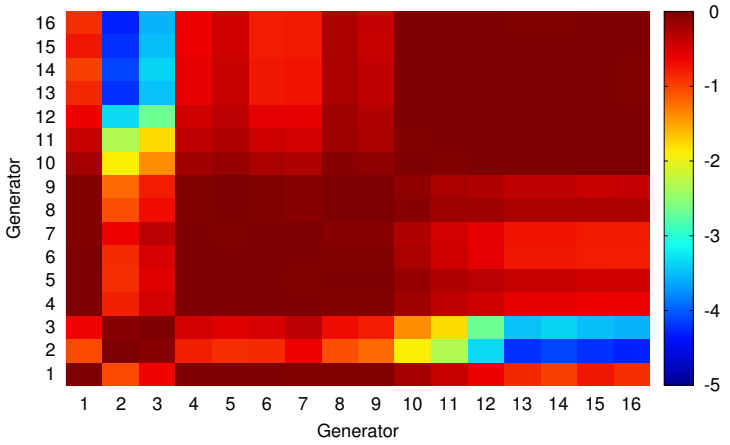

(b) Matrix ΔH computed just after clearance of the short-circuit

Figure 2.9: Case II: Critical machine identification in a stable test scenario, where a short-circuit on the line connecting bus 4 and bus 5 was applied.

are forming clusters. Moreover, the proposed clustering algorithm correctly identified the most critical group of generators. However, further tests and investigations are needed to confirm and verify the approach.

Chapter 3

Sensitivity based assessment and prediction of transient voltage sags

In this chapter the derivation of sensitivities to assess transient voltage sags caused by rotor angle swings and the development of a method for early prediction of these voltage sags is described. The detailed derivation and the results of the sensitivities as well as the prediction method can be found in the Appendix in the papers E, F and G, respectively.

3.1 Voltage sags caused by rotor angle swings

Voltage sags, also known as voltage dips, are depressions of the measured voltage magnitude lasting for a short period of time. The first international definition and measurement method for voltage dips was described in the standard IEC Standard IEC 61000-4-30 [67].

> "Voltage dip: Temporary reduction of the voltage at a point in the electrical system below a threshold."

In literature on power quality, the topic is frequently addressed and discussed [68]. A primary cause of voltage sags are faults in the power system and the observed voltage sags are dependent on the types of loads, e.g. induction machine, which are connected to the buses in the region of the fault. However, a less recognized origin of voltage sags is rotor angle swings or, rather, the angular separation of groups of generators. This kind of voltage sags is less dependent on the type of load present in the power system, since the dominating mechanism is the angular separation.

New England & New York example case: In this chapter, the simulation results are obtained using the New England & New York system, which consists of 68 buses and 16 generators, and was adopted from [65]. Detailed information and

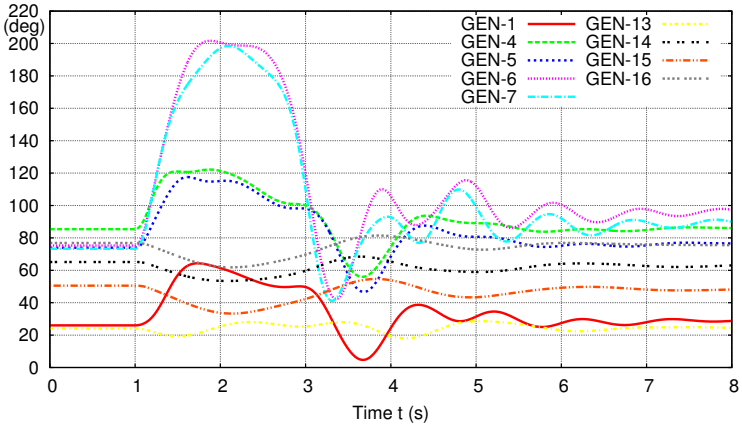

(a) Rotor angles over time

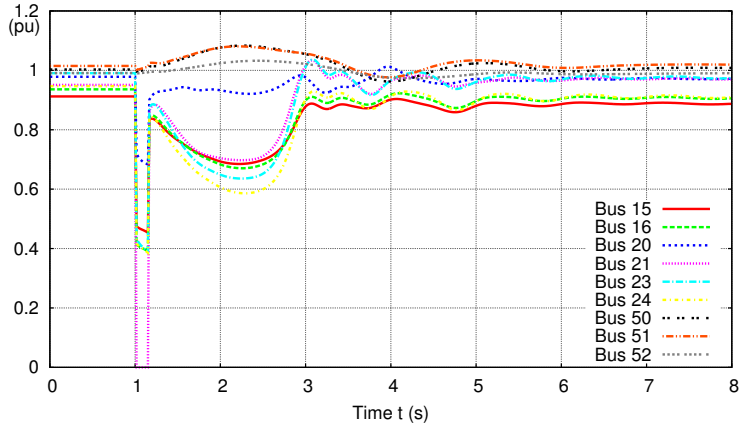

(b) Voltages over time

Figure 3.1: Example of a voltage sag caused by rotor angle swings

a one-line diagram can be found in Appendix I.1. The initial conditions of the test scenario were as well adopted from [65]. In this case, the considered contingency is a three-phase short-circuit on the transmission line connecting buses 16 and 21. The short-circuit occurs one second after the simulation begins and is assumed to be very close to bus 21. It is cleared after 150 ms by opening the breakers at both ends of the faulted transmission line. Figure 3.1 shows a selection of the bus voltages and the rotor angles of a selection of generators over time. The fault leads to acceleration and, subsequently, angular separation of certain generators as seen in Fig. 3.1(a).

In Fig. 3.1(b), it can be observed that the short circuit leads to a depression of the voltage magnitudes at the system buses. However, the voltages begin to recover immediately after fault clearance. Following, at a selection of buses voltage sags can be observed which coincides with the rotor angle swings depicted in Fig. 3.1(a).

Since the voltage sags may lead to further disturbances in the system for example disconnection of loads and, hence, to deterioration of the system condition, it is crucial to study the mechanism behind these voltage sags.

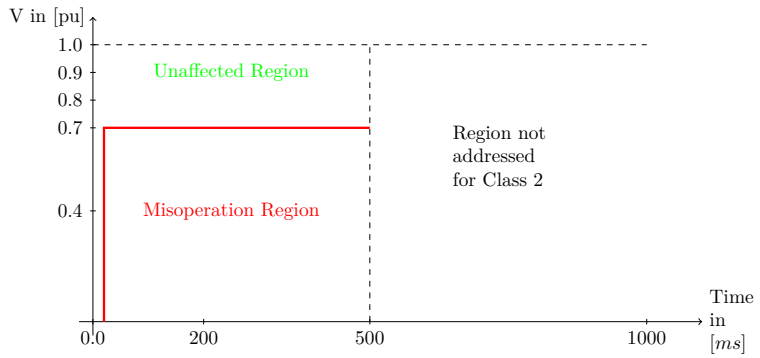

(a) Class 2: PCC and IPC

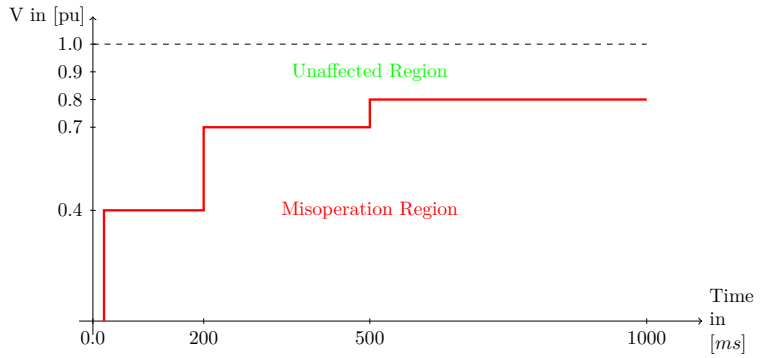

(b) Class 3: Only IPC

Figure 3.2: IEC-61000-4-34: Voltage Dip envelopes defined by the IEC for class 2 and class 3 loads with input current more than 16 A per phase

3.1.1 IEC standard on voltage sags

In IEC-61000-4-34 requirements for different load types with input currents of more than 16 A per phase are defined with respect to voltage dips.

- Class 1: Highly sensitive loads, usually equipped with protection such as uninterrupted power supply, filters, etc.
- Class 2: Points of common coupling for consumer systems (PCC) and points of common coupling for industrial systems (IPC)
- Class 3: Only IPC's with higher compatibility level as class 2
- Class X: User defined class

For the classes 2 and 3 the standard defined voltage envelops to determine regions of unaffected and misoperation (see Fig. 3.2).

The norm required that Class 2 devices stay connected to the power grid, if the voltage recovers to a value above 0.7 pu after fault clearance, else the devices may disconnect. For Class 3 the requirements are more stringent, the loads need to remain connected in the first 200 ms after fault clearance, if the voltage recovers to a value above 0.4 pu. In the period of $200 - 500$ ms, the loads need to stay connected, if the voltage is higher than 0.7 pu. Afterwards, the voltage needs to have recovered to a value above 0.8 pu to guarantee that the Class 3 loads operate

normally. If the voltage magnitude at a bus is not recovering fast enough and the "Misoperation Region" is entered, the connected loads may malfunction, e.g. an induction machine may stall, and eventually trip.

3.1.2 Investigation of the mechanism behind voltage sags

The mechanism behind voltage sags caused by rotor swings can be discussed and illustrated graphically under consideration of a simple example power system as the one shown in Fig. 3.3.

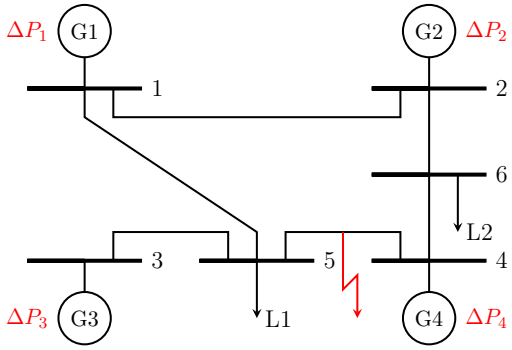

Figure 3.3: One-line diagram of a simple example test system with 6 buses.

The generators are represented by the so-called "classical" transient stability model, where each generator is represented by an e.m.f. $\bar{E}'$ of constant voltage magnitude behind the transient reactance X'_d (see Fig. 3.4(a)). The angle of the e.m.f. can then be used to represent the rotor angle of the generator [27, Sec. 5.3, p. 187]. In this example, for sake of simplicity the generators' mechanical power input is assumed constant and the loads are modelled as constant impedances. When representing each generator by its Norton equivalent, as shown in Fig. 3.4(b), then the following linear algebraic equation can be used to describe the relation of the complex bus voltages $\bar{\mathbf{V}}$ and the complex current injections $\bar{\mathbf{I}}$, where $\mathbf{Y}$ is the "augmented" admittance matrix.

$$\bar{\mathbf{I}} = \mathbf{Y}\bar{\mathbf{V}} \tag{3.1}$$

Assuming a system with n buses and m generators ($n > m$), the equations in (3.1) can be sorted, in order that the buses where generators are connected are numbered from $n - m + 1$ to n.

$$\begin{bmatrix} 0 \\ \vdots \\ 0 \\ \bar{E}'_1/(jX'_{d,1}) \\ \vdots \\ \bar{E}'_m/(jX'_{d,m}) \end{bmatrix} = \mathbf{Y} \begin{bmatrix} \bar{V}_1 \\ \vdots \\ \bar{V}_{n-m} \\ \bar{V}_{n-m+1} \\ \vdots \\ \bar{V}_n \end{bmatrix} \tag{3.2}$$

Equation (3.2) reveals that the complex voltage at a bus is a result of the sum of the contributions of the generators in the system. The contribution of a generator is

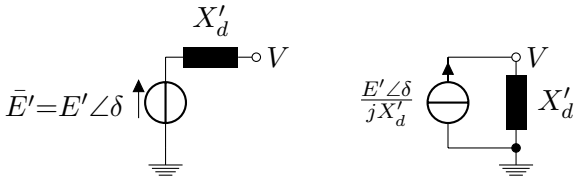

(a) Thevenin Equivalent (b) Norton Equivalent

Figure 3.4: Thévenin and Norton equivalents of generator

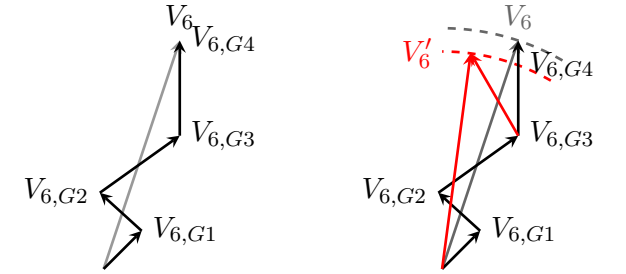

(a) Bus voltage at initial state

(b) Effect of rotor angle increase of generator G4

Figure 3.5: Example of complex voltage at bus 6 as sum of generator contributions

determined by its e.m.f., which is scaled and rotated corresponding to the entry in the inverse of the admittance matrix divided by the respective transient reactance.

Figure 3.5(a) shows the complex voltage at bus 6 (from the simple example system) and the contribution of the individual generators, which amount to the voltage measured at the respective bus. Under the aforementioned assumptions, the effect of an increase in rotor angle, e.g. due to a transient disturbance, on a particular bus voltage can be assessed under consideration of the linear algebraic equation (3.2).

In the example shown in Fig. 3.3, a short-circuit occurs on the transmission line connecting bus 4 and 5. The fault alters the admittance matrix and leads to changes of the electric power injections of the generators in the system. Since the mechanical power is assumed to be constant, the change will result in a power mismatch ΔP in the system's generators and, consequently, cause a relative acceleration or deceleration of the generators' rotors. In the example, it is assumed that the fault mainly affects generator G4 causing an acceleration of the machine and an advancing of the rotor angle relative to the remaining generators.

The effect on the voltage at bus 6 is shown in Fig. 3.5(b) and it can be observed that the relative increase in rotor angle depressed the voltage magnitude at the bus. This observation gave the impulse for the investigation of transient voltage sags using sensitivities derived from the linear algebraic network equations.

3.2 State-of-the-art assessment of transient voltage sags

Similar to the assessment of transient stability, the voltage sags caused by rotor swings can be assessed by using detailed time-domain simulation, simplified/direct methods or combinations of the prior two.

In 1990 the authors of [69] presented a method based on the TEF, which can be used to determine the depth of the voltage sag. The authors suggest computing the maximum rotor angle during the swing through an approximation of the post-fault angle trajectory and utilizing that the total system energy described by TEF is constant after fault clearance. Under the assumption that the generators are represented by their Norton Equivalent, the generators' current injections can be determined at the maximum rotor angle excursion and, subsequently, utilizing (3.1) the voltages in the grid can be computed. Finally, voltage sag prediction results are presented from three different test systems, which look promising. However, it should be mentioned that the computational complexity associated with the TEF approach and in particular the identification of the controlling unstable equilibrium point is high as discusses in Sec. 2.4 and paper A. In [70] the authors used the same TEF based approach to compute the voltage sag and derive sensitivities, which allow relating the depth of the observed voltage sag to certain pre-fault parameters such as terminal voltages and power generation.

A voltage sag/dip assessment method, which uses detailed time-domain simulation and a simple two-dimensional look-up table, where the critical voltage level and critical voltage dip duration are specified, was proposed in [71]. Furthermore, the authors investigate the transient voltage stability of dynamic loads such as induction machines.

A contingency filtering and ranking method with respect to voltage sags was presented in [72]. The method carries out detailed time-domain simulation for the individual contingencies and classifies them according to the depth of the voltage sag in satisfactory, harmless, potentially dangerous and dangerous. The voltage magnitude thresholds for the classification are adopted from NERC stability performance criteria, which can be found in e.g. [73], where a survey of current practices for transient voltage sag criteria related to power system stability was presented.

3.3 Sensitivity based assessment of transient voltage sags

This section solely presents a short summary of the derivation and findings concerning the transient voltage sag assessment using sensitivities. The detailed derivation and results can be found in paper E in the appendix of this thesis.

In the paper two sensitivities were proposed. In the following, the derivation of the sensitivities will be briefly discussed and their application potential will be presented by means of the example shown in Fig 3.1.

3.3.1 Load voltage sensitivity

This sensitivity provides a measure of the impact of a generator on the voltage magnitude at a particular bus. The sensitivity of the voltage magnitude at the l-th bus with respect to the k-th generator is defined as:

$$(\mathbf{s}_{V,Gk})_\ell = \frac{|\bar{V}_\ell^\dagger| - |\bar{V}_\ell|}{\epsilon \cdot \pi/180} \quad \ell = 1, \ldots, m-n \tag{3.3}$$

where ϵ corresponds to a small change of the rotor angle of generator k, which is simulated through a shift of the phase angle of $\bar{E}'_k$, and $\bar{V}_l^\dagger$ is the complex voltage at bus ℓ after altering the rotor angle, which can be computed as follows.

$$\begin{bmatrix} 0 \\ \vdots \\ 0 \\ \bar{E}'_1/(jX'_{d,1}) \\ \vdots \\ \bar{E}'_k\, e^{j\epsilon}/(jX'_{d,k}) \\ \vdots \\ \bar{E}'_m/(jX'_{d,m}) \end{bmatrix} = \mathbf{Y} \begin{bmatrix} \bar{V}_1^\dagger \\ \vdots \\ \bar{V}_{n-m}^\dagger \\ \bar{V}_{n-m+1}^\dagger \\ \vdots \\ \vdots \\ \vdots \\ \bar{V}_n^\dagger \end{bmatrix} \tag{3.4}$$

New England & New York example case: Figure 3.6 shows the load voltage sensitivities in the test case at a selection of load buses and for a subset of generators computed just after fault clearance. The sensitivities allow identifying critical generator-load pairs in the system, such as generators GEN-6 & GEN-7 and the load buses 21, 23 and 24. These findings are confirmed by the time-domain simulation results, which were presented in Fig. 3.6 and showed a large rotor angle excursion of GEN-6 & GEN-7 causing voltage sags at the mentioned buses. The results of a possible application are presented in Fig. 3.7. Here, these sensitivities are used to determine the contribution of the individual generators to the observed voltage sags. In this case, it allows identifying generator GEN-6 and GEN-7 as being the origin of the voltage sags, where the contributions from GEN-6 are generally greater. This information can be very useful e.g. when determining effective locations for preventive controls, which aim at reducing the voltage sags, and is discussed in more detail in paper E.

3.3.2 Generator power sensitivity

The second sensitivity assesses the impact of a change in load consumption on the electric power injection of the generators in the power system. The derivation of this sensitivity was motivated due to the fact that certain loads may disconnect, when the voltage dip is deeper than a certain threshold and its duration longer than a certain time limit.

The derivation of the generator power sensitivity is described in detail in paper E in the appendix, a short summary is presented here. In order to estimate the impact

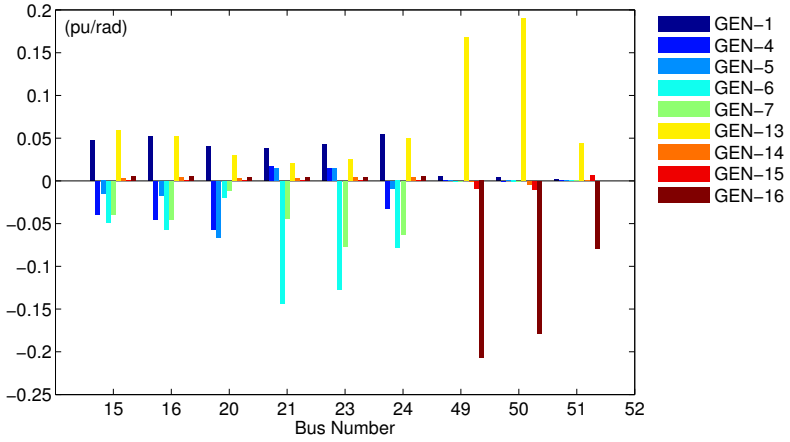

Figure 3.6: Selection of load voltage sensitivities showing the estimated change in voltage magnitude to a 1° increase of rotor angle of a particular generator (colour code) for a selection of load buses (x-axis)

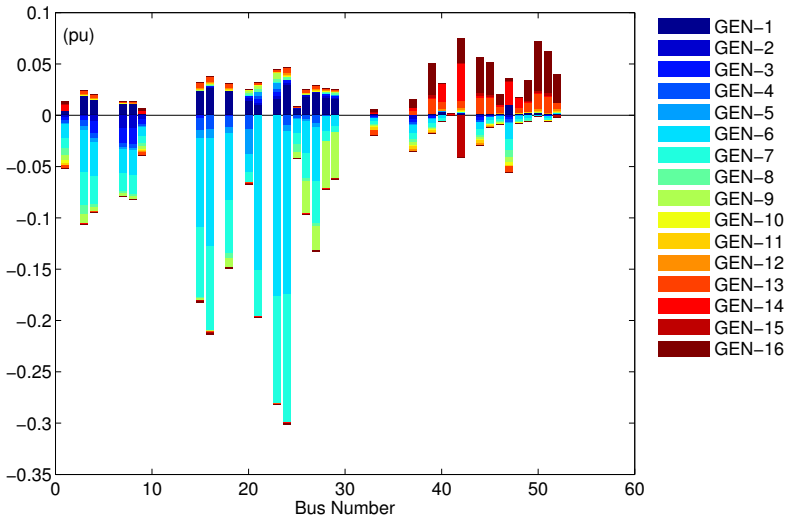

Figure 3.7: Contribution of individual generators to voltage depressions

of a load variation Δy at the k-th bus, first the complex bus voltages after the change $\overline{\mathbf{V}}$ are estimated in the whole power system using the following equation, which was derived from (3.2).

$$\overline{\mathbf{V}} = \overline{\mathbf{V}}^{\circ} - \frac{\overline{V}_k^{\circ}}{[\mathbf{Y}^{-1}]_{kk} + \frac{1}{\Delta y}} \mathbf{Y}^{-1} e_k \tag{3.5}$$

where e_k is the unit vector with the k-th entry equal to one and $\mathbf{Y}^{-1}$ corresponds to the inverse of the admittance matrix. The index k and the superscript $^\circ$ represent values at the k-th bus and values before the load change respectively.

Under the assumption that the generators are represented by their Norton equivalent, then the variation in current injection can be determined for the i-th generator

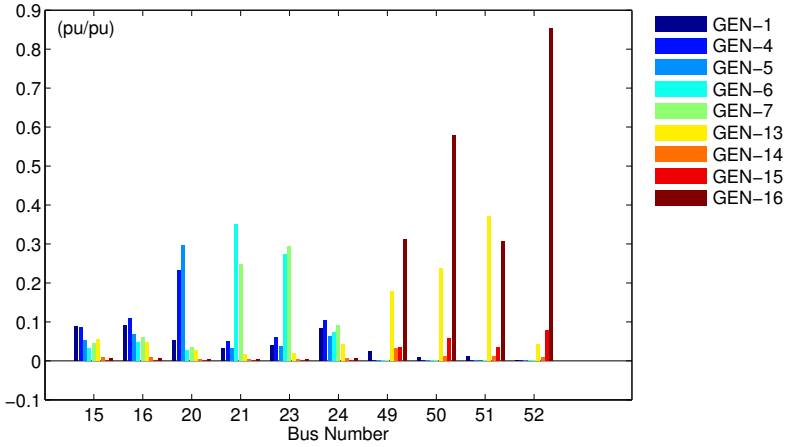

Figure 3.8: Selection of generator load sensitivities displaying the estimated change in active power injection of each generator (y-axis) to a 1 pu increase of load admittance at particular system buses (x-axis). The results correspond to the case shown in Fig. 3.1

connected to the k-th bus as follows.

$$\overline{I}_i = \frac{\overline{E}'_i - \overline{V}_k}{jX'_{d,i}} \tag{3.6}$$

The resulting change in active power injection can then be computed.

$$\Delta P_i = Re\left(\overline{V}_k \overline{I}_i^* - \overline{V}_k^0 \left(\overline{I}_i^0\right)^*\right) \tag{3.7}$$

In this manner the effects of changes in load consumption on each generator can be estimated.

New England & New York example case: Figure 3.8 depicts the generator power sensitivities of a selection of generators and at a subset of load buses in the test case. The sensitivities reveal that a change of load consumption at the buses 21 and 23 will mainly affect the critical generators GEN-6 and GEN-7. Hence, it is expected that an increase in load consumption increases the electric power injection of the generators and vice versa.

Figure 3.9 shows a comparison of three cases: a base case, a second case, where load tripping leads to further deterioration of the system conditions and loss of synchronism of generator GEN-7, and a third case, where load tripping is leading to faster system recovery. Figure 3.9(a) shows the electric power injection of generator GEN-7 and Fig. 3.9(b) displays the voltage magnitude at bus 23 over time in the three cases. In the second case, load is tripped at bus 23, which was identified as a location where changes in load consumption mainly impact the power injection of GEN-6 and GEN-7. Figure 3.9(a) reveals that the load tripping leads to slight reduction of the power injection of the generator, which is enough to cause instability in this marginal case. In the third case load tripping occurs at a bus, which has a dominant effect on generators in the vicinity of GEN-6 & GEN-7 (GEN-4 & GEN-5) and not on the two generators themselves. In this case the load tripping causes a slight acceleration of the generators GEN-4 and GEN-5, which decreases

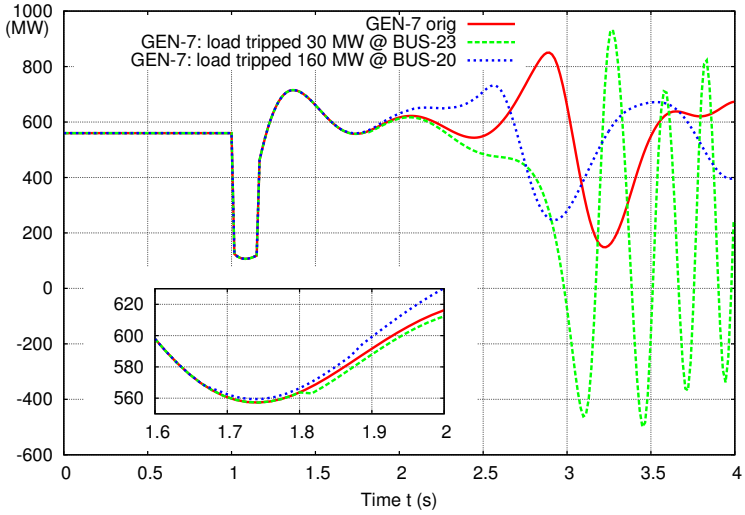

(a) Effect of load shedding on active power of generator GEN-7

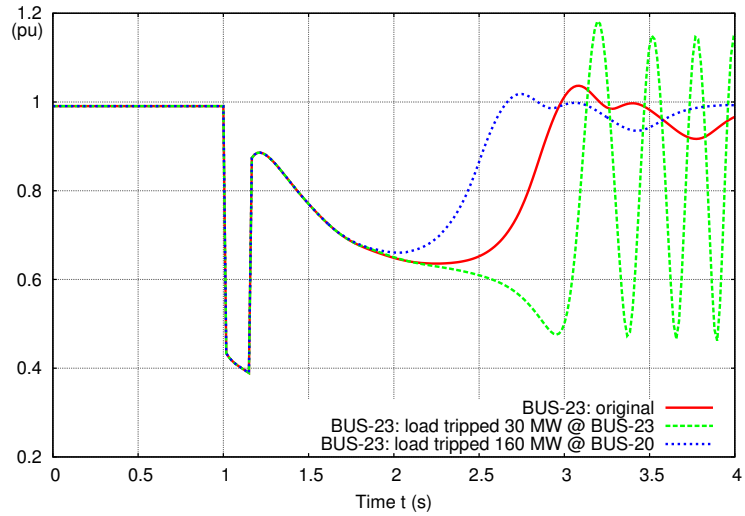

(b) Effect of load shedding on the voltage magnitude at bus 23

Figure 3.9: Example of the application of generator power sensitivities. Comparison of a base case with two cases, where different load tripping events were applied.

the relative rotor angle difference between the two groups of generators and enables a faster resynchronization. Figure 3.9(b) shows that this load tripping has a positive effect and leads to a faster recovery of the voltage at bus 23. These findings show, that the generator power sensitivities can be very useful, when e.g. designing under-voltage load shedding schemes. A more detailed discussion of the results can be found in paper E.

3.4 Early prediction of transient voltage sags

The prior described sensitivities allow assessment of voltage dips after they were observed, but also enable determination of efficient locations for preventive or remedial control. This information is very valuable, if dangerous voltage sags are identified early with appropriate prediction methods. For that purpose, three different voltage sag prediction methods were developed and compared in paper G. The methods were assessed with respect to their ability to early, accurately and consistently predict the crossing of a critical voltage threshold.

3.4.1 Voltage sag prediction methods

The three methods are using different approaches to solve the task of early predicting the voltage sag and are described in more detail in the following.

Utilizing PMU measurements: The first approach assumes that measurements of the bus voltages are available at high sampling rates from phasor measurement units (PMUs). A recursive least square (RLS) estimator is used to predict the evolution of the voltage magnitudes at the respective buses with a quadratic function. The extreme values of the function can then be utilized to determine the depth of the respective voltage sag.

Using the phase angle of the e.m.f: The second approach addresses the problem of voltage sag prediction under consideration of the underlying mechanism, which was described in Sec. 3.1.2. Here the assumption is that the relative angular deviation of certain generators causes the depression of the voltage magnitude. When representing a generator by its classical model, the phase angle of the e.m.f. $\overline{E}'$ corresponds to the angle of the generator's rotor. Hence, in this approach the evolution of the rotor angles of the individual generators are predicted using a RLS estimator and corresponding estimations of the complex bus voltage trajectories are computed by solving the following equation.

$$\begin{bmatrix} 0 \\ \vdots \\ 0 \\ \bar{E}'_1\, e^{j\Delta\delta_1}/(jX'_{d,1}) \\ \vdots \\ \bar{E}'_m\, e^{j\Delta\delta_m}/(jX'_{d,m}) \end{bmatrix} = \mathbf{Y} \begin{bmatrix} \bar{V}_1^{\dagger} \\ \vdots \\ \bar{V}_{n-m}^{\dagger} \\ \bar{V}_{n-m+1}^{\dagger} \\ \vdots \\ \bar{V}_n^{\dagger} \end{bmatrix} \tag{3.8}$$

where $\Delta\delta_i$ is the deviation of the rotor angle of the i-th generator to its initial value.

Using E-SIME: The third method combines the knowledge on the identified mechanism causing the voltage sag with a sophisticated transient stability assessment (TSA) method. The used TSA method is called Emergency SIngle Machine Equivalent (E-SIME) method, which is described in detail in [25] and the recent achievements were published in [74]. E-SIME uses on-line measurements to identify the critical group of generators, meaning the group of generators likely to lose synchronism, and determines a single machine equivalent for the dynamic interaction of the critical generator group and the remaining generators. For this equivalent the

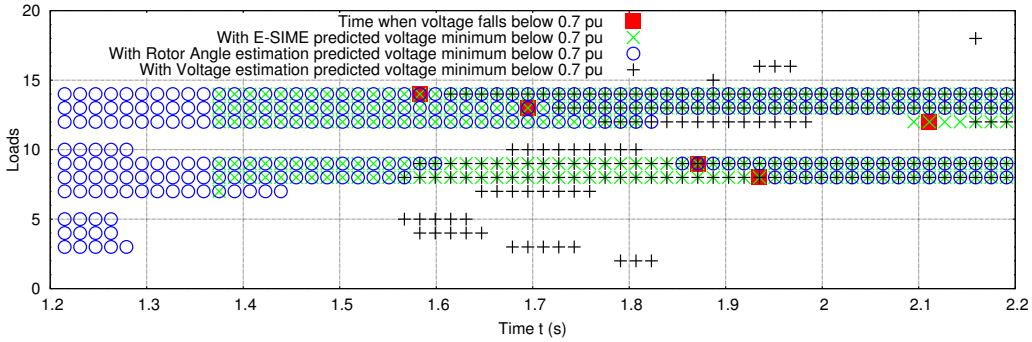

Figure 3.10: Early and consistent detection of load bus voltages falling below the critical value of 0.7 pu: The x-axis shows the simulation time and the y-axis the loads in the system. A marker indicates that at the time instance in the simulation the respective method predicted the voltage to fall below 0.7 pu. The red squares indicate when the voltage actually crossed 0.7 pu. The results correspond to the case shown in Fig. 3.1

equal area criterion can be applied to determine stability. In this approach E-SIME is slightly modified to predict for a stable case the return angle of the critical group of generators. Under the assumption that the voltage sag reaches its minimum at the maximum angular separation of the critical generators and, hence, at the return angle, the bus voltages at that point can be computed by advancing the rotor angles of the critical machines and employing (3.8). In this case $\Delta\delta$ is zero for the non-critical generators and for the critical generators their angular distance to the return angle.

3.4.2 Comparison of the prediction method

The three methods were evaluated with respect to their ability to correctly predict voltage sags. The criteria to measure the performance of the different methods were the following.

- *Earliness:* How early can the method identify critically low voltage sags?
- *Consistency:* How consistent is the prediction? Are only the actual critical buses flagged as critical?
- *Accuracy:* Is the voltage sag minimum predicted with satisfactory accuracy?

The assessment results are documented in detail in the Appendix in paper G and show that each of the approaches predicts the voltage sags to a certain extent.

New England & New York example case: Figure 3.10 shows a comparison of the earliness and consistency of the assessment results. The findings indicate that, in contrast to the other prediction methods, the method based on E-SIME allows an early and consistent prediction of critical load buses. The method does not flag non-critical buses as critical and allows identification of critical buses approximately $200 - 500$ ms before the critical voltage level is underrun. These findings together with the results on the accuracy of the voltage minimum prediction, which can be found in paper G, suggest that the method using E-SIME is promising to early, accurately and consistently predict voltage sags.

Chapter 4

Remedial action using wide-area measurements

The work described in this chapter is building up on [75], where a method was developed to prevent blackouts. As part of the PhD project the method was extended and tested on a different system. Moreover, it was further developed to allow the filing of a patent [76]. In the following, the addressed instability mechanism and the remedial action method are briefly introduced with the help of an example case. The detailed documentation of the method can be found in paper H.

4.1 State-of-the-art of wide-area remedial actions

In order to operate a system reliable, efficient remedial action schemes (RAS) or special protection schemes (SPS) are required as mentioned in [77]. Several utilities tried to implement RAS, which are to a certain extend centralized and automated. Moreover, the authors of [77] describe a real-world implementation of a Centralized Remedial Action Scheme (CRAS) implemented in the grid from Southern California Edison. Contrary, to other systems in the CRAS the measurements of monitoring relays are transferred to a central location, where they are evaluated. In case of required remedial action, control signal are send to mitigation relays from the center. In this manner, the system executes corrective actions such as load or generation reduction to ensure reliable and safe system operation after fault occurrence.

Another real-world implementation of an automatic and system-wide RAS arming system was described in [78]. In the system, a transient stability analysis tool is used periodically to determine the RAS arming patterns. In order to achieve real-time performance of the system, a large case database is used. The database is generated from extensive off-line system studies.

A new methodology for determining the security region of transmission systems with respect to its current operating point was proposed in [79]. The actual calculation of the security region is carried out off-line, but the result can be used to monitor the operating point and condition of the system. Furthermore, the authors

suggest that the off-line calculated stability boundaries, which make up the security region, may be used to identify efficient remedial actions. When the operating point of the system approaches the boundary of the security region, then pre-determined remedial actions can be executed to bring the system back into a secure state.

The remedial action methods, which were described so far, apply actions such as load tripping and generation shedding to secure system operation. Another type of remedial action may be automated adaptation of controller parameters, e.g. based on wide-area measurements and in correspondence to the current system condition. In [80] an adaptive damping control scheme was proposed, which uses wide-area measurements to adapt the controller parameters to fit to the current system conditions. The initial controller parameters are determined off-line and are derived using a large database of common system operation conditions.

In [81] two different approaches for damping of inter-area oscillations are compared. The conclusion of the paper suggests that wide-area control methods are more effective than local controls.

The method described in [82] addresses the same instability mechanism, namely aperiodic small signal rotor angle instability, as the one proposed later in this chapter. The authors developed a method, which applies changes to the consumption pattern with the goal to restore stability and security of the system with respect to the stability boundary. In order to achieve this goal, the method proposes changes to a number of loads, which were identified to be the most effective locations for applying countermeasures.

4.2 From voltage instability to a collapse in voltage

In some of the cases where aperiodic small signal rotor angle instability causes a collapse in voltage, the power system had earlier entered a state of voltage unstable operation. The topic was discussed in [83], where a method for early warning against aperiodic small signal rotor angle stability was developed. In the following a short summary of the discussion will be presented. The explanations are supported by a state diagram shown in Fig. 4.1.

When after a fault a power system enters the state of voltage instability, the point of maximum deliverable power has been reached at certain system nodes. This state is shown in the upper right corner of Fig 4.1. If the condition subsequently evolves into a blackout depends on a variety of system characteristics such as long term voltage dependency of system loads and voltage control equipment.

In the following a degradation mechanism is described, which may eventually lead from voltage unstable operation to a collapse in voltage. A ULTC-Transformer connected to a voltage unstable bus will attempt to boost the depressed voltage by adjusting the transformer ratio. However, in such a condition each tap action will further deteriorate the system condition by decreasing the system voltage and increasing the line currents. The lower system voltages suppress the voltage at neighboring buses, which may lead to spreading of the voltage instability to other buses.

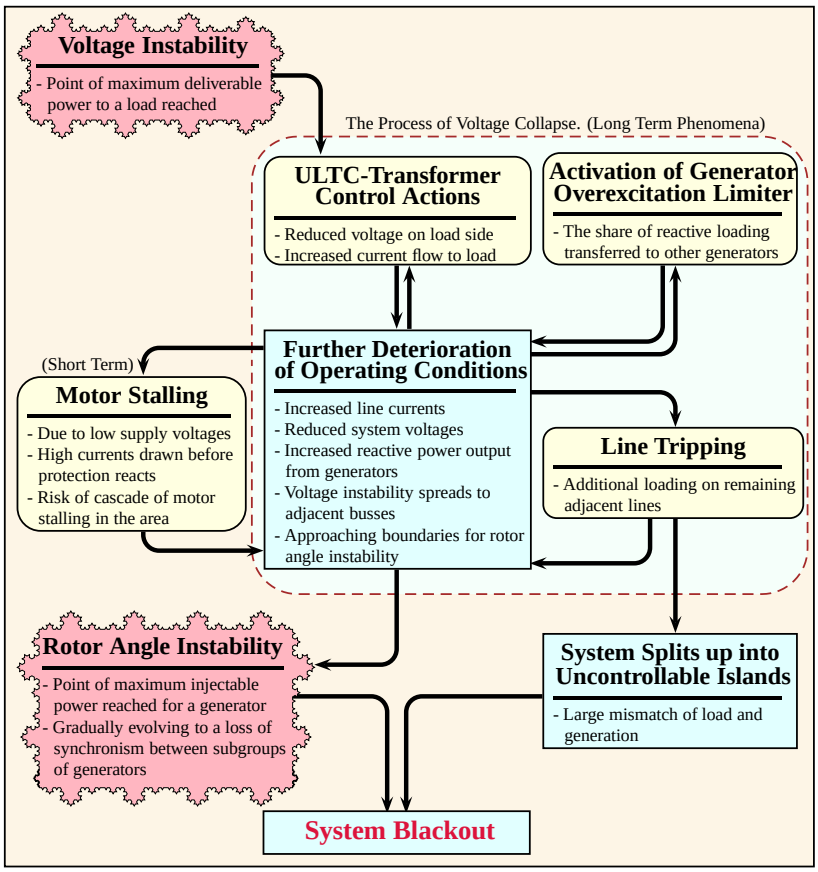

Figure 4.1: From voltage instability to a collapse in voltage (adopted from [83])

Furthermore, the depressed system voltage and the increased line currents lead to higher reactive power demand, which needs to be provided by the generators in the system. This may result in the activation of overexcitation current limiters (OEL) at individual generators. Then the generator is no longer capable of keeping the voltage magnitude at the respective remote bus constant and its share of reactive power generation needs to be transfered to other generators. This may lead to overloading of other generators and cascading activation of OELs (see Fig. 4.1).

Due to the increasing line currents, transmission lines may experience overloading, which may lead to further line tripping, system deterioration and eventually split the system into uncontrollable islands. Another possibility is that individual generators reach the point of maximum injectable power into the system and lose synchronism with the remaining generators in the system, which eventually may lead to a blackout.

As described in [83], voltage instability describes the operating condition where the point of maximum deliverable power is reached at certain nodes. While aperiodic small signal rotor angle stability is associated with the capability of a generator to inject power into a system node or rather the condition that a generator has reached the maximum injectable power.

4.3 Aperiodic small signal rotor angle stability

The proposed remedial action method determines countermeasures with respect to the boundary of a particular instability mechanism, which is called aperiodic small signal rotor angle stability (ASSRAS) and, according to [9], refers to...

> "...the capability of each generator to generate sufficient synchronizing torque so that operation at stable equilibrium point can be maintained. The lack of sufficient steady-state synchronizing torque causes aperiodic increase in rotor angle and a loss of synchronism."

By focusing on a particular mechanism, the power system can be represented by a simplified model, which allowed the development of the real-time stability assessment method described in [9].

Nordic32 example case: The Nordic32 system as described in [84] is in the following employed to support the description of the instability mechanism, the assessment method and the remedial action method. A one-line diagram as well as a description of the modification applied to the system can be found in Appendix I.2. In order to trigger aperiodic small signal rotor angle instability in the case of the Nordic32 system, the transmission line connecting bus 4021 and 4042 was tripped at $t = 5$ s. The system response can be seen in Fig. 4.2.

Figure 4.2(a) shows the voltage magnitudes at a selection of system buses over time. The loss of the transmission line at $t = 5$ s causes oscillation in the system, which damp out, but lead to the activation of several over excitation limiters (OELs) between $t = 18.3$ s and $t = 47.1$ s (for details see paper H). After the last activation of an OEL, the voltages appear to stabilize again before a collapse in voltage occurs.

Figure 4.2(b) depicts the change in rotor speed relative to nominal speed of a selection of generators. It can be observed that the speed of the generators varies due to the loss of the transmission line and the activation of the OELs. Moreover, the magnified detail in the graph reveals that generator $G7$ experiences a speed up and, subsequently, a loss of synchronism, at the same time as the collapse in voltage occurs.

The observed collapse in voltage and the simultaneous loss of synchronism of a generator confirm that the observed instability is aperiodic small signal rotor angle instability.

4.4 Aperiodic small signal rotor angle stability assessment method

The method carries out an element-wise assessment (see Fig. 4.3), which allows to monitor the ASSRAS of each individual generator in the power system in real-time. In the figure the stability boundary is represented by a red curve, which divides the graph into an area of stable and unstable operation. The current operating points (OPs) of the individual generator are depicted by the "$\times$" and their respective distance to the boundary corresponds to their stability margin.

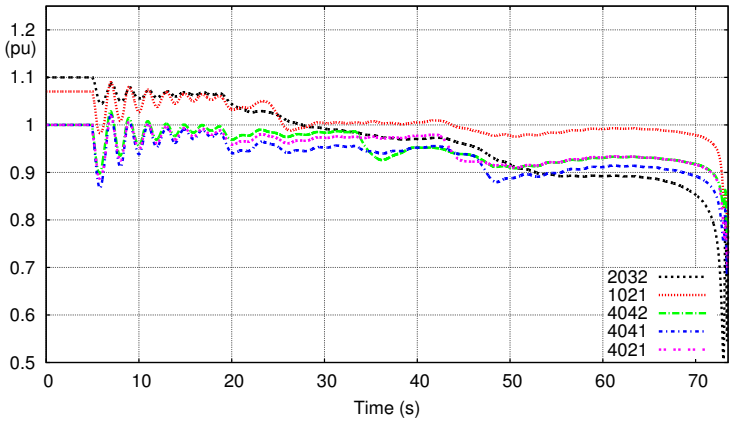

(a) Voltages at a selection of buses

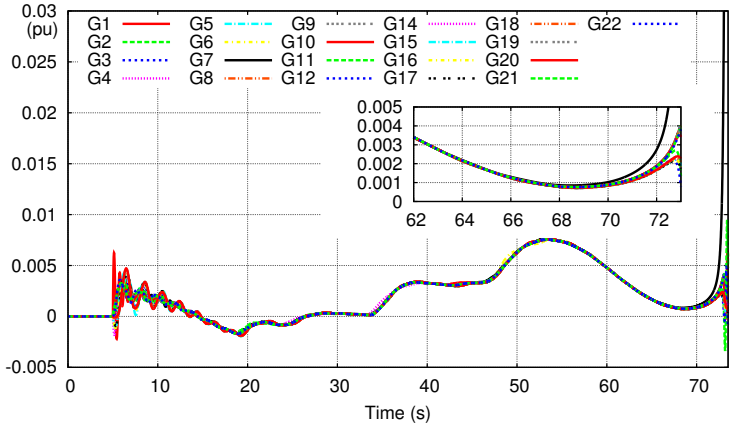

(b) Generator speed deviations from nominal speed of all generators

Figure 4.2: Nordic32: System response to the tripping of the line connecting bus 4021 and 4042 resulting in a collapse of voltage

In order to display the stability of each generator in such way, the authors of [9] simplified the considered power system model by introducing the following assumptions:

1. Power injection occurs at nodes with constant voltage magnitude.
   - Hence, the generators are represented by voltage sources with constant magnitude. Dependent on the excitation system of the generator this source is either directly connected to the terminal or to an internal node behind the saturated direct axis reactance.
2. Power consumption in the system can be represented by impedance loads.
   - The method relies on the availability of real-time measurements, which allow determining the load impedance in the current system state.

These assumptions are sufficient in the case that system snapshots of the current system condition are received at a high sampling rate, e.g. from PMUs which provide full system observability. The snapshots are used to determine the complex voltages at the nodes of power injection, the impedances corresponding to the

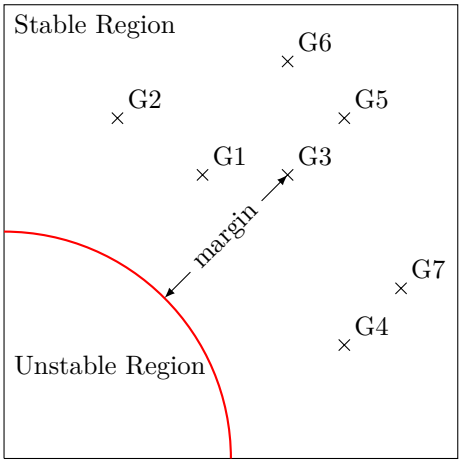

Figure 4.3: Element-wise assessment of stability, monitoring the aperiodic small signal rotor angle stability of each individual system generator.

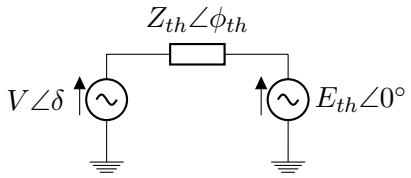

Figure 4.4: Two bus equivalent: Node of constant voltage magnitude and Thévenin equivalent

current load consumption and to update the admittance matrix to the current system condition.

Under these assumptions seen from each node of constant voltage magnitude the rest of the system can be represented by a Thévenin equivalent as shown in Fig. 4.4.

In [85] the authors mapped critical and characteristic curves of the PQV-surface of a two-bus system into the injection impedance plane, which corresponds to the load impedance plane, but the resistance can be both positive and negative.
Critical curves:

- $\frac{\partial P}{\partial V} = \frac{\partial Q}{\partial V} = 0$. Maximum injectable active power when E_{th} and ϕ_{th} are fixed
- $\frac{\partial Q}{\partial P} = \frac{\partial V}{\partial P} = 0$. Maximum or minimum injectable reactive power when V and E_{th} are constant
- $\frac{\partial P}{\partial Q} = \frac{\partial V}{\partial Q} = 0$. Maximum injectable active power when V and E_{th} are fixed

Characteristic curves:

- Constant active power injection P
- Constant reactive power injection Q
- Constant voltage magnitude V
- Constant voltage angle δ

It was shown and analytically derived that these critical and characteristic curves appear as circles in the injection impedance plane.

The critical curve, which corresponds to the maximum injectable active power, when the voltage magnitudes at both ends are fixed, is identical to the circle, which is the characteristic curve of constant voltage angle, when $\delta = 180° - \phi_{th}$. This is due to the fact that the active power injection of a two bus system, such as in Fig. 4.4, becomes solely a function of the voltage phase angle δ, when the voltage magnitudes at both ends and the impedance $\bar{Z}_{th}$ are assumed to be fixed. Then the power injection may be computed as follows.

$$P_{inj} = \frac{E_{th}V}{Z_{th}} \cos(\delta + \phi_{th}) - \frac{V^2}{Z_{th}} \cos(\phi_{th}) \tag{4.1}$$

Consequently, the maximum power injection $\hat{P}_{inj}$ at $\delta = 180° - \phi_{th}$ is equal to:

$$\hat{P}_{inj} = -\frac{E_{th}V}{Z_{th}} - \frac{V^2}{Z_{th}} \cos(\phi_{th}) \tag{4.2}$$

This critical curve represents the ASSRAS boundary and in the injection impedance plane the boundary for a particular generator can be expressed in polar coordinates as:

$$Z_{inj,i} = -\frac{Z_{th,i} \sin\theta}{\sin\phi_{th,i}} \tag{4.3}$$

When representing the operating point of a generator by its injection impedance $\bar{Z}_{inj}$, it was shown in [9] that an operation outside the corresponding circle represents a stable operation, while an operation inside is unstable and leads to a loss of synchronism of the respective machine. This allows determining a stability criterion for each machine, which is described by the following set of inequalities.

$$\left| \frac{\bar{Z}_{inj,i}(2\sin\phi_{th,i}) + jZ_{th,i}}{Z_{th,i}} \right| \begin{cases} > 1 \text{ Stable} \\ = 1 \text{ On the boundary} \\ < 1 \text{ Unstable} \end{cases} \tag{4.4}$$

Moreover, in [9] the authors derived an equation to determine the stability margin of each generator to its stability boundary in terms of active power, which is very useful when developing a remedial action method.

When the remaining system is represented by a Thévenin equivalent, the active power injection of a generator can be computed utilizing (4.1) and the maximum power using (4.2). Knowing the maximum and the current power injection allows computing the current active power margin as follows.

$$\Delta P_{inj} = \hat{P}_{inj} - P_{inj} = \frac{E_{th}V}{Z_{th}} \left(\cos(\delta + \phi_{th}) + 1\right) \tag{4.5}$$

This margin can also be expressed in percentage of the maximum power injection as follows:

$$\%\Delta P_{inj} = \frac{\cos(\delta + \phi_{th}) + 1}{1 + \frac{V}{E_{th}} \cos\phi_{th}} \cdot 100\% \tag{4.6}$$

The developed stability criterion (4.4) together with the derivation of a useful stability margin allowed the authors to develop an assessment algorithm, which is shown in Fig. 4.5.

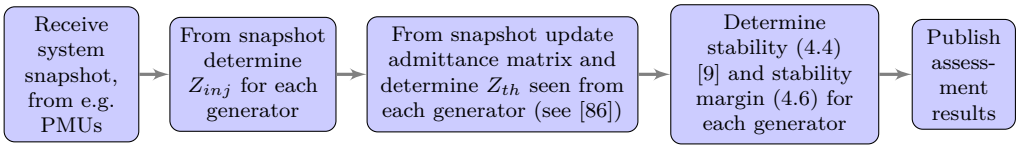

Figure 4.5: Function blocks of the ASSRAS assessment method [9]

The algorithm receives a snapshot of the system, which contains the complex bus voltages and complex transmission line currents, and may be obtained from synchronized PMU measurements or a fast state estimator. This snapshot is then used to evaluate ASSRAS and to determine the stability margin of each generator in the system. These assessment results together with some of the mapped characteristic curves, e.g. curves of constant voltage magnitude and curves of constant phase angle, enabled the development of the remedial action method (RAM) described in the next section.

N − 1 operating points: Due to the assumption that active power is injected at nodes of constant voltage magnitude, the generator is either represented by a voltage source with constant magnitude directly connected to the terminal of the machine or connected to an internal node of the generator, which is situated behind the synchronous reactance. This is depending on the excitation system of the generator and its state. For generators equipped with an AVR and OEL, this allows to monitor the actual operating (OP) as well as the $N-1$ OP, which corresponds to the condition of an activated OEL and, consequently, the generator lost its capability to keep the voltage magnitude at the terminal constant.

Table 4.1: Location of the node of constant voltage magnitude in different generator configuration and operation conditions during computation of stability criteria and margin

Excitation system	OEL	Actual OP	$N-1$ OP
Manually	–	at internal node	–
AVR with OEL	inactive	at terminal	at internal node
	active	at internal node	–

Table 4.1 shows for the different configurations and conditions, where the voltage magnitude is assumed to be constant, when computing stability criteria and margin of the generators.

Nordic32 example case: In the following the assessment results when applying the prior described method to the test case, which was introduced in Sec. 4.3, will be discussed. The results will be shown in the normalized injection impedance plane. The normalization as described in [9] corresponds to mapping of the operating point of each generator and allows displaying them with respect to one normalized ASSRAS boundary, while maintaining the characteristic that the distance of an OP to the boundary reflects its stability margin.

Figure 4.6(b) shows the operating points of the generators in the system at a selection of time instances (numbered from $I-IV$) in the normalized injection impedance plane. Figure 4.6(a) shows again the voltages over time for a selection

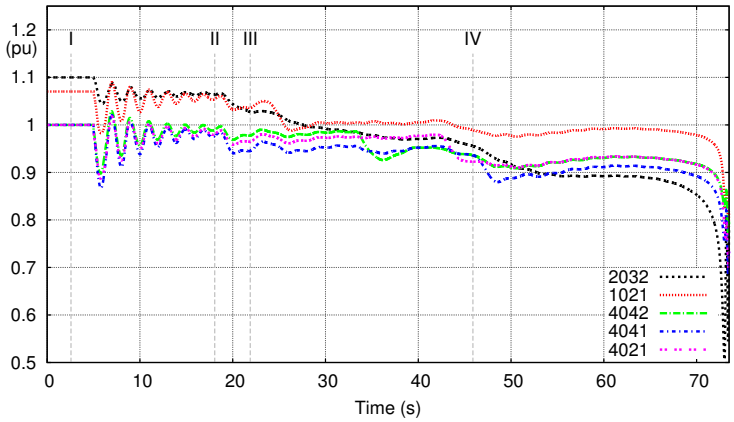

(a) Voltages at a selection of buses with time instances $I - IV$ marked

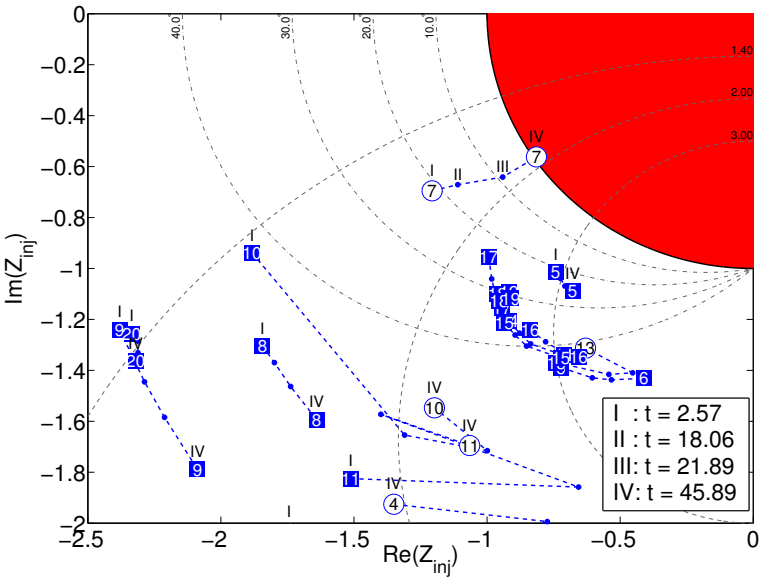

(b) Assessment results displayed in the normalized injection impedance plane

Figure 4.6: Nordic32: Stability assessment results of the test case

of buses and the time instances $I - IV$ are indicated by vertical dashed grey lines. The red area, in Fig. 4.6(b), corresponds to the unstable region and its boundary is the section of the circle, which corresponds to the normalized ASSRAS boundary. The $N - 1$ OPs are displayed by blue filled squares and the actual OPs by blue circles. The numbers inside the OPs correspond to the respective generator, e.g. 1 corresponds to $G1$.

The graph shows that, due to the disturbance and the subsequent activations of the OELs, the OPs of the generators are moving in the injection impedance plane. It can also be observed that for those generators, which experience an activation of the OEL, the $N - 1$ OPs turn into actual OPs, e.g. $G10$ and $G11$.

Finally, it should be noticed that the OP of generator $G7$ gets closer and closer to the stability boundary until it crosses it at $t = 45.89$ s. Hence, the assessment method could detect the imminent instability approximately 28 s before the collapse in voltage occurred (see Fig. 4.6(a)). It should be mentioned that Fig. 4.2(b) showed that it was also $G7$, which was identified from the time-domain simulation results as the generator that first lost synchronism.

4.5 Remedial action method

Figure 4.7 shows the block diagram of the proposed remedial action method (RAM). The method proposes an active power re-dispatch solution, which aims at moving the critical generator away from the stability boundary by reducing its active power injection. The reduction is counterbalanced by an increase of power generation of the remaining (supporting) generator.

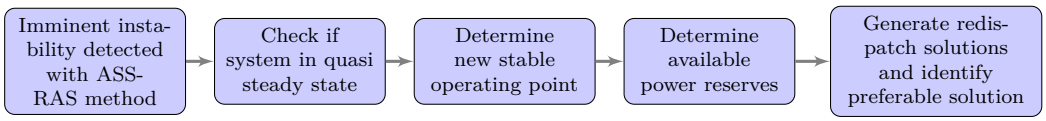

Figure 4.7: Function blocks of the proposed remedial action method

4.5.1 Imminent instability detection

The ASSRAS assessment method is used to monitor the stability of the system and to determine the stability margin of each generator. Since it is preferable that RAM is executed before the stability boundary is crossed, a trigger margin and a security margin as percentage of the maximum power injection are introduced. If the stability margin of an operating point of a generator crosses the trigger margin RAM is executed. In order to avoid a crossing of the trigger margin by supporting generators and to provide a target margin for the critical generator a second margin called security margin was introduced.

It is suggested that the trigger/security margins for actual OPs and $N-1$ OPs differ, since a crossing of the stability boundary of an $N-1$ OP solely represents an insecure system state, while the crossing of an actual OP corresponds to an unstable system state.

In paper H the trigger and security margins were chosen as shown in Tab. 4.2.

Table 4.2: Trigger and security margins for the different operating point types

Type of OP	Trigger margin	Security margin
Actual OP	1 %	2 %
$N-1$ OP	0.1 %	0.5 %

Under the assumption that the ratio between the voltage magnitude at the node of power injection and the voltage magnitude of the Thévenin equivalent is constant ($V/E_{th} = const.$), then the trigger and security margin correspond to certain curves of constant δ in the injection impedance plane.

4.5.2 Quasi steady state

Aperiodic small signal rotor angle instability occurs in a quasi steady state, since it occurs when a generator can no longer produce sufficient steady state electromechanical torque. During system dynamics OPs of generators may enter the region

of unstable operation. Therefore, it is necessary to determine a criterion to assess, if a new quasi steady state was reached.

Due to the assumption of constant voltage magnitude at nodes of power injection when computing the stability boundary and margin, it is reasonable to determine quasi steadiness of the system based on the error introduced by variations of the voltage magnitude. If the voltage magnitude fluctuates, then the computed maximum power injection will vary. Therefore, the system is considered to be in a quasi steady state, when the variation of the maximum power injection is within acceptable limits, which was chosen to be 0.5 %.

4.5.3 Determine new stable operating point & available power reserves

When the system is in quasi steady state and the critical generator has been identified, then the new stable operating of the critical generator has to be determined and the available power reserves of the remaining generators have to be computed.

In order to utilize the characteristic curves, which were described in [85] and mentioned in Sec. 4.4, it is assumed that throughout the remedial action the voltage magnitudes at the nodes of power injection remain constant. Table 4.3 shows for the different operating point types and depending on the generator's excitation system in which node the voltage is assumed to be constant during the remedial action.

Table 4.3: Location of node of constant voltage magnitude during remedial action in different generator configuration and operation conditions

Excitation system	OEL	Actual OP	$N-1$ OP
Manually	–	behind X_d	–
AVR with OEL	inactive	at terminal	at terminal
	active	behind X_d	-

Due to the assumption of constant voltage magnitude, the power injection of the generator is again solely a function of the voltage angle. Therefore, in the injection impedance plane the OP of each generator where their margin is equal to the trigger or security margin corresponds to the intersection of the curve of constant V and the respective curve of constant δ. This observation is the basis for the computation of the new stable operating point and the available power reserves.

As priorly mentioned, if the assumption of constant V is extended to the assumption of constant ratio V/E_{th}, then the trigger and security margin correspond to curves of constant δ.

In the following, the determination of a new stable and secure operating point is exemplified on the instability scenario in the Nordic32 system from the previous sections.

Nordic32 example case: In Sec. 4.4 generator $G7$ was identified as the critical generator that first crosses the stability boundary. However, the remedial action method is already executed when the stability margin of the respective machine fell

below the trigger margin (see Tab. 4.2) and the system is in quasi steady state (as described in Sec. 4.5.2). In the test case the actual OP of generator $G7$ crosses the first time the trigger margin boundary in quasi steady state at $t = 21.89$ s, which corresponds to time instance III in Fig. 4.6.

Below the computation of a new stable and secure OP for an actual operating point will be described. The computation of a new stable OP for a crossing of the stability boundary by an $N-1$ OP as well as the determination of the available power reserves follow a similar approach and the reader is encouraged to find the detailed derivations in paper H.

Figure 4.8 graphically explains, how the new stable and secure OP is determined for an actual OP that caused the insecure situation. The OP of generator $G7$ is here displayed by its injection impedance Z_{inj} and has just crossed the trigger margin represented by the red dotted circle.

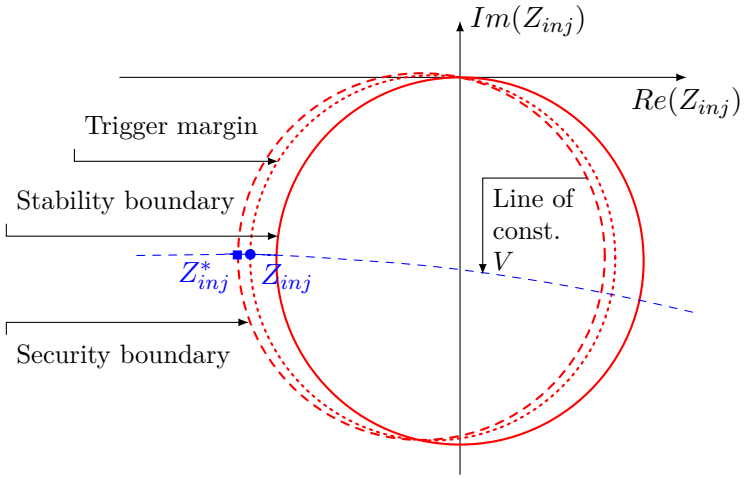

Figure 4.8: Graphical representation of the computation of a new secure operating point for the case of imminent instability due to an actual operating point

The desired margin after the remedial action is defined by the security margin m_{sec} (see Tab. 4.2) and is known as a percentage of the maximum power injection. Under the assumption that the voltage magnitude ratio V/E_{th} remains constant throughout the remedial action, (4.6) can be used to compute the voltage angle δ^* at the new stable and secure OP.

$$\delta^* = \arccos\left[\frac{m_{sec}}{100\%}\left(1+\frac{V}{E_{th}}\cos(\phi_{th})\right)-1\right]-\phi_{th} \tag{4.7}$$

Then the power injection at δ^* can be computed employing (4.1). The power reduction needed to bring the generator back into a stable and secure state can then be determined as the difference in power injection.

$$\Delta P_{inj} = P_{inj}(\delta) - P_{inj}(\delta^*) \tag{4.8}$$

In this case the remedial action method determines that a reduction of the power generation of $G7$ by 8.25 MW is sufficient to bring it back to a secure operating point. In a similar way, the power reserves of the remaining generators with respect to their security boundary can be computed.

4.5.4 Identify re-dispatch solution

After the required power reduction for the critical generator and the power reserves of the remaining generators are determined, then re-dispatch solutions can be developed. Depending on the available power reserves and the amount of required power reduction, the adjustment of the OP of the critical generator can be counterbalanced by one or several of the remaining generators.

Nordic32 example case: In the discussed case, the required power reduction is relatively small and the power reserves of the remaining generators are sufficiently large. It was chosen that generator $G11$ is used to counterbalance, due to the short electrical distance between the two generators. The sequence of OEL activations at certain generators in the system caused three times a crossing of the trigger margin by generator $G7$, each time the remedial action method was triggered and an active power re-dispatch was conducted. Table 4.4 shows the three re-dispatch solutions, which includes time of trigger margin violation, the critical generator, stability margin before the re-dispatch, required power reduction, supporting generator and stability margin of the critical generator after the remedial action.

Table 4.4: Nordic32: Active power re-dispatch

Time s	Critical Gen.	Margin $\%\Delta P_{inj}$	Necessary ΔP	Supp. Gen.	Margin after red.
21.89	G7	0.98%	8.25 MW	G11	1.53%
27.05	G7	0.81%	9.44 MW	G11	1.05%
49.46	G7	0.83%	9.09 MW	G11	2.14%

The table shows that the method only with the last remedial action achieves to bring the generator's OP back to the secure region. The deviations after the first two remedial actions may be explained by the dynamics induced by the activation of the OELs. Figure 4.9 shows with solid lines the bus voltages when remedial actions are applied and dashed when no countermeasures are taken. The graph confirms

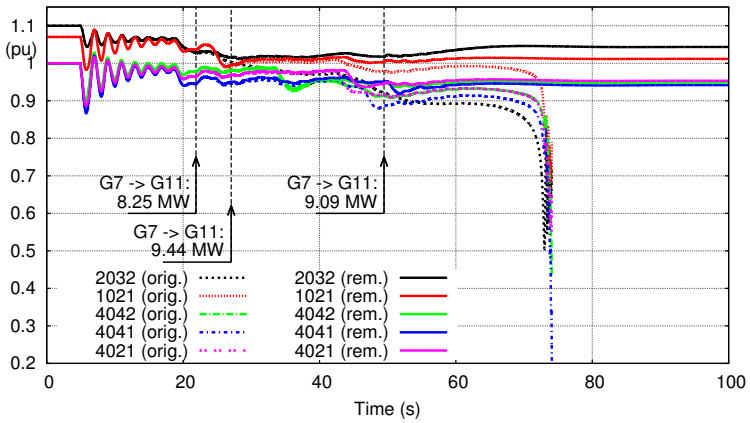

Figure 4.9: Nordic32: Scenario with applied remedial actions voltages at a selection of buses

that the proposed method succeeds in stabilizing the system and in avoiding the imminent blackout.

Chapter 5

Conclusion

The PhD project concerned the development of tools and methods suitable for a future on-line dynamic security assessment system. For that purpose, the assumptions were the availability of a database, which contains detailed models of the system components, and system snapshots, which provide full observability at a high sampling rate, e.g. provided from a fast state estimator or PMUs. Furthermore, it was assumed that due to the paradigm shift in power system operation and the reduced predictability of generation and load patterns, approaches based on large case and simulation databases, which are periodically generated off-line, are unfavorable. The ambition of the PhD project was to develop on-line stability and security assessment methods, which are independent of such case databases. Therefore, approaches, which solely utilize on-line measurements and parameters, were chosen or developed. The results of the PhD project are methods and tools, which origin from in-depth studies of the underlying instability mechanisms.

The PhD project resulted in the development of the following methods:

- *Fast Contingency Screening and On-line TSA*: An efficient and reliable contingency screening method is a central part of an on-line DSA. The screening method developed in this thesis aims at quickly assessing and classifying the credible contingencies in the system. The focus was on first-swing transient stability.
- *Critical machine cluster identification:* In order to further improve the performance of the contingency screening and on-line TSA method, a new approach for early and accurately identifying the critical machine cluster was developed. For that purpose, a coupling coefficient was developed, which is a measure of the coupling strength between two generators.
- *Transient Voltage sag assessment and prediction*: A case can only be determined as being transient stable when all generators remain in synchronism and the bus voltages remain within acceptable limits. This is due to the fact that voltages below a certain threshold may cause subsequent events in the system, which may further deteriorate the system condition and may cause instability. In order to address this issue, sensitivities were derived to assess voltage sags and a method for early prediction of voltage sags was developed.

- *Remedial Actions:* When assessment methods are available, which are capable of monitoring stability in real-time, and an insecure state has been detected, then the next logical step is to determine and apply remedial actions to restore security. The developed method aims at restoring stability through an active power generation re-dispatch with respect to aperiodic small signal rotor angle instability.

5.1 Fast contingency screening and on-line transient stability assessment

The aim was to develop a contingency screening method, which assesses the security of the system in terms of its capability of surviving the transient response to any credible contingency. Moreover, the ambition was to develop a method, which could perform this task in a time frame suitable for on-line application.

In order to develop such a method, first the available transient stability assessment methods were reviewed and their adaptability to real-time operation was assessed. For that purpose, the computational complexities of the respective assessment algorithms were analyzed. The results showed that a hybrid method called SIME, which combines the advantages of detailed time-domain simulation and a direct method, was promising.

In the next step, it was investigated, if the used power system model can be simplified to speed up the stability assessment, while preserving the instability mechanism correctly and allowing accurate as well as early stability assessment with the SIME method. The results showed that, in order to display the true instability mechanism, it is of crucial importance to represent the components in the power system with sufficiently detailed models and in case of the synchronous generator with models of 4^{th}-order or higher.

The prior findings were utilized to develop a fast contingency screening and on-line transient stability assessment method. Moreover, the method employs a new approach to fast identify created islands in the power system utilizing the efficient algorithms from graph theory. The presented results showed that the proposed screening method determines stability with high reliability, where the success rate for identification of unstable cases was higher than for stable cases. Furthermore, the performance assessment showed that most of the computation time is spend on the detailed time-domain simulations and that the computation related to the actual stability assessment calculations is negligible. Finally, it was shown that the proposed contingency categorization criterion is promising and may provide better system awareness. However, a reliable and early identification of the critical group of generator, which are those likely to lose synchronism, may lead to improved classification results, a higher success rate for identification of stable cases and lower the required simulation time in certain cases. Hence, in order to improve the contingency screening and assessment results, a new approach for identifying the critical machine cluster was proposed. For that purpose, a cluster coefficient was derived, which utilizes the equal area criterion. These cluster coefficients were then used to identify the critical machine cluster after fault clearance. The proposed approach was tested on two scenarios, where the method succeeded in identifying

the critical group of machines.

5.2 Assessment and prediction of transient voltage sags

The ambition was to develop methods and indices to assess transient voltage sags, which are caused by large rotor angle swings of generators in the system. For that purpose, first the mechanism behind them was investigated thoroughly and related to known theory. This enabled the derivation of two sensitivities, which provide valuable information on the voltage sags.

The first sensitivity identifies which bus voltages are affected by changes in rotor angle of a certain generator. It was shown that this sensitivity can be used to determine the contribution of a generator to observed voltage sags and it allows identifying favorable locations for preventive control. The second sensitivity reveals which generators are impacted by a change in load consumption. It was shown that this sensitivity can be used to assess if load tripping has a detrimental or beneficial impact on the voltage sag as well as the power system's dynamic performance.

In conclusion, the derived sensitivities can provide valuable information on location and type of preventive or remedial control. However, in order to apply counter measures an early detection of critical voltage sags is crucial. For that purpose, three different voltage sag prediction methods were derived and their performances were assessed with respect to earliness, consistency and accuracy of the prediction. The results showed that a modified version of the transient stability assessment method SIME performed best.

5.3 Remedial control against aperiodic small signal rotor angle instability

A further developed version of the remedial action method described in [75] was presented and its performance was demonstrated on basis of an example case. In order to develop the remedial control action method, the instability mechanism causing aperiodic small signal rotor angle instability as well as the real-time stability assessment method were studied in detail. Characteristic curves of the PQV-surface of a two-bus system mapped into the injection impedance plane turned out to be very useful, when determining remedial control actions in terms of generation re-dispatch. These curves allow to analytically determine generation re-dispatch solutions, which restore stability and security in the system with respect to aperiodic small signal rotor angle stability. The results showed that the method succeeds in stabilizing the system, even if a series of disturbances such as the activations of over excitation limiter cause repetitive crossing of the security boundary.

5.4 Future work

In the following an outlook on future work and research challenges is presented.

5.4.1 Contingency screening and on-line transient stability assessment

- **Further speed up of the contingency screening method:** A possible way to further speed up the assessment could be parallelization, for example by only initializing the simulation once and parallel computation of several contingencies at the same time. Moreover, a seamless implementation of SIME into a time-domain simulation tool could enable further performance improvements.
- **Investigation of transient stability of other generator types:** The number of generators, which are not synchronously connected, is growing, e.g. due to the increasing installation of wind turbine generators. Consequently, investigation of the transient stability of these types of generators could be useful and, following, an adaptation of the developed transient stability assessment methods may be needed.
- **Reliability of the proposed screening method:** In order to further assess the reliability, tests on other and larger power systems may be performed.
- **Extension of the contingency screening method:** In order to ensure security of the system, it is not sufficient to solely assess the systems stability with respect to rotor angle stability. Hence, the screening method should be extended to include security assessment with respect to other instability mechanisms, e.g. transient voltage sags.
- **Critical machine cluster identification:** The proposed method performed well in the presented test cases. However, the approach should be further investigated and the results should be compared to other approaches.
- **Application possibilities in other approaches:** A major challenge in transient stability assessment with methods based on the Lyapunov approach is to fast determine the controlling unstable equilibrium point. An early identification of the critical machine cluster with the proposed algorithm could speed up the process of finding the CUEP and improve the existing methods.
- **Implementation into test environment:** In order to validate the proposed methods, an implementation into the real-time simulation environment in PowerLabDK could be realized.

5.4.2 Voltage sags caused by rotor swings

In order to develop an efficient defense mechanism against critical voltage sags, e.g. a closed-loop emergency control, a plurality of methods and indicators need to be developed.

- *Firstly*, a method to early predict voltage sags and to determine their severity.
- *Secondly*, indicators to identify preferable locations for applying remedial controls and efficient means for controls.

- *Lastly*, methods to determine the required size and, possibly, duration of the control.

In this work the first two points were addressed and methods/criteria were proposed.

Below a list of future work is presented:

- **Severity of voltage sags:** A measures for assessing the severity of observed voltage sags could be another important indicator for a closed-loop emergency control.
- **Implementation into test environment:** In order to test the proposed sensitivities and the prediction method in a real-time environment, the methods could be implemented in the real-time simulation environment in PowerLabDK.
- **Benefits for other approaches:** It will be investigated, how other approaches could benefit from the proposed sensitivities. Application possibilities are anticipated in the area of machine learning in particular decision trees, where the computed sensitivities could be attributes in a decision tree, which is used to assess system security. Moreover, the sensitivities could support the selection of appropriate test scenarios when building up learning sets.

5.4.3 Remedial action method using wide-area measurements

- **Implementation into real-time test environment:** In order to validate the proposed method, an implementation into the real-time simulation environment in PowerLabDK could be realized.
- **Consideration of other stability and security boundaries:** The proposed method determines remedial action with the aim to improve the system condition with respect to aperiodic small signal rotor angle stability. An extension of the method to determine remedial action under consideration of other instability mechanisms could be one of the next development steps.
- **Transient stability:** It will be further investigated, how the assessment results from the developed contingency screening approach can be used to determine remedial control actions to bring the system back in a secure state.
- **Transient voltage sags:** To realize a closed-loop emergency control against transient voltage sags it will be necessary to develop means to determine the required size of remedial control.

Bibliography

[1] U.S.-Canada Power System Outage Task Force, "Final Report on the August 14, 2003 Blackout in the United States and Canada: Causes and Recommendations," U.S. Department of Energy, Washington DC, USA, Tech. Rep. April, 2004.

[2] European Comission, "A Roadmap for moving to a competitive low carbon economy in 2050," 2011.

[3] F. Li, W. Qiao, H. Sun, H. Wan, J. Wang, Y. Xia, Z. Xu, and P. Zhang, "Smart Transmission Grid: Vision and Framework," *IEEE Transactions on Smart Grid*, vol. 1, no. 2, pp. 168–177, Sep. 2010.

[4] A. Phadke, J. Thorp, and M. Adamiak, "A New Measurement Technique for Tracking Voltage Phasors, Local System Frequency, and Rate of Change of Frequency," *IEEE Transactions on Power Apparatus and Systems*, vol. 102, no. 5, pp. 1025–1038, May 1983.

[5] A. Phadke and J. Thorp, *Synchronized Phasor Measurements and Their Applications*. Springer Verlag, 2008.

[6] A. Phadke and R. De Moraes, "The Wide World of Wide-Area Measurement," *IEEE Power and Energy Magazine*, vol. 6, no. 5, pp. 52–65, Sep. 2008.

[7] S. Skok, I. Ivankovic, and Z. Cerina, "Applications Based on PMU Technology for Improved Power System Utilization," in *Power Engineering Society General Meeting, 2007. IEEE*, Jun. 2007, pp. 1–8.

[8] D. Novosel, V. Madani, B. Bhargava, K. Vu, and J. Cole, "Dawn of the grid synchronization," *IEEE Power and Energy Magazine*, vol. 6, no. 1, pp. 49–60, Jan. 2008.

[9] H. Jóhannsson, A. H. Nielsen, and J. Østergaard, "Wide-Area Assessment of Aperiodic Small Signal Rotor Angle Stability in Real-Time," *IEEE Transactions on Power Systems*, pp. 1–13, 2013.

[10] M. Glavic and T. Van Cutsem, "Wide-Area Detection of Voltage Instability From Synchronized Phasor Measurements. Part I: Principle," *IEEE Transactions on Power Systems*, vol. 24, no. 3, pp. 1408–1416, Aug. 2009.

[11] ——, "Wide-Area Detection of Voltage Instability From Synchronized Phasor Measurements. Part II: Simulation Results," *IEEE Transactions on Power Systems*, vol. 24, no. 3, pp. 1417–1425, Aug. 2009.

[12] K. Morison, L. Wang, and P. Kundur, "Power system security assessment," *IEEE Power and Energy Magazine*, vol. 2, no. october, pp. 30–39, 2004.

[13] Working Group Cigré C4.601, "Review of on-line dynamic security assessment tools and techniques," 2007.

[14] S. C. Savulescu, *Real-Time Stability in Power Systems*. New York: Springer Verlag, 2006.

[15] P. Kundur, J. Paserba, V. Ajjarapu, G. Andersson, A. Bose, C. Canizares, N. Hatziargyriou, D. Hill, A. Stankovic, C. Taylor, T. Van˜Cutsem, and V. Vittal, "Definition and Classification of Power System Stability," *IEEE Transaction on Power Systems*, vol. 19, no. 2, pp. 1387–1401, May 2004.

[16] R. Treinen, V. Vittal, and A. A. Fouad, "Application of a modal-based transient energy function to a large-scale stressed power system: assessment of transient stability and transient voltage dip," *International Journal of Electrical Power & Energy Systems*, vol. 15, no. 2, pp. 117–125, 1993.

[17] S. C. Savulescu, *Real-Time Stability in Power Systems*, 2nd ed., ser. Power Electronics and Power Systems, S. C. Savulescu, Ed. Cham: Springer International Publishing, 2014.

[18] Y. Tada and H.-D. Chiang, "Design and Implementation of On-line Dynamic Security Assessment," *IEEJ TRANSACTIONS ON ELECTRICAL AND ELECTRONIC ENGINEERING*, vol. 4, no. 3, pp. 313–321, May 2009.

[19] H.-D. Chiang, C.-S. Wang, and Hua Li, "Development of BCU classifiers for on-line dynamic contingency screening of electric power systems," *IEEE Transactions on Power Systems*, vol. 14, no. 2, pp. 660–666, May 1999.

[20] Y. Tada, A. Kurita, and K. Koyanagi, "BCU-guided time-domain method for energy margin calculation to improve BCU-DSA system," in *IEEE/PES Transmission and Distribution Conference and Exhibition*, vol. 1. IEEE, 2002, pp. 366–371.

[21] K. Sun, S. Likhate, V. Vittal, V. S. Kolluri, and S. Mandal, "An Online Dynamic Security Assessment Scheme Using Phasor Measurements and Decision Trees," *IEEE Transactions on Power Systems*, vol. 22, no. 4, pp. 1935–1943, Nov. 2007.

[22] P. Lund, C. L. Bak, P. Thogersen, Z. Chen, C. Liu, K. Sun, and Z. H. Rather, "A Systematic Approach for Dynamic Security Assessment and the Corresponding Preventive Control Scheme Based on Decision Trees," *IEEE Transactions on Power Systems*, vol. 29, no. 2, pp. 717–730, 2014.

[23] M. He, V. Vittal, and J. Zhang, "Online Dynamic Security Assessment With Missing PMU Measurements : A Data Mining Approach," *Power Systems, IEEE Transactions on*, vol. 28, no. 2, pp. 1969–1977, 2013.

[24] A. Dissanayaka, U. D. Annakkage, B. Jayasekara, and B. Bagen, "Risk-Based Dynamic Security Assessment," *IEEE Transactions on Power Systems*, vol. 26, no. 3, pp. 1302–1308, Aug. 2011.

[25] M. Pavella, D. Ernst, and D. Ruiz-Vega, *Transient Stability of Power Systems: A Unified Approach to Assessment and Control.* Kluwer Academic Publishers, 2000.

[26] O. G. C. Dahl, *Electric Power Circuits. Vol.II: Power System Stability.* Mc Graw Hill, 1938.

[27] P. Kundur, *Power System Stability and Control*, N. J. Balu and M. G. Lauby, Eds. McGraw-Hill Inc., 1994.

[28] C. Fu and A. Bose, "Contingency Ranking Based on Severity Indices in Dynamic Security Analysis," *IEEE Transaction on Power Systems*, vol. 14, no. 3, pp. 980–986, Aug. 1999.

[29] A. A. Fouad and V. Vittal, "The transient energy function method," *International Journal of Electrical Power & Energy Systems*, vol. 10, no. 4, pp. 233–246, Oct. 1988.

[30] V. Chadalavada, V. Vittal, G. C. Ejebe, G. D. Irisarri, J. Tong, G. Pieper, and M. McMullen, "An On-Line Contingency Filtering Scheme for Dynamic Security Assessment," *IEEE Transaction on Power Systems*, vol. 12, no. 1, pp. 153–161, Feb. 1997.

[31] S. Khaitan and A. Gupta, *High Performance Computing in Power and Energy Systems*, Springer, 2012.

[32] H.-D. Chiang, Y. Tada, H. Li, and T. Takazawa, "TEPCO-BCU for On-line Dynamic Security Assessments of Large-Scale Power Systems," in *Advances in Power System Control, Operation and Management (APSCOM 2009), 8th International Conference on*, Nov. 2009, pp. 1–14.

[33] Y. Xue and M. Pavella, "Extended equal-area criterion: an analytical ultra-fast method for transient stability assessment and preventive control of power systems," *International Journal of Electrical Power & Energy Systems*, vol. 11, no. 2, pp. 131–149, Apr. 1989.

[34] Y. Xue, T. Huang, and F. Xue, "Effective and Robust Case Screening for Transient Stability Assessment," in *2013 IREP Symposium Bulk Power System Dynamics and Control - IX Optimization, Security and Control of the Emerging Power Grid*, 2013, pp. 1–8.

[35] Y. Xue, P. Rousseaux, Z. Gao, L. Wehenkel, M. Pavella, R. Belhomme, E. Euxibie, and B. Heilbronn, "Dynamic Extended Equal Area Criterion: Part 1. Basic formulation," in *IEEE/NTUA Athens Power Tech Conference*, vol. 71, no. 2, Athens, Greece, Sep. 1993, pp. 889–895.

[36] Y. Xue, P. Rousseaux, Z. Gao, L. Wehenkel, M. Pavella, Y. Zhang, M. Trotignon, A. Duchamp, and B. Heilbronn, "Dynamic Extended Equal Area Criterion Part 2. Embedding fast valving and automatic voltage

regulation," in *IEEE/NTUA Athens Power Tech Conference*, vol. 71, no. 2, Athens, Greece, Sep. 1993, pp. 896–900.

[37] B. Lee, S.-H. Kwon, J. Lee, H.-K. Nam, J.-B. Choo, and D.-H. Jeon, "Fast contingency screening for online transient stability monitoring and assessment of the KEPCO system," *IEEE Proc., Gener. Transm. Distrib.*, vol. 150, no. 4, pp. 399–404, Jul. 2003.

[38] G. E. Gless, "Direct Method of Liapunov Applied to Transient Power System Stability," *IEEE Transactions on Power Apparatus and Systems*, vol. PAS-85, no. 2, pp. 159–168, Feb. 1966.

[39] A. H. El-Abiad and K. Nagappan, "Transient Stability Regions of Multimachine Power Systems," *IEEE Transaction on Power Apparatus and Systems*, vol. PAS-85, no. 2, pp. 169–179, Feb. 1966.

[40] T. Athay, R. Podmore, and S. Virmani, "A practical Method for the Direct Analysis of Transient Stability," *IEEE Transactions on Power Apparatus and Systems*, vol. PAS-98, no. 2, pp. 573–584, Mar. 1979.

[41] N. Kakimoto, Y. Ohsawa, and M. Hayashi, "Tansient Stability Analysis of Multimachine Power Systems with Field Flux Decays via Lyapunov's Direct Method," *IEEE Transactions on Power Apparatus and Systems*, vol. PAS-99, no. 5, pp. 1819–1827, Sep. 1980.

[42] M. Ribbens-Pavella and F. J. Evans, "Direct Methods for Studying Dynamics of Large-scale Electric Power Systems A Survey," *Automatica*, vol. 21, no. 1, pp. 1–21, Jan. 1985.

[43] H.-D. Chiang, F. F. Wu, and P. P. Varaiya, "Foundations of the Potential Energy Boundary Surface Method for Power Systern Transient Stability Analysis," *IEEE Transactions on Circuits and Systems*, vol. 35, no. 6, pp. 712–728, Jun. 1988.

[44] A. A. Fouad, V. Vittal, and T. K. Oh, "Critical Energy for Direct Transient Stability Assessment of a Multimachine Power System," *IEEE Transaction on Power Apparatus and Systems*, vol. PAS-103, no. 8, pp. 2199–2206, Aug. 1984.

[45] H.-D. Chiang, F. F. Wu, and P. P. Varaiya, "A BCU Method for Direct Analysis of Power System Transient Stability," *IEEE Transactions on Power System*, vol. 9, no. 3, pp. 1194–1208, Aug. 1994.

[46] A. R. Bergen and D.J. Hill, "A Structure Preserving Model for Power System Stability Analysis," *IEEE Transactions on Power Apparatus and Systems*, vol. PAS-100, no. 1, pp. 25–35, Jan. 1981.

[47] Y. Zou, M.-H. Yin, and H.-D. Chiang, "Theoretical Foundation of the Controlling UEP Method for Direct Transient-Stability Analysis of Network-Preserving Power System Models," *IEEE Transactions on Circuits and Systems - I: Fundamental Theory and Applications*, vol. 50, no. 10, pp. 1324–1336, Oct. 2003.

[48] L. B. Jocic, M. Ribbens-Pavella, and D. D. Siljak, "Multimachine Power Systems: Stability, Decomposition, and Aggregation," *IEEE Transactions on Automatic Control*, vol. AC-23, no. 2, pp. 325–332, Apr. 1978.

[49] M. Araki, M. Saeki, and B. Kondo, "Application of a New Stability criterion of Composite Systems to Multimachine Power Systems," *IEEE Transactions on Automatic Control*, vol. AC-25, no. 3, pp. 480–483, Jun. 1980.

[50] A. N. Michel, A. A. Fouad, and V. Vittal, "Power System Transient Stability Using Individual Machine Energy Functions," *IEEE Transactions on Circuits and Systems*, vol. 30, no. 5, pp. 266–276, May 1983.

[51] Y. Zhang, L. Wehenkel, P. Rousseaux, and M. Pavella, "SIME: A hybrid approach to fast transient stability assessment and contingency selection," *Electrical Power & Energy Systems*, vol. 19, no. 3, pp. 195–208, Mar. 1997.

[52] D. Ernst, D. Ruiz-Vega, M. Pavella, P. M. Hirsch, and D. Sobajic, "A Unified Approach to Transient Stability Contingency Filtering, Ranking and Assessment," *IEEE Transactions on Power Systems*, vol. 16, no. 3, pp. 435–443, Aug. 2001.

[53] D. Ruiz-Vega and M. Pavella, "A Comprehensive Approach to Transient Stability Control: Part I - Near Optimal Preventive Control," *IEEE Transactions on Power Systems*, vol. 18, no. 4, pp. 1446–1453, Nov. 2003.

[54] C.-W. Liu and J. Thorp, "Application of synchronised phasor measurements to real-time transient stability prediction," in *Generation, Transmission and Distribuion, IEE Proceedings*, vol. 142, no. 4, Jul. 1995, pp. 355–360.

[55] C.-W. Liu and J. S. Thorp, "New Methods for Computing Power System Dynamic Response for Real-Time Transient Stability Prediction," *IEEE Transactions on Circuits and Systems - I: Fundamental Theory and Applications*, vol. 47, no. 3, pp. 324–337, Mar. 2000.

[56] L. Wehenkel, T. Van Cutsem, and M. Ribbens-Pavella, "Decision Trees applied to on-line Transient Stability Assessment of Power Systems," in *IEEE International Symposium on Circuits and Systems, 1988.*, vol. 2, Jun. 1988, pp. 1887–1890.

[57] ——, "An Artificial Intelligence Framework for on-line Transient Stability Assessment of Power Systems," *IEEE Transactions on Power Systems*, vol. 4, no. 2, pp. 789–800, May 1989.

[58] H.-Z. Guo, H. Xie, B.-H. Zhang, G.-L. Yu, P. Li, Z.-Q. Bo, and A. Klimek, "Study on power system transient instability detection based on wide area measurement system," *European Transactions on Electrical Power*, vol. 20, no. 2, pp. 184–205, Mar. 2010.

[59] V. Kolluri, S. Mandal, M. Vaiman, M. Vaiman, S. Lee, and P. Hirsch, "Fast Fault Screening Approach to Assessing Transient Stability in Entergy's Power System," in *Power Engineering Society General Meeting, 2007. IEEE*, Jun. 2007, pp. 1–6.

[60] J. Kleinberg and E. Tardos, *Algorithm Design*, M. Suarez-Rivas, Ed. Boston: Pearson Addison Wesley, 2006.

[61] F. Pruvost, T. Cadeau, P. Laurent-Gengoux, F. Magoules, F. X. Bouchez, and B. Haut, "Numerical accelerations for power systems transient stability simulations," in *17th Power System Computation Conference*, Zurich, Switzerland, 2011.

[62] F. Dörfler, and F. Bullo, "Kron Reduction of Graphs with Applications to Electrical Networks," *Dynamical Systems*, pp. 1–28, Feb. 2011.

[63] IEEE Std 1110-2002 (Revision of IEEE Std 1110-1991), *IEEE Guide for Synchronous Generator Modeling Practices and Applications in Power System Stability Analyses*, 2003, no. November.

[64] P. Sauer and M. A. Pai, *Power System Dynamics and Stability*, E. Svendson, M. Horton, and B. M. de Leon, Eds. Prentice Hall, 1998.

[65] G. Rogers, *Power System Oscillations*. Springer, 2000.

[66] D. Fabozzi, B. Haut, A. S. Chieh, and T. Van Cutsem, "Accelerated and Localized Newton Schemes for Faster Dynamic Simulation of Large Power Systems," *IEEE Transactions on Power Systems*, pp. 1–12, 2013.

[67] International Electrotechnical Commission, "International standard iec 61000-4-30," Geneva, Switzerland, 2003.

[68] M. H. Bollen, *Understanding power quality problems*, vol. 3 ed. New York: IEEE press, 2000.

[69] A. A. Fouad and R. Sreedhara, "Transient Voltage Dip Analysis using the Transient Energy Function Method," in *Proceedings of the Twenty-Second Annual North American Power Symposium*. IEEE Comput. Soc. Press, 1990, pp. 264–273.

[70] F. Dominguez, A. S. Debs, and J. Anasis, "Transient voltage dip in power systems: computation and sensitivity analysis using the hybrid method," in *Decision and Control, 1992., Proceedings of the 31st IEEE Conference on*, 1992, pp. 576–581 vol.1.

[71] Y. Xue, T. Xu, B. Liu, and Y. Li, "Quantitative assessments for transient voltage security," *Proceedings of the 21st International Conference on Power Industry Computer Applications. Connecting Utilities. PICA 99. To the Millennium and Beyond (Cat. No.99CH36351)*, pp. 101–106, 1999.

[72] A. Tiwari and V. Ajjarapu, "Contingency assessment for voltage dip and short term voltage stability analysis," *2007 iREP Symposium - Bulk Power System Dynamics and Control - VII. Revitalizing Operational Reliability*, pp. 1–8, Aug. 2007.

[73] D. Shoup, J. Paserba, and C. Taylor, "A survey of current practices for transient voltage dip/sag criteria related to power system stability," *IEEE PES Power Systems Conference and Exposition, 2004.*, pp. 1499–1506, 2004.

[74] M. Glavic, D. Ernst, D. Ruiz-Vega, L. Wehenkel, and M. Pavella, "E-SIME - A Method for Transient Stability Closed-Loop Emergency Control : Achievements and Prospects Fundamentals of E-SIME," in *2007 iREP Symposium-Bulk Power System Dynamics and Control - VII, Revitalizing Operational Reliability*, 2007.

[75] T. Weckesser, "Power System Instability and Blackout Prevention," Technical University of Denmark, Kgs. Lyngby, Tech. Rep., 2011.

[76] T. Weckesser and H. Jóhannsson, "Method of determining remedial control actions for a power system in an insecure state," 2011.

[77] J. Wen, W.-h. E. Liu, P. L. Arons, and S. K. Pandey, "Evolution Pathway Towards Wide Area Monitoring and Protection - A Real-World Implementation of Centralized RAS System," *IEEE Transactions on Smart Grid*, vol. 5, no. 3, pp. 1506–1513, May 2014.

[78] Z. Yao, V. R. Vinnakota, Q. Zhu, C. Nichols, G. Dwernychuk, and T. Inga-Rojas, "Forewarned Is Forearmed: An Automated System for Remedial Action Schemes," *IEEE Power and Energy Magazine*, vol. 12, no. 3, pp. 77–86, May 2014.

[79] Y. Makarov, S. Lu, X. Guo, J. Gronquist, P. Du, T. Nguyen, and J. Burns, "Wide Area Security Region," Pacific Northwest National Laboratory, Richland, Washington 99352, Tech. Rep. March, 2010.

[80] J. Ma, T. Wang, S. Wang, X. Gao, X. Zhu, Z. Wang, and J. S. Thorp, "Application of Dual Youla Parameterization Based Adaptive Wide-Area Damping Control for Power System Oscillations," *IEEE Transactions on Power Systems*, vol. 29, no. 4, pp. 1602–1610, Jul. 2014.

[81] A. Heniche and I. Kamwa, "Assessment of two methods to select wide-area signals for power system damping control," *IEEE Transactions on Power Systems*, vol. 23, no. 2, pp. 572–581, 2008.

[82] E. Dimitrova, M. L. Wittrock, H. Jóhannsson, and A. H. Nielsen, "Early Prevention Method for Power System Instability," *IEEE Transactions on Power Systems*, vol. PP, no. 99, pp. 1–9, 2014.

[83] H. Jóhannsson, "Development of early warning methods for electric power systems," Ph.D. dissertation, The Technical University of Denmark, 2011.

[84] M. Stubbe, "Long-term dynamics-phase II (report of CIGRE Task Force 38.02.08)," CIGRE, Tech. Rep. March, 1995.

[85] H. Jóhannsson, J. Østergaard, and A. H. Nielsen, "Identification of critical transmission limits in injection impedance plane," *International Journal of Electrical Power & Energy Systems*, vol. 43, no. 1, pp. 433–443, Dec. 2012.

[86] S. Sommer and H. Jóhannsson, "Real-time thevenin impedance computation," in *2013 IEEE PES Innovative Smart Grid Technologies Conference (ISGT)*. IEEE, Feb. 2013, pp. 1–6.

[87] D. Molina, J. Liang, R. G. Harley, and G. K. Venayagamoorthy, "Virtual Generators: Simplified Online Power System Representations for Wide-Area Damping Control," in *IEEE Power and Energy Society General Meeting*, Jul. 2012, pp. 1–8.

Appendix A

Investigation of the Adaptability of Transient Stability Assessment Methods to Real-Time Operation

---

This paper has been presented at the IEEE PES Innovative Smart Grid Technologies (ISGT) Europe Conference in Berlin, Germany and has been published as part of the conference proceedings.

Investigation of the Adaptability of Transient Stability Assessment Methods to Real-Time Operation

Tilman Weckesser, *Student Member, IEEE*, Hjörtur Jóhannsson, *Member, IEEE*,
Stefan Sommer, *Student Member, IEEE*, Jacob Østergaard, *Senior Member, IEEE*

***Abstract*—In this paper, an investigation of the adaptability of available transient stability assessment methods to real-time operation and their real-time performance is carried out. Two approaches based on Lyapunov's method and the equal area criterion are analyzed. The results allow to determine the runtime of each method with respect to the number of inputs. Furthermore, it allows to identify, which method is preferable in case of changes in the power system such as the integration of distributed power resources (DER). A comparison of the performance of the analyzed methods leads to the suggestion that matrix reduction and time domain simulation are the most critical operations.**

***Index Terms*—Power system stability, Stability analysis, Lyapunov method, Wide area measurements, Phasor measurement units**

I. Introduction

ONE of the fundamental requirements of a modern society is a stable and secure operation of the electric power system and this is not expected to change in the future. In many countries a shift from fossil energy sources to renewable energy sources is taking place. In order to reach the future vision of a danish society with minimal dependency on fossil fuels [1], the power system faces a great challenge. It has to evolve into a system with minimal environmental impact, while continuing to provide its service satisfactory and at a competitive price. Therefore, a big share of the power production will use non-controllable sources, such as wind and solar radiation [1].

This will lead to increased fluctuations of the power system's operating point, which will make the planning of a stable and secure operation a challenging task, and a planning hours ahead may no longer be feasible. Hence, the state-of-the-art stability assessment methods, which are based on computationally demanding off-line calculations, will no longer be sufficient. A need for real-time assessment tools will arise.

Smart grid solutions are often suggested for coping with the fluctuating nature of wind and photo-voltaic power generation, where control of distributed energy resources is used for power balancing purpose. It is of paramount importance, that the smart grid control actions do not cause other stability problems in the system, while solving the power balancing problem. The need for real-time stability information in a future smart grid power system was accentuated e.g. in [2].

The phasor measurement technology [3]–[5] is seen as the enabling technology for the development of real-time wide area monitoring and control applications [6], [7].

Recent publications focus on the task of on-line security and stability assessment by utilizing synchronized phasor measurements. In [8], [9] an entirely new approach was developed for real-time assessment of the power system. However, in [10], [11] an existing method, used for off-line stability assessment, was adapted to real-time operation.

The potentials of adapting existing off-line assessment methods are further explored in this paper, where the focus is on methods for transient stability assessment. The computational complexity of several methods is investigated to identify the approaches that are well suited for real-time operation. This complexity investigation as well applies to future systems with changed topology. In contrast, an analysis based on simulations would only be representative for a current system.

The authors are with the Centre for Electric Technology, Department of Electrical Engineering, Technical University of Denmark, 2800 Lyngby, Denmark. (email: jtgw@elektro.dtu.dk)

This research was supported by the Danish Strategic Research Council.

II. Overview of existing methods

Figure 1 shows a mind-map of available transient stability assessment methods and depicts as well how research gradually developed towards more specific assessment methods. In the following, two approaches for transient stability assessment are discussed.

A. Lyapunov's Direct Method

Direct methods for transient stability assessment using Lyapunov functions have been developed since the 1960s (e.g. [12], [13]). The challenges are to determine a Lyapunov function, which represents the system with satisfactory accuracy, and, furthermore, to determine the most suitable critical energy, which allows the evaluation of the transient stability.

1) Transient Energy Function: A widely used energy function was derived in [14], which is nowadays most often referred to as transient energy function (TEF) (e.g. [16], [37]). This function is used in scalar Lyapunov approaches to assess transient stability in the power system.

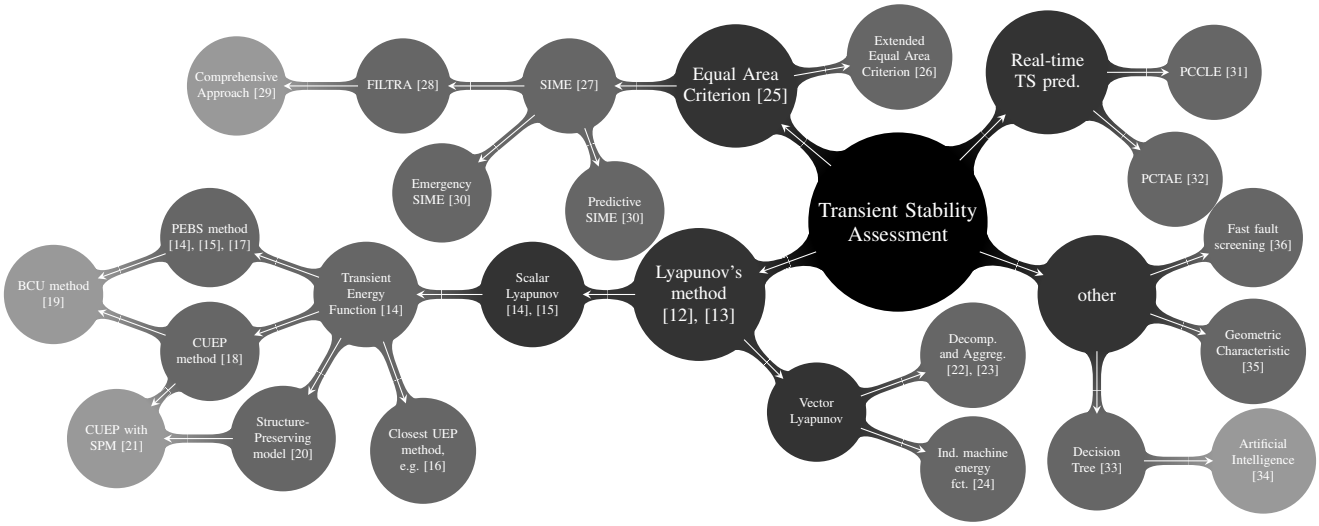

Fig. 1. Available methods and their development steps (not intended to be exhaustive)

$$V = \sum_{i=1}^{n}(\overbrace{\frac{1}{2}M_i\tilde{\omega}_i^2}^{E_{kin}=} - \overbrace{P_i(\theta_i-\theta_i^s)}^{E_{pot,r}=}) - \sum_{i=1}^{n-1}\sum_{j=i+1}^{n}[\underbrace{C_{ij}(\cos\theta_{ij}-\cos\theta_{ij}^s)}_{E_{mag}} - \underbrace{\int_{\theta_i^s+\theta_j^s}^{\theta_i+\theta_j} D_{ij}\cos\theta_{ij}\, d(\theta_i+\theta_j)]}_{E_{dis}} \quad (1)$$

E Constant voltage behind the transient reactance
G_{ii} Driving point conductance
P_{mi} Mechanical power input of the i^{th} machine
V Transient Energy

The terms in eq. (1) can be interpreted as:

- E_{kin}: Total change in rotor kinetic energy with respect to the center of inertia (COI) (M_i and $\tilde{\omega}_i$ are the inertia constant and angular velocity relative to COI respectively)
- $E_{pot,r}$: The change in potential energy of the rotor with respect to COI ($P_i = P_{mi} - E_i^2 G_{ii}$ and θ_i represents the rotor angle relative to the COI, the index s denotes conditions at the stable equilibrium point (SEP))
- E_{mag}: Change in stored magnetic energy in the branch connecting machine i and j (C_{ij} is the product of the voltages E_i, E_j and the transfer susceptance B_{ij})
- E_{dis}: Change in dissipated energy of the branch connecting machine i and j (D_{ij} is the product of the respective voltages E_i, E_j and the transfer conductance G_{ij})

The term E_{dis} causes that the total energy for a system with transfer conductances cannot be expressed in a closed form expression. One way to circumvent the problem is to neglect those when determining the reduced admittance matrix. The admittance matrix includes the transmission line impedances and loads, which are modeled as constant impedances. Neglecting the resistances is generally not acceptable [14].

2) Lyapunov Function: In order to use Lyapunov's method and the transient energy function, it has to be shown that eq. (1) exhibits the properties of a Lyapunov function.

Moreover, the power system has to have an asymptotic stability characteristic to be transient stable. In order to prove asymptotic stability with the Lyapunov method, the corresponding function $V(x)$ has to be a strong Lyapunov function ($V(x) > 0$; $\dot{V}(x) < 0$) [38]. This can be relaxed to $\dot{V}(x) \leq 0$, if LaSalle's invariance principle is invoked and the stability of $V(x)$ is only analyzed around the origin [37], [38].

The transient energy function (1) exhibits these characteristics, when using the classical model and assuming certain constraints such as neglecting the transfer conductances $G_{ij} = 0$, [16], [39]. The Lyapunov function is then.

$$V = \sum_{i=1}^{n}(E_{kin}(\tilde{\omega}_i) - E_{pot,r}(\theta_i)) - \sum_{i=1}^{n-1}\sum_{j=i+1}^{n} E_{mag}(\theta_{ij}) \quad (2)$$

3) Accounting for transfer conductances: Several approaches were developed to account for or to approximate the effects of the transfer conductances and only a few will be mentioned in the following. For a more complete discussion of the different approaches the reader is referred to [16].

a) Numerical integration: Some approaches utilize numerical integration to approximate the effects of transfer conductances. This additional term may cause the loss of the Lyapunov properties of the function. Furthermore, different integration paths may lead to different assessment results.

In [14] and [37] a linear approach is assumed and the additional term is integrated using the trapezoidal rule.

$$\sum_{i=1}^{n-1}\sum_{j=i+1}^{n}\int_{\theta_i^s+\theta_j^s}^{\theta_i+\theta_j} D_{ij}\cos\theta_{ij} d(\theta_i+\theta_j) \equiv \sum_{i=1}^{n-1}\sum_{j=i+1}^{n} I_{ij} \quad (3)$$

where

$$I_{ij} = D_{ij}\frac{\theta_i+\theta_j-\theta_i^s-\theta_j^s}{\theta_{ij}-\theta ij^s}\left(\sin\theta_{ij}-\sin\theta_{ij}^s\right) \quad (4)$$

Another approach was chosen by the authors of [15], here the sustained fault trajectory in the relative angle space determines the integration path [16].

b) Structure Preserving Model: A third approach was described by *Bergen and Hill* in [20], where the loads are preserved in the reduced admittance matrix, instead of being absorbed by it. Contrary to neglecting the transfer conductances of the transmission lines, neglecting the real part of the load impedances may not be a valid assumption [16].

In this approach the authors are considering a frequency dependent load (FDL) model, which load variations are linear about nominal frequency. This leads to a modification of the swing equation considered for the derivation of the TEF (eq. (1)) and, eventually, to a modified Lyapunov function [40].

The structure preserving model was further developed by other research groups (see also [16], [40]).

4) Critical Energy: In order to determine the stability of the system, the critical energy has to be computed. A straightforward theoretical approach to identify the critical energy is described in [16]: *Step 1:* Find all the unstable equilibrium points (UEPs) surrounding the new SEP of the post-fault system; *Step 2:* Define the critical energy V_{crit} as the value corresponding to the UEP 'closest' to the SEP (lowest value). This theoretical approach is not feasible and several practical attempts were made to identify the critical energy.

a) Closest UEP approach: In [16] only all type-1 UEPs are considered to determine the closest unstable equilibrium and the corresponding critical energy. These are the operating points, where one of the machines looses synchronism. In order to identify the type-1 UEPs, an operating point of the following structure can be chosen as a starting point.

$$\theta^{sj} = [\theta^s_{1,n}, \theta^s_{2,n}, \ldots, \pi - \theta^s_{j,n}, \ldots, \theta^s_{n-1,n}] \tag{5}$$

The critical energy can be approximated by:

$$V_{crit} = \min_{j=1,\ldots,n-1} V(\theta^{sj}, 0) \tag{6}$$

This approach reduces the computational time, but does not have an effect on the conservativeness of the method.

b) Controlling Unstable Equilibrium Point (CUEP): The method of the controlling UEP was first considered by *Fouad et al.* [41]. The controlling UEP is the unstable equilibrium, which is closest to the particular trajectory of the disturbed system. At the UEP, in order to satisfy the swing equation (see e.g. [42]), the angular speed is equal to zero and, consequently, the critical energy in that point is determined by eq. (1) and (3) as follows.

$$V_{crit} = -\sum_{i=1}^{n} E_{pot,r}(\theta^u_i) - \sum_{i=1}^{n-1}\sum_{j=i+1}^{n} \left[E_{mag}(\theta^u_{ij}) + I^u_{ij}\right] \tag{7}$$

In order to identify the controlling UEP *Fouad et al.* propose in [18] a criterion as follows: *"The post-disturbance trajectory approaches (if the disturbance is large enough) the controlling u.e.p. This is the u.e.p. with lowest normalized potential energy margin at the instant the disturbance is removed."* This criterion can be computed using the following:

$$\Delta V_{PE,norm} = \Delta V_{PE}/V_{KE,corr} \tag{8}$$

where the energy absorbing capacity of the post-disturbance system ΔV_{PE} can be determined as the difference between potential energy at the UEP and at fault clearance. The equations for determining the corrected kinetic energy $V_{KE,corr}$ are provided in [18]. The correction is necessary due to the finding that not all the kinetic energy contributes to the separation of the critical generators [37], [41], [43].

In order to determine the minimum normalized potential energy margin $\Delta V_{PE,norm}$, the actual values of θ^u for the possible UEPs have to be known. In [18] it is proposed, that approximate values of θ^u are used, which can be obtained from the knowledge of the post-disturbance stable equilibrium point. After identification of the candidate CUEP the corresponding θ^u is calculated accurately and, eventually the critical energy corresponding to the CUEP can be calculated utilizing eq. (7). The critical energy computed can then be compared to the value of the energy function at the time of fault clearance and the stability of the system can be determined.

A more detailed description of the approach is provided in [18] or [39]. This approach clearly reduces the conservativeness of the method compared to the closest UEP method.

c) Potential Energy Boundary Surface (PEBS): *Kakimoto et al.* [15] as well as *Athay et al.* [14] proposed to determine the transient stability region by analyzing the potential energy function (V_p). According to [14] the V_p has within a periodic frame of rotor angles at most one relative minimum (new SEP). The rest of the extreme values correspond to relative maxima and saddle-points (UEPs). The authors of [15] propose a stability boundary, where the saddle-points surrounding the SEP are connected through curves (O_x), which are orthogonal to equipotential curves ($V_p(\theta, E) = C_i$). The authors argue that, due to the fact that the direction of the total torque applied to the system is orthogonal to the equipotential curves, the system will loose synchronism after crossing a curve O_x. In [15] it is suggested that the fault-on trajectory is simulated until it crosses a curve O_x. The point of crossing the boundary can be detected by analyzing the time derivative of the kinetic energy.

A theoretical foundation of the PEBS method was later presented by *Chiang et al.* in [17]. The authors define the PEBS as the stability boundary of the gradient system

$$\dot{\theta} = -\partial V_p/\partial\theta \tag{9}$$

and conclude that it is a local approximation of the stability boundary of a power system described by the swing equation.

d) Boundary of stability region based controlling unstable equilibrium point method (BCU method): The BCU method, described in [19], is based on the relationship of the stability boundary of the original and the reduced system determined by eq. (9) [17]. Where the reduced system is described by:

$$\dot{\theta}_{in} = (P_i - P_{ei}) - (M_i/M_n)(P_n - P_{en}) \tag{10}$$

P_{ei} Injected electrical power of the ith machine

Roughly speaking, the BCU method analyzes the fault-on trajectory and detects when the boundary of the reduced-state model is crossed. This point is called exit point and is

used as the initial condition when integrating the post-fault reduced system. The integration yields a new approximation of θ corresponding to the controlling UEP and is used as an initial guess to find the actual CUEP by solving eq. (9) equal to zero. The transient stability of the system can then be determined utilizing the CUEP, provided by the BCU method, and applying the CUEP method described in section II-A4b.

B. Methods based on the Equal Area Criterion (EAC)

The equal area criterion was developed in the late 1930's, though the origin is not really clear [30].

1) Equal Area Criterion (EAC): The method allows the determination of transient stability of an one-machine infinite bus system (OMIB) without computing the swing curves. Therefore, the following simplifications and assumptions were considered. The synchronous machine (SM) is represented by a constant voltage magnitude behind the synchronous reactance and the mechanical power input is assumed to be constant. Furthermore, the damping of the machine is neglected and the loads are represented by constant impedances. It was later shown that the simplifications can be relaxed [30].

When the damping is neglected and after manipulation, the swing equation can be written for an OMIB as follows [44]:

$$[d\delta/dt]^2 = \int (2/M)(P_m - P_e)\, d\delta \tag{11}$$

$P_{e/m}$ Electric power injection / mechanical power input
δ Relative rotor angle

Initially, the derivative of the angle is zero and changes after the disturbance. For a stable case the angle reaches a maximum at δ_m and changes the direction thereafter. From this the following stability criteria can be formulated [44].

$$\int_{\delta_0}^{\delta_m} (2/M)(P_m - P_e)\, d\delta = 0 \tag{12}$$

The integral can be split up into two areas, which can be calculated as follows (indices D and P denote conditions during and after fault clearance respectively).

$$A_{acc} = \int_{\delta_0}^{\delta_c} (P_{mD} - P_{eD})\, d\delta = \int_{\delta_0}^{\delta_c} P_a\, d\delta \tag{13}$$

$$A_{dec} = -\int_{\delta_c}^{\delta_m} (P_{mP} - P_{eP})\, d\delta = -\int_{\delta_c}^{\delta_m} P_a\, d\delta \tag{14}$$

P_a Accelerating power

A stability margin η can then be determined as follows, where δ_u is the rotor angle at the UEP.

$$\eta = -\int_{\delta_0}^{\delta_u} P_a d\delta = A_{dec}(\delta_m = \delta_u) - A_{acc} \tag{15}$$

A positive margin represents a stable case, a negative an unstable and in the case that $\eta = 0$ it is a critical case.

2) Extended Equal Area Criterion (EEAC): In order to determine the stability of the power system as a response to a certain disturbance, the method described in [26] decomposes the multi-machine system into a set of critical machine(s) and a set of the 'remaining' generators. The machines in the two groups are aggregated and then transformed into two equivalent machines to form an OMIB system. Furthermore, in order to achieve simple algebraic equations for the assessment criteria, a modified Taylor series expansion is applied to determine the rotor angle.

a) Aggregation of Machines and Formulation of the OMIB system: The two sets of machines are aggregated as follows.

$$M_{a,s} = \sum_{i \in A,S} M_i;\ \delta_{a,s} = M_{a,s}^{-1} \sum_{i \in A,S} M_i \delta_i; \tag{16}$$

where S is the set of the machines of the critical cluster; s is its equivalent aggregated to one machine and $t_0^+ = 0^+$ is the time immediately following the disturbance. In the same way the 'remaining' machines can be aggregated, where A is the set of the 'remaining' machines; a is its equivalent aggregated to one machine. The OMIB system is then described by

$$M\ddot{\delta} = P_m - P_e = P_m - [P_c + P_{max} \sin(\delta - v)] \tag{17}$$

The equations for P_m, P_c, P_{max} and v can be found in [26].

b) Determine acceleration and deceleration area: The two areas can be computed as follows.

$$\begin{aligned} A_{acc} &= (P_m - P_{cD})(\delta_\tau - \delta_0) \\ &+ P_{maxD}[\cos(\delta_\tau - v_D) - \cos(\delta_0 - v_D)] \end{aligned} \tag{18}$$

$$\begin{aligned} A_{dec} &= (P_{cP} - P_m)(\pi - \delta_\tau - \delta_P + 2v_P) \\ &+ P_{maxP}[\cos(\delta_\tau - v_P) - \cos(\delta_P - v_P)] \end{aligned} \tag{19}$$

c) Critical Clearing Time (CCT): In order to determine the CCT, the rotor angle is expressed in a Taylor series.

$$\delta_\tau = \delta_0 + \alpha_1^{-1}\alpha_2^{-2}\gamma(\tau^2/2) + \alpha_1^{-1}\alpha_2^{-4}\dddot{\gamma}(\tau^4/24);\ \gamma = \ddot{\delta} \tag{20}$$

where $\alpha_{1,2}$ are corrective factors to compensate for the truncation error [26]. The Taylor series expansion solely contains even derivatives of δ, this is due to continuity which dictates that $\dot{\delta}$ is equal to zero at t_0^+ and that causes the cancellation of all higher-order odd derivatives of δ [26].

The stability of the power system with respect to a certain contingency can be assessed by determining the CCT. Therefore, (18) and (19) are solved for δ_c and (20) is utilized to calculate t_c. A simple comparison of the CCT and the actual clearing time yields the stability assessment result.

d) Identification Critical Machine(s): In order to identify a (cluster of) critical machine(s), the authors of [26] suggest the acceleration criterion σ_i.

$$\sigma_i = (P_{mi} - P_{ei}(\delta(t_0^+)))/M_i \tag{21}$$

The machines with the largest acceleration criterion are the critical machines. Critical groups can be identified, when considering the CCTs of the machines and their interconnection. A critical group is formed if two to three generators at the top of the list have similar CCTs and are strongly interconnected.

3) SIME: SIngle Machine Equivalent (SIME) poses an hybrid approach, which combines the advantages of a direct method and the time domain simulation approach.

In [30] different applications of the method are described. For fast stability assessment the *predictive SIME* seems to be appropriate and is considered in this analysis.

In the following a short description of the method is given. It solely comprises the most important features and the reader is referred to [27], [30] for a complete description.

a) Identification of Critical Machines: In order to identify the critical machines, the rotor angles of the generators are analyzed in every time step of the post-fault time domain simulation. In [28], [30] the generators are sorted according to their rotor angles and the angles of consecutive generators are compared to detect the 'maximum gap'. The generators above each gap are considered to form the set of critical generators and a corresponding candidate OMIB is formed. The time-domain simulation is continued until a candidate OMIB fulfills the instability criteria stated in (22).

b) Formulation of OMIB: After the critical machines are identified the system generators can be transformed into two equivalent machines and the OMIB system can be set up. The inertia coefficients of the equivalent machines can be calculated utilizing (16). The OMIB can then be described by (17), after P_m, P_c, P_{max} and v are determined.

c) Stability criterion: In [27] the stability criteria for the OMIB trajectories are determined as follows.

Unstable trajectory is a trajectory, which reaches an angel δ_u at time t_u where

$$P_a(t_u) = 0;\ dP_a/dt|_{t=t_u} > 0 \tag{22}$$

Stable trajectory is a trajectory, which reaches an angel $\delta_r < \delta_u$ at time t_r, where $\omega(t_r) = 0;\ P_a(t_r) < 0$.

d) Stability margin: The stability margin can then be determined as follows.

$$\eta = -\int_{\delta_i}^{\delta_u} P_a d\delta - (1/2)M\omega_i^2 \tag{23}$$

$\delta_i = \delta(t_i)$ OMIB angle at time t_i short after fault clearance

In order to determine the stability margin, a weighted least-square approximation (WLS) is used in [30] and $P_a(\delta)$ is extrapolated between δ_r to δ_u. The parameters a, b and c in eq. (24) are determined using values of P_a at three successive time steps

$$P_a(\delta) = a\delta^2 + b\delta + c \tag{24}$$

e) Predictive SIME: In [30] the predictive SIME method is used within a closed emergency control loop. The method is assumed to receive real-time measurements, which contain the rotor angles, speeds and accelerations. Subsequently, the method is used to carry out a predictive stability assessment, which can be used to determine appropriate control actions.

The procedure of the predictive SIME is described in [30] as follows. *Step 1:* At a time shortly after the disturbance clearance, consider three successive incoming measurements of the individual machines. *Step 2:* Use Taylor series to predict machine angles some time ahead and identify critical machines as described in section II-B3a. *Step 3:* Construct the corresponding OMIB as described in section II-B3b. *Step 4:* Determine OMIB parameters from the received measurements. *Step 5:* Approximate $P_a - \delta$ curve with WLS approximation. *Step 6:* Solve eq. (24) to determine δ_u. *Step 7:* Determine stability margin as described in section II-B3d.

f) Modification of Predictive SIME: In order to use the predictive SIME method for a fast stability assessment, the real-time measurements are used as initial conditions for a time domain simulation. The simulation is run until shortly after the disturbance is cleared and the simulated values are used instead of the measured values in the predictive SIME.

The stability analysis can then be carried out following the steps described in the previous section.

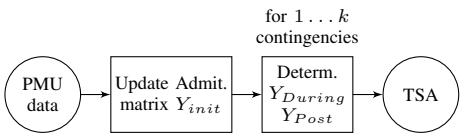

Fig. 2. PMU data utilization

TABLE I
COMPLEXITY ESTIMATION, b: NUMBER OF BRANCHES; m:NUMBER OF GENERATORS; n: NUMBER OF BUSES; k: NUMBER OF CONTINGENCIES

Function	Time	Frequency	
PMU data	$O(n+b)$	1	$O(n+b)$
Admittance matrix	$O(m+n+b)$	1	$O(m+n+b)$
Y_{During}, Y_{Post}	$O(m+n+b)$	k	$kO(m+n+b)$
TOTAL			$kO(m+n+b)$

III. RESULTS

The runtime analysis of the examined methods are presented in the following. It is assumed that PMU data providing full observability of the system are received in real-time.

The complexity of the algorithms of the distinct methods are compared in the following. This estimation should be valid for future power system and, consequently, the effects of structural changes, such as the increasing installation of DER, should be reflected in the results. Therefore, the algorithms of the different methods are compared using the big O-notation, which is common practice when analyzing algorithms [45]. If simulations were carried out instead, the analysis would be tied to the particular test case, and effects of structural changes would not be accounted for. A simulation of a relatively small test power system such as the IEEE test system cases would assess runtime on current power systems, and the results would fail to capture dependence on the system size and topology.

A. PMU data utilization

The procedure to extract the needed information from the received PMU measurements is shown in figure 2. It is assumed that voltage measurements from each node are received as well as current measurements from both ends of each branch. These measurements are used to update the admittance matrix and with a list of contingencies the admittance matrices for the during- and post-fault condition are set up.

The matrices are extended by the internal nodes of the machines behind their transient reactance X'_d, since some of the methods assume the voltages behind X'_d to be constant.

The number of operations to update these matrices is proportional to the number of branches, nodes and machines in the system. The results in O-notation are shown in table I.

B. Scalar Lyapunov's Direct method

The discussed methods assessing transient stability using Lyapunov's method are only differing in the way the critical

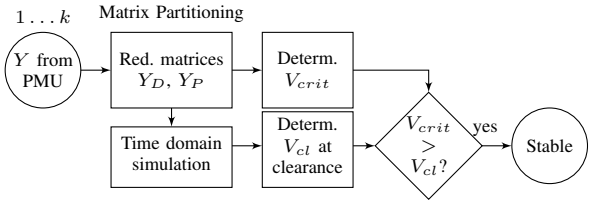

Fig. 3. Flow diagram scalar Lyapunov method

transient energy is determined. Therefore, the general procedure is shown in fig. 3 and in subsequent sections it is solely described how each method calculates the critical energy.

The methods based on a scalar Lyapunov function use the reduced admittance matrix, which means that the nodes where no current enters or leaves the network are eliminated. This elimination is carried out using matrix algebra and partitioning of the admittance matrix [46]. The most complex step, in determining the reduced admittance matrix, is to find the inverse of the $(n \times n)$ admittance matrix. However, the matrix is highly sparse, which enables to determine the inverse much faster than for the case of a full matrix. In order to use the algorithm proposed by Takahishi *et al.* [47], the matrix has to be transformed into a banded matrix by applying the reverse Cuthill-McKee algorithm, which complexity was shown in [48] to be proportional to the number of edges and, hence, proportional to $O(b)$. The complexity of calculating the whole inverse of a banded matrix can be approximated by $O(n^2 d)$ [49], where d is the bandwidth. It can be argued that in the case of power system networks the bandwidth of the ordered admittance matrix is small compared to the number of nodes and in large system smaller than the number of machines. In the IEEE 14-bus system d is larger than m. In the IEEE 300-bus system the bandwidth is considerably smaller than the number of machines (d: 35, m: 68).

In order to determine the transient energy of the system at the point of fault clearance, a time domain simulation of the whole system until the clearance has to be carried out. An explicit integration method such as Runge-Kutta (R-K) method is used to calculate the time response. In order to carry out the time domain simulation a set of algebraic equations and differential equations has to be solved. When utilizing the R-K method the complexity of solving the differential equation is proportional to $O(m^2)$. In order to solve the algebraic equation fast the sparsity of the admittance matrix is utilized and corresponding fast algorithms are used. By performing a LU-factorization and through forward and backward substitution the process can be considerably accelerated. The LU-factorization is, however, the operation with the highest computational cost and can be approximated by $O(d^2 n)$ [49].

After the values of the state variables at fault clearance are determined, the transient energy of the system at that point in time can be determined. The complexity of calculating the transient energy itself is $O(m^2)$, due to the double sum (see eq. (1)). Additionally to the state variables at fault clearance, the state variables at the during-fault stable equilibrium need to be known. To find the SEP the Newton Raphson (N-R) method is used and this leads to a complexity of $O(m^3)$.

TABLE II
COMPLEXITY ESTIMATION PROCESSES SHARED BY THE TWO SCALAR LYAPUNOV METHODS, d: BANDWIDTH OF BANDED MATRIX

Function	Time	Freq.	
Y from PMU	$O(m+n+b)$	1	$O(m+n+b)$
Reduce Matrices$^{\diamond}$	$O(dn^2)$	1	$O(dn^2)$
Time domain simulation†	$O(d^2 n)$	x	$xO(d^2 n)$
Determine V_{cl}	$O(m^3)$	1	$O(m^3)$
Determine V_{crit}			III-B1 & III-B2
Compare V_{cl} and V_{crit}	1	1	1
TOTAL‡(one disturbance)			$O(dn^2)$

$^{\diamond}$: Matrix reduction by partitioning of the matrix, see [46, section 2.1]
†: Using an explicit integration method Runge-Kutta with x time steps
‡: Runtime evaluation without determination of the critical energy

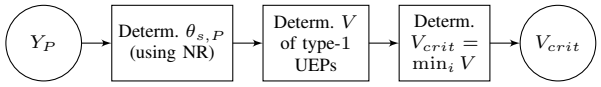

Fig. 4. Flow diagram determine V_{crit} in the closest UEP method

TABLE III
COMPLEXITY ESTIMATION CLOSEST UEP

Function	Time	Freq.	
Lyapunov method frame$^{\diamond}$	$O(dn^2)$	1	$O(dn^2)$
Determine V of type-1 UEPs	$O(m^3)$	m	$O(m^4)$
Determine V_{crit} (merge sort)	$O(m \log m)$	1	$O(m \log m)$
TOTAL(one disturbance)			$O(m^4)$

$^{\diamond}$: see table II

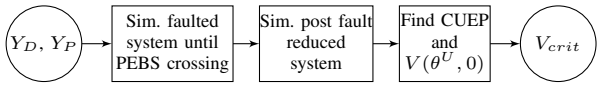

Fig. 5. Flow diagram determine V_{crit} in the BCU method

Finally, the determined transient energy at fault clearance and the critical energy of the post-fault system are compared.

1) Closest UEP: Figure 4 shows the block diagram of the closest UEP method, which determines the critical energy of the post-fault system by considering all type-1 UEP. The procedure to determine all m type-1 UEPs is the computational most expensive step, because the UEPs are identified using N-R method which comprises the inversion of an $2m \times 2m$-matrix resulting in a complexity proportional to $O(m^3)$.

The next step to identify the lowest critical energy is fast with $O(m \log m)$, when applying the merge sort algorithm.

The runtime evaluation results are presented in tab. III.

2) BCU method: The procedure to determine the critical energy when applying the BCU method is depicted as block diagram in fig. 5. The corresponding estimation of the runtime is depicted in table IV. When applying an explicit integration method to carry out the time domain simulation, its complexity is proportional to the square of the number of machines in the system. The second time domain simulation, which is of the reduced system, comprises a reduced number of differential equation, the number of equations and the complexity to solve those is, however, still proportional to the number of machines squared $O(m^2)$. In both cases in each simulation step a set of algebraic equations has to be solved using LU-factorization with complexity proportional to $O(d^2 n)$.

TABLE IV
COMPLEXITY ESTIMATION BCU

Function	Time	Freq.	
Lyapunov method frame$^{\diamond}$	$O(dn^2)$	1	$O(dn^2)$
Sim. until PEBS crossing †	$O(d^2n)$	y	$yO(d^2n)$
Sim. reduced system ‡	$O(d^2n)$	z	$zO(d^2n)$
Find CUEP	$O(m^3)$	1	$O(m^3)$
Determine V_{crit}	$O(m^2)$	1	$O(m^2)$
TOTAL(one disturbance)			$O(dn^2)$

$^{\diamond}$: see table II
†: Time dom. sim. continued using R-K with y time steps
‡: Time dom. sim. of red. system using R-K with z time steps

TABLE V
COMPLEXITY ESTIMATION EEAC

Function	Time	Freq.	
Y from PMU	$O(m+n+b)$	1	$O(m+n+b)$
Reduce Matrices$^{\diamond}$	$O(dn^2)$	1	$O(dn^2)$
Acceleration criteria	$O(m)$	m	$O(m^2)$
Identify critical	$O(m \log m)$	1	$O(m \log m)$
Aggregate & form OMIB	$O(m^2)$	1	$O(m^2)$
Determine δ_c, CCT	1	1	1
Compare t_{cl} and CCT	1	1	1
TOTAL(one disturbance)			$O(dn^2)$

$^{\diamond}$: Matrix reduction by partitioning of the matrix, see [46, section 2.1]

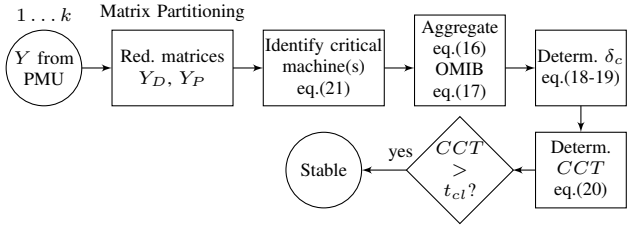

Fig. 6. Flow diagram extended equal area criterion

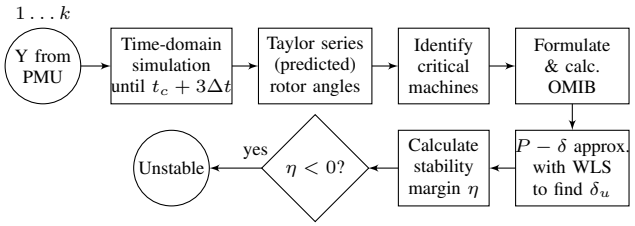

Fig. 7. Flow diagram modified predictive SIME

In order to find the controlling UEP, the N-R method is applied, where the results of the time domain simulation serve as an initial guess. The complexity of this step is consequently proportional to $O(m^3)$ and the calculation of V_{crit} is proportional to $O(m^2)$.

C. Equal Area Criterion Methods

The equal area in its pure form is promising to be very fast due to the lack of time domain simulation, the results, however, are expected to be conservative, because of the assumed constant voltage magnitude behind the transient reactance frozen at the time just before the fault occurrence. The SIME method tries to overcome these challenges through the combination of a direct method with time domain simulation.

1) Extended Equal Area Criterion: Figure 6 shows the procedure to determine stability using the EEAC method depicted as a block diagram. The method utilizes the admittance matrices provided from the PMU data procedure. The matrices are reduced as described in the preceding section ($O(dn^2)$). Following, the acceleration criterion is calculated for each machine, which allows to determine the critical machine(s). Therefore, the electrical power injection of each machine at fault occurrence has to be calculated $O(m^2)$.

The critical machines can then be identified after sorting the calculated acceleration criteria and identifying the machines with the largest values, this can be achieved by employing the merge sort algorithm ($O(m \log m)$).

In the next step the machines are aggregated into two equivalent machines and the OMIB system is determined. The number of operations associated with this process is proportional to the square of the number of machines.

Eventually, the critical angle and the CCT can be calculated and the results can be compared to the settings of the associated protection relays to evaluate stability. The results of the runtime assessment are shown in table V.

TABLE VI
COMPLEXITY ESTIMATION SIME

Function	Time	Freq.	
PMU data	$O(m+n+b)$	1	$O(m+n+b)$
Time domain sim.†	$O(d^2n)$	x	$xO(d^2n)$
Rotor angle (pred.)	1	m	$O(m)$
Ident. critical mach.	$O(m \log m)$	1	$O(m \log m)$
Aggregate & form OMIB ‡	$O(m)$	1	$O(m)$
$P - \delta$ approx.	1	1	1
Det. stability margin	1	1	1
TOTAL(one dist.)			$xO(d^2n)$

†: Explicit integration method (R-K method) with x time steps
‡: Differs to EEAC see text for explanation

2) Modified Predictive SIME: Figure 7 shows the transient stability assessment using the SIME method in a block diagram. The first step in the method based on SIME is to carry out a time-domain simulation until three time steps after the fault clearance. For the time domain simulation a number of differential equations proportional to the number of machines in the system have to be solved using an explicit integration method. The complexity of the individual differential equations varies and in some cases, e.g. the derivative of the rotor speed depends on the remaining generators, which leads to a total complexity estimation proportional to $O(m^2)$. The second step in the time domain simulation is to update the network parameters, therefore n algebraic equations have to be solved. Due to the fact that the admittance matrix is highly sparse special algorithms can be used to solve these equations and this results in a complexity approximated by $O(d^2n)$. In the following, the rotor angle of each individual machine advancing in time are predicted through a Taylor series expansion, where complexity is estimated to be proportional to $O(m)$. The predicted rotor angles are sorted and the critical machine candidates are identified through the biggest 'gap' (merge sort $O(m \log m)$). After identification of the critical machines, the machines can be aggregated and transformed into an OMIB system, this processes is less complex than in

the EEAC method due to the availability of parameters from the time domain simulation. The $P-\delta$-curve is then approximated with the simulated data and equation (24). Thereupon, the angle δ_u and time t_u, which meet the conditions stated in eq. (22), are identified and used to determine the stability margin utilizing (23). Eventually, by evaluating the stability margin the stability can be determined. The overall complexity of the SIME method can then be approximated by $xO(d^2n)$.

IV. Discussion

The results in tab. I to VI make it possible to identify the dominant operation in all methods. The complexity of the processes of handling the PMU data and updating of the matrices is linear and negligible in all the analyzed methods.

In the analysis of the closest UEP method it was shown that identification of all the type-1 UEPs is the most complex step with an associated complexity proportionally $O(m^4)$. In the case of the BCU method and the EEAC the operation with the highest associated computational costs is the reduction of the admittance matrix $O(dn^2)$, which is for the case of the EEAC in good agreement with the results in [26]. The SIME method overcomes some of the challenges of the EEAC method by including time domain simulation. This results in a complexity proportional to $O(d^2n)$.

In direct comparison with the closest UEP method, the BCU method is faster and less conservative because of the determination of the CUEP. The use of Lyapunov's methods compared to the EEAC allows more detailed models of the system and the machines. While the EEAC is restricted to the classic model, more complex structure-preserving models can be utilized in Lyapunov's method. The SIME circumvents the restriction to the classical model by using a detailed time domain simulation. It should be noted that the needed simulation is shorter compared to the BCU method.

In the complexity analysis the time domain simulation was assumed to be carried out using an explicit integration method, this method is not A-stable and, consequently, requires a small integration time step [44]. An improvement of the accuracy of the time domain simulation and the usage of larger time steps could be enabled by employing an implicit integration method, which uses for example the trapezoidal rule. However, this may lead to an increase of the complexity to $xO(dn^2)$. Because the aim of the paper is to investigate the method's real-time capability, it was decided to use a faster but less accurate integration method.

The results of the analysis of the time domain simulation are as well dependent on the accuracy of the representation of the loads. For this analysis it was assumed that the impedances of the loads vary during the disturbance and, consequently, the admittance matrix needs to be updated and factorized in each simulation step. When load impedances are assumed to be constant, the simulation is still dominated by the LU-factorization, but it has to be carried out only two times.

Another critical issue is the comparison of complexities proportional to the number of machines and proportional to the number of nodes in the system. Nowadays, due to the centralized power generation, in a power system the number of machines is considerably lower than the number of nodes. This ratio is to change in the future, due to increasing installation of DER. Consequently, the number of machines in the system could approach values closer to the number of nodes, which may lead to changes in the complexity evaluation, e.g. domination of the Lyapunov method frame by $O(m^3)$.

Under the consideration that in the future power system the number of machines in the system will be considerably higher than today, the analysis of the complexity suggest that the SIME method may provide the fastest stability evaluation of the system. However, an additional uncertainty is introduced due to the prediction of the rotor angles using a Taylor series and a weighted least-square approximation of the $P-\delta$-curve.

V. Conclusion

The paper begins with a review of methods using Lyapunov's method and the EAC, which are further analyzed.

When using the Lyapunov approach the challenge is to derive an appropriate energy function, which fulfills the criteria for a Lyapunov function, and to identify the appropriate critical energy for the stability evaluation. The BCU method combined with a structure-preserving model seems to overcome these challenges in a promising way.

The second approach uses the equal area criterion. The EEAC method allows to carry out the transient stability assessment without the need for time domain simulations, but requires the reduced admittance matrix and is limited to the use of the classical model, which leads to conservative results.

SIME overcomes some of the limitation of the EEAC method through the use of a detailed time domain simulation.

The results suggest that the methods utilizing the equal area criterion are faster than the methods using energy functions when assessing transient stability in large systems with distributed power generation. The SIME method may be the preferable tool to fast evaluate the transient stability of a large power system, due to the less conservative results.

VI. References

[1] The Danish Ministry of Climate and Energy, "Energy Strategy 2050 - from coal, oil and gas to green energy," The Danish Ministry of Climate and Energy, Stormgade 2-6 1470 Copenhagen K Denmark, Tech. Rep., Feb. 2011.

[2] F. Li *et al.*, "Smart Transmission Grid: Vision and Framework," *IEEE Trans. Smart Grid*, vol. 1, no. 2, pp. 168–177, Sep. 2010.

[3] A. Phadke, J. Thorp, and M. Adamiak, "A New Measurement Technique for Tracking Voltage Phasors, Local System Frequency, and Rate of Change of Frequency," *IEEE Trans. Power App. Syst.*, vol. 102, no. 5, pp. 1025–1038, May 1983.

[4] A. Phadke and J. Thorp, *Synchronized Phasor Measurements and Their Applications*. Springer Verlag, 2008.

[5] A. Phadke and R. De Moraes, "The Wide World of Wide-Area Measurement," *IEEE Power Energy Mag.*, vol. 6, no. 5, pp. 52–65, Sep. 2008.

[6] S. Skok, I. Ivankovic, and Z. Cerina, "Applications Based on PMU Technology for Improved Power System Utilization," in *Power Engineering Society General Meeting, 2007. IEEE*, Jun. 2007, pp. 1–8.

[7] D. Novosel *et al.*, "Dawn of the grid synchronization," *IEEE Power Energy Mag.*, vol. 6, no. 1, pp. 49–60, Jan. 2008.

[8] H. Jóhannsson, "Development of early warning methods for electric power systems," Ph.D. dissertation, 2011.

[9] H. Jóhannsson *et al.*, "Real-time stability assessment based on synchrophasors," in *Proceedings of 2011 IEEE Trondheim PowerTech*, Jun. 2011, pp. 1–8.

[10] M. Glavic and T. Van Cutsem, "Wide-Area Detection of Voltage Instability From Synchronized Phasor Measurements. Part I: Principle," *IEEE Trans. Power Syst.*, vol. 24, no. 3, pp. 1408–1416, Aug. 2009.

[11] ——, "Wide-Area Detection of Voltage Instability from Synchronized Phasor Measurements. Part II: Simulation Results," *IEEE Trans. Power Syst.*, vol. 24, no. 3, pp. 1417–1425, Aug. 2009.

[12] G. E. Gless, "Direct Method of Liapunov Applied to Transient Power System Stability," *IEEE Trans. Power App. Syst.*, vol. PAS-85, no. 2, pp. 159–168, Feb. 1966.

[13] A. H. El-Abiad and K. Nagappan, "Transient Stability Regions of Multimachine Power Systems," *IEEE Trans. Power App. Syst.*, vol. PAS-85, no. 2, pp. 169–179, Feb. 1966.

[14] T. Athay, R. Podmore, and S. Virmani, "A practical Method for the Direct Analysis of Transient Stability," *IEEE Trans. Power App. Syst.*, vol. PAS-98, no. 2, pp. 573–584, Mar. 1979.

[15] N. Kakimoto, Y. Ohsawa, and M. Hayashi, "Tansient Stability Analysis of Multimachine Power Systems with Field Flux Decays via Lyapunov's Direct Method," *IEEE Trans. Power App. Syst.*, vol. PAS-99, no. 5, pp. 1819–1827, Sep. 1980.

[16] M. Ribbens-Pavella and F. J. Evans, "Direct Methods for Studying Dynamics of Large-scale Electric Power Systems A Survey," *Automatica*, vol. 21, no. 1, pp. 1–21, Jan. 1985.

[17] H.-D. Chiang, F. F. Wu, and P. P. Varaiya, "Foundations of the Potential Energy Boundary Surface Method for Power Systern Transient Stability Analysis," *IEEE Trans. Circuits Syst.*, vol. 35, no. 6, pp. 712–728, Jun. 1988.

[18] A. A. Fouad, V. Vittal, and T. K. Oh, "Critical Energy for Direct Transient Stability Assessment of a Multimachine Power System," *IEEE Trans. Power App. Syst.*, vol. PAS-103, no. 8, pp. 2199–2206, Aug. 1984.

[19] H.-D. Chiang, F. F. Wu, and P. P. Varaiya, "A BCU Method for Direct Analysis of Power System Transient Stability," *IEEE Trans. Power Syst.*, vol. 9, no. 3, pp. 1194–1208, Aug. 1994.

[20] A. R. Bergen and D.J. Hill, "A Structure Preserving Model for Power System Stability Analysis," *IEEE Trans. Power App. Syst.*, vol. PAS-100, no. 1, pp. 25–35, Jan. 1981.

[21] Y. Zou, M.-H. Yin, and H.-D. Chiang, "Theoretical Foundation of the Controlling UEP Method for Direct Transient-Stability Analysis of Network-Preserving Power System Models," *IEEE Trans. Circuits Syst. - I: Fundam. Theory Appl.*, vol. 50, no. 10, pp. 1324–1336, Oct. 2003.

[22] L. B. Jocic, M. Ribbens-Pavella, and D. D. Siljak, "Multimachine Power Systems: Stability, Decomposition, and Aggregation," *IEEE Trans. Autom. Control*, vol. AC-23, no. 2, pp. 325–332, Apr. 1978.

[23] M. Araki, M. Saeki, and B. Kondo, "Application of a New Stability criterion of Composite Systems to Multimachine Power Systems," *IEEE Trans. Autom. Control*, vol. AC-25, no. 3, pp. 480–483, Jun. 1980.

[24] A. N. Michel, A. A. Fouad, and V. Vittal, "Power System Transient Stability Using Individual Machine Energy Functions," *IEEE Trans. Circuits Syst.*, vol. 30, no. 5, pp. 266–276, May 1983.

[25] O. Dahl, *Electric Power Circuits. Vol. II: Power System Stability*. New York: McGraw-Hill, 1938.

[26] Y. Xue and M. Pavella, "Extended equal-area criterion: an analytical ultra-fast method for transient stability assessment and preventive control of power systems," *International Journal of Electrical Power & Energy Systems*, vol. 11, no. 2, pp. 131–149, Apr. 1989.

[27] Y. Zhang *et al.*, "SIME: A hybrid approach to fast transient stability assessment and contingency selection," *Electrical Power & Energy Systems*, vol. 19, no. 3, pp. 195–208, Mar. 1997.

[28] D. Ernst *et al.*, "A Unified Approach to Transient Stability Contingency Filtering, Ranking and Assessment," *IEEE Trans. Power Syst.*, vol. 16, no. 3, pp. 435–443, Aug. 2001.

[29] D. Ruiz-Vega and M. Pavella, "A Comprehensive Approach to Transient Stability Control: Part I - Near Optimal Preventive Control," *IEEE Trans. Power Syst.*, vol. 18, no. 4, pp. 1446–1453, Nov. 2003.

[30] M. Pavella, D. Ernst, and D. Ruizvega, *Transient Stability of Power Systems: A Unified Approach to Assessment and Control*. Kluwer Academic Publishers, 2000.

[31] C.-W. Liu and J. Thorp, "Application of synchronised phasor measurements to real-time transient stability prediction," *Generation, Transmission and Distribuion, IEE Proceedings*, vol. 142, no. 4, pp. 355–360, Jul. 1995.

[32] C.-W. Liu and J. S. Thorp, "New Methods for Computing Power System Dynamic Response for Real-Time Transient Stability Prediction," *IEEE Trans. Circuits Syst. - I: Fundam. Theory Appl.*, vol. 47, no. 3, pp. 324–337, Mar. 2000.

[33] L. Wehenkel, T. Van Cutsem, and M. Ribbens-Pavella, "Decision Trees applied to on-line Transient Stability Assessment of Power Systems," in *IEEE International Symposium on Circuits and Systems, 1988.*, vol. 2, Jun. 1988, pp. 1887–1890.

[34] ——, "An Artificial Intelligence Framework for on-line Transient Stability Assessment of Power Systems," *IEEE Trans. Power Syst.*, vol. 4, no. 2, pp. 789–800, May 1989.

[35] H.-Z. Guo *et al.*, "Study on power system transient instability detection based on wide area measurement system," *European Transactions on Electrical Power*, vol. 20, no. 2, pp. 184–205, Mar. 2010.

[36] V. Kolluri *et al.*, "Fast Fault Screening Approach to Assessing Transient Stability in Entergy's Power System," in *Power Engineering Society General Meeting, 2007. IEEE*, Jun. 2007, pp. 1–6.

[37] A. A. Fouad and V. Vittal, "The transient energy function method," *International Journal of Electrical Power & Energy Systems*, vol. 10, no. 4, pp. 233–246, Oct. 1988.

[38] J. D. Meiss, *Differential Dynamical Systems*, A. Aceves *et al.*, Eds. SIAM, 2007, vol. 1.

[39] H.-D. Chiang, F. F. Wu, and P. P. Varaiya, "Foundations of Direct Methods for Power System Transient Stability Analysis," *IEEE Trans. Circuits Syst.*, vol. 34, no. 2, pp. 160–173, Feb. 1987.

[40] P. P. Varaiya, F. F. Wu, and R.-L. Chen, "Direct Methods for Transient Stability Analysis of Power Systems: Recent Results," in *Proceedings of the IEEE*, vol. 73, no. 12, Dec. 1985, pp. 1703–1715.

[41] A. A. Fouad and S. E. Stanton, "Transient Stability of a Multi-Machine Power System Part I: Investigation of System Trajectories," *IEEE Trans. Power App. Syst.*, vol. PAS-100, no. 7, pp. 3408–3416, Jul. 1981.

[42] P. Sauer and M. A. Pai, *Power System Dynamics and Stability*, E. Svendson, M. Horton, and B. M. de Leon, Eds. Prentice Hall, 1998.

[43] A. A. Fouad and S. E. Stanton, "Transient Stability of a Multi-Machine Power System Part II: Critical Transient Energy," *IEEE Trans. Power App. Syst.*, vol. PAS-100, no. 7, pp. 3417–3424, Jul. 1981.

[44] P. Kundur, *Power System Stability and Control*, N. J. Balu and M. G. Lauby, Eds. McGraw-Hill Inc., 1994.

[45] J. Kleinberg and E. Tardos, *Algorithm Design*, M. Suarez-Rivas, Ed. Boston: Pearson Addison Wesley, 2006.

[46] F. Dorfler and F. Bullo, "Kron Reduction of Graphs with Applications to Electrical Networks," *Dynamical Systems*, pp. 1–28, Feb. 2011. [Online]. Available: http://arxiv.org/abs/1102.2950

[47] K. Takahishi, J. Fagan, and M. S. Chen, "Formation of a sparse bus admittance matrix and its application to short circuit study," *8th PICA Conference Proceedings*, pp. 63–69, 1973.

[48] W. M. Chan and A. George, "A linear time implementation of the reverse cuthill-McKee Algorithm," *BIT Numerical Mathematics*, vol. 20, no. 1, pp. 8–14, Aug. 1980.

[49] H. Niessner and K. Reichert, "On computing the inverse of a Sparse Matrix," *International Journal for Numerical Methods in Engineering*, vol. 19, no. 10, pp. 1513–1526, Oct. 1983.

VII. Biographies

Tilman Weckesser (S'12) received the M.Sc. degree in sustainable energy engineering from the Technical University of Denmark (DTU), Lyngby, in 2011. He is currently a Ph.D. student at the Centre for Electric Technology (CET), DTU.

His research interests are in the field of power system stability with a focus on the development of fast stability assessment methods.

Hjörtur Jóhannsson (M'10) received the M.Sc. and the PhD degree in Electrical Engineering from Technical University of Denmark, in 2007 and 2011 respectively. He is currently an assistant professor at CET, Department of Electrical Engineering, Technical University of Denmark.

His research interests concern the development of methods that provide an early warning for instability in electric power systems, and power systems dynamics, stability and control.

Stefan Sommer (S'11) received the M.Sc. degree in Mathematics in 2008 and the Ph.D. degree in Computer Science in 2012, both from the University of Copenhagen (UCPH). He is currently holding a position as postdoctoral researcher at the Technical University of Denmark (DTU), CET.

His research interests cover computational aspects of power system stability and control with focus on numerical algorithms and mathematical modeling.

Jacob Østergaard (M'95-SM'09) received the M.Sc. degree in electrical engineering from the Technical University of Denmark (DTU), Lyngby, in 1995. He was with the Research Institute of Danish Electric Utilities for 10 years. Since 2005 he has been Professor and Head of Centre for Electric Technology, DTU.

His research interests cover smart grids with focus on system integration of renewable energy and distributed energy resources, control architecture for future power system, and flexible demand.

Appendix B

Impact of Model Detail of Synchronous Machines on Real-time Transient Stability Assessment

This paper has been presented at the 2013 IREP Symposium-Bulk Power System Dynamics and Control - IX (IREP) in Rethymnon, Greece and has been published as part of the conference proceedings.

2013 IREP Symposium-Bulk Power System Dynamics and Control –IX (IREP), August 25-30, 2013, Rethymnon, Greece

Impact of Model Detail of Synchronous Machines on Real-time Transient Stability Assessment

Tilman Weckesser, Hjörtur Jóhannsson and Jacob Østergaard
Centre for Electric Power and Energy, Department
of Electrical Engineering, Technical University of Denmark, 2800 Lyngby

Abstract

In this paper, it is investigated how detailed the model of a synchronous machine needs to be in order to assess transient stability using a Single Machine Equivalent (SIME). The results will show how the stability mechanism and the stability assessment are affected by the model detail. In order to identify the transient stability mechanism, a simulation with a high-order model was used as reference. The Western System Coordinating Council System (WSCC) and the New England & New York system are considered and simulations of an unstable and a stable scenario are carried out, where the detail of the machine models is varied. Analyses of the results suggest that a 4^{th}-order model may be sufficient to represent synchronous machines in transient stability studies.

Introduction

Today's society is highly dependent on a stable and secure supply of electric power. In the future, this is not expected to change. The shift from fossil energy sources to renewable energy sources, which can be observed in many countries around the world and the aim of reaching a Danish society with minimal dependency on fossil fuels [1], represents a great challenge for the power system. These ambitious plans can only be achieved, when a large share of the electric power generation uses renewable energy sources, whose energy sources are non-controllable sources such as wind and solar radiation [1].
The integration of such non-controllable sources will lead to increased fluctuations of the power system's operating point. This will make the planning of secure and stable operation hours ahead no longer feasible and the need for real-time stability assessment tools will arise.
In [2], [3], [4] phasor measurement technology is said to be the technology enabling the development of real-time wide area monitoring and control applications [5], [6].
Consequently, recently developed stability assessment methods try to solve the task of on-line security and stability assessment by utilizing synchronized phasor measurements. This is done by either developing an entirely new approach such as in [7], [8] or by adaption of an off-line method to real-time operation, e.g. in [9], [10].
In [11] the adaptability of various direct transient stability assessment (TSA) methods to real-time operation was investigated. The analysis showed that the SIME method allows the fastest TSA. The method utilizes input from time-domain simulation. In order to achieve fast computation, it is desirable to reduce the number of differential equations to be solved. Hence, in the following it is investigated, how detailed the model of a synchronous generator needs to be to depict the transient stability mechanism accurately enough to allow a detection of the instability and its origin. However, it should be noted that in this work the focus is solely on assessing first swing instability.
In this work the RAMSES software [12] developed at the University of Liège was used to perform the dynamic time-domain simulations.

Transient Stability Assessment

Transient stability assessment (TSA) analyzes the system's ability to sustain large transient disturbances such as loss of generation or failure on transmission facilities [13]. These disturbances lead to large excursion of the machines rotor angle, which are described by the strongly non-linear relations governing the dynamics in power systems. Consequently, transient stability cannot be assessed through linearization of the system equations.

Direct methods

In order to allow fast transient stability assessment, direct TSA methods were developed. These methods try to avoid explicitly solving the system differential equations. One of the main approaches is based on Lyapunov's method [14] and a second main approach is applying the equal area criterion [15].

Lyaponov's method. In order to apply Lyapunov's method the system is described by a transient energy function, which allows determining transient stability after identification of the stable and unstable equilibrium point (UEP) of the post-fault system [14]. However, since the system is described by one single transient energy

This research was supported by the Danish Strategic Research Council.

978-1-4799-0199-9/13/$31.00 ©2013 IEEE

function, it is difficult to determine the origin of the instability. One of the most recent developments applying this approach is the so called BCU method [16].

Equal Area Criterion. The equal area criterion (EAC) allows assessing transient stability of one-machine infinite bus (OMIB) systems without explicitly solving the swing equation [13]. The criterion essentially states that the system needs to be capable of absorbing the kinetic energy of the generator gained during the fault. The gained kinetic energy and the energy absorbing capability are represented by areas defined by the mechanical power and the $P-\delta$-curve, which describes the non-linear relation of the electric power injection and the rotor angle. Hence, with certain assumptions and simplifications the stability criteria can be formulated as an integral.
This approach was further developed with the extended equal area criterion [17] and most recently with the hybrid method SIME [15].
An analysis of the computational burden of the two mentioned methods with respect to real-time implementation was carried out in [11]. The results suggest that methods based on the EAC are faster than methods using Lyapunov's method. Hence, in the following SIME is considered for the fast screening method.

Single Machine Equivalent (SIME) Method

Transient stability assessment with a SIngle Machine Equivalent (SIME) is based on the Equal Area Criterion and considered to be a hybrid method, since it combines the advantages of a direct method and time-domain simulation. A detailed description of the method can be found in [15].

Concept. The SIME method determines in each simulation step parameters of a candidate one-machine infinite bus (OMIB) system, which describes the dynamics of a critical generator group and a group of remaining (non-critical) generators. The machines in the system are split up into the critical and the non-critical group corresponding to their rotor angles. The machines in each group are aggregated and the parameters of the OMIB system are determined. After aggregation of the machines the transient stability of the resulting OMIB can be assessed using the equal area criterion.

Transient stability margin. The stability margin of such a system can be calculated as follows [15].

$$\eta = -\int_{\delta_i}^{\delta_u} P_a d\delta - 1/2\, M\omega_i^2 \quad (1)$$

M	Inertia coefficient of candidate OMIB $[s^2/rad]$
P_a	Accelerating power of candidate OMIB $[pu]$
δ_i	Current rotor angle of candidate OMIB $[rad]$
δ_u	Rotor angle at UEP of candidate OMIB $[rad]$
η	Transient stability margin in $[rad]$
ω_i	Current rotor speed of candidate OMIB $[rad/s]$

Here a negative margin represents an unstable case and a positive margin a stable case [15]. The unit of the stability margin computed with eq. (7) is radians. Often the margin is normalized with respect to the inertia coefficient of the OMIB, which results in a normalized stability margin with unit $(rad/s)^2$.

Implementation. In this case the implementation of SIME is used to carry out a fast screening of the current system condition with respect to N-1-contingencies and first swing transient stability. The implementation is derived from E-SIME, e.g. described in [15], [18]. E-SIME uses measurements of the post-fault system, which are acquired in real-time. These measurements are replaced in this implementation by data received from the time-domain simulation software RAMSES. This implementation of SIME is called preventive SIME [15]. With the application of SIME the aim is to get an early stop criterion for the simulation, which declares a contingency to be definitely stable or unstable.
In order to determine first swing stability of the particular contingency scenario, a time-domain simulation is run until at least three data sets of the post-fault system are available. Then the predictive SIME method is executed the first time and, subsequently, the stability assessment is updated with data sets acquired in each successive simulation step.
In the following the procedure of preventive SIME is described in more detail (see also [11] and [15]).
Step 1: Consider the first three data sets received from the time-domain simulation in the post-fault configuration. *Step 2:* Predict the rotor angle of each individual generator some time ahead ($\sim 100ms$) using Taylor series expansion truncated after the quadratic term. *Step 3:* Rank generators according to the predicted rotor angles and identify the critical machine candidates looking for the maximum angular deviation of two successive machines. The machines above this gap form the candidate critical machines and the ones below the candidate the non-critical machines. The machines are then aggregated accordingly and the candidate OMIB is determined. *Step 4:* Subsequently, the parameter of the candidate OMIB can be computed and, utilizing the accelerating power and the rotor angle from at least three successive data sets, the $P_a - \delta$ curve can be estimated as follows.

$$P_a(\delta) = a\delta^2 + b\delta + c \quad (2)$$

Note: First, the parameters a, b and c can be determined using the three acquired data sets and, in the following, with additional acquired data the prediction can be refined using a weighted least square technique. *Step 5:* The angle δ_u at the unstable equilibrium point is determined by solving $P_a(\delta_u) = 0$ and by checking if the instability conditions of eq. (3) are met.

$$P_a(\delta_u) = 0;\ \dot{P}_a(\delta_u) > 0 \quad (3)$$

If the instability conditions (3) are not met, then a new set of data is acquired and the procedure is repeated from *Step 2*. If the conditions are met the stability margin is computed utilizing eq. (1), then a new set of data is

acquired and the *Steps 2* to *5* are repeated to refine the computed δ_u and the estimated stability margin η. The procedure is terminated when the stability margin converged to a constant value or the angle of maximum excursion δ_r is reached where the following conditions are met.

$$P_a(\delta_r) < 0;\ \omega_r = 0 \tag{4}$$

Since the method to determine transient stability requires time-domain simulation a speed up of the assessment can be achieved, when the model detail of the power system components, used in the simulation, can be reduced. Hence, in the following the method is tested with reduced order synchronous machine models.

Synchronous machine models

In the following section the described synchronous machine (SM) models were adopted from [19]. The 6th- and 4th-order model are readily integrated in RAMSES. The 3rd-order and 2nd-order model were realized through appropriate selection of the time constants in the 4th-order model.

Four winding model (6th-order)

In the 6th-order model, four windings are considered, two on the q-axis and two on the d-axis. However, the network and stator transients are neglected. According to [13] the dynamics introduced by these transients may be neglected and this will lead to slightly conservative results, which is preferable in stability studies and in particular for fast screening where all critical and unstable scenarios should be identified.

In dynamic analysis, when using the 6th-order model, the synchronous machine is described by the following six equations [19].

$$\begin{aligned} T'_{do}\frac{dE'_q}{dt} = {} & -E'_q - (X_d - X'_d)\Big[I_d \\ & - \frac{X'_d - X''_d}{(X'_d - X_{ls})^2}\big(\psi_{1d} \\ & + (X'_d - X_{ls})I_d + E'_q\big)\Big] \\ & + E_{fd} \end{aligned} \tag{5}$$

$$T''_{do}\frac{d\psi_{1d}}{dt} = -\psi_{1d} + E'_q - (X'_d - X_{ls})I_d \tag{6}$$

$$\begin{aligned} T'_{qo}\frac{dE'_d}{dt} = {} & -E'_d + \big(X_q - X'_q\big)\Big[I_q \\ & - \frac{X'_q - X''_q}{\big(X'_q - X_{ls}\big)^2}\big(\psi_{2q} \\ & + \big(X'_q - X_{ls}\big)I_q + E'_d\big)\Big] \end{aligned} \tag{7}$$

$$T''_{qo}\frac{d\psi_{2q}}{dt} = -\psi_{2q} + E'_d - \big(X'_q - X_{ls}\big)I_q \tag{8}$$

$$\frac{d\delta}{dt} = \omega - \omega_s \tag{9}$$

$$\begin{aligned} \frac{2H}{\omega_s}\frac{d\omega}{dt} = {} & T_M - \frac{X''_d - X_{ls}}{(X'_d - X_{ls})}E'_q I_q \\ & - \frac{X'_d - X''_d}{(X'_d - X_{ls})}\psi_{1d} I_q \\ & - \frac{X''_q - X_{ls}}{\big(X'_q - X_{ls}\big)}E'_d I_d \\ & + \frac{X'_q - X''_q}{\big(X'_q - X_{ls}\big)}\psi_{2q} I_d \\ & - \big(X''_q - X''_d\big)I_d I_q - T_{FW} \end{aligned} \tag{10}$$

$E'_{d,q}$	Transient voltage in d-/q-axis
E_{fd}	Field voltage
H	Inertia constant
$I_{d,q}$	Current in d-/q-axis
$T'_{do,qo}$	Transient time constant of d- /q-axis
$T''_{do,qo}$	Subtransient time constant of d- /q-axis
T_{FW}	Additional damping torque prop. to rotor speed
T_M	Mechanical torque
$X'_{d,q}$	Transient reactance in d- /q-axis
$X''_{d,q}$	Subtransient reactance in d-/q-axis
X_{ls}	Leakage reactance
δ	Rotor angle
ψ_{1d}	Flux linkage d-axis damper winding
ψ_{2q}	Flux linkage q-axis damper winding
ω	Rotor speed
ω_s	Synchronous rotor speed: $2\pi f$

Equation (5) and (6) describe the dynamics in the d-axis, while equation (7) and (8) describe the dynamics in the q-axis. Equation (9) and (10) represents the well-known swing equation.

In all models additional damping may be added through the optional torque component T_{FW}, which introduces a damping torque proportional to the rotational speed.

Two-axis model (4th-order)

In the 4th-order two axis model, the damper winding dynamics ψ_{1d} and ψ_{2q} are neglected. As described in [19], this is achieved by setting T''_{do} and T''_{qo} equal to zero, which leads to the following mathematical description of the synchronous machine.

$$T'_{do}\frac{dE'_q}{dt} = -E'_q - (X_d - X'_d)I_d + E_{fd} \tag{11}$$

$$T'_{qo}\frac{dE'_d}{dt} = -E'_d + \big(X_q - X'_q\big)I_q \tag{12}$$

$$\frac{d\delta}{dt} = \omega - \omega_s \tag{13}$$

$$\begin{aligned} \frac{2H}{\omega_s}\frac{d\omega}{dt} = {} & T_M - E'_q I_q - E'_d I_d - \big(X'_q - X'_d\big)I_d I_q \\ & - T_{FW} \end{aligned} \tag{14}$$

It should be noted that, while the ψ_{1d} and ψ_{2q} dynamics are neglected, the E'_d and E'_q dynamics are maintained.

One-axis model (3rd-order)

In the one-axis model, the representation of the synchronous machine is reduced by another degree. Therefore, the damper windings dynamics E'_d are eliminated. This reduction is achieved by setting T'_{qo} equal to zero and results in the following equations [19].

$$T'_{do}\frac{dE'_q}{dt} = -E'_q - (X_d - X'_d)I_d + E_{fd} \quad (15)$$

$$\frac{d\delta}{dt} = \omega - \omega_s \quad (16)$$

$$\frac{2H}{\omega_s}\frac{d\omega}{dt} = T_M - E'_q I_q - (X_q - X'_d)I_d I_q - T_{FW} \quad (17)$$

Classical model (2nd-order)

The last synchronous machine model, which is considered in this analysis, is the classical model. In this model the voltage behind the transient reactance is assumed to be constant. For such a representation only the swing equation is needed to describe the dynamics of a synchronous machine.

$$\frac{d\delta}{dt} = \omega - \omega_s \quad (18)$$

$$\frac{2H}{\omega_s}\frac{d\omega}{dt} = T_M - \frac{E'V_T}{X'_d}\sin(\delta - \theta_T) - T_{FW} \quad (19)$$

E' Internal voltage behind transient reactance
V_T Terminal voltage

Test systems and scenarios

Two test systems, namely the Western System Coordinating Council system as well as the New England & New York system, were considered for the analysis. For each of the test systems a transient stable and a transient unstable test scenario were considered.

Western System Coordinating Council (WSCC)

The WSCC system is a 9-bus system with 3 generators. The load flow and the dynamic data were adopted from [19]. However, in order to further stress the system, the system loading was increased by approximately 50%. The power generation of the generators was increased correspondingly.
The parameters of the synchronous machine models can be seen in Table 1. In the original WSCC system the generators are solely described by a 4th-order model. Consequently, for the 6th-order model standard parameter were added, which were taken from [13].
In order to allow assessment of solely the influence of the generator model, the excitation systems were removed from the model and the excitation was assumed to be manually. Furthermore, no governor model was implemented.

Table 1 Parameter of the three generators in the WSCC test system on machine basis adopted from [15]

Parameter	GEN-1	GEN-2	GEN-3
MVA_{base}	500.0	300.0	300.0
$H[s]$	4.728	2.133	1.003
$X_d[pu]$	0.7300	2.6874	3.9375
$X'_d[pu]$	0.3040	0.3594	0.5439
$X''_d[pu]$[1]	0.2500	0.2500	0.3000
$X_q[pu]$	0.4845	2.5935	3.7734
$X'_q[pu]$	0.3040	0.3594	0.5439
$X''_q[pu]$[1]	0.2500	0.2500	0.3000
$T'_{do}[s]$	8.690	6.000	5.890
$T''_{do}[s]$[1]	0.030	0.045	0.030
$T'_{qo}[s]$	0.310	0.535	0.600
$T''_{qo}[s]$[1]	0.040	0.035	0.040

[1]: Standard parameter chosen from [13]

In order to assess how detailed the synchronous machine model needs to be to depict the instability mechanism of the first swing accurately and to allow correct stability assessment using SIME, two test scenarios are considered, an unstable and a stable case.
In [20] it is stated that it is sufficient to represent turbogenerators by their 6th-order model in stability analysis. Therefore, the simulations using the 6th-order generator model serve as a reference case and it is assumed to reflect reality sufficiently.

Unstable case. In the unstable case, the stressed system is driven to instability through the loss of the heavily loaded line connecting bus 7 and 8 100 ms after simulation begin. In this case, it is assumed that the line is tripped due to overloading and it is not reconnected.

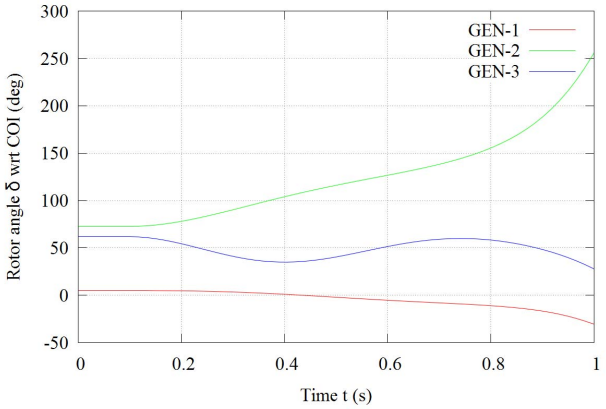

Fig. 1: Unstable response of the rotor angles of the generators to the transient disturbance

Figure 1 shows that the loss of the heavily loaded transmission line triggers a first swing instability and causes generator 2 to lose synchronism.

Stable case. In the stable case the same fault as in the unstable case is considered, but the transmission line is reconnected after $150ms$. This reconnection leads to a relative deceleration of the affected generators and

eventually the system reaches a new steady state operating point. Figure 2 displays the rotor angle response of all three generators.

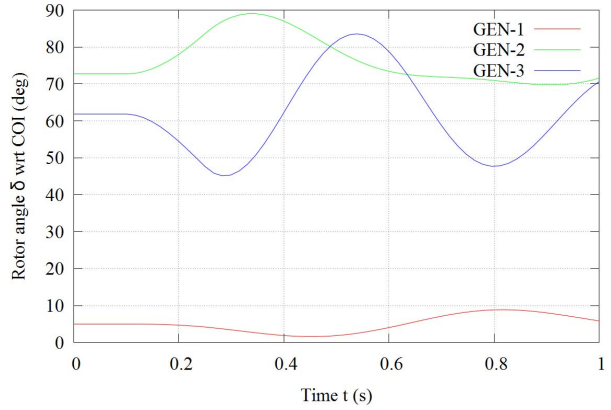

Fig. 2: Stable response of the rotor angles of the generators to the transient disturbance

New England and New York

The second test system represents the New England and New York system. The system was adopted from Graham Rogers [21] and consists of sixteen generators and 68 buses. The synchronous generators are modeled using a 6th-order model, thermal turbine/governor model and static exciters. All generators but generator 7 and 14 are equipped with a PSS. The parameters and a detailed model description can be found in [21]. In the following two transient stability scenarios are considered.

Stable case. The stable case is adopted from chapter 5 in [21]. The considered fault is a three phase short circuit very close to bus 21 applied $1s$ after simulation begin. The fault is cleared after $150ms$ by opening the breakers at both ends of the transmission line connecting bus 16 and bus 21. The case represents a marginal stable scenario, which is apparent due to the large angular excursion of the rotor angles of the generators 6 and 7. Figure 3 shows the rotor angles over time, when the synchronous machines are represented by a 6th-order model. Like before this simulation will serve as reference for the TSA when using SIME.

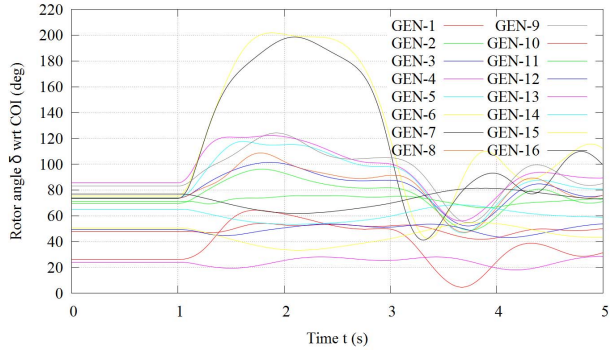

Fig. 3: Stable response of the rotor angles of the generators to the transient disturbance

Unstable case. In order to obtain an unstable case, the power flow of the marginal stable case was modified. To further stress the system, the power generation of the critical generators was increased. Therefore, the power generation of generator 4 was decreased by $10MW$ and at the same time the power output of generator 6 was increased by the same amount. This accounts to a change in power generation of approx. 1.5% at both generators.
This modification of the power flow and the same fault as in the stable case triggered a transient first swing instability and the loss of synchronism of generators 6 and 7. The reference unstable case using 6th-order synchronous machine models and the rotor angles over time of all 16 generators can be seen in Figure 4.

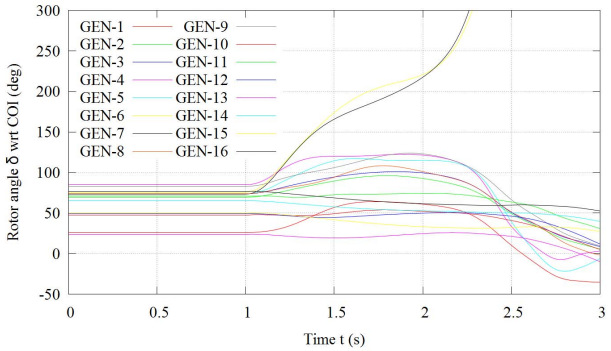

Fig. 4: Unstable response of the rotor angles of the generators to the transient disturbance

Simulation results

In the following section, the simulation results using the various generator models are discussed with respect to representation of the stability mechanism and possibility to assess transient stability using preventive SIME.

Representation of the stability mechanism

In order to detect instability correctly, the stability mechanism has to be depicted accurately. For the case of transient stability, the rotor angles of the machines allow to detect loss of synchronism and the origin of the stability problem. Hence, a comparison of the rotor angles may give an indication on the needed model detail. In the following, the rotor angle responses of the critical machines are compared when using varying SM models.

WSCC unstable and stable case. In the two cases generator 2 was identified as the critical machine. A comparison of the unstable rotor angle responses of generator 2 using the four different machine models is shown in Figure 5.
It can be seen that approximately for the first $400\,ms$ after the fault, the development of the rotor angles of generator 2 over time are differing only slightly. However, thereafter the development begins to diverge. The generator appears to be first swing stable, when using low order generator models such as the 2nd- and 3rd-order

model. The simulation using a 4th-order model shows the same instability mechanism as the reference case using the 6th-order model. It even seems to be slightly pessimistic since the rotor angle is increasing faster than in the reference case.

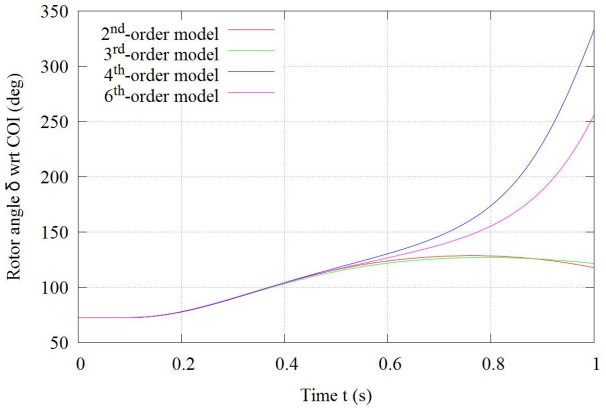

Fig. 5: Unstable case: Rotor angle response of generator 2 using the four different generator model details

A comparison of the rotor angle trajectories of the stable case lead to a similar conclusion. Figure 6 shows that the rotor angle trajectories are similar for the first $200\,ms$ after the disturbance, but begin to deviate subsequently. The deviations for 2nd- and 3rd-order models are larger than for the 4th-order model. However, the first swing characteristic is the same for all four models, where the 4th-order model is, with respect to the maximum angle excursion, slightly more pessimistic and the 3rd-order model slightly more optimistic.

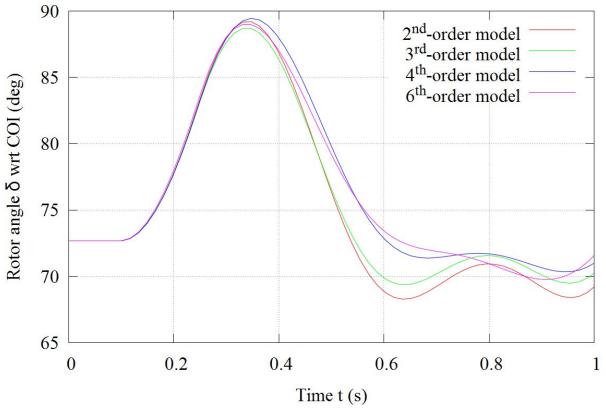

Fig. 6: Stable case: Rotor angle response of generator 2 using the four different generator model details

New England and New York. For the two scenarios of the second test system the generators 6 and 7 were identified as critical. Subsequently, the rotor angle trajectories of one of the critical generators (generator 6) are compared for the stable and unstable case. The different rotor angle curves are obtained from varying the SM model.
Figure 7 shows the rotor angle responses for the stable case and it can be seen that only the simulation using the second order model fails to represent the correct stability mechanism; meaning that all but the 2nd-order model simulation show a stable rotor response.

Approximately, for the first $400ms$ the different rotor angle trajectories only vary slightly. However, afterwards a clear separation is visible. When excluding the 2nd-order model, it can be observed that with decreasing order of detail, the maximum return angle decreases and it seems that the angle response is becoming less critical.

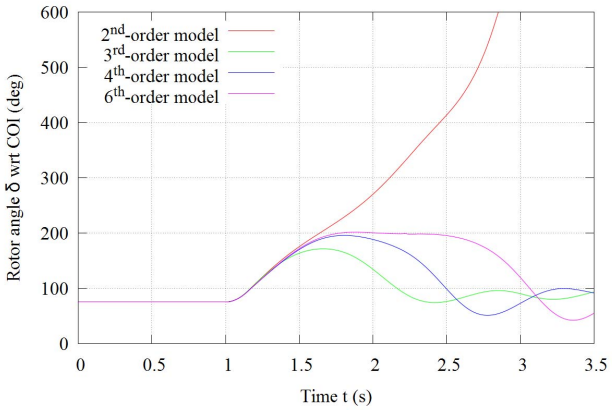

Fig. 7: Stable case: Rotor angle response of generator 6 using the four different generator models

Figure 8 shows the rotor angle response of generator 6 for the unstable case and varying model. Again it can be observed that for the first $400ms$ the rotor angle trajectories vary only slightly. In this case only the simulation with 3rd-order model does not depict the correct instability mechanism, since the machine appears to be first swing stable. However, the simulations utilizing 2nd- and 4th-order models show a similar behavior as the reference case with 6th-order model, namely the loss of synchronism of the generator within the first swing.

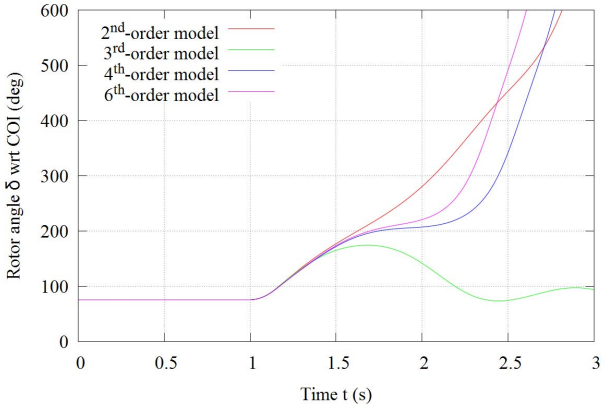

Fig. 8: Unstable case: Rotor angle response of generator 6 using the four different generator model details

Stability Assessment Results using SIME

Determination of the stability margin. In the following, the determined stability margins are analyzed for the discussed transient stability scenarios of the two test systems. The aim is to investigate if a reduced order model of a synchronous machine is sufficient to represent its dynamics during and following a transient disturbance.
In the stable as well as in the unstable case of the WSCC test system, the estimation of the $P-\delta$ curve and the

calculation of the stability margin led to the conclusion that only generator 2 is critical and, hence, the following analysis solely considers the stability assessment of this generator as the critical generator group.

It is expected that the estimation of the stability margin is improving with increasing number of considered simulated data. Furthermore, it is expected that the stability margin converges to a constant value. Figure 9 shows the determined margin for the unstable case. For the four simulations with differing generator model, it can be seen that the margins converge to a constant value.

The simulations, when using low order generator models, showed that the system is first swing stable in the unstable reference case (see Figure 5). The transient stability assessment of the first swing using SIME confirms this, since the stability margin converges to a positive value. The rotor angles over time for simulations with higher order generator model showed a loss of synchronism within the first swing. The TSA of these cases correctly predicts this loss of synchronism, which is apparent due to the convergence to a negative stability margin

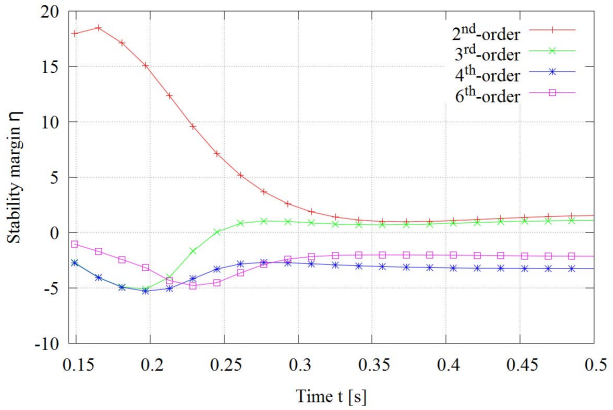

Fig. 9: Stability margins over time for the critical generator group consisting only of generator 2 and with differing degree of model detail

Consequently, SIME determined stability in the four simulations accurately. However, the stability mechanism is only depicted correctly with models of 4th-order and higher.

In the section analyzing the stability mechanism of the stable case, it was shown that the first swing characteristic was similar for all the generator models. Consequently, it is expected that SIME will determine all the four simulations to be first swing stable. Figure 10 shows the calculated stability margin of the stable case. Due to the rather fast first swing and the few data sets available to extrapolate the $P-\delta$ curve, the estimated stability margin seems to converge to a constant value, but does not reach it. Hence, for the presented stable case any of the considered synchronous machine models seems to be sufficient to assess stability.

For the case of the New England and New York system generator 6 and 7 were identified as the critical generator group in both scenarios. Since the stable case is marginally stable and the unstable case marginally unstable, it is expected that the stability margin will converge to a value very close to zero in both cases. Figure 11 shows the computed stability margin over time of the stable case.

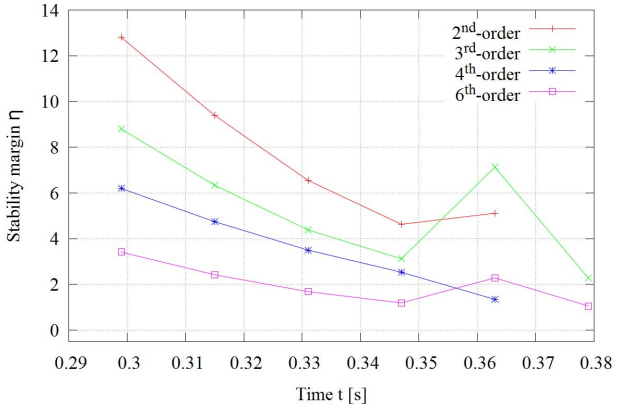

Fig. 10: Stability margins over time of the stable scenario for the critical generator group consisting only of generator 2 and with differing degree of model detail

The analysis of the rotor angle of generator 6 (see Figure 7) showed a stable response using SM models of 3rd-order and higher. Consequently, SIME determines those simulations as stable and only the simulation using a 2nd-order SM model as unstable.

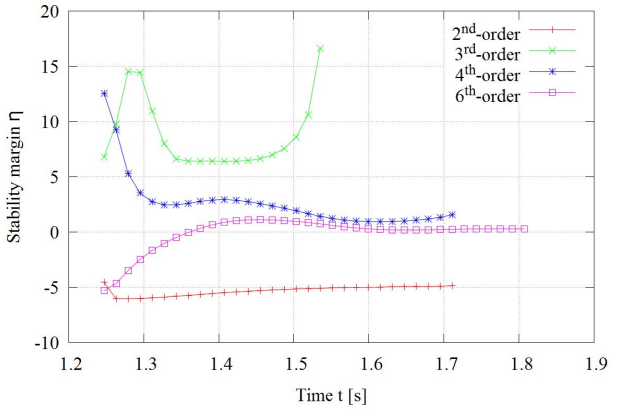

Fig. 11: Stability margins over time of the stable scenario for the critical generator group consisting of generator 6 and 7 with differing degree of model detail

The stability margin determined for the 2nd-order model simulation changes only slightly with time. This may be explained by the fact that TSAs using EAC are derived from the assumption of fixed voltage behind the transient reactance, which is also assumed for the case of a 2nd-order model. The stability margin of the simulation using a 3rd-order model is the next fastest simulation to reach a (temporarily) constant stability margin. The subsequent rise of the stability margin may be explained by the observance that very close to the return angle the quadratic estimation of the $P_a-\delta$ curve is no longer sufficient. For the 4th-order model the stability margin remains positive until the end of the simulation. However, the stability margin does not reach a constant value. The stability margin computed from values of the simulation using 6th-order SM models begin with a negative margin,

but it converges over time and with improving estimation of the $P_a - \delta$ curve to a slightly positive value.
Figure 12 shows the stability margin of the unstable case of the New England and New York system. Recall Figure 8 for this case all simulations but the simulation using 3rd-order generator model depicted an unstable rotor angle response similar to the reference case. The stability margin of the 2nd-order simulation is slightly more negative than in the prior case, but as steady as before. The simulation with 3rd-order models is much too optimistic and the stability assessment indicates a stable case. With a fourth order model the stability margin begins with a positive value, but slowly converges to a slightly negative margin indicating an unstable case. The stability margin determined from the 6th-order model simulation begins with a negative margin and converges to a negative margin close to zero, which was expected since the case is marginal unstable. In this case the simulations with 4th- and 6th-order models allowed a correct stability assessment, where the results with 4th-order were slightly more optimistic.

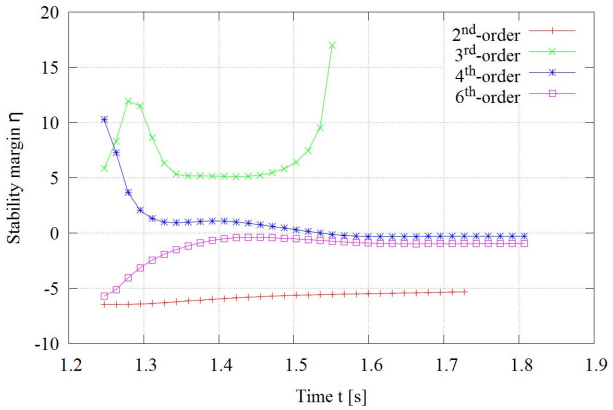

Fig. 12: Stability margins over time of the unstable case for the critical generator group consisting only of generator 6 and 7 with differing degree of model detail

Conclusion

The paper begins with a short description of the SIngle Machine Equivalent (SIME) method, which is based on the equal area criterion, and can be used to assess transient stability. SIME is a hybrid method combining the advantages of using time-domain simulation and using a direct method for transient stability assessment (TSA).
In this paper SIME is used to carry out a fast transient stability screening of the current power system condition. For that purpose the computational burden of the TSA method should be minimized. In order to speed up the necessary time-domain simulation, a reduction of the synchronous machine model is considered in this work. The modeling degree of the synchronous generators was varied in two test power systems and two transient stability scenarios. For that purpose 6th-, 4th-, 3rd- and 2nd-order models were considered, the stability mechanism by means of the rotor angle trajectories of the critical machines were compared and the resulting transient stability assessment results using the preventive SIME implementation were investigated. In all cases the simulation with 6th-order model was used as reference.
The results showed that simulations using a synchronous machine model of 3rd-order and below do not exhibit the correct stability mechanism and, consequently, the transient stability assessment with SIME fails. Furthermore, it was shown that a representation of the synchronous machines by a 4th-order model may be sufficient, since the simulation displayed in all four cases the right stability mechanism and allowed to correctly determine transient stability. It should be mentioned that in the case of the New England and New York system the TSA with the 4th-order model led to slightly more optimistic stability assessment results than in the reference case. It should be noted the stable and unstable scenario of the New England and New York system were marginal stable and unstable and nevertheless, the 4th-order generator model representation was sufficient.
The simulation results at hand may suggest that a representation of the synchronous machine by their 4th-order model is sufficient to assess transient first swing stability.

References

[1] The Danish Ministry of Climate and Energy, “Energy Strategy 2050 - from coal, oil and gas to green energy,” The Danish Ministry of Climate and Energy, Stormgade 2-6 1470 Copenhagen K Denmark, Tech. Rep., Feb. 2011.

[2] A. Phadke, J. Thorp, and M. Adamiak, “A New Measurement Technique for Tracking Voltage Phasors, Local System Frequency, and Rate of Change of Frequency,” IEEE Trans. on Power App. and Syst., vol. 102, no. 5, pp. 1025–1038, May 1983.

[3] A. Phadke and J. Thorp, Synchronized Phasor Measurements and Their Applications. Springer Verlag, 2008.

[4] A. Phadke and R. De Moraes, “The Wide World of Wide-Area Measurement,” IEEE Power and Energy Mag., vol. 6, no. 5, 2008.

[5] S. Skok, I. Ivankovic, and Z. Cerina, “Applications Based on PMU Technology for Improved Power System Utilization,” in PES General Meeting, 2007. IEEE, Jun. 2007, pp. 1–8.

[6] D. Novosel, V. Madani, B. Bhargava, K. Vu, and J. Cole, “Dawn of the grid synchronization,” IEEE Power and Energy Mag., vol. 6, no. 1, pp. 49–60, Jan. 2008.

[7] H. Jóhannsson, “Development of early warning methods for electric power systems,” Ph.D. dissertation, 2011.

[8] H. Jóhannsson, R. Garcia-Valle, T. Weckesser, A. Nielsen, and J. Østergaard, “Real-time stability assessment based on synchrophasors,” in Proc. of 2011 IEEE Trondheim PowerTech, Jun. 2011, pp. 1–8.

[9] M. Glavic and T. Van Cutsem, “Wide-Area Detection of Voltage Instability From Synchronized Phasor Measurements. Part I: Principle,” IEEE Trans. Power Syst., vol. 24, no. 3, pp. 1408–1416, Aug. 2009.

[10] ——, “Wide-Area Detection of Voltage Instability from Synchronized Phasor Measurements. Part II: Simulation Results,” IEEE Trans. Power Syst., vol. 24, no. 3, pp. 1417–1425, 2009.

[11] T. Weckesser, H. Jóhannsson, S. Sommer, and J. Østergaard, “Investigation of the Adaptability of Transient Stability Assessment Methods to Real-Time Operation,” in IEEE Proc., Innovative Smart Grid Technologies, Oct. 2012, pp. 1–9.

[12] Fabozzi, D., Haut, B., Chieh, A. S., & Van~Cutsem, T. (2013). Accelerated and Localized Newton Schemes for Faster Dynamic Simulation of Large Power Systems. IEEE Transactions on Power Systems, 1–12.

[13] Kundur, P. Power System Stability and Control. (N. J. Balu & M. G. Lauby, Eds.). McGraw-Hill Inc. 1994.

[14] Athay, T., Podmore, R., & Virmani, S. (1979). A practical Method for the Direct Analysis of Transient Stability. IEEE Transactions on Power Apparatus and Systems, PAS-98(2), 573–584.
[15] M. Pavella, D. Ernst, and D. Ruiz-Vega, Transient Stability of Power Systems: A Unified Approach to Assessment and Control. Kluwer Academic Publishers, 2000.
[16] Chiang, H.-D., Wu, F. F., & Varaiya, P. P. (1994). A BCU Method for Direct Analysis of Power System Transient Stability. *IEEE Transactions on Power System*, *9*(3), 1194–1208.
[17] Xue, Y., & Pavella, M. (1989). Extended equal-area criterion: an analytical ultra-fast method for transient stability assessment and preventive control of power systems. *International Journal of Electrical Power & Energy Systems*, *11*(2), 131–149.
[18] Glavic, M., Ernst, D., Ruiz-Vega, D., Wehenkel, L., & Pavella, M. (2007). E-SIME - A Method for Transient Stability Closed-Loop Emergency Control : Achievements and Prospects Fundamentals of E-SIME. 2007 iREP Symposium- Bulk Power System Dynamics and Control - VII, Revitalizing Operational Reliability.
[19] P. Sauer and M. A. Pai, Power System Dynamics and Stability, Prentice Hall, 1998.
[20] IEEE Std 1110-2002 (Revision of IEEE Std 1110-1991). (2003). *IEEE Guide for Synchronous Generator Modeling Practices and Applications in Power System Stability Analyses*. doi:10.1109/IEEESTD.2003.94408
[21] Rogers, G. (2000). *Power System Oscillations* (p. 328). Springer.

Appendix C

On-line Contingency Screening using Wide-Area Measurements

This paper has been submitted to IET Generation, Transmission & Distribution.

On-line Contingency Screening using Wide-Area Measurements

Tilman Weckesser, Hjörtur Jóhannsson, and Jacob Østergaard
Centre for Electric Power and Energy
Department of Electrical Engineering
Technical University of Denmark
2800 Lyngby, Denmark.
Email: jtgw@elektro.dtu.dk

Abstract

This paper presents a framework for an on-line implementation of a contingency screening method using wide-area measurements. For that purpose, a fast method is proposed, which carries out contingency screening and on-line stability assessment with respect to first-swing transient stability. The proposed method utilizes the single machine equivalent (SIME) method and attempts to improve the prior developed contingency screening methods. The proposed method only carries out one time-domain simulation per contingency and in average requires only a few hundred milliseconds of simulation after fault clearance. The method provides an assessment of the system's stability and classifies the respective contingency. The contingencies are categorized under the consideration of the parameters of the determined equivalent one machine infinite bus (OMIB) system. Furthermore, a method to detect islanding is proposed, which is appropriate for on-line operation, since it utilizes the efficient algorithms from graph theory. This enables the stability assessment of individual islands. The New England & New York system is used to test the proposed method with respect to assessment accuracy and computation time.

Index Terms

PMU, power system stability, transient stability, contingency screening, island detection

I. Introduction

In several countries around the world, power systems are going through major changes, which are induced by political decisions and are leading to increased penetration of renewable energy sources (RES). The European Commission published in 2010 a roadmap on how to reach a greenhouse gas emission reduction of 80 % compared to 1990 by 2050 [1]. This will be a great challenge for the operators of power systems, which have to ensure a reliable as well as stable and secure supply.

Research supported by the Danish Council for Strategic Research (DSF).

In the future power system energy generation will be based on RES, such as wind and sunlight. These sources are non-controllable and the generation planing will be dependent on forecasting accuracy. In contrast to today's power system, the production pattern in such a future system may change fast and will lead to increased fluctuations of the power system's operating point. This will introduce a need for real-time assessment methods for the future transmission grid [2]. The current tools and methods for stability assessment are based on extensive off-line calculations and, consequently, may no longer be sufficient. The development of individual assessment methods, where each addresses a particular instability mechanism, was proposed in [3]. The assessment method proposed in [3] uses algebraically derived stability boundaries [4] and was reported to allow assessment of 1325 generators in a 7917 bus system in a few milliseconds [5]. Further methods for real-time stability and security assessment have been presented in [6]–[8].

In this paper a fast stability assessment and contingency screening method is proposed, which assesses transient stability of the system and can be part of an extensive dynamic security assessment (DSA) toolbox. Due to the aforementioned changes in the power system, the transmission grid might be often operated at its limits and, hence, a fast online-DSA is of crucial importance [9]. Moreover, a framework for the implementation of the method into a real-time environment is presented.

A wide range of approaches and methods have been proposed for DSA [10] and fast contingency screening. In [11] the authors discussed various severity indices for dynamic security analysis and ranking of contingencies. The indices are based on coherency, transient energy conversion or on dot products of certain system states. A detailed time-domain simulation is carried out until 500 ms after fault clearance. Then the indices are computed to determine stability of the system and rank the respective contingency. In [12] a screening method utilizing the transient energy function was proposed, which filters out the non-severe disturbances in three steps. A recent case screening approach based on the extended equal area criterion (EEAC) was presented in [13]. Here the main idea was to filter out the majority of the stable cases with data gathered just after fault clearance and to carry out detailed time domain simulation combined with the integrating EEAC on the remaining yet undetermined cases. In [14] the authors propose a SIME based contingency, filtering, ranking and assessment (FILTRA) method. The method consists of two blocks. The first block filters stable contingencies and the second block ranks and assesses the remaining possible harmful contingencies according to their estimated critical clearing times (CCTs). For that purpose, up to two time-domain simulations have to be carried out for each contingency. The fast contingency screening approach presented in [15] is also based on the SIME method. The authors introduce a new index for grouping of the generators and a classification based on the power-angle shape of the OMIB. In order to classify and rank the contingencies, the presented method carries out one to three time-domain simulations with varying fault clearing time for each contingency.

The method proposed in this paper builds on the prior developed approaches based on the SIME method, since it was identified in [16] as being potentially the fastest direct transient stability assessment (TSA) method. In the present paper the idea of classifying the contingencies by considering the power-angle shape was further developed, in order to allow the use of only one simulation per contingency. The fault clearing time is chosen corresponding

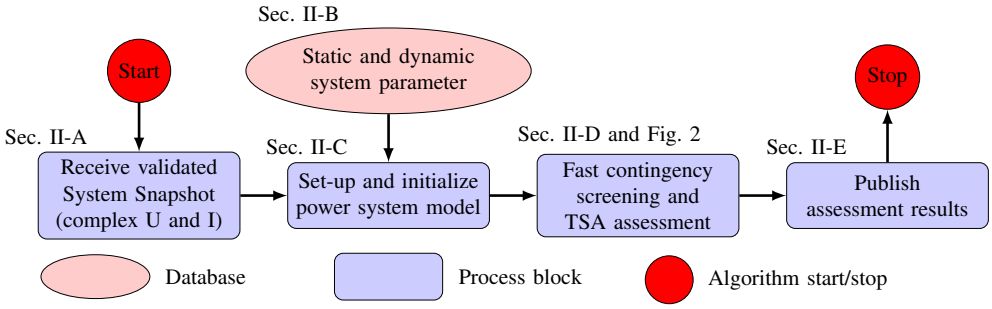

Fig. 1. Block diagram of the proposed screening and assessment method integrated into a framework for online assessment

to the respective protective relay settings and the aim is to extract from the simulation sufficient information to get an estimate of the security and stability condition of the power system. Furthermore, the paper proposes a method to detect the formation of islands and to identify the generators and loads in each island. The method utilizes the efficient algorithms from graph theory and, hence, it is suitable for on-line application. Finally, the paper presents a detailed runtime assessment of the proposed screening method.

II. Method

Figure 1 shows the block diagram of the proposed transient stability assessment (TSA) and contingency screening method integrated into an on-line power system assessment framework, similar to the power system simulation platform described in [17]. In the following, each block will be described in detail.

A. System Snapshot

This block reads validated system snapshots consisting of complex bus voltages from all system buses as well as currents flowing in and out of each transmission line or transformer. These snapshots are determined from wide-area measurements and provide full system observability.

B. Static and dynamic system parameters

The database contains the model parameter for all electric components in the monitored power system. It is assumed that the provided parameters are sufficient to represent the power system components (e.g. generators, transformers, loads, etc.) with enough detail to allow accurate simulation of the transient system response. This means that e.g. the rotor dynamics of synchronous generators are at least represented by a 4^{th}-order model, which was suggested in [18].

C. Power system model

In this block the obtained system snapshot and the system parameters are utilized to set-up a power system model including the admittance matrix $\mathbf{Y}$. Furthermore, the data are used to initialize the model to represent the current

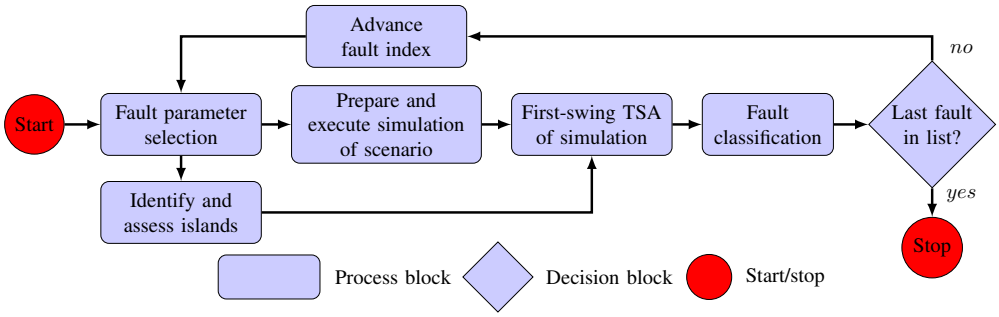

Fig. 2. Block diagram of the fast contingency screening and TSA assessment algorithm

system state. Finally, a list of contingencies is generated which will be used for the contingency screening and stability assessment.

D. Fast contingency screening and TSA assessment

Figure 2 shows the block diagram of the proposed on-line contingency screening and stability assessment algorithm.

1) Fault parameter selection: The parameters of the fault next on the contingency list are extracted from the system model. These include type of fault (e.g. three-phase short circuit), fault location, fault clearing time and fault clearance. The fault location corresponds to the bus or branch where the fault occurs. The fault clearing time is given by the protection relays in the vicinity of the fault. The fault clearance provides information on e.g. breakers to be opened to isolate the fault.

2) Prepare and execute simulation: After the fault parameters have been determined, the time-domain simulation of the scenario can be prepared. The simulation is initialized with the current system state provided by the snapshot. The model database provides all the needed component data to set-up the models used in the simulation and to compute the dynamic system response.

3) Identify and assess islands: In this block it is determined, if the fault and its clearance are causing a splitting of the power system into separated islands. In order to use the efficient algorithms from graph theory, the power grid model needs to be converted into a graph. Therefore, the admittance matrix is imported and altered according to the assumed fault clearance. For example, if the fault is cleared by disconnecting a particular branch, the branch admittance is added to the respective off-diagonal entries and subtracted from the diagonal entries of the buses connected by the branch. If the only direct connection between two buses was the respective branch, the corresponding off-diagonal entries will be equal to zero after the modification, which indicates that there is no longer a transmission line connecting the two buses. Hence, the admittance matrix can easily be converted into an adjacency matrix ($\mathbf{Adj}$) of an undirected graph by generating a copy of $\mathbf{Y}$ and setting all non-zero values equal to one. Then the efficient algorithms from graph theory can be applied. Algorithm 1 shows the implementation of the island identification and assessment algorithm as pseudocode. It uses a recursive depth-first search (DFS) algorithm

Algorithm 1 Algorithm to identify and assess islands

Input: Admittance matrix $\mathbf{Y}$, $from$-bus,to-bus and data of tripped branch b_data
Output: Buses isl, generators gen and loads $load$ in each island
Compute admittance of tripped branch utilizing b_data
Alter $\mathbf{Y}$ in correspondence to tripping of the branch
Convert $\mathbf{Y} \rightarrow \mathbf{Adj}$
Execute DFS starting at $from$-bus with target to-bus ▷ DFS returns $Ind = 1$, if graph remains connected, and a vector of $explored$ buses
if Ind is equal to 0 **then** ▷ If islands were created
    Store $explored$ buses in isl
    Store generator connected to $explored$ buses in gen
    Store loads connected to $explored$ buses in $load$
    $next \leftarrow$ first not-explored bus
    while Graph not completely explored **do**
        Execute DFS starting at $next$
        Store $explored$ buses in isl
        Store generator connected to $explored$ buses in gen
        Store loads connected to $explored$ buses in $load$
        if All nodes in the graph were explored **then**
            Graph completely explored
        else
            $next \leftarrow$ first not-explored bus
        end if
    end while
end if

[19] to identify the creation of islands and to determine if generator or loads are in the respective island. The algorithm's output indicates if islands were created or not. If the power system was split, it provides information on the buses, generators and loads in each island.

4) First-swing TSA of simulation results: The simulation as well as the island identification & assessment results are forwarded to the TSA block, where in each time step the transient stability of the system or, if fault clearance created islands, of each island is assessed using the preventive SIME method.

Preventive SIME is a hybrid transient stability assessment method, which combines the advantages of both detailed time-domain simulation and equal area criterion (EAC). In [14] a detailed description of the method can be found and [20] recently presented a discussion of the achievements and prospects of Emergency SIME. SIME is derived based on the assumption that the post-fault dynamics of a multi-machine power system can be represented by a suitable OMIB equivalent. EAC can then be applied to assess transient stability. Figure 3 shows the proposed first-swing TSA algorithm, which is described in more detail in the following.

a) Required data sets: In order to assess transient stability, the method requires only a limited number of data and parameters from the system and the generators. The only time invariant parameters required are the inertia coefficient of each generator and, if islands were created, the generators in each island. Apart from that the method needs at least three successive data sets of rotor angles, rotor speeds, mechanical powers and electrical active powers from all generators in the post-fault configuration. In this implementation of the method up to six successive data

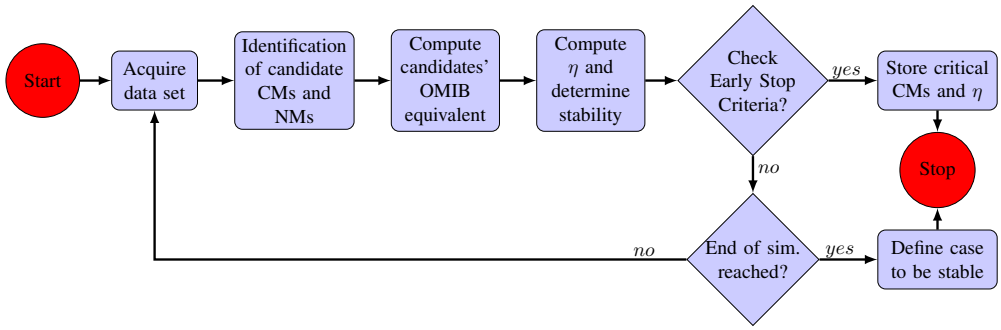

Fig. 3. First-swing transient stability assessment algorithm

sets are considered.

b) Identification of critical and non-critical machine candidates: In order to determine an OMIB equivalent, which represents the dynamics of the system, the generators are split into two groups: a group of critical machines (CMs), which is the group of generators that are likely to lose synchronism, and a group of non-critical machines (NMs). Candidate CMs and NMs are identified under consideration of the evolution of the generators' individual rotor angles. For that purpose, the rotor angles are predicted some time ahead (e.g. 100 ms) using Taylor series expansion. The candidate CMs are then determined by ranking the machines according to the predicted rotor angle and searching for the largest angular gaps between two successive machines. The machines above the gap are identified to be the CMs and the NMs are the machines below the gap. In this implementation in each assessment step up to three candidate CM and NM groups were selected.

c) Formulation of the OMIB parameters: In the next step, the gathered simulation data sets are used to formulate the OMIB equivalent, which represents the dynamics between a group of CMs and NMs. This is done for each candidate group of CMs and NMs. The OMIB is characterized by its rotor angle $\delta(t)$, speed $\omega(t)$, inertia coefficient M and acceleration power $P_a(t)$. The rotor angle δ of the OMIB is defined as the difference of the center of angle (COA) of the CMs and NMs.

$$\delta(t) = \delta_{CM}(t) - \delta_{NM}(t) \tag{1}$$

The COAs of the CMs $\delta_{CM}(t)$ and NMs $\delta_{NM}(t)$ are defined as follows.

$$\begin{aligned} \delta_{CM}(t) &= M_{CM}^{-1} \textstyle\sum_{k \in CM} M_k \delta_k(t) \\ \delta_{NM}(t) &= M_{NM}^{-1} \textstyle\sum_{j \in NM} M_j \delta_j(t) \end{aligned} \tag{2}$$

$M_{k,j}$ and $\delta_{k,j}(t)$ are the inertia coefficients and the rotor angles of the individual machines in the respective group. M_{CM} and M_{NM} are corresponding to the aggregated inertias of the individual generators in the two groups, which are computed as follows.

$$M_{CM} = \sum_{k \in CM} M_k; \quad M_{NM} = \sum_{j \in NM} M_j \tag{3}$$

The rotor speed of the OMIB is defined as the difference between the speed of the aggregated NCs and NMs.

$$\omega(t) = \omega_{CM}(t) - \omega_{NM}(t) \tag{4}$$

where $\omega_{CM}(t)$ and $\omega_{NM}(t)$ are computed in the same manner as the rotor angles (2). The acceleration power $P_a(t)$ of the OMIB is computed as the difference between its mechanical power $P_m(t)$ and electrical power $P_e(t)$.

$$P_a(t) = P_m(t) - P_e(t) \tag{5}$$

The parameters $P_m(t)$ and $P_e(t)$ are computed as follows.

$$P_m(t) = M\left(M_{CM}^{-1}\sum_k P_{mk}(t) - M_{NM}^{-1}\sum_j P_{mj}(t)\right)$$
$$P_e(t) = M\left(M_{CM}^{-1}\sum_k P_{ek}(t) - M_{NM}^{-1}\sum_j P_{ej}(t)\right)$$

Finally, the inertia coefficient M of the OMIB is defined by:

$$M = \frac{M_{CM}M_{NM}}{M_{CM} + M_{NM}} \tag{6}$$

d) Computation of stability margin and determination of stability: By employing the EAC, the determined parameter of the candidate OMIB allow to compute the transient stability margin η, which is negative for an unstable and positive for a stable case [14]:

$$\eta = -\int_{\delta_i}^{\delta_u} P_a d\delta - 1/2\, M\omega_i^2 \tag{7}$$

where δ_i and ω_i correspond to $\delta(t_i)$ and $\omega(t_i)$ and δ_u is the angle where the following instability conditions are met:

$$P_a(\delta_u) = 0 \text{ and } \dot{P}_a(\delta_u) > 0 \tag{8}$$

In the Preventive SIME method the angle δ_u is estimated through an approximation of the $P_a(\delta)$-curve of the OMIB. To this purpose, (at least) three successive data sets of the OMIB, consisting of P_a and δ, are used to compute a quadratic approximate of the curve:

$$P_a(\delta) = a\delta^2 + b\delta + c \tag{9}$$

of which the parameters a, b and c are computed from the three data sets and, subsequently, are refined using a weighted least square technique.

Theory dictates that the $P_a(\delta)$-curve of the OMIB opens upwards, which results in the requirement of parameter a being larger than zero. If the parameter a is zero or less for the approximated $P_a(\delta)$-curve, it is rejected and the next set of data is acquired. The two curves shown in Fig. 4 represent valid approximation of the $P_a(\delta)$-curve and the stability margin computation is straight forward. In Case I (see Fig. 4a), the angle δ_u is found employing the condition in (8) and the stability margin is computed with (7). When the OMIB does not have an equilibrium point, meaning that the estimated $P_a(\delta)$-curve does not intersect $P_a = 0$, as shown in Case II in Fig. 4b, a stability

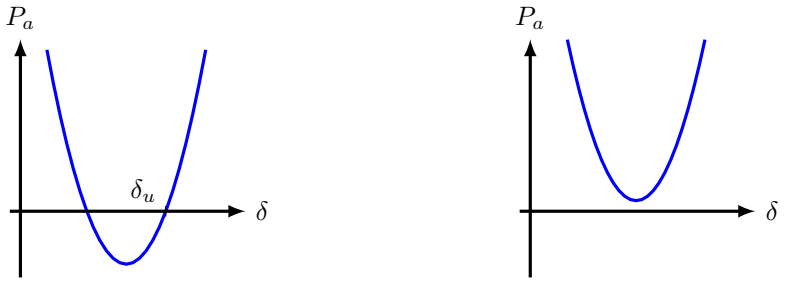

(a) Case I: $a > 0$, stable or unstable

(b) Case II: $a > 0$, definitely unstable

Fig. 4. Considered $P_a(\delta)$-curve shapes

margin cannot be computed with (7). However, in that case, as suggested in [14], the kinetic energy of the OMIB can be used to represent the negative stability margin and can be computed as follows.

$$\eta = -1/2\, M\omega_i^2 \tag{10}$$

e) Early Stop Criteria: The time-domain simulation and the stability assessment can be stopped, when from the candidate OMIBs the most critical one is identified and the computed stability margin converged to a constant value. The most critical OMIB in an unstable case is either the one, which first crosses δ_u and, hence, the unstable equilibrium point (UEP), or the one, which first reaches the minimum of the $P_a(\delta)$-curve in case that no post-fault equilibrium exists. In a stable case, the most critical OMIB is the one, which is the last one to reach the return angle δ_r, where the following stability conditions are met.

$$P_a(\delta_r) < 0 \text{ and } \omega_r = 0 \tag{11}$$

For that purpose, the candidate OMIBs are assessed with respect to the criteria identifying the most critical OMIB and when the most critical has been identified, the assessment is continued until the stability margin reached a constant value. Once the two conditions are satisfied the stability margin and the CMs of the respective OMIB are stored and forwarded to the contingency classification block (see Fig. 2).

5) Classification of faults: In order to classify the faults, a classification index is introduced. It utilizes characteristics of the approximated $P_a(\delta)$-curve and states of the OMIB at the time the early stop criteria were satisfied. Therefore, it also allows the classification of a contingency with respect to individual islands. The proposed classification is similar to the one proposed in [15] and is shown in Table I. A contingency is classified to be Definitely Unstable (DU), if the $P_a(\delta)$-curve, as shown in Fig. 4b, does not intersect zero and a post-contingency equilibrium point does not exist. Moreover, in case of a splitting of the power system into islands, a contingency is rated DU for an island, when the island only contains generators, but no loads. A contingency is classified Unstable (U), if the determined stability margin is negative. If the most critical OMIB has reached its return angle δ_r and δ_r is lying on the side of the $P_a(\delta)$-curve, where $dP_a/d\delta > 0$, then the contingency is assessed to be Marginal Stable

TABLE I
CLASSIFICATION OF CONTINGENCIES (WHERE g: NUMBER OF GENERATORS AND l: NUMBER OF LOADS)

Classifier	η	$\frac{dP_a}{d\delta}\big\vert_{\delta=\delta_r}$	ω	Number of generators & loads
Definitely Unstable (DU)	$-$ $-$	$-$ $-$	$-$ $-$	$-$ $g \geq 1;\ l = 0$
Unstable (U)	< 0	$-$	$-$	$-$
Not Classifiable (NC)	$-$	$-$	$-$	$g = 1;\ l \geq 1$
Marginal Stable (MS)	> 0 $-$	> 0 > 0	$-$ < 0	$g \geq 2;\ l \geq 1$ $g \geq 2;\ l \geq 1$
Stable (S)	> 0 $-$	< 0 < 0	$-$ < 0	$g \geq 2;\ l \geq 1$ $g \geq 2;\ l \geq 1$
Definitely Stable (DS)	$-$	$-$	$< \omega_{lim}$	$g \geq 2;\ l \geq 1$

(MS). However, if δ_r lies on the side of the $P_a(\delta)$-curve, where $dP_a/d\delta < 0$, then it is classified Stable (S). A contingency is only classified Definitely Stable (DS), if the relative rotor speed of all the candidate OMIBs after fault clearance are below a certain threshold (e.g. $\omega_{lim} < 0.1$ rad/s) or if the maximum simulation time was reached without identification of the most critical OMIB. Finally, if an island only contains one generator and loads, the method cannot determine stability of the island, since no reference is available to determine loss of synchronism. Hence, it is categorized as Not Classifiable (NC). Table I summarizes the classifiers and the criteria used to classify.

The classification of the contingencies can be used to determine further assessment strategies. For example, NC or MS cases could be investigated in more detail e.g. with extensive time-domain simulation and DU cases could be prioritized, when determining preventive control actions.

E. Publish assessment results

After fault screening and TSA assessment, the obtained results are published (see Fig. 1) to make them available for other function or method, e.g. visualization tools or methods determining preventive controls. This may be realized through a client as described in [17].

III. RESULTS

A. Test system, cases and set-up

1) Test system: The test system employed to validate the presented screening method is the New England & New York system described in [21]. It consists of 68 buses and 16 generators. The loads are modelled as constant impedances in the time-domain simulation. The generators are represented by a sixth order model. They all have a simple excitation and voltage regulation system, as well as a thermal turbine/governor model. Moreover, all generators, but GEN-7 and GEN-14, are equipped with a power system stabilizer.

TABLE II
PERFORMED TESTS AND ASSESSMENT RESULTS FROM TIME-DOMAIN SIMULATION

Test	Clearing time $[ms]$	Number of stable	Number of unstable
Test I	50	168	40
Test II	200	137	71
Test III	500	55	153

2) Test cases: For the purpose of testing the on-line contingency screening method, a set of contingencies was defined. The set includes two three-phase fault scenarios per transmission line, where one time the fault is close to the from-bus and the second time the fault is close to the to-bus. This resulted in 172 cases. Furthermore, the method was tested with three different fault clearing times to vary the total number of stable and unstable cases (see Table II). In order to determine if the stability assessment with the on-line screening method is correct, the result needs to be compared against a reference. For this purpose, the rotor angle of the generators within an island are assessed at the end of the time domain simulation of 4 s, which is sufficient to ensure capturing of the first swing. If at the end of the simulation the rotor angle of at least two generators within an island are more than 120° apart, then the island is identified to be unstable, else stable. This maximum angle was chosen, since it is a common setting for generator out-of-step protection [22]. The reference stability assessment results are shown in Table II. The total number of assessments is larger than the number of test cases, because in cases, where the fault clearance leads to splitting of the system, the stability of each individual island is determined, which leads to a total of 208 stability assessments.

3) Test set-up: The tests were carried out on a standard laptop with the following characteristics: Intel®Core™ i7-2620M, 2.7 GHz, 8 GB DDR3 RAM, running on 64-bit Ubuntu Linux 14.04 LTS. The time-domain simulations were carried out using the software RAMSES developed at the Univ. of Liège [23]. The entire method, which was shown in Fig. 1, was implemented in MATLAB. The CPU times were measured directly in MATLAB and include all steps of the contingency screening. Due to the use of a fast external time-domain simulator and not an integrated numerical integrator, the system variables are not accessible during the simulation. Hence, the simulations are carried out for a fixed time (e.g. 4 s) and the trajectories of the needed system variables are stored in a file, which is imported into MATLAB to be used in the contingency screening algorithm.

B. Contingency screening and stability assessment results

In the following, the results of the screening method of the assessment of the New England & New York test system are presented. First, the accuracy of the method will be evaluated by comparing the stability assessment results with the reference. Second, the performance of the method will be presented in terms of the runtime. Finally, the classification results are presented and discussed.

1) Accuracy of the proposed method: The accuracy will be presented by assessing the number of correctly identified stable/unstable cases, where the reference stability assessment results were extracted from time-domain

TABLE III
ACCURACY OF FAST SCREENING METHOD

Test	Clearing time $[ms]$	Identified stable cases	Identified unstable cases
Test I	50	94.64%	100.00%
Test II	200	93.43%	98.59%
Test III	500	90.91%	100.00%

TABLE IV
PERFORMANCE OF FAST SCREENING METHOD WITH FIXED SIMULATION TIME (HERE 4 S)

Test	Runtime with simulation $[s]$		Runtime of assessment $[s]$		Needed average sTDI $[s]$
	per cont.	total	per cont.	total	
Test I	0.449	77.30	0.057	9.78	0.667
Test II	0.536	92.17	0.055	9.53	0.570
Test III	0.636	109.36	0.051	8.85	0.609

simulation. Table III shows the results of the accuracy assessment for the three different tests, where the fault clearing time was varied between 50, 200 and 500 ms. First of all, it should be mentioned that the success rates of the proposed contingency screening method are very high. Between $90.91 - 94.64$ % of the stable cases are correctly identified by the proposed contingency screening method and the success rate for identifying unstable cases is even higher with $98.59 - 100.0$ %. It should be noticed that the rate for identifying an unstable case is generally higher, which corresponds to a slightly more conservative characteristics of the method. This is preferable since a progressive characteristic would increase the rate of unstable cases being assessed as stable.

2) Performance of the screening method with fixed simulation time: The performance of the method is assessed in two ways. First, the runtime of the implementation is assessed and, afterwards, the potential speed up is estimated, for the case that the method would be seamlessly integrated with a time-domain simulator, which enables stopping the simulation when the early stop criteria are satisfied.

Table IV displays the runtimes obtained in the three tests, where each time the 172 contingencies were assessed. It shows the total runtime and the average runtime per contingency for two setups. In the first setup, the time-domain simulation is included. In the second, the already computed simulation data are solely read and utilized for the stability assessment. The total runtimes including the simulation are in the range of 77.30 s to 109.36 s, which corresponds to an average runtime of $449 - 636$ ms per contingency. It can be observed, that the runtime increases quite significantly with increasing fault clearance time and, consequently, with growing number of unstable cases. This may be explained by the increase of the runtime of the time-domain simulation. In order to speed up the time-domain (T-D) simulation a variable step size is used, in the case of a stable case the step size can be increased soon after fault clearance, while for an unstable case the step size needs to be kept small for a longer period. Consequently, an increase of the number of unstable cases leads to an increase of the runtime. Without the

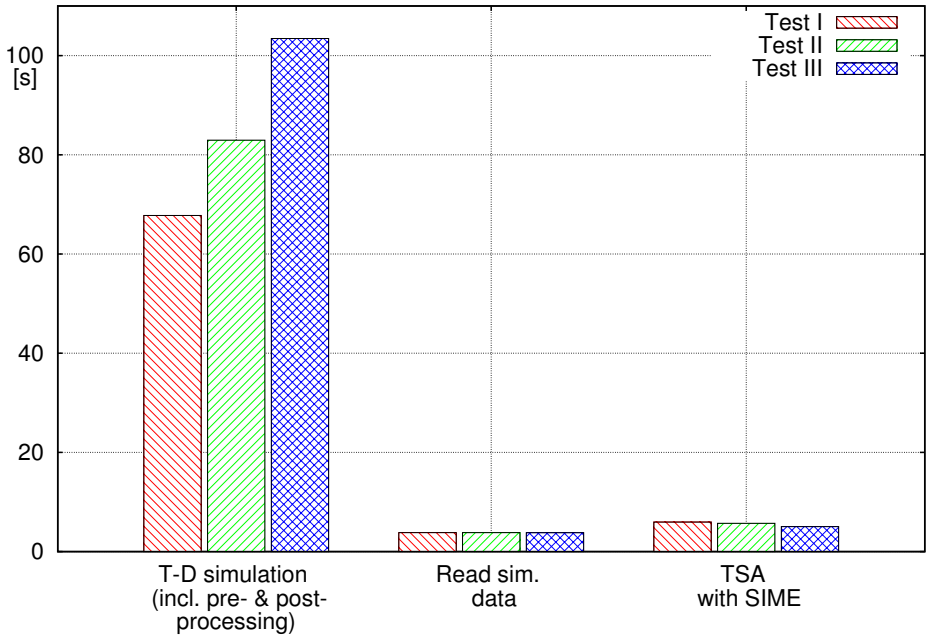

Fig. 5. Runtime of the major parts of the screening method with fixed simulation time

simulation, the total runtimes are in the range of 8.85 s to 9.78 s corresponding to $51 - 57$ ms per contingency.

Figure 5 shows the runtime of the three tests split up into three parts, namely time-domain simulation, which includes the time of data preparation and post-processing, reading of simulation data and stability assessment. The graph shows that around 90 % of the runtime is spend on the time-domain simulation with fixed simulation time. Hence, a variable simulation time has a large potential for reducing the runtime, where an early stability prediction with SIME enables the early simulation stop.

In [14], it was proposed to measure the performance of SIME based methods in needed seconds of time-domain integration (sTDI) until determination of stability. The sTDI's for each contingency and the three tests are shown in Fig. 6 and the needed average for each test was presented in Table IV. In the graph the average simulation time needed is indicated by a horizontal dashed line, the maximum simulation time by a solid line and the colours indicate the corresponding test. The graph shows that in the majority of the cases a simulation time of less than a second is sufficient and that there are only very few cases, where the maximum simulation time was reached.

3) Performance of the screening method with variable simulation time: In the previous section, it was shown that time-domain simulation with fixed simulation time is dominating the runtime of the screening method. In order to further speed up the screening, the three tests were conducted with variable simulation time, where the simulation is stopped once the TSA method has determined stability of the particular case. Hence, the simulation time of the individual cases correspond to the sTDI, shown in Fig. 6, plus pre-fault simulation and fault clearing time (here 100 ms and, depending on the test, $50 - 500$ ms respectively).

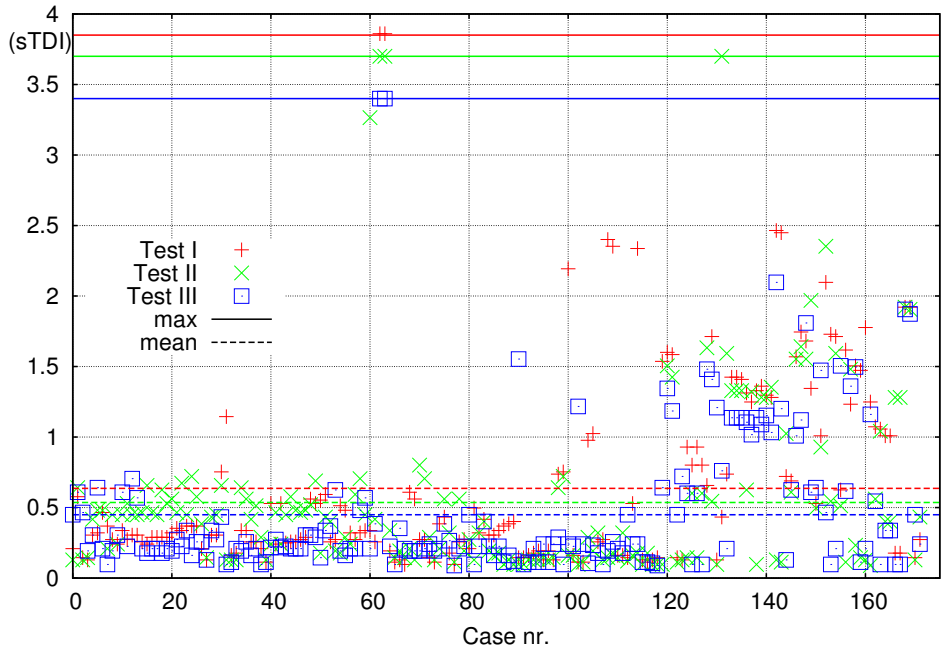

Fig. 6. Seconds of Time-Domain Integration (sTDI) required from fault clearance and until stability determination

TABLE V
PERFORMANCE OF FAST SCREENING METHOD WITH VARIABLE SIMULATION TIME

Test	Runtime with simulation $[s]$		Runtime of assessment $[s]$		Needed average sTDI $[s]$
	per cont.	total	per cont.	total	
Test I	0.263	45.31	0.045	7.54	0.667
Test II	0.275	47.32	0.042	7.24	0.570
Test III	0.296	51.05	0.038	6.53	0.609

Table V shows the runtime of the three tests of the screening method with variable simulation time and reveals that this leads to considerable shorter runtimes in the first setup, where the time-domain simulations were included. The runtimes are reduced by 41.4 % to 53.3 % and are in the range of $45.31 - 51.05$ s for the assessment of the 172 contingencies. It should be noticed that it also led to shorter runtimes for the setup without time-domain simulation, which is due to a reduction of the time needed to read the simulation data.

Figure 7 shows a comparison of the runtimes with fixed and variable simulation time. The graph shows as expected that the main runtime reduction stems from the reduced time spent on time-domain simulation. Firstly, it is noticeable that the reduction is significant in particular in the third test with clearing time of 500 ms and, consequently, a large number of unstable cases. This can be explained by the fact that the needed time step for unstable cases is required to be smaller and that the simulation of an unstable system response can be shortened due to the early stop criteria, described in section II-D4e. Secondly, a reduction of the time needed to read the simulation

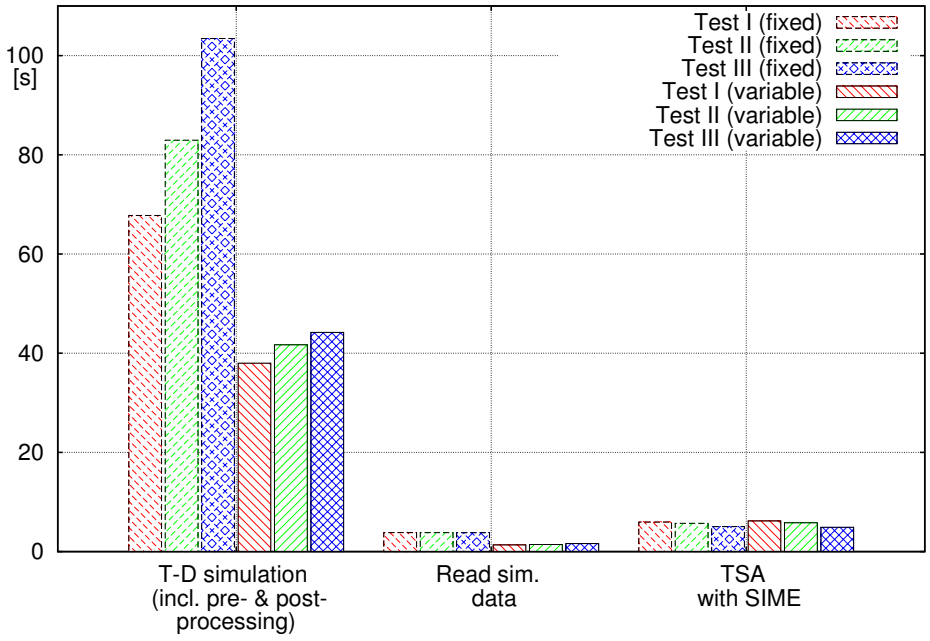

Fig. 7. Comparison of the runtime of the major parts of the screening method with fixed and variable simulation time

data is noticeable and this results from the lower number of simulation data, which was already mentioned earlier. Finally, it should be noted that the time needed for the TSA assessment using SIME is not affected by the variation of the simulation time, which was expected.

4) Classification of faults: The bar graph in Fig. 8 summarizes the results of the classification of the contingencies as proposed in section II-D5. It should be mentioned that in this section only the results of the contingencies are depicted, which were correctly assessed by the proposed assessment method. The different contingency categories are shown on the x-axis. The number of identified contingencies in each test in the respective category are displayed by the bars belonging to the left y-axis. The bar graph shows that with longer clearing times the number of definitely unstable (DU) as well as unstable (U) cases increases and vice versa the number of definitely stable (DS) cases increases with shorter clearing times. Moreover, it should be noticed that the number of marginal stable (MS) cases peaks in the test with intermediate clearing time. These results are in good agreement with intuition. It should be mentioned, that independent of the fault clearing time two cases always were identified as not classifiable (NC). These are corresponding to faults that lead to islanding, where one island consists of one generator and a load. In the case of a single machine in an island, stability can not be determined as mentioned earlier.

The data points in Fig. 8 depict the average critical clearing times (CCTs) of the contingencies in the respective categories and tests (shown on the right y-axis). Furthermore, an error bar is added to each average critical clearing time, which stretches from the minimum to the maximum CCT in the respective category and test. It should be noted that the algorithm used to identify CCTs stopped the search for CCTs when the clearing time became larger

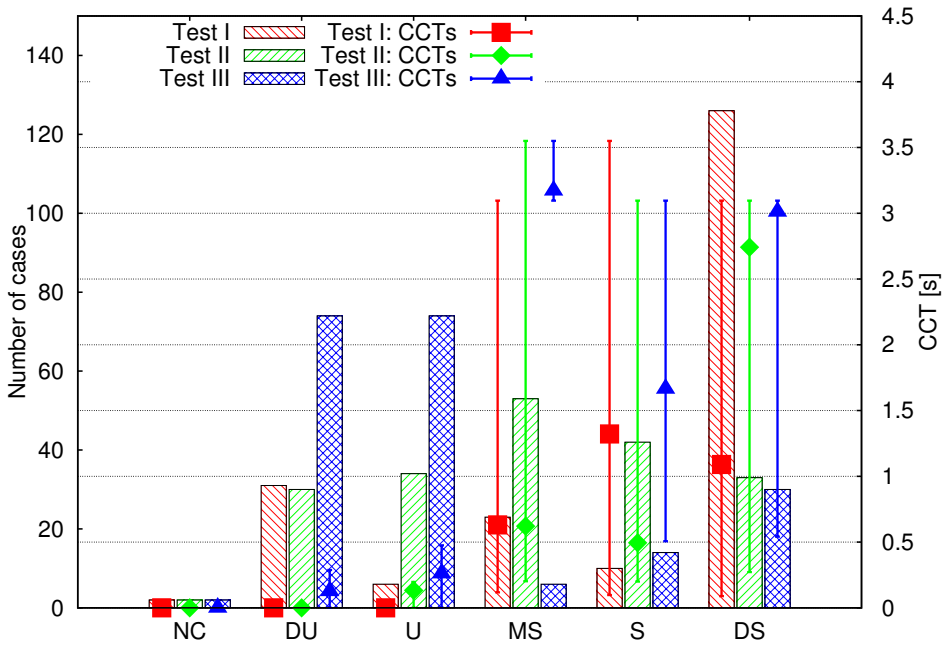

Fig. 8. Fault ranking results: Bar graph (left y-axis) indicates number of cases in a particular category and test. The data points and error bars show average and range of CCTs in the corresponding category and test (right y-axis).

than 3 s. It is assumed that these cases are stable in the during fault as well as post fault condition. The CCTs of the contingencies in the unstable categories (DU + U) are, as expected, always below the respective actual clearing times ($50/200/500$ ms). Furthermore, it can be observed, that the average clearing time in the category DU is lower than in the category U, which confirms the effectiveness of the categorization. The results obtained for the stable cases and categories (MS, S, DS) are less clear. The maximum and minimum CCTs in each stable category vary greatly. However, it may be argued that a general upward trend can be observed for the average CCTs from DU to DS, when ignoring outliers such a the few MS cases in Test III, which correspond to only 3 % of the correctly assessed cases. The upward trend of the CCTs indicates again the effectiveness of the proposed classification of the contingencies. The problem of precisely classifying the stable cases may be explained by the difficulty to determine the correct critical group of machines. A method or criteria to early and accurately identifying this group could lead to an improvement of the classification of stable cases. Finally, it should be mentioned that the categories are not intended to strictly split the contingencies with respect to their CCTs, but allow a categorization relative to the fault clearing time and the severity of the disturbance in the current system condition.

IV. Discussion

This paper proposed a framework for on-line contingency screening using wide-are measurements and a fast stability and contingency screening method, which aims at identifying first-swing unstable contingencies and providing a classification of the stable as well as the unstable cases with respect to their severity. The method

uses a system snapshot and data from a corresponding model database to determine the current admittance matrix of the system. Following, for each considered contingency the admittance matrix is modified to represent the post-fault condition and a graph theory based approach is used to identify islanding. If islands are detected, it is assessed which generators and loads are in the individual islands. The system snapshot is used to initialize a time-domain simulation, where a particular contingency is applied. The simulation data are forwarded to the TSA block, where the stability of the case is evaluated employing SIME and the assessment is stopped once the early stop criteria are fulfilled. Furthermore, each contingency is categorized with information extracted from the $P_a(\delta)$ curve of the OMIB. The accuracy and speed of the method was tested on the New England & New York test system. Three tests with different fault clearing times were carried out, where each was composed of 172 contingencies. The accuracy assessment showed a very high success rate with respect to stability assessment. It was shown, that the proposed method filters between $90.9 - 94.6$ % of the stable cases and correctly identifies $98.6 - 100$ % of the unstable cases. Consequently, the method is slightly more conservative, which is preferable for a screening method. The assessment of the runtime exposed that the majority of the CPU time is spent on the time-domain simulation and it was shown that by introducing a variable simulation time a considerable speed up can be achieved. Finally, the results of the classification of contingencies were presented by comparing the results to the CCTs of the individual contingencies, which showed that the categorization approach is promising. However, it is expected that the results, particular for stable cases, could be further improved through an early and accurate identification of the correct critical and non-critical group of generators.

REFERENCES

[1] European Comission, "Roadmap 2050: A Practical Guide To a Prosperous, Low-Carbon Europe," Tech. Rep., 2010.

[2] F. Li, W. Qiao, H. Sun, H. Wan, J. Wang, Y. Xia, Z. Xu, and P. Zhang, "Smart Transmission Grid: Vision and Framework," *IEEE Transactions on Smart Grid*, vol. 1, no. 2, pp. 168–177, Sep. 2010.

[3] H. Jóhannsson, A. H. Nielsen, and J. Østergaard, "Wide-Area Assessment of Aperiodic Small Signal Rotor Angle Stability in Real-Time," *IEEE Transactions on Power Systems*, pp. 1–13, 2013.

[4] H. Jóhannsson, J. Østergaard, and A. H. Nielsen, "Identification of critical transmission limits in injection impedance plane," *International Journal of Electrical Power & Energy Systems*, vol. 43, no. 1, pp. 433–443, Dec. 2012.

[5] S. Sommer and H. Jóhannsson, "Real-time thevenin impedance computation," in *2013 IEEE PES Innovative Smart Grid Technologies Conference (ISGT)*. IEEE, Feb. 2013, pp. 1–6.

[6] A. Perez, H. Jóhannsson, P. Vancraeyveld, and J. Østergaard, "Suitability of voltage stability study methods for real-time assessment," in *Proceedings of the 2013 IEEE PES Innovative Smart Grid Technologies Conference*, Copenhagen, Denmark, 2013.

[7] T. Weckesser, H. Jóhannsson, and T. Van Cutsem, *Early Prediction of Transient Voltage Sags caused by Rotor Swings*. IEEE, 2014.

[8] H. Jóhannsson and M. Wache, "System security assessment in real-time using synchrophasor measurements," in *IEEE PES ISGT Europe 2013*. IEEE, Oct. 2013, pp. 1–5.

[9] S. C. Savulescu, *Real-Time Stability in Power Systems*. New York: Springer Verlag, 2006.

[10] Working Group Cigré C4.601, "Review of on-line dynamic security assessment tools and techniques," 2007.

[11] C. Fu and A. Bose, "Contingency Ranking Based on Severity Indices in Dynamic Security Analysis," *IEEE Transaction on Power Systems*, vol. 14, no. 3, pp. 980–986, Aug. 1999.

[12] V. Chadalavada, V. Vittal, G. C. Ejebe, G. D. Irisarri, J. Tong, G. Pieper, and M. McMullen, "An On-Line Contingency Filtering Scheme for Dynamic Security Assessment," *IEEE Transaction on Power Systems*, vol. 12, no. 1, pp. 153–161, Feb. 1997.

[13] Y. Xue, T. Huang, and F. Xue, "Effective and Robust Case Screening for Transient Stability Assessment," in *2013 IREP Symposium Bulk Power System Dynamics and Control - IX Optimization, Security and Control of the Emerging Power Grid*, 2013, pp. 1–8.

[14] M. Pavella, D. Ernst, and D. Ruiz-Vega, *Transient Stability of Power Systems: A Unified Approach to Assessment and Control*. Kluwer Academic Publishers, 2000.

[15] B. Lee, S.-H. Kwon, J. Lee, H.-K. Nam, J.-B. Choo, and D.-H. Jeon, "Fast contingency screening for online transient stability monitoring and assessment of the KEPCO system," *IEEE Proc., Gener. Transm. Distrib.*, vol. 150, no. 4, pp. 399–404, Jul. 2003.

[16] T. Weckesser, H. Jóhannsson, S. Sommer, and J. Østergaard, "Investigation of the Adaptability of Transient Stability Assessment Methods to Real-Time Operation," in *IEEE Proc., Innovative Smart Grid Technologies*, Oct. 2012, pp. 1–9.

[17] H. Morais, P. Vancraeyveld, A. Pedersen, M. Lind,H. Jóhannsson and J. Østergaard, "SOSPO - SP: Secure Operation of Sustainable Power Systems Simulation Platform for Real - Time System State Evaluation and Control," *IEEE Transactions on Industrial Informatics*, vol. 3203, no. c, 2014.

[18] T. Weckesser, H. Jóhannsson, and J. Østergaard, "Impact of Model Detail of Synchronous Machines on Real-time Transient Stability Assessment," in *2013 IREP Symposium Bulk Power System Dynamics and Control - IX Optimization, Security and Control of the Emerging Power Grid*, Rethymnon, Greece, Aug. 2013.

[19] J. Kleinberg and E. Tardos, *Algorithm Design*, M. Suarez-Rivas, Ed. Boston: Pearson Addison Wesley, 2006.

[20] M. Glavic, D. Ernst, D. Ruiz-Vega, L. Wehenkel, and M. Pavella, "E-SIME - A Method for Transient Stability Closed-Loop Emergency Control : Achievements and Prospects Fundamentals of E-SIME," in *2007 iREP Symposium- Bulk Power System Dynamics and Control - VII, Revitalizing Operational Reliability*, 2007.

[21] G. Rogers, *Power System Oscillations*. Springer, 2000.

[22] P. Kundur, *Power System Stability and Control*, N. J. Balu and M. G. Lauby, Eds. McGraw-Hill Inc., 1994.

[23] D. Fabozzi, B. Haut, A. S. Chieh, and T. Van Cutsem, "Accelerated and Localized Newton Schemes for Faster Dynamic Simulation of Large Power Systems," *IEEE Transactions on Power Systems*, pp. 1–12, 2013.

Appendix D

Critical Machine Cluster Identification using the Equal Area Criterion

---

This paper has been accepted for presentation at the *IEEE PES General Meeting (IEEE PES GM'15)* in Denver, Colorado, USA.

Critical Machine Cluster Identification using the Equal Area Criterion

Tilman Weckesser Hjörtur Jóhannsson Jacob Østergaard

***Abstract*—The paper introduces a new method to early identify the critical machine cluster (CMC) after a transient disturbance. For transient stability assessment with methods based on the equal area criterion it is necessary to split the generators into a group of critical and non-critical machines. The generators in the CMC are those likely to lose synchronism. The early and reliable identification of the CMC is crucial and one of the major challenges. The proposed new approach is based on the assessment of the rotor dynamics between two machines and the evaluation of their coupling strength. A novel coupling coefficient is derived and a cluster identification algorithm is developed. The algorithm determines the CMC based on the impact of the fault on the derived coupling coefficient of individual generator pairs. The results from two cases are presented and discussed, where the CMC is successfully determined just after fault clearance.**

I. Introduction

STABLE and secure supply of electric energy is a fundamental requirement of modern society. In order to ensure operation of the power system within stability and security limits, the system operator is dependent on tools and methods, which provide situational awareness. Analysis that determine if a system can remain within the stability & security boundaries for a given set of credible contingencies are referred to as dynamic security assessment (DSA) [1]. An efficient transient stability assessment (TSA) method is an important part of a DSA toolbox. In order to reach real-time performance in TSA, approaches using so-called direct methods are appealing. A large number of these methods are either using the transient energy function, such as the BCU method [2], or the equal area criterion (EAC), such as the EEAC method [3] and the SIME method [4]. The mentioned methods employing the EAC are requiring that the generators in the system are split into a group of critical generators also called critical machine cluster (CMC), which is the group likely to lose synchronism, and a group of non-critical generators. This stems from the assumption that no matter how complex a system is the transient stability problem arises from the separation of two generator groups [4]. An early and reliable identification of the CMC is crucial to enable correct stability assessment.

In [4] it is proposed to extrapolate the individual rotor angle trajectories using a set of measurements and e.g. Taylor series expansion. The extrapolations are used to predict the individual rotor angles some time ahead. The predicted rotor angles are sorted descending and the gaps between entries are assessed. The generators are split into the critical and the non-critical group according to the maximum angular gap. [5] proposes

The authors are with the Centre for Electric Power and Energy, Department of Electrical Engineering, Technical University of Denmark, 2800 Lyngby, Denmark. (email: jtgw@elektro.dtu.dk)

Research supported by the Danish Council for Strategic Research (DSF).

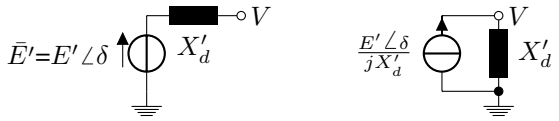

(a) Thevenin Equivalent (b) Norton Equivalent

Fig. 1. Thévenin and Norton equivalents of generator

an index for grouping the generators, which is called angle increment. It is a measure of the relative rotor angle change of an individual generator since fault clearance and with respect to the average change of the rotor angles of all generators.

In this paper a new method is proposed to identify the CMC, which utilizes efficient algorithms from graph theory. For that purpose, a novel coupling coefficient is derived, which represents the coupling strength between pairs of generators. The rest of the paper is structured as follows. In Sec. II the model used for the computation of the clustering coefficient as well as the EAC are briefly described. This is followed by the derivation of the one-machine equivalent (OME) of pairs of machines and the coupling strength coefficient. In Sec. III the cluster identification algorithm is introduced. Afterwards, in Sec. IV the results from test cases are presented and discussed. Finally, in Sec. V some concluding remarks are offered.

II. Derivation of Coupling Coefficients

A. Modelling for coupling analysis

In order to derive the coupling coefficients, the synchronous generators are represented by the so-called "classical" transient stability model [6]. Each generator is represented by its Thévenin equivalent and correspondingly by an e.m.f. E' of constant magnitude behind the transient reactance X'_d (see Fig. 1a). This simple generator model is only valid for a very short time period, due to e.g. fast automatic voltage regulators. Therefore, the model is fitted to the current operating point using the latest measurements or simulation data. When the complex voltage $\bar{V}$ and the complex current injection $\bar{I}$ at the machine terminal are known, the e.m.f. can be computed.

$$\bar{E}' = E'\angle\delta = \bar{V} + jX'_d\bar{I} \tag{1}$$

where δ corresponds to the rotor angle of the machine. When each generator is represented by its Norton equivalent (see Fig. 1b) and, hence, by a current source $\bar{E}'/jX'_d$ in parallel with the admittance corresponding to X'_d, then the algebraic network equations describe the relation between the bus voltages, current injections and network admittances.

$$\bar{\boldsymbol{I}} = \boldsymbol{Y}\bar{\boldsymbol{V}} \tag{2}$$

Here, $\bar{\boldsymbol{I}}$ corresponds to the vector of the complex current injections at the generator buses, $\bar{\boldsymbol{V}}$ to the vector of complex

bus voltages and $\boldsymbol{Y}$ to the "augmented" admittance matrix, which is obtained by adding the admittances corresponding to the transient reactances of the generators and loads to the original admittance matrix.

In order to compute the power injection of a generator as a function of the e.m.f.s of the remaining generators, the augmented admittance matrix $\boldsymbol{Y}$ needs to be extended to the internal nodes of the generators, which correspond to fictive nodes behind the respective X'_d. Then the resulting extended admittance matrix $\boldsymbol{Y}_{ex}$ will be reduced to the internal nodes.

$$\boldsymbol{Y}_{ex} = \begin{pmatrix} \boldsymbol{Y} & \boldsymbol{Y}_{bg} \\ \boldsymbol{Y}_{bg}^T & \boldsymbol{Y}_{gg} \end{pmatrix} \tag{3}$$

$\boldsymbol{Y}_{bg}$ corresponds to the matrix representing the connection of the machine internal nodes to the respective machine terminal buses and $\boldsymbol{Y}_{bg}^T$ is its transpose. $\boldsymbol{Y}_{gg}$ corresponds to the square admittance matrix of order m, where m is the number of generators and which holds the admittances to the corresponding X'_d on its diagonal. This extended and augmented admittance matrix allows computing the current injections $\bar{\boldsymbol{I}}_{\boldsymbol{tr}}$ into the internal nodes as follows.

$$\begin{pmatrix} \boldsymbol{0} \\ \bar{\boldsymbol{I}}_{tr} \end{pmatrix} = \begin{pmatrix} \boldsymbol{Y} & \boldsymbol{Y}_{bg} \\ \boldsymbol{Y}_{bg}^T & \boldsymbol{Y}_{gg} \end{pmatrix} \begin{pmatrix} \bar{\boldsymbol{V}} \\ \bar{\boldsymbol{E}}' \end{pmatrix} \tag{4}$$

where $\bar{\boldsymbol{E}}'$ corresponds to a vector of the e.m.f.s. Here, the generators are again represented by their Thévenin equivalent.

In order to reduce the matrix to the internal nodes and eliminate all nodes, where no current injection takes place, a Kron reduction is carried out, which results in a reduced matrix $\boldsymbol{Y}_{red}$ and the algebraic equations of the reduced network.

$$\bar{\boldsymbol{I}}_{\boldsymbol{tr}} = \boldsymbol{Y}_{\boldsymbol{red}} \bar{\boldsymbol{E}}' \tag{5}$$

With (5) the apparent power injection $\bar{\boldsymbol{S}}$ into the internal node of each machine can be computed as:

$$\bar{\boldsymbol{S}} = \bar{\boldsymbol{E}}' \bar{\boldsymbol{I}}_{tr}^* \tag{6}$$

where $\bar{\boldsymbol{I}}_{tr}^*$ represents the vector of the complex conjugate of the current injections into the internal nodes. Following, the active power injection $P_{e,k}$ of generator k can then be computed as a function of the e.m.f.s of the remaining generators.

$$P_{e,k} = \sum_{l=1}^{m} E'_k E'_l Y_{k,l} \cos(\delta_k - \delta_l - \theta_{k,l}) \tag{7}$$

with $\theta_{k,l}$ and $Y_{k,l}$ being the angle and the magnitude of the admittance $[\boldsymbol{Y}_{red}]_{k,l} = Y_{k,l} \angle \theta_{k,l}$. Under consideration of the "classical" model, the dynamics of the k-th machine are governed by the swing equation [6].

$$\dot{\delta}_k = \omega_k \tag{8}$$

$$\dot{\omega}_k = \ddot{\delta}_k = \tfrac{\omega_0}{M_k}(P_{m,k} - P_{e,k}) \tag{9}$$

where ω_0 corresponds to the synchronous speed, M_k is the inertia coefficient and $P_{m,k}$ is the mechanical power.

B. Equal area criterion

The equal area criterion (EAC) allows determining transient stability of a one-machine infinite bus system (OMIB) without carrying out time-domain simulation. Therefore, a number of simplifications and assumptions are considered. The synchronous machine is represented by its Thévenin equivalent and the mechanical power is assumed to be constant. Furthermore, the machine's damping is neglected and the loads are represented by constant impedances. Under these assumptions, for a OMIB (9) can be rearranged as follows [6]:

$$\left[\tfrac{d\delta}{dt}\right]^2 = \int \tfrac{2}{M}(P_m - P_e(\delta))\, d\delta \tag{10}$$

If a function for the active electric power $P_e(\delta)$ is known, a stability margin can be computed as shown below.

$$\eta = -\int_{\delta_c}^{\delta_u} [P_m - P_{e,P}(\delta)]\, d\delta - \int_{\delta_0}^{\delta_c} [P_m - P_{e,D}(\delta)]\, d\delta \tag{11}$$

The subscripts D and P denote conditions during and after fault clearance respectively. δ_c is the rotor angle at fault clearance and δ_u the angle at the unstable equilibrium point. A positive margin represents a stable case, a negative an unstable.

C. Formulation of a one-machine equivalent (OME)

The proposed aggregation is similar to the one used in [7], where a OMIB equivalent of two aggregated groups of machines is computed. However, here the aim was to assess the dynamics of pairs of machines. For that purpose, a relative rotor angle ϕ_{ij} for each pair is determined as the difference of the rotor angles of generator i and j.

$$\phi_{ij} = \delta_i - \delta_j \tag{12}$$

Similarly, the relative speed ω_{ij} and acceleration $\ddot{\phi}_{ij}$ can be computed.

$$\begin{aligned} \dot{\phi}_{ij} = \omega_{ij} = \omega_i - \omega_j = \dot{\delta}_i - \dot{\delta}_j \\ \ddot{\phi}_{ij} = \dot{\omega}_i - \dot{\omega}_j = \ddot{\delta}_i - \ddot{\delta}_j \end{aligned} \tag{13}$$

With (9) the relative acceleration may be rewritten as follows:

$$\ddot{\phi}_{ij} = \tfrac{\omega_0}{M_i}(P_{m,i} - P_{e,i}) - \tfrac{\omega_0}{M_j}(P_{m,j} - P_{e,j}) \tag{14}$$

As in [7] the inertia coefficient of the OME is computed as:

$$M_{ij} = M_i M_j / M_T \text{ with } M_T = M_i + M_j \tag{15}$$

Following, the dynamics of the OME of a pair of machines can be described by a new swing equation.

$$\ddot{\phi}_{ij} = \tfrac{\omega_0}{M_{ij}}\,(P_{m,ij} - P_{e,ij}) \tag{16}$$

where

$$P_{m,ij} = M_T^{-1}\,(M_j P_{m,i} - M_i P_{m,j}) \tag{17}$$

$$P_{e,ij} = M_T^{-1}\,(M_j P_{e,i} - M_i P_{e,j}) \tag{18}$$

Under the assumption that the mechanical power of both generators remains constant, the relative acceleration of the OME is dependent on the electric power of the individual machines. It can be shown that (18) can be reformulated as:

$$P_{e,ij}(\phi_{ij}) = P_{c,ij} + P_{max,ij} \sin(\phi_{ij} - \nu_{ij}) \tag{19}$$

where

$$P_{c,ij} = \frac{1}{M_T}\left[M_j {E'_i}^2 Y_{ii} cos(\theta_{ii}) - M_i {E'_j}^2 Y_{jj} cos(\theta_{jj})\right]$$
$$P_{max,ij} = \sqrt{D_{ij}^2 + C_{ij}^2} \text{ and } \nu_{ij} = -\tan^{-1}\frac{C_{ij}}{D_{ij}} \quad (20)$$

with

$$\begin{aligned} C_{ij} = \; & \frac{1}{M_T}\left[M_j \sum_{k=1}^{m} E'_i E'_k Y_{ik} \cos(\delta_j - \delta_k - \theta_{ik})\right. \\ & \left. -M_i \sum_{k=1}^{m} E'_j E'_k Y_{jk} \cos(\delta_i - \delta_k - \theta_{jk})\right] \\ D_{ij} = \; & -\frac{1}{M_T}\left[M_j \sum_{k=1}^{m} E'_i E'_k Y_{ik} \sin(\delta_j - \delta_k - \theta_{ik})\right. \\ & \left. +M_i \sum_{k=1}^{m} E'_j E'_k Y_{jk} \sin(\delta_i - \delta_k - \theta_{jk})\right] \end{aligned} \quad (21)$$

With (19) the swing equation of the OME can be expressed as follows, which allows computation of the EAC.

$$\ddot{\phi}_{ij} = \frac{\omega_0}{M_{ij}}\left[P_{m,ij} - (P_{c,ij} + P_{max,ij}\sin(\phi_{ij} - \nu_{ij}))\right] \quad (22)$$

D. Coupling coefficients

In this analysis the coupling strength between two generators is defined as the available excess dissipation energy and, hence, it can be computed as the difference between available dissipation energy after fault clearance and kinetic energy gained during the fault. In order to determine the coupling coefficient, (10) can be reformulated as follows.

$$\tfrac{1}{2}\frac{M_{ij}}{\omega_0}\dot{\phi}_{ij}^2 = \int P_{a,ij} d\phi_{ij} \quad (23)$$

where $\dot{\phi}_{ij} = \omega_{ij}$ and $P_{a,ij}$ with (17) & (19) is described as:

$$P_{a,ij} = P_{m,ij} - [P_{c,ij} + P_{max,ij}\sin(\phi_{ij} - \nu_{ij})] \quad (24)$$

Under consideration of the EAC, in (23) the left-side term represents the kinetic energy $E_{kin,ij}$ and the right-side the dissipation energy $E_{dis,ij}$, which corresponds to the maximum kinetic energy that the OME can absorb. The OME is stable, if the available $E_{dis,ij}$ is greater or equal to $E_{kin,ij}$ induced by the fault. Therefore, it is proposed that the coupling strength is approximated by the coupling coefficient c_{ij}.

$$c_{ij} = E_{dis,ij} - E_{kin,ij} \quad (25)$$

where

$$\begin{aligned} E_{dis,ij} = \; & -\int_{\phi_{c,ij}}^{\phi_{u,ij}} P_{m,ij} - P_{e,ij}(\phi_{ij}) d\phi_{ij} \\ E_{kin,ij} = \; & \tfrac{1}{2}\frac{M_{ij}}{\omega_0}\omega_{ij}^2 \end{aligned} \quad (26)$$

The proposed coupling strength c_{ij} is negative, when the coupling is very weak and the two machines are likely to lose synchronism, and it is positive, when there is strong coupling, which makes it likely that the two machines remain in synchronism. By computing the coupling strength between each pair of machines a coupling matrix $\mathbf{H}$ can be constructed.

E. Impact of fault on coupling strength

The coupling matrix $\mathbf{H}$ can be computed for steady state and dynamic system conditions. In steady state the relative speed between the generators is equal to zero and, hence, the coupling coefficients are solely determined by the available dissipation energy. In order to determine the CMC after the occurrence and the clearance of a fault, the change in coupling strength due to the fault was found to be essential. Therefore,

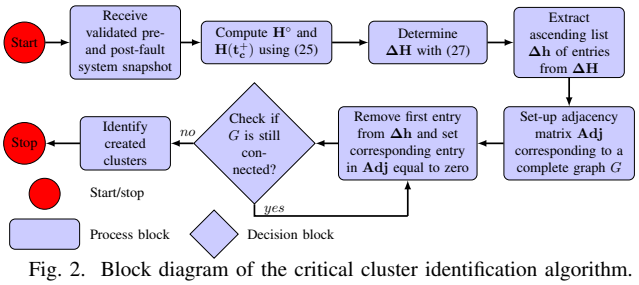

Fig. 2. Block diagram of the critical cluster identification algorithm.

it is proposed to use $\mathbf{\Delta H}$, which is the difference in coupling strength between post- and pre-fault condition.

$$\mathbf{\Delta H} = \mathbf{H}(t_c^+) - \mathbf{H}^\circ \quad (27)$$

where $\mathbf{H}(t_c^+)$ is the coupling matrix determined at the time just after fault clearance t_c^+ and $\mathbf{H}^\circ$ is the coupling matrix determined at steady state before the fault. By using the difference in coupling strength, focus is set on changes, structural as well as dynamic, due to the fault. If the coupling between two generators is weakened in the post-fault condition the corresponding entry in $\mathbf{\Delta H}$ becomes negative, while a strengthening of the coupling results in a positive value.

III. Critical Machine Cluster Identification

In order to identify the CMC, an algorithm was developed. A block diagram of the algorithm is shown in Fig. 2. In this approach two snapshots, one of the pre- and one of the post-fault system condition, are used to compute the coupling matrices $\mathbf{H}^\circ$ and $\mathbf{H}(t_c^+)$. These matrices are then used to compute the change in coupling strength between individual generators due to the fault, which results in the matrix $\mathbf{\Delta H}$. The entries of $\mathbf{\Delta H}$ are copied into the vector $\mathbf{\Delta h}$, where the entries are sorted ascending. Moreover, an adjacency matrix Adj is initialized with the same dimension as $\mathbf{\Delta H}$ and corresponding to a complete graph G, where each node of G corresponds to a generator. In order to identify the CMC, individual edges are removed one by one from G until the graph is split. The edges are removed beginning with the lowest change in coupling strength and according to the list of increasing changes in $\mathbf{\Delta h}$. After each removal a depth-first search (DFS) is carried out to check if G is still connected. If a splitting of the graph occurred, a second DFS based algorithm is executed to identify the created clusters. Since each node of G corresponds to a generator in the system, a splitting of the graph corresponds to a separation of the generators into clusters and the proposed approach is designed to identify the weakest coupled clusters.

IV. Results for CMC Identification

A. Test system and scenario

The power system model, employed to test the presented method, is the New England & New York system described in [8]. It consists of 68 buses and 16 generators. The loads are modelled as constant impedances and the generators are represented by a sixth order model in the time-domain simulation. All generators have a simple excitation and voltage regulation system as well as a thermal turbine/governor model. Moreover,

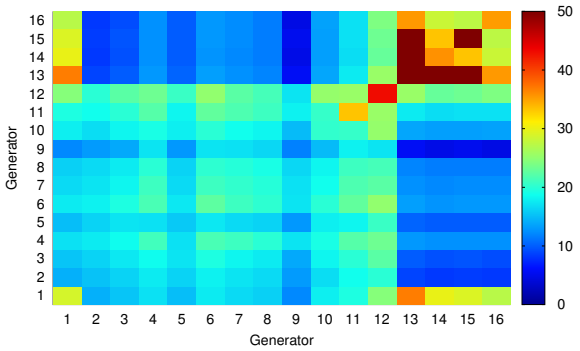

Fig. 3. Coupling matrix computed by (25) in steady state initial conditions.

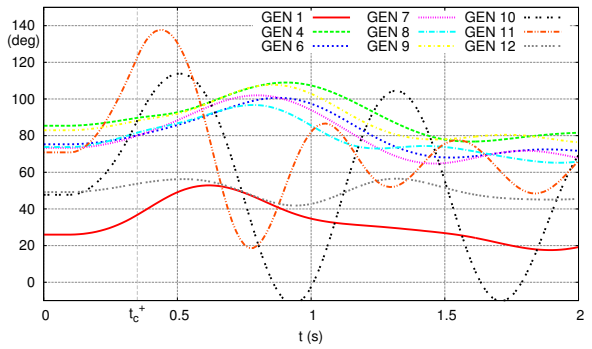

Fig. 4. Case 1: Rotor angle response of a selection of generators.

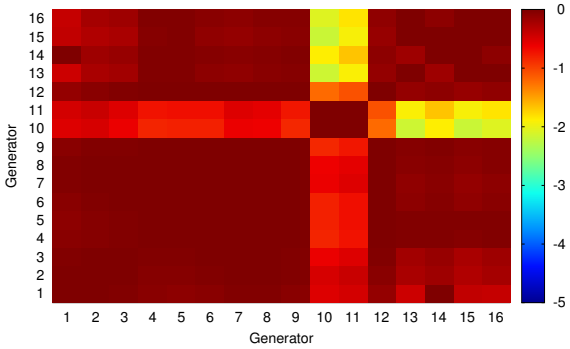

Fig. 5. Case 1: $\mathbf{\Delta H}$ computed by (27) at t_c^+.

all generators, but GEN 7 and GEN 14, are equipped with a power system stabilizer. The initial state of the system was as well adopted from [8]. To test the proposed method three-phase short circuits on individual transmission lines were considered, which last for 250 ms and are cleared by opening of the breakers at both ends of the respective transmission line.

B. Coupling strength at initial conditions

In the following the coupling strength matrix is computed for the pre-fault steady state conditions with the equations derived in Sec. II-D, the results are used to show the apparent correlation of the proposed coupling coefficients and the structure of the power system. The coupling matrix in the initial conditions is shown in Fig. 3. The obtained coupling coefficients of the generators are compared to each other relatively, where greater values, e.g. above 25, indicate a stronger coupling, while lower values, e.g. below 20, correspond to a weaker coupling. Visual inspection of the graph allows identifying patterns, which may indicate a stronger coupling between certain generators. The coupling coefficients between the generators GEN 1 & $13-16$ may suggest a tight coupling. In the one-line diagram, which can be found in e.g. [9], it can be seen that the generators GEN $14-16$ are close and well connected. Moreover, generator GEN 1 is strongly connected with two transmission lines to the area, which may explain the strong coupling to this generator group. The generators GEN $4-8$ & $10-11$ seem to be tightly coupled as well. The coupling strength of generator GEN 12 appears to be relatively high with respect to all generators but generator GEN 9. This could indicate that generator GEN 12 has a large impact on all generators, which may also be explained by its central location in the system. GEN 9 appears to have weaker coupling to the other generators. This may be explained by its remote location and the few lines connecting it to the rest of the system.

C. Case 1: Transient stable

In this section an example case is shown, where a transient disturbance occurs but does not lead to a loss of synchronism of generators. The considered contingency is a three-phase short circuit on the transmission line connecting bus 1 and 30.

1) Rotor angle response: The rotor angle response of a selection of generators is shown in Fig. 4. The selection contains the two generators GEN 10 & 11, which are strongest effected by the fault, six generators (GEN 1, 4 & $6-9$), which experience a less significant deviation in rotor angle, and generator GEN 12, which is in the vicinity of the fault but barely effected. Although the fault causes significant oscillation of the rotor angles of generator GEN 10 & 11, the system remains stable and returns to a new steady state.

2) Critical cluster identification: The matrix $\mathbf{\Delta H}$ can be displayed as a two-dimensional grid, where the matrix entries and, consequently, the changes in coupling strength are displayed by different colors. Figure 5 shows the changes in coupling strength computed at t_c^+. The graph suggests that the coupling strength between most generators was barely affected by the fault. However, the coupling of GEN 10 & 11 to the remaining generators appears to be weakened by the fault, which is well aligned with the observations from Fig. 4.

When the proposed algorithm is employed, individual connections of the graph corresponding to the values in $\mathbf{\Delta H}$ are removed beginning with the largest negative change. The removing of the connections is done by setting the corresponding entries in the adjacency matrix to zero. Figure 6 shows the adjacency matrix at the instance when the proposed clustering algorithm splits the graph into two. The proposed method identifies by employing the DFS based algorithm presented in Fig. 2 that GEN 10 & 11 are the generators with the weakest coupling to the remaining system. This is well aligned with the observations described in Sec. IV-C1.

D. Case 2: Transient unstable

In this section the performance of the method is presented on a transient unstable case. The contingency is a three-phase short circuit on the transmission line connecting bus 4 and 5.

1) Rotor angle response: The rotor angle responses of a selection of generators are shown in Fig. 7. The selection

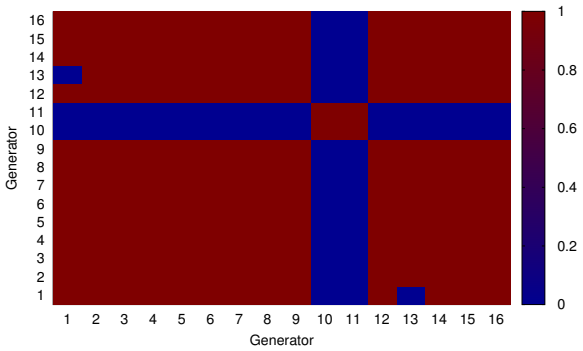

Fig. 6. Case 1: Adjacency matrix after graph split into two disjoint subsets.

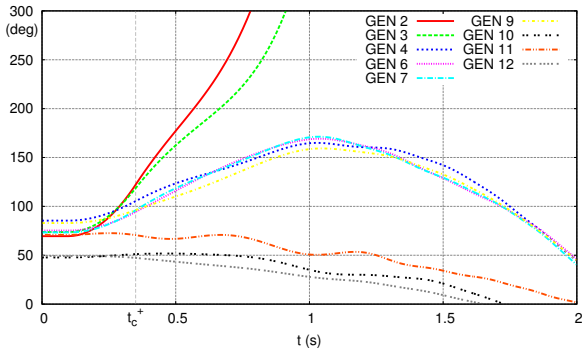

Fig. 7. Case 2: Rotor angle response of a selection of generators.

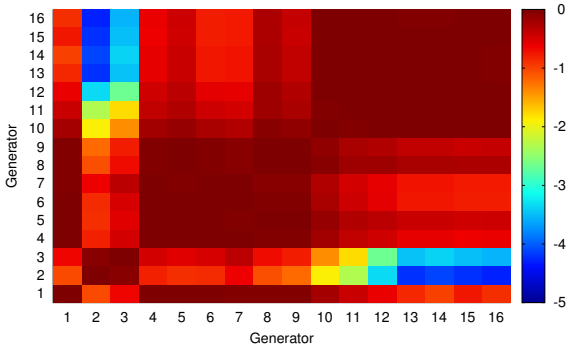

Fig. 8. Case 2: $\mathbf{\Delta H}$ computed by (27) at t_c^+.

contains the two generators GEN 2 & 3, which are losing synchronism, the generators GEN 4, 6, 7 & 9, which are also significantly impacted by the fault, and GEN $10-12$, which are initially less affected by the fault. The loss of generator GEN 2 & 3 is leading to a considerable lag of power, which leads to a system collapse. The rotor angles at t_c^+ may suggest that the generators initially splits into two clusters, where the first consists of GEN $2-4$, 6, 7 & 9 and the second of GEN $10-12$. Later the generators split into three groups namely, GEN 2 & 3, GEN 4, 6, 7 & 9 and GEN $10-12$.

2) Critical cluster identification: Figure 8 shows the change in coupling strength. The visual inspection of the graph allows identifying three machine clusters. The first cluster is GEN 1 & $4-9$, the second cluster is GEN $10-16$ and the third cluster is GEN 2 & 3. This is in good agreement with the observations extracted from the rotor angles shown in Fig. 7.

The $\mathbf{\Delta H}$ matrix is again forwarded to the cluster identification algorithm, where the matrix is converted into a graph. Figure 9 shows the adjacency matrix of the corresponding

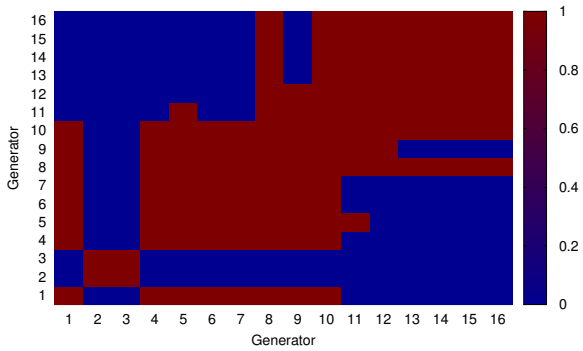

Fig. 9. Case 2: Adjacency matrix after graph split into two disjoint subsets.

graph, when the first decoupled set of generators is identified with the proposed algorithm. It can be seen that all connections from generators GEN 2 & 3 are removed and, hence, already at t_c^+ the algorithm identifies those generators as the CMC.

V. Conclusion

In this paper a new approach was proposed for identifying the CMC after a transient disturbance. For that purpose, a novel coupling coefficient was derived, which is determining the coupling strength of each pair of generators. This coefficient can be used to set up a coupling matrix, which describes the coupling strength between all generators in the system. In order to determine the CMC after a fault, the coupling strength matrix is determined for the initial condition and just after fault clearance. The difference of the two matrices is a new matrix, which describes the change of the coupling strength due to the fault and can be utilized to identify the CMC. A method, which uses efficient algorithms from graph theory, was proposed to identify the CMC. In two test cases it was demonstrated that although the coupling coefficients do not encompass all the existing controls, the clustering algorithm allows early and correct determination of the CMC. Another application of the developed cluster coefficients may be the early identification of stable cases, which will be further investigated.

References

[1] K. Morison, L. Wang, and P. Kundur, "Power system security assessment," *IEEE Power and Energy Magazine*, vol. 2, no. october, 2004.

[2] H.-D. Chiang, F. F. Wu, and P. P. Varaiya, "A BCU Method for Direct Analysis of Power System Transient Stability," *IEEE Transactions on Power System*, vol. 9, no. 3, pp. 1194–1208, Aug. 1994.

[3] Y. Xue, T. Van Cutsem, and M. Ribbens-Pavella, "Extended equal area criterion justifications, generalizations, application," *IEEE Transaction on Power Systems*, vol. 4, no. 1, pp. 44–52, Feb. 1989.

[4] M. Pavella, D. Ernst, and D. Ruiz-Vega, *Transient Stability of Power Systems: A Unified Approach to Assessment and Control*. Kluwer Academic Publishers, 2000.

[5] J. Lee, B. Lee, S.-H. Kwon, H.-K. Nam, J.-B. Choo, and K. Yi, "Fast contingency screening for on-line transient stability monitoring of the KEPCO system," in *2001 PES Summer Meeting. Conference Proceedings*, vol. 1. IEEE, 2001, pp. 314–319.

[6] P. Kundur, *Power System Stability and Control*, N. J. Balu and M. G. Lauby, Eds. McGraw-Hill Inc., 1994.

[7] Y. Xue and M. Pavella, "Extended equal-area criterion: an analytical ultra-fast method for transient stability assessment and preventive control of power systems," *Int. J. Elec. Power*, vol. 11, no. 2, Apr. 1989.

[8] G. Rogers, *Power System Oscillations*. Springer, 2000.

[9] D. Molina, J. Liang, R. G. Harley, and G. K. Venayagamoorthy, "Virtual Generators: Simplified Online Power System Representations for Wide-Area Damping Control," in *IEEE PES General Meeting*, Jul. 2012.

Appendix E

Sensitivity based Assessment of Transient Voltage Sags caused by Rotor Swings

---

This paper has been presented at the 18^{th} Power System Computation Conference (PSCC 2014) in Wroclaw, Poland and has been published as part of the conference proceedings.

Sensitivity based Assessment of Transient Voltage Sags caused by Rotor Swings

Tilman Weckesser Hjörtur Jóhannsson Jacob Østergaard Thierry Van Cutsem

***Abstract*—The paper introduces an approach to investigate voltage sags, which are caused by large generator rotor swings following a transient disturbance. Therefore, the method exploits sensitivities derived from the algebraic network equations. These provide information on the impact of a generator on the voltage magnitude at a load bus and the effect of load variation on the generator's power injection. It is shown that these sensitivities give valuable information to identify critical generator-load pairs and locations for applying preventive control measures.**

***Index Terms*—power system stability, sensitivity to rotor swings, transient stability, voltage sag**

I. Introduction

In literature on power quality, voltage sags/dips is a topic vastly addressed [1]. While the primary cause is the occurrence of a fault, a less pointed out reason for voltage sags is rotor angle swing, more precisely angular separation of generators, resulting from a fault. From a practical viewpoint, a scenario may be assessed transiently stable considering that generators remain in synchronism, while voltage sags due to the relative rotor angle displacement already result in transiently low voltages for which the system response should be considered unacceptable.

The prediction of this type of voltage sag using the Transient Energy Function was described in the early reference [2]. In [3] sensitivities relative to voltage dip were derived using this method as well. The sensitivities relate the voltage sag depths to certain parameters such as terminal voltages and power generation. The authors of [4] address the transient voltage dip acceptability problem using a two-dimensional table of critical voltage level and critical voltage dip duration. Moreover, the issue of transient voltage stability of dynamic loads such as induction machines is analysed. In the more recent reference [5] the authors use sensitivities to carry out contingency filtering and ranking with respect to voltage dips. Furthermore, the assessment addresses power quality issues and short-term voltage stability. In [6], the authors present a survey of current practices for transient voltage sag criteria related to power system stability.

T. Weckesser, H. Jóhannsson and J. Østergaard are with the Center for Electric Power and Energy (CEE) at the Technical University of Denmark (DTU), Kgs. Lyngby, Denmark, email: {jtgw}{hjjo}{joe}@elektro.dtu.dk

T. Van Cutsem is with the Fund for Scientific Research (FNRS) at the University of Liège, Belgium, email: t.vancutsem@ulg.ac.be

Paper submitted to Power Systems Computation Conference, August 18-22, 2014, Wroclaw, Poland, organized by Power Systems Computation Conference and Wroclaw University of Technology.

Research supported by the Danish Council for Strategic Research (DSF).

The present paper also investigates voltage sags with focus on power system stability rather than power quality. Transient voltage sags are identified using time-domain simulation. Then, sensitivities are derived which provide information on tight couplings between relative change of rotor angles and load voltage magnitudes. These sensitivities are easier to compute than those considered in the above references.

The sensitivities can be used, for instance, to identify the contribution of each generator to a drop in voltage magnitude experienced at a particular load bus. A voltage depression at a load bus can trigger consecutive events such as load tripping. Therefore, a second sensitivity is derived, which assesses the impact of a change of load power on generator active powers.

This paper is organized as follows. In Section II the power system model used for the computation of sensitivities is described and the voltage sensitivities are derived. This is followed by the presentation of the corresponding results in Section III. The derivation of the second sensitivities, addressing the effect of variation of load on generator power, can be found in Section IV and the corresponding results are shown in Section V. Finally, in Section VI concluding remarks are offered.

II. Derivation of Load Voltage Sensitivities

A. Modelling for sensitivity analysis

The model used for sensitivity analysis is the so-called "classical" transient stability model [7]. Each generator is modeled by an e.m.f. $\bar{E}'$ of constant magnitude behind the transient reactance X'_d (see Fig. 1(a)), the mechanical power input is assumed constant, and loads are converted to constant shunt admittances. The simple generator model is valid in the first second after fault clearance and the justification for using it is twofold. First, this model is used for sensitivity analysis. As indicated in the Introduction, this analysis is aimed at complementing a detailed time-domain simulation in which much more refined models can be used. Second, the classical model is not used with constant e.m.f. throughout the whole simulation: instead, the e.m.f. is adjusted so that the classical model fits specific operating points where the sensitivity analysis is carried out.

For convenience each generator is represented by its Norton equivalent (see Fig. 1(b)), i.e. a current source $\bar{E}'/(jX'_d)$ in parallel with the admittance $1/(jX'_d)$. Based on these assumptions, the following well-known linear algebraic equations can be used:

$$\bar{\boldsymbol{I}} = \boldsymbol{Y}\bar{\boldsymbol{V}} \tag{1}$$

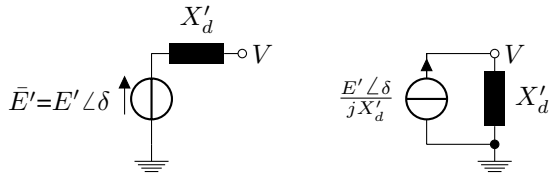

(a) Thevenin Equivalent (b) Norton Equivalent

Fig. 1. Thévenin and Norton equivalents of generator

where $\bar{\boldsymbol{I}}$ is the vector of complex currents injected at the generator buses (stemming from the Norton equivalents), $\bar{\boldsymbol{V}}$ is the vector of complex bus voltages, and $\boldsymbol{Y}$ is the "augmented" bus admittance matrix obtained by adding the contribution of generators and loads to the matrix relative to the network.

A system with n buses and m machines is considered $(n > m)$. It is assumed, without loss of generality, that the buses where machines are connected are numbered from $n-m+1$ to n. Hence, Eq. (1) can be detailed as:

$$\begin{bmatrix} 0 \\ \vdots \\ 0 \\ \bar{E}'_1/(jX'_{d,1}) \\ \vdots \\ \bar{E}'_m/(jX'_{d,m}) \end{bmatrix} = \boldsymbol{Y} \begin{bmatrix} \bar{V}_1 \\ \vdots \\ \bar{V}_{n-m} \\ \bar{V}_{n-m+1} \\ \vdots \\ \bar{V}_n \end{bmatrix} \tag{2}$$

where the zero sub-vector has dimension $n-m$ and $\bar{V}_i$ is the complex voltage at the i-th bus.

B. Load voltage sensitivities

In this section, sensitivities are derived to identify the load buses whose voltage magnitudes are strongly affected by changes of the rotor angle of particular generators. They are referred to as "load voltage sensitivities". The latter will be used to determine the contribution of individual generators to an observed voltage sag at a load bus.

The effect of a small rotor angle change is assessed through modification of Eq. (2). To this purpose, the e.m.f. phasor of the k-th generator, $\bar{E}'_k$, is slightly rotated, while the other generators remain unchanged. This corresponds to a small change of the rotor angle, when generators are represented by the classical model. The new bus voltages $\overline{\boldsymbol{V}}^{\dagger}$ that result from a small increase ϵ in the phase angle of $\bar{E}'_k$ are easily computed by solving the modified linear system:

$$\begin{bmatrix} 0 \\ \vdots \\ 0 \\ \bar{E}'_1/(jX'_{d,1}) \\ \vdots \\ \bar{E}'_k\, e^{j\epsilon}/(jX'_{d,k}) \\ \vdots \\ \bar{E}'_m/(jX'_{d,m}) \end{bmatrix} = \boldsymbol{Y} \begin{bmatrix} \bar{V}_1^{\dagger} \\ \vdots \\ \bar{V}_{n-m}^{\dagger} \\ \bar{V}_{n-m+1}^{\dagger} \\ \vdots \\ \vdots \\ \vdots \\ \bar{V}_n^{\dagger} \end{bmatrix} \tag{3}$$

Clearly, in order to speed up computations, the admittance matrix $\boldsymbol{Y}$ is LU-factorized once for all, and Eq. (3) is solved for each change ϵ in the left-hand-side vector.

The changes of magnitudes between the "new" and the reference bus voltages are calculated and normalized. The sensitivities of the various bus voltage magnitudes to the i-th generator rotor angle are computed as:

$$(\boldsymbol{s}_{V,Gi})_{\ell} = \frac{|\bar{V}_{\ell}^{\dagger}| - |\bar{V}_{\ell}|}{\pi\epsilon/180} \quad \ell = 1, \ldots, m-n \tag{4}$$

where ϵ is expressed in degrees. The resulting sensitivity vector has the unit $[pu/rad]$ or $[V/rad]$. This vector can be determined for each generator in the system and the aggregation of the individual vectors gives a sensitivity matrix $\boldsymbol{S}_{V,G}$, where each column corresponds to a generator and each row to a load bus. This matrix allows identifying the generators having a dominant impact on a certain load bus voltage magnitude. The entries also indicate whether increasing a rotor angle will increase a voltage magnitude or will depress it.

C. Contribution of individual generators to a voltage sag

Once it has been found from time simulation that a significant voltage sag is experienced at some load bus, the voltage sensitivities presented in the previous sub-section can be utilized to identify the contribution of each individual generator. The procedure described hereafter was found to provide the most accurate results.

The time-domain simulation is carried out until the minimum voltage is reached at the load bus of interest. In order to ignore bus voltage variations caused by topological changes, the voltage magnitude reduction is considered between the time t_c of fault clearing and the instant t_{Vmin} where the minimum of voltage is reached. The excursions $\Delta\delta_j$ $(j = 1, \ldots, m)$ of rotor angles are considered over the time interval $[t_c\ t_{Vmin}]$. Furthermore, the load voltage sensitivities $\boldsymbol{S}_{V,G}$ are determined at time t_c^+. Therefore, the bus voltages $V(t_c^+)$ and the power consumption of the loads just after the system has entered its post-fault configuration are used to update the admittance matrix and, subsequently, to compute the Norton equivalent of the generators.

Therewith, an estimate of the voltage magnitude drop at bus i can be calculated through linearisation, using the load voltage sensitivities, as follows:

$$\Delta V_i = \textstyle\sum_{j=1}^{m} [\boldsymbol{S}_{V,G}]_{ij}\, \Delta\delta_j = \sum_{j=1}^{m} \Delta V_{i,j} \tag{5}$$

Finally, the share of the k-th generator in the total change of voltage magnitude can be determined as:

$$f_{i,k} = \frac{\Delta V_{i,k}}{\left|\sum_{j=1}^{m} \Delta V_{i,j}\right|} \tag{6}$$

Using this fraction and the voltage trajectory obtained from time-domain simulation, the actual share of the k-th generator in the voltage sag at the i-th bus can be computed as:

$$\Delta V^*_{i,k} = f_{i,k}\, \left|V_i(t_c^+) - V_i(t_{Vmin})\right| \tag{7}$$

where $V_i(t_c^+)$ is the voltage at bus i immediately after fault clearing and $V_i(t_{Vmin})$ its minimum value.

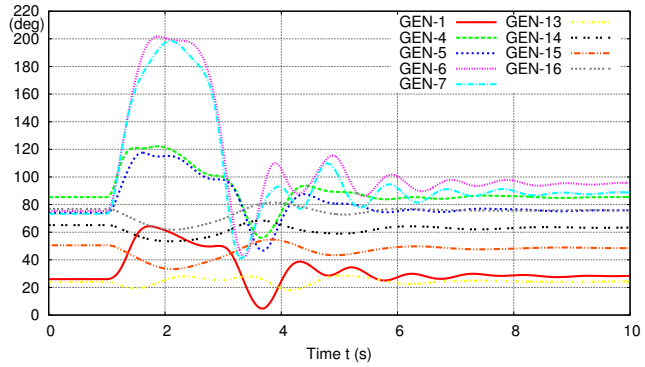

Fig. 2. Evolution of rotor angles of a selection of generators (with respect to center of inertia)

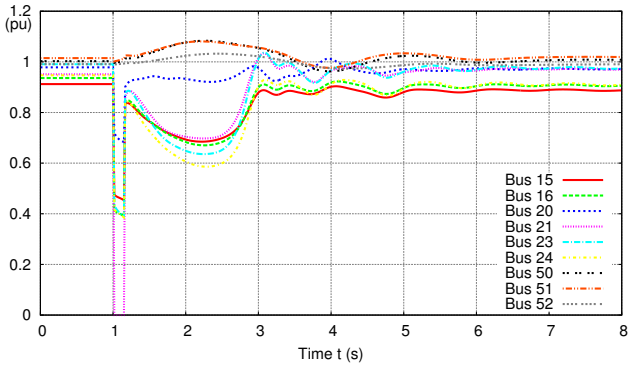

Fig. 3. Evolution of voltage magnitudes at a selection of load buses

III. Results for Load Voltage Sensitivities

A. Test system and example case

1) Test system: The test system employed to validate the presented sensitivities is the well-known New England & New York system described in [8]. It consists of 68 buses and 16 generators. The loads are modelled as constant impedances in the time-domain simulation. The generators are represented by a sixth order model. They all have a simple excitation and voltage regulation system, and a thermal turbine/governor model. Furthermore, all generators, but GEN-7 and GEN-14, are equipped with a power system stabilizer.

2) Test scenario: The test scenario was as well adopted from [8]. In this case, the considered contingency is a three-phase short-circuit on the transmission line connecting buses 16 and 21. The short-circuit occurs one second after the simulation begins and is assumed to be very close to bus 21. It is cleared after 150 ms by opening the breakers at both ends of the faulted transmission line.

The disturbance causes some generators to accelerate relative to the others, which leads to a significant separation of the generator rotor angles. Figure 2 shows the evolution of the rotor angles of nine among the sixteen generators: the five generators with the largest increase of rotor angle (GEN-1, GEN-4, GEN-5, GEN-6 and GEN-7), the three generators with the largest decrease (GEN-14, GEN-15 and GEN-16) and one which is barely affected (GEN-13). The graph shows that the generators are affected to different degrees by the disturbance; in particular, GEN-6 and GEN-7 are experiencing large rotor angle excursions. However, all generators remain in synchronism and reach a new stable equilibrium point. Consequently, the scenario is assessed to be stable. Figure 3 displays the time evolution of voltage magnitudes at a selection of load buses. The selection consists of the five buses which experience the lowest voltages (buses 15, 16, 21, 23 and 24), the three buses whose voltage magnitude are slightly increased (buses 50, 51 and 52), and one bus barely affected (bus 20). As expected the voltage magnitudes drop dramatically in the fault-on period, and recover immediately after fault clearing. However, in the subsequent evolution, a voltage sag can be observed at certain buses. At some buses the voltage drops

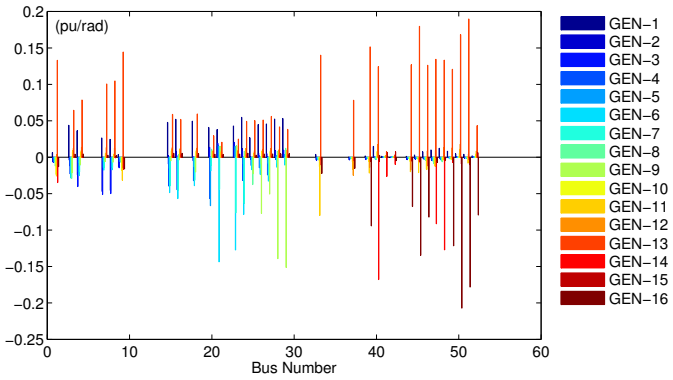

Fig. 4. Load voltage sensitivities

below the critical value of 0.7 pu, which is unacceptably low and long lasting.

B. Identification of critical generator-load pairs

In order to clearly identify which generators strongly impact load bus voltage magnitudes, the load voltage sensitivities described in the previous section are computed using Eq. (4) and data obtained from time-domain simulation, just after fault clearance. Figure 4 shows the resulting sensitivities. The bar graph shows for all load buses the expected change in voltage magnitude (in pu/rad) resulting from an increase of individual generator rotor angle. The values clearly indicate that an angle increase can either depress or boost a voltage magnitude.

In the example scenario, GEN-6 and GEN-7 experience large rotor angle excursions and are likely to cause the observed voltage sags. Indeed, Fig. 4 indicates that GEN-6 and GEN-7 mainly affect the voltage magnitudes at buses with numbers in the range of $15-24$. Furthermore, from Fig. 2 it can be observed that GEN-14, GEN-15 and GEN-16 experience a slight decrease of their rotor angle. The sensitivities in Fig. 4 indicate that GEN-16 strongly affects the load buses with numbers in the range of $49-52$. In the following, a more detailed analysis of this group is considered.

Figure 5 shows a selection of sensitivities displayed in the bar graph of Fig. 4, relative to above mentioned subset of generators and load buses. Dominant negative sensitivities indicate that increasing the corresponding rotor angles

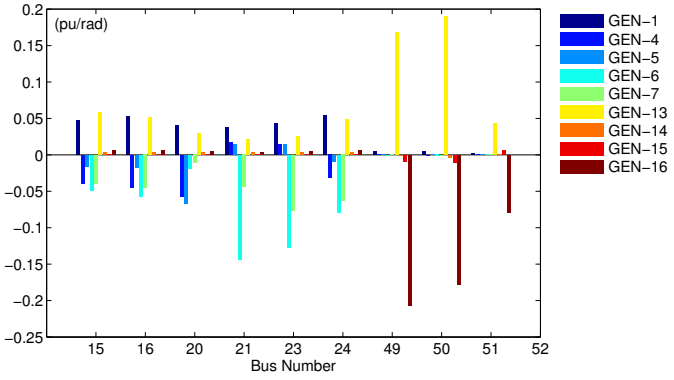

Fig. 5. Load voltage sensitivities for a subset of loads and generators

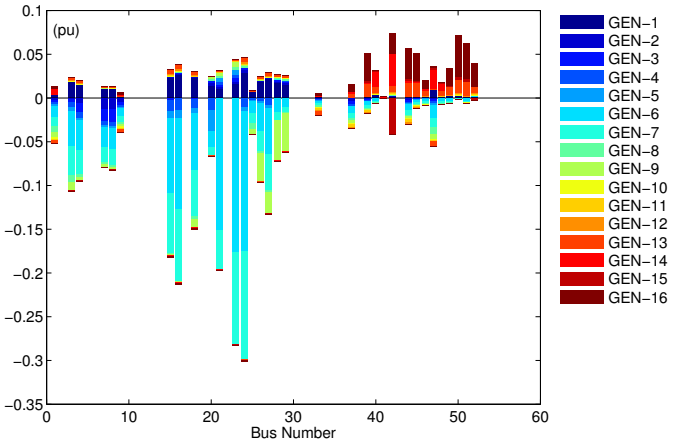

Fig. 6. Contribution of individual generators to voltage depressions

would decrease the voltage magnitude at the respective load buses, and vice versa. These high sensitivities combined with the generator rotor angle deviations can explain the voltage magnitude evolutions at the load buses shown in Fig. 3. The sensitivities in Fig. 5 suggest that the load buses where GEN-6 and GEN-7 are dominant, will experience a voltage depression, which is the case for buses 15, 16, 21, 23 and 24. The voltage at bus 20 is less affected, which is in good correlation with the lower sensitivities to the critical generators GEN-6 and GEN-7. Furthermore, Fig. 5 suggests that the load buses where GEN-16 is dominant experience a slight increase of their voltage magnitudes corresponding to the negative sensitivity and the decreasing rotor angle of GEN-16. This is in very good agreement with the voltage evolutions shown in Fig. 3.

C. Contribution of individual generators

Another use of the load voltage sensitivities is to determine the contribution of each generator to an observed voltage sag at a particular bus, as described in Section II-C, more precisely by Eq. (7). For the same test scenario, the contributions $\Delta V^*_{i,k}$ of each generator to the voltage sags are presented in Fig. 6.

As for the load voltage sensitivities, the individual contributions of the generators show that each generator strongly impacts load buses in a certain vicinity and can have either a positive or a negative effect on the voltage magnitude.

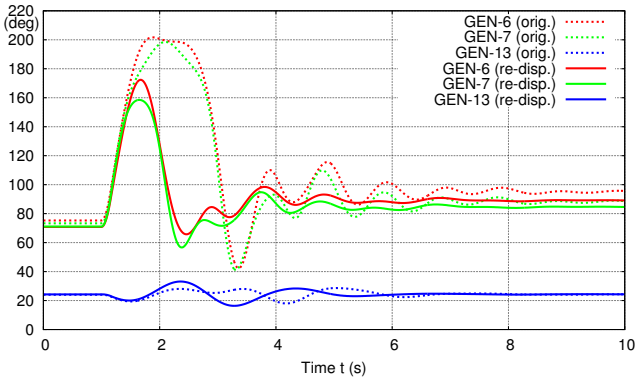

Fig. 7. Rotor angle responses before and after power re-dispatch

Moreover, it can be seen that, at an individual load bus, either a positive or a negative contribution can be dominant (see for instance buses 23, 24, 50 and 51), or the contributions of various generators compensate each other to a large extent (see for instance buses 37 and 42).

D. Application to generator re-dispatch

The above individual generator contributions also point out effective locations for preventive control aimed at mitigating the voltage sags.

In the scenario under concern, GEN-6 has been identified as one major source of the voltage sags. Consequently, a reduction of its rotor angle excursion due to the fault could significantly improve the post-fault voltage evolutions. This can be achieved by reducing the critical generator's pre-fault active power and re-dispatching the power difference to appropriate non-critical generators.

The results of such a re-dispatch are presented next. The power output of GEN-6 was reduced by merely 50 MW (from 700 to 650 MW) while the power output of GEN-13 was increased to cover the difference. These two generators were chosen, because GEN-6 has a large contribution to the severe voltage sags at buses 15, 16, 21, 23 and 24, while the sensitivities shown in Fig. 5 suggest that a rotor angle increase of GEN-13 tends to increase the same voltage magnitudes. Alternatively, any other generator with a negligible sensitivity could have been chosen to compensate the power reduction of the critical generator. In this test scenario the critical group of machines, which is the group that will loose synchronism in case of a fault cleared a little after the critical clearing time, consists of GEN-6 and GEN-7. Due to the tight coupling of those two generators, a preventive control applied to one of them will as well have a positive affect on the other.

Figure 7 shows a comparison of the rotor angle responses of GEN-6, GEN-7 and GEN-13, before and after the re-dispatch, respectively. It can be observed that, due to the active power re-dispatch, the large rotor angle excursion is significantly reduced for GEN-6 and GEN-7. Furthermore, the duration of the first swing is almost halved. The beneficial effect on the voltage evolutions is evident in Fig. 8, showing the voltage evolutions at the load buses 15, 16, 21, 23 and 24. The depth

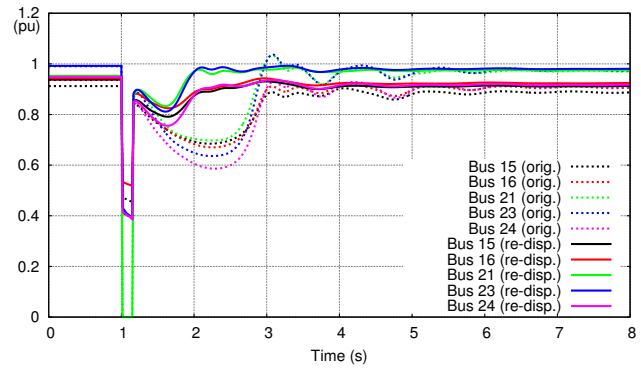

Fig. 8. Voltage magnitude evolutions before and after power re-dispatch

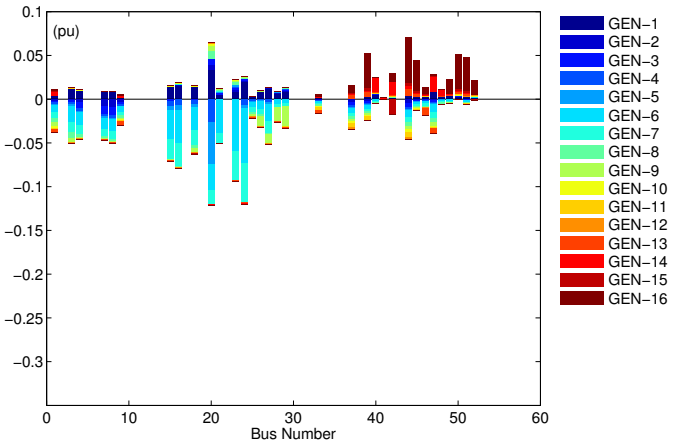

Fig. 9. Contribution of individual generators to voltage depressions after power re-dispatch

of the voltage sag at each load bus is reduced dramatically and the duration of the swing is more than halved.

The individual generator contributions updated after the power re-dispatch are shown in Fig. 9. It can be observed that all the negative contributions are significantly lower in magnitude. At the same time, the load voltage sensitivities have been little affected by the small power re-dispatch. Consequently, the voltage improvement results essentially from the decreased rotor angle excursion of the critical generators.

The above example has demonstrated the usefulness of load voltage sensitivities and individual generator contributions to identify the source of voltage sags and appropriate locations for preventive control. It should be noted that, at this stage, those indexes do not provide information on the required amount of preventive control.

IV. Derivation of Generator Power Sensitivities

A. Motivation

A depressed voltage, falling below a certain critical level, may trigger consecutive events such as load disconnection by internal protections, or possibly under-voltage load shedding in a system provided with this integrity protections scheme. The subsequent reduction of power consumption at some load buses may lower the maximum of the $P(\delta)$-curves of some generators. This leads to a reduction of the available deceleration area, which is detrimental for stability if those generators belong to the critical group, and beneficial if they belong to the non-critical one [9].

In order to investigate the effect of load variations on generator active powers, a second type of sensitivities is considered, based on the same model as in Section II-A. The increase of load consumption is obtained from an extra load admittance Δy added at the bus of concern, and the goal is to determine the effect on the generator active powers. It was found that these sensitivities provide the most accurate results when calculated directly after fault clearance, at time t_c^+.

B. Derivation of generator power sensitivities

The first step consists in estimating the bus voltages after increasing the load admittance at the k-th bus by a small value Δy. To this purpose, let us assume that this additional admittance draws a current $\Delta\bar{I}_k$ from the network. The resulting change in bus voltages is given by:

$$\Delta\bar{\boldsymbol{V}} = -\Delta\bar{I}_k\ \boldsymbol{Y}^{-1}\boldsymbol{e}_k \tag{8}$$

where $\boldsymbol{e}_k$ is the unit vector with the k-th entry equal to one. The bus voltages after variation of the load admittance are given by:

$$\bar{\boldsymbol{V}} = \bar{\boldsymbol{V}}^o + \Delta\bar{\boldsymbol{V}} = \bar{\boldsymbol{V}}^o - \Delta\bar{I}_k\ \boldsymbol{Y}^{-1}\boldsymbol{e}_k \tag{9}$$

where the upper script ^{o} denotes a value before the load change. This equation particularized to the k-th bus gives:

$$\bar{V}_k = \bar{V}_k^o - \Delta\bar{I}_k\ \left[\boldsymbol{Y}^{-1}\boldsymbol{e}_k\right]_k = \bar{V}_k^o - \Delta\bar{I}_k\ \left[\boldsymbol{Y}^{-1}\right]_{kk} \tag{10}$$

where $\left[\boldsymbol{Y}^{-1}\right]_{kk}$ is nothing but the Thévenin impedance seen from bus k. Furthermore, the current $\Delta\bar{I}_k$ relates to the bus voltage $\bar{V}_k$ through:

$$\Delta\bar{I}_k = \Delta y\ \bar{V}_k \tag{11}$$

Combining Eqs. (10) and (11) and solving for $\Delta\bar{I}_k$ yields:

$$\Delta\bar{I}_k = \frac{\bar{V}_k^o}{[\boldsymbol{Y}^{-1}]_{kk} + \dfrac{1}{\Delta y}} \tag{12}$$

Replacing $\Delta\bar{I}_k$ by this expression in Eq. (9) provides the expression of bus voltages resulting from the addition of the admittance Δy at the k-th bus:

$$\bar{\boldsymbol{V}} = \bar{\boldsymbol{V}}^o - \frac{\bar{V}_k^o}{[\boldsymbol{Y}^{-1}]_{kk} + \dfrac{1}{\Delta y}}\boldsymbol{Y}^{-1}\boldsymbol{e}_k \tag{13}$$

The second step consists in determining the variations of generator active powers that result from the change of voltages from $\bar{\boldsymbol{V}}^o$ to $\bar{\boldsymbol{V}}$. From the Thévenin equivalent of the j-th generator (Fig. 1(a)), one easily derives the current before the load change:

$$\bar{I}_j^o = (\bar{E}' - \bar{V}_j^o)/jX_j' \tag{14}$$

and after the load change:

$$\bar{I}_j = (\bar{E}' - \bar{V}_j)/jX_j' \tag{15}$$

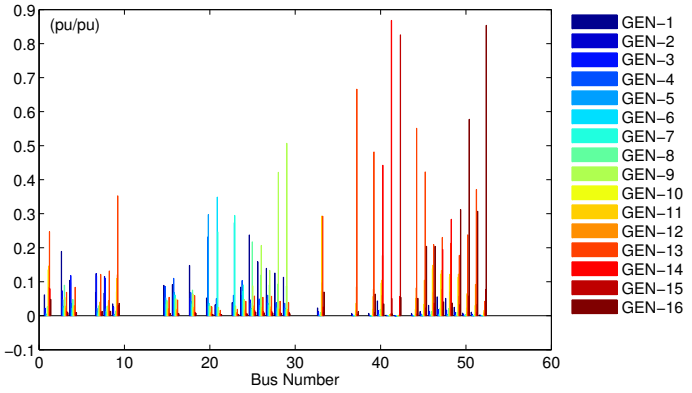

Fig. 10. Generator power sensitivities

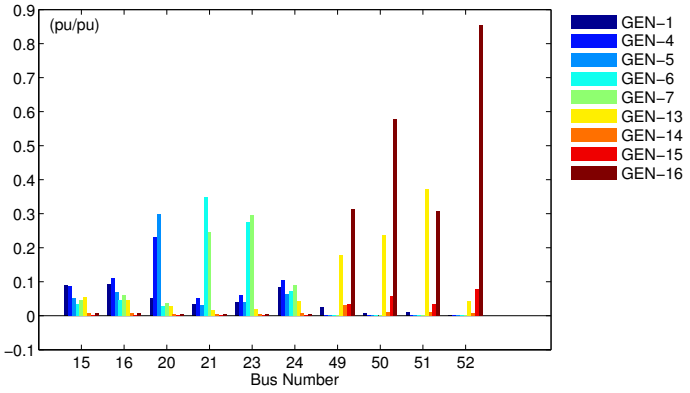

Fig. 11. Excerpt of generator power sensitivities at prior selected buses

The variation of active power of the j-th generator is merely given by:

$$\Delta P_j = Re\left(\bar{V}_j \bar{I}_j^* - \bar{V}_j^o (\bar{I}_j^o)^*\right) \tag{16}$$

where * denotes the complex conjugate.

Equation (16) provides the sensitivities of the generator active powers to a change of the load admittance at the k-th bus. The main computational effort involves solving one sparse linear system from the LU factors of $\boldsymbol{Y}$ with the sparse independent term $\boldsymbol{e}_k$. By repeating the computation for the various load buses of interest, a sensitivity matrix can be assembled column by column. As shown in the sequel, this matrix gives useful information on e.g. the effect of load tripping/shedding on generators during a transient voltage sag.

V. Results for Generator Power Sensitivities

A. Investigation of the effect of load variation

In the following an application of the power injection sensitivities is presented, where the sensitivities are used to estimate the effect of under-voltage load tripping.

Figure 10 shows the generator power sensitivities computed from Eq. (16) for the same scenario as in Section III. The bar graph shows how much a 1 pu increase of the load admittance under constant power factor (of 0.89) affects the active powers of generators. It can be seen that increasing load power generally results in increasing generator active powers. However, in some rare cases, depending on the load power factor, the opposite effect can be observed. It can be also seen that, as for the load voltage sensitivities, there is a strong coupling between certain loads and certain generators.

Figure 11 shows a detail of the bar graph of Fig. 10. It can be seen that the power injection of GEN-6 and GEN-7, which experience a large rotor angle excursion and were found to have high impact on the voltages at buses 21 and 23, are as well sensitive to the load power consumed at these buses.

All in all, the relations between, on the one hand, voltage magnitudes at load buses and rotor angles and, on the other hand, active power of generators and load consumptions yield a more complete picture of the system response observed. Namely, the fault causes GEN-6 and GEN-7 to have their rotor angles significantly increased. This, in turn, causes the voltage magnitudes at load buses 21 and 23 to drop significantly, with the consequence that the voltage-sensitive load power is reduced. Eventually, the reduction of the power consumed by these loads further reduces the active powers of both generators, which results in a lower deceleration and, hence, a larger rotor angle excursion.

B. Effect of load tripping/shedding

Hereafter, the detrimental or beneficial effect of load tripping is discussed, based on the same scenario as before.

Figure 12 shows the voltage evolution at bus 23 in three different cases. The red solid curve refers to the original scenario with a pronounced voltage sag. The green dashed curve is the same voltage evolution when 30 MW of load are tripped at the same bus, under constant power factor, 100 ms after the voltage has dropped below the critical value of 0.7 pu. A loss of synchronism results, which can be explained from the sensitivities of Fig. 11. Indeed, reducing the load power at bus 23 decreases the active power of GEN-6 and GEN-7, which make up the critical group. The blue dotted curve shows the voltage evolution at bus 23 when load is tripped at bus 20. Stability is improved, the depth of the voltage sag is reduced and voltage recovery is faster. This is to be expected from the sensitivities of Fig. 11 which indicate that acting at bus 20 little affects the critical generators GEN-6 and GEN-7 but reduces the active power of GEN-4 and GEN-5 which belong to the non-critical group.

This observation could be at the heart of an intelligent load shedding scheme, detecting a voltage sag caused by rotor angle separation and selecting the loads to curtail in order to improve the system response. The case shown with the blue dotted curve in Fig. 11 was obtained by assuming a response-based scheme of this type, acting in several steps in order to apply a proper amount of corrective control. In this very simple example, a first block of 40 MW of load is curtailed when the voltages stay below 0.7 pu for more than 100 ms, followed by one block of 40 MW every 200 ms until all bus voltages recover above 0.7 pu. The power factor is kept constant. In the scenario of concern, this scheme leads to shedding a total of 160 MW. The effect on generator active powers is illustrated in Fig. 13, relative to the critical

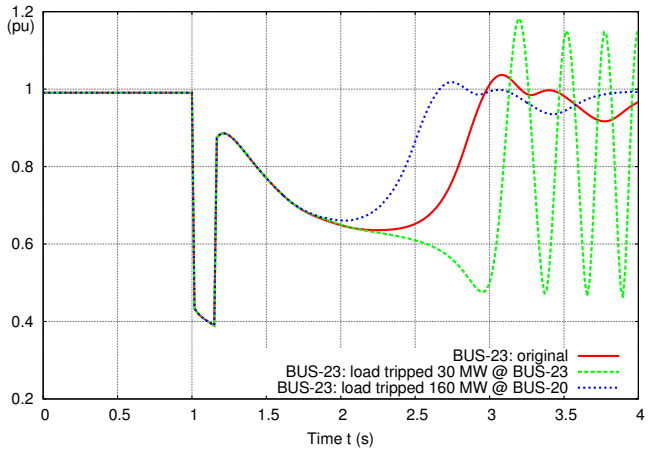

Fig. 12. Effect of load shedding on the voltage magnitude at bus 23

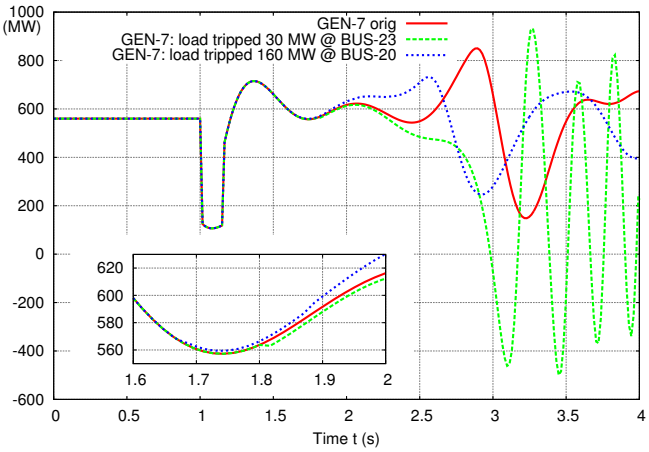

Fig. 13. Effect of load shedding on active power of generator GEN-7

generator GEN-7. The red solid curve shows the evolution of its active power in the base case with no load shedding. The counterproductive load tripping scenario (30 MW shed at bus 23) is depicted by the green dashed curve. Load tripping takes place at $t = 1.80$ s. The magnified plot in Fig. 13 shows that this slightly reduces the power injected by the generator. This decreases the deceleration power (i.e. the difference better the active and mechanical powers) and eventually results in a loss of synchronism. In the stabilizing load tripping scenario, shown by the blue dotted curve (160 MW shed at bus 20), the active power of the same generator is not reduced by the shedding. It is even higher than in the base case. This increase may be explained by a lower relative rotor angle between the critical and non-critical machines as well as a less pronounced voltage drop and, consequently, a higher power consumption.

VI. Conclusion

In this paper, a method is proposed to assess transient voltages sags caused by rotor swings. This can occur when generators experience large relative rotor angle displacements after a fault. The system may be assessed transiently stable, since no loss of synchronism takes place, but the voltage sag leads to critically low voltage levels and the system response should be considered unacceptable.

The voltage sag assessment uses new sensitivities, derived from the well-known linear algebraic network equations and aimed at complementing detailed time-domain simulations. To this purpose, generators are represented by the classical model adjusted to fit some points of the system evolution. Under these assumptions, two sensitivities were developed.

The first sensitivity provides information on the impact of rotor angle changes on the voltage magnitude of load buses. This sensitivity can be used to detect critical generator-load pairs. Furthermore, it allows computing the contribution of a generator to an observed voltage sag, which gives valuable information to point out a location for preventive control. Presently, the sensitivity must be complemented with information on the amount of preventive measure. The second sensitivity reveals the impact of load consumption variation on the active power injected by generators. Simulations have shown that this sensitivity can be used to determine if under-voltage load tripping/shedding will improve or deteriorate transient stability and, thereby, identify critical locations for under-voltage load shedding.

Since the sensitivities are obtained from a very fast computation, they could be used to determine preventive actions in real time. Assuming the availability of fast communication means, the sensitivities could also be used for emergency control. This, however, requires a reliable early detection of voltage sags and proper tools to compute the amount and type of control.

References

[1] M. H. Bollen, *Understanding power quality problems*, vol. 3 ed. New York: IEEE press, 2000.

[2] A. A. Fouad and R. Sreedhara, "Transient Voltage Dip Analysis using the Transient Energy Function Method," in *Proceedings of the Twenty-Second Annual North American Power Symposium*. IEEE Comput. Soc. Press, 1990, pp. 264–273.

[3] F. Dominguez, A. S. Debs, and J. Anasis, "Transient voltage dip in power systems: computation and sensitivity analysis using the hybrid method," in *Decision and Control, 1992., Proceedings of the 31st IEEE Conference on*, 1992, pp. 576–581 vol.1.

[4] Y. Xue, T. Xu, B. Liu, and Y. Li, "Quantitative assessments for transient voltage security," *Proceedings of the 21st International Conference on Power Industry Computer Applications. Connecting Utilities. PICA 99. To the Millennium and Beyond (Cat. No.99CH36351)*, pp. 101–106, 1999.

[5] A. Tiwari and V. Ajjarapu, "Contingency assessment for voltage dip and short term voltage stability analysis," *2007 iREP Symposium - Bulk Power System Dynamics and Control - VII. Revitalizing Operational Reliability*, pp. 1–8, Aug. 2007.

[6] D. Shoup, J. Paserba, and C. Taylor, "A survey of current practices for transient voltage dip/sag criteria related to power system stability," *IEEE PES Power Systems Conference and Exposition, 2004.*, pp. 1499–1506, 2004.

[7] P. Kundur, *Power System Stability and Control*, N. J. Balu and M. G. Lauby, Eds. McGraw-Hill Inc., 1994.

[8] G. Rogers, *Power System Oscillations*. Springer, 2000.

[9] M. Pavella, D. Ernst, and D. Ruiz-Vega, *Transient Stability of Power Systems: A Unified Approach to Assessment and Control*. Kluwer Academic Publishers, 2000.

Appendix F

Derivation and Application of Sensitivities to Assess Transient Voltage Sags caused by Rotor Swings

---

This paper is an extension of the paper on sensitivities published as part of the proceedings of the PSCC 2014. It will appear in a special issue of the International Journal of Electrical Power and Energy Systems (IJEPES).

Electrical Power and Energy Systems xxx (2015) xxx–xxx

Contents lists available at ScienceDirect

Electrical Power and Energy Systems

journal homepage: www.elsevier.com/locate/ijepes

Derivation and application of sensitivities to assess transient voltage sags caused by rotor swings ☆

Tilman Weckesser [a,*], Hjörtur Jóhannsson [a], Jacob Østergaard [a], Thierry Van Cutsem [b]

[a] Center for Electric Power and Energy (CEE) at the Technical University of Denmark (DTU), Kgs. Lyngby, Denmark
[b] Fund for Scientific Research (FNRS) at the University of Liège, Belgium

ARTICLE INFO

Article history:
Received 1 February 2015
Accepted 16 February 2015
Available online xxxx

Keywords:
Power system stability
Sensitivity to rotor swings
Transient stability
Voltage sag

ABSTRACT

The paper introduces an approach to investigate voltage sags, which are caused by large generator rotor swings following a transient disturbance. Therefore, the method exploits sensitivities derived from the algebraic network equations. These provide information on the impact of a generator on the voltage magnitude at a load bus and the effect of load variation on the generator's power injection. It is shown that these sensitivities give valuable information to identify critical generator–load pairs and locations for applying preventive control measures.

Introduction

In literature on power quality, voltage sags/dips is a topic vastly addressed [2]. While the primary cause is the occurrence of a fault, a less pointed out reason for voltage sags is rotor angle swing, more precisely angular separation of generators, resulting from a fault. From a practical viewpoint, a scenario may be assessed transiently stable considering that generators remain in synchronism, while voltage sags due to the relative rotor angle displacement already result in transiently low voltages for which the system response should be considered unacceptable.

The prediction of this type of voltage sag using the Transient Energy Function was described in the early reference [3]. In [4] sensitivities relative to voltage dip were derived using this method as well. The sensitivities relate the voltage sag depths to certain parameters such as terminal voltages and power generation. The authors of [5] address the transient voltage dip acceptability problem using a two-dimensional table of critical voltage level and critical voltage dip duration. Moreover, the issue of transient voltage stability of dynamic loads such as induction machines is analyzed. In the more recent reference [6] the authors use sensitivities to carry out contingency filtering and ranking with respect to voltage dips. Furthermore, the assessment addresses power quality issues and short-term voltage stability. In [7], the authors present a survey of current practices for transient voltage sag criteria related to power system stability.

The present paper also investigates voltage sags with focus on power system stability rather than power quality. Transient voltage sags are identified using time-domain simulation. Then, sensitivities are derived which provide information on tight couplings between relative change of rotor angles and load voltage magnitudes. These sensitivities are easier to compute than those considered in the above references. The sensitivities can be used, for instance, to identify the contribution of each generator to a drop in voltage magnitude experienced at a particular load bus. A voltage depression at a load bus can trigger consecutive events such as load tripping. Therefore, a second sensitivity is derived, which assesses the impact of a change of load power on generator active powers.

This paper is organized as follows. In Section "Voltage sags caused by rotor angle swings" the power system model used for the discussion of voltage sags and the computation of sensitivities is described. Moreover, a brief discussion of the mechanism causing these transient voltage sags is presented. The voltage sensitivities are derived in Section "Derivation of load voltage sensitivities". This is followed by the presentation of the corresponding results in Section "Results for load voltage sensitivities". The derivation of the second sensitivities, addressing the effect of variation of load on generator power, can be found in Section "Derivation of generator power sensitivities" and the

☆ An earlier version of the paper [1] was published as part of the proceedings of the Power Systems Computation Conference, August 18–22, 2014, Wroclaw, Poland.
Research supported by the Danish Council for Strategic Research (DSF).

* Corresponding author.
E-mail addresses: jtgw@elektro.dtu.dk (T. Weckesser), hjjo@elektro.dtu.dk (H. Jóhannsson), joe@elektro.dtu.dk (J. Østergaard), t.vancutsem@ulg.ac.be (T. Van Cutsem).

http://dx.doi.org/10.1016/j.ijepes.2015.02.013
0142-0615/

corresponding results are shown in Section "Results for generator power sensitivities". Finally, in Section "Conclusion" concluding remarks are offered.

Voltage sags caused by rotor angle swings

Modelling for discussion of the mechanism causing the voltage sags and for sensitivity analysis

The model used for synchronous generator is the so-called "classical" transient stability model [8]. Each generator is modeled by an e.m.f. $\bar{E}'$ of constant magnitude behind the transient reactance X'_d (see Fig. 1(a)), the mechanical power input is assumed constant, and loads are converted to constant shunt admittances. The simple generator model is valid in the first second after fault clearance and the justification for using it is twofold. First, this model is used for sensitivity analysis and, as indicated in the Introduction, this analysis is aimed at complementing a detailed time-domain simulation in which much more refined models can be used. Second, the "classical" model is not used with constant e.m.f. throughout the whole simulation: instead, the e.m.f. is adjusted so that the "classical" model fits specific operating points where the sensitivity analysis is carried out.

For convenience each generator is represented by its Norton equivalent (see Fig. 1(b)), i.e. a current source $\bar{E}'/(jX'_d)$ in parallel with the admittance $1/(jX'_d)$. Based on these assumptions, the following well-known linear algebraic equations can be used:

$$\bar{\boldsymbol{I}} = \boldsymbol{Y}\bar{\mathbf{V}} \tag{1}$$

where $\bar{\boldsymbol{I}}$ is the vector of complex currents injected at the generator buses (stemming from the Norton equivalents), $\bar{\mathbf{V}}$ is the vector of complex bus voltages, and $\boldsymbol{Y}$ is the "augmented" bus admittance matrix obtained by adding the contribution of generators and loads to the matrix relative to the network.

A system with n buses and m machines is considered ($n > m$). It is assumed, without loss of generality, that the buses where machines are connected are numbered from $n-m+1$ to n. Hence, Eq. (1) can be detailed as:

$$\begin{bmatrix} 0 \\ \vdots \\ 0 \\ \bar{E}'_1/(jX'_{d,1}) \\ \vdots \\ \bar{E}'_m/(jX'_{d,m}) \end{bmatrix} = \boldsymbol{Y} \begin{bmatrix} \bar{V}_1 \\ \vdots \\ \bar{V}_{n-m} \\ \bar{V}_{n-m+1} \\ \vdots \\ \bar{V}_n \end{bmatrix} \tag{2}$$

where the zero sub-vector has dimension $n-m$ and $\bar{V}_i$ is the complex voltage at the i-th bus.

Voltage sag mechanism

The mechanism behind voltage sags caused by rotor swings can be discussed and illustrated graphically under consideration of a simple example system such as the one shown in Fig. 2.

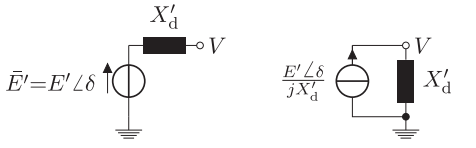

(a) Thevenin Equivalent (b) Norton Equivalent

Fig. 1. Thévenin and Norton equivalents of generator.

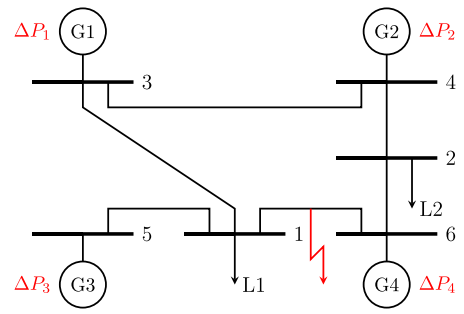

Fig. 2. One-line diagram of a simple example test system with 6 buses. A three-phase short-circuit on the transmission line connecting Buses 1 and 6, which is indicated by the red zigzag arrow, causes a change ΔP_i in the power injection of each generator Gi.

As mentioned in the previous section the generators are represented by the "classical" transient stability model. The angle of the e.m.f. can then be used to represent the rotor angle of the generator [8]. Moreover, in this example the generators' mechanical powers are assumed constant and the loads are modeled as constant impedances for sake of simplicity.

With these and the aforementioned assumptions, Eq. (2) reveals that the complex voltage at a bus is the sum of contributions of the generators. The contribution of a generator is determined by its e.m.f., which is scaled and rotated corresponding to the entry in the inverse of the admittance matrix divided by the respective transient reactance.

Fig. 3(a) shows the complex voltage at Bus 2 (from the simple example system) and the contributions of the individual generators, which add up to the voltage measured at the respective bus.

The effect of an increase in rotor angle, e.g. due to a transient disturbance, on a particular bus voltage can be assessed under consideration of the linear algebraic equation Eq. (2).

In the example shown in Fig. 2, a short-circuit occurs on the transmission line connecting Buses 4 and 5. The fault alters the admittance matrix and leads to a change of the electric power injection of the generators, which causes a relative acceleration or deceleration of the generator rotors. In the example, it is assumed for clarity that the fault only affects generator G4 resulting in its acceleration and an advancing of its rotor angle relative to the remaining generators.

The effect on the voltage at Bus 6 is shown in Fig. 3(b) from which it can be observed that the relative increase in rotor angle depresses the voltage magnitude at the bus. This observation gave the impulse for the investigation of transient voltage sags using sensitivities.

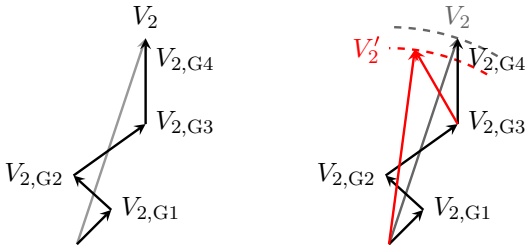

(a) Bus voltage at initial state (b) Effect of rotor angle increase of generator G4

Fig. 3. Example of complex voltage at Bus 2 as sum of generator contributions.

Please cite this article in press as: Weckesser T et al. Derivation and application of sensitivities to assess transient voltage sags caused by rotor swings. Int J Electr Power Energ Syst (2015), http://dx.doi.org/10.1016/j.ijepes.2015.02.013

Derivation of load voltage sensitivities

Load voltage sensitivities

In this section, sensitivities are derived to identify the load buses whose voltage magnitudes are strongly affected by changes of the rotor angle of particular generators. They are referred to as "load voltage sensitivities". The latter will be used to determine the contribution of individual generators to an observed voltage sag at a load bus.

The effect of a small rotor angle change is assessed through modification of Eq. (2). To this purpose, the e.m.f. phasor of the k-th generator, $\overline{E}'_k$, is slightly rotated, while the other generators remain unchanged. This corresponds to a small change of the rotor angle, when generators are represented by the "classical" model. The new bus voltages $\overline{\mathbf{V}}^{\dagger}$ that result from a small increase ϵ in the phase angle of $\overline{E}'_k$ are easily computed by solving the modified linear system:

$$\begin{bmatrix} 0 \\ \vdots \\ 0 \\ \overline{E}'_1/(jX'_{d,1}) \\ \vdots \\ \overline{E}'_k\, e^{j\epsilon\pi/180}/(jX'_{d,k}) \\ \vdots \\ \overline{E}'_m/(jX'_{d,m}) \end{bmatrix} = \boldsymbol{Y} \begin{bmatrix} \overline{V}^{\dagger}_1 \\ \vdots \\ \overline{V}^{\dagger}_{n-m} \\ \overline{V}^{\dagger}_{n-m+1} \\ \vdots \\ \vdots \\ \vdots \\ \overline{V}^{\dagger}_n \end{bmatrix} \tag{3}$$

In order to speed up computations and make the approach well suited for real-time application, the admittance matrix $\boldsymbol{Y}$ is LU-factorized once for all, and Eq. (3) is solved for each change ϵ in the left-hand-side vector.

The changes of magnitudes between the "new" and the reference bus voltages are calculated and normalized. The sensitivities of the various bus voltage magnitudes to the i-th generator rotor angle are computed as:

$$\left(\boldsymbol{s}_{V,Gi}\right)_{\ell} = \frac{|\overline{V}^{\dagger}_{\ell}| - |\overline{V}_{\ell}|}{\pi\epsilon/180} \quad \ell = 1,\ldots,m-n \tag{4}$$

where ϵ is expressed in degrees. The resulting sensitivity vector has the unit $[pu/rad]$ or $[V/rad]$. This vector can be determined for each generator in the system and the aggregation of the individual vectors gives a sensitivity matrix $\boldsymbol{S}_{V,G}$, where each column corresponds to a generator and each row to a load bus. This matrix allows identifying the generators having a dominant impact on a certain load bus voltage magnitude. The entries also indicate whether increasing a rotor angle will increase a voltage magnitude or will depress it.

Contribution of individual generators to a voltage sag

Once it has been found from time simulation that a significant voltage sag is experienced at some load bus, the voltage sensitivities presented in the previous sub-section can be utilized to identify the contribution of each individual generator. The procedure described hereafter was found to provide the most accurate results.

The time-domain simulation is carried out until the minimum voltage is reached at the load bus of interest. In order to ignore bus voltage variations caused by topological changes, the voltage magnitude reduction is considered between the time t_c of fault clearing and the instant $t_{V\min}$ where the minimum of voltage is reached. The excursions $\Delta\delta_j \quad (j = 1,\ldots,m)$ of rotor angles are considered over the time interval $[t_c\ t_{V\min}]$. Furthermore, the load voltage sensitivities $\boldsymbol{S}_{V,G}$ are determined at time t_c^+. Therefore, the bus voltages $V(t_c^+)$ and the power consumption of the loads just after the system has entered its post-fault configuration are used to update the admittance matrix and, subsequently, to compute the Norton equivalent of the generators.

Therewith, an estimate of the voltage magnitude drop at Bus i can be calculated through linearization, using the load voltage sensitivities, as follows:

$$\Delta V_i = \sum_{j=1}^{m} [\boldsymbol{S}_{V,G}]_{ij} \Delta\delta_j = \sum_{j=1}^{m} \Delta V_{i,j} \tag{5}$$

Finally, the share of the k-th generator in the total change of voltage magnitude can be determined as:

$$f_{i,k} = \frac{\Delta V_{i,k}}{\left|\sum_{j=1}^{m} \Delta V_{i,j}\right|} \tag{6}$$

Using this fraction and the voltage trajectory obtained from time-domain simulation, the actual share of the k-th generator in the voltage sag at the i-th bus can be computed as:

$$\Delta V^*_{i,k} = f_{i,k} \left| V_i(t_c^+) - V_i(t_{V\min}) \right| \tag{7}$$

where $V_i(t_c^+)$ is the voltage at Bus i immediately after fault clearing and $V_i(t_{V\min})$ its minimum value.

Results for load voltage sensitivities

Test system and example case

Test system

The test system employed to validate the presented sensitivities is the well-known New England and New York system described in [9]. It consists of 68 buses and 16 generators. A one-line diagram is shown in Fig. 4. The loads are modeled as constant impedances in the time-domain simulation. The generators are represented by a sixth order model. They all have a simple excitation and voltage regulation system, and a thermal turbine/governor model. Furthermore, all generators, but GEN-7 and GEN-14, are equipped with a power system stabilizer.

Test scenario

The test scenario was as well adopted from [9]. In this case, the considered contingency is a three-phase short-circuit on the transmission line connecting Buses 26 and 28. The short-circuit occurs one second after the simulation begins and is assumed to be very close to Bus 28. It is cleared after 120 ms by opening the breakers at both ends of the faulted transmission line.

The disturbance causes some generators to accelerate relative to the others, which leads to a significant separation of the generator rotor angles. Fig. 5 shows the evolution of the rotor angles of nine among the sixteen generators: the five generators with the largest increase of rotor angle (GEN-4, GEN-5, GEN-6, GEN-7 and GEN-9), the three generators with the largest decrease (GEN-14, GEN-15 and GEN-16) and one which is little affected (GEN-8). The graph shows that the generators are affected to different degrees by the disturbance; in particular, GEN-9 is experiencing a large rotor angle excursion. However, all generators remain in synchronism and reach a new stable equilibrium point. Consequently, the scenario is assessed to be stable. Fig. 6 displays the time evolution of voltage magnitudes at a selection of load buses. The selection consists of the four buses which experience the lowest voltages (Buses 26, 27, 28 and 29), the three buses whose voltage magnitude are slightly increased (Buses 50, 51 and 52), and two buses little affected (Buses 18 and 25). As expected the voltage magnitudes drop dramatically in the fault-on period, and

Please cite this article in press as: Weckesser T et al. Derivation and application of sensitivities to assess transient voltage sags caused by rotor swings. Int J Electr Power Energ Syst (2015), http://dx.doi.org/10.1016/j.ijepes.2015.02.013

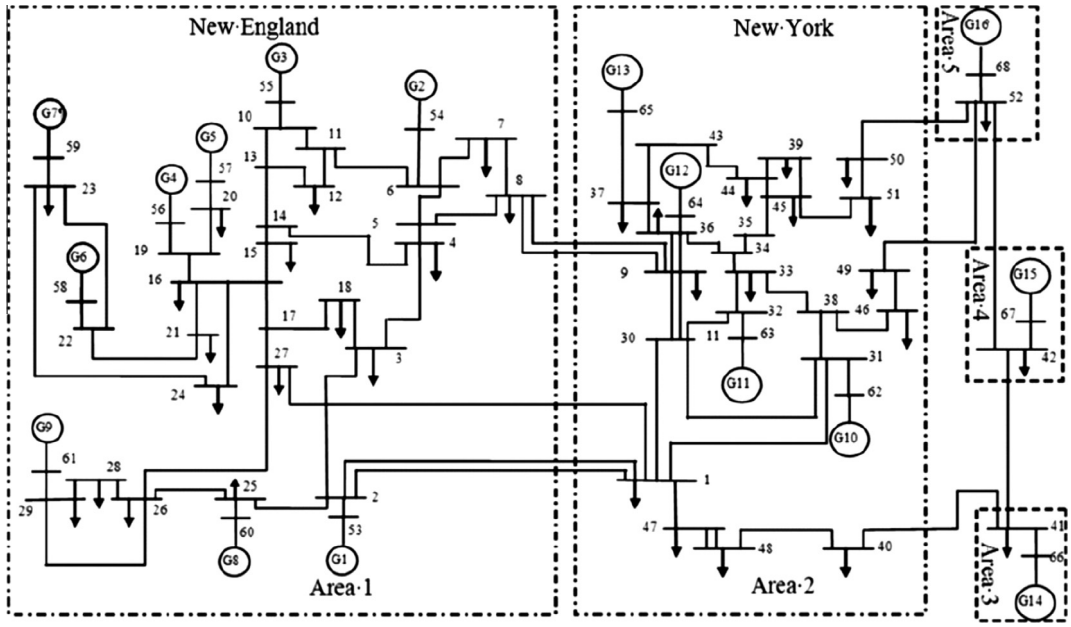

Fig. 4. One-line diagram of the New England and New York system [10].

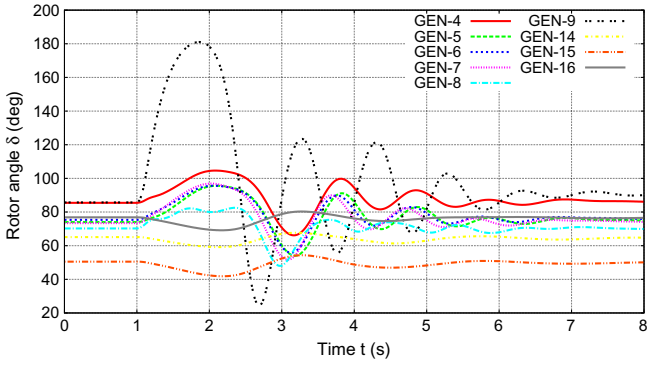

Fig. 5. Evolution of rotor angles of a selection of generators (with respect to center of inertia).

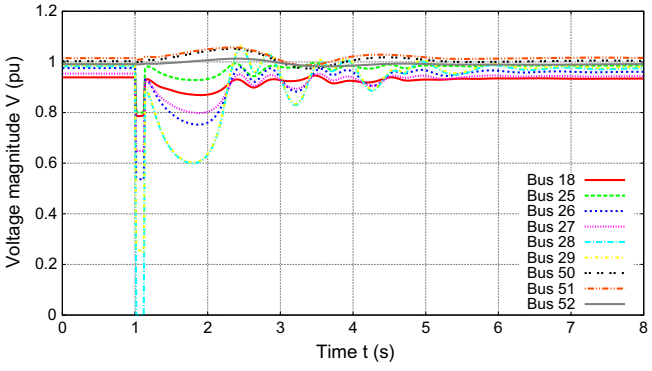

Fig. 6. Evolution of voltage magnitudes at a selection of load buses.

recover immediately after fault clearing. However, in the subsequent evolution, a voltage sag can be observed at certain buses. At some buses the voltage drops below the critical value of 0.7 pu, which is unacceptably low and long lasting.

Identification of critical generator–load pairs

In order to clearly identify which generators strongly impact load bus voltage magnitudes, the load voltage sensitivities described in the previous section are computed using Eq. (4) and data obtained from time-domain simulation, just after fault clearance. Fig. 7 shows the resulting sensitivities. The bar graph shows for all load buses the expected change in voltage magnitude (in pu/rad) resulting from the increase of one individual generator rotor angle. The values clearly indicate that an angle increase can either depress or boost a voltage magnitude.

In the example scenario, GEN-9 experiences a large rotor angle excursions and is likely to cause the observed voltage sags. Indeed, Fig. 7 indicates that GEN-9 mainly affects the voltage magnitudes at Buses 18 and 25–29. Furthermore, from Fig. 5 it can be observed that GEN-14, GEN-15 and GEN-16 experience a slight decrease of their rotor angle. The sensitivities in Fig. 7 indicate that GEN-16 strongly affects the load buses with numbers in the range of 50–52. In the following, a more detailed analysis of this group is considered.

Fig. 8 shows a selection of sensitivities displayed in the bar graph of Fig. 7, relative to above mentioned subset of generators and load buses. Dominant negative sensitivities indicate that increasing the corresponding rotor angles would decrease the voltage magnitude at the respective load buses, and vice versa. These high sensitivities combined with the generator rotor angle deviations can explain the voltage magnitude evolutions at the load buses shown in Fig. 6. The sensitivities in Fig. 8 suggest that the load buses where GEN-9 is dominant, will experience a voltage depression, which is the case for Buses 26, 27, 28 and 29. The voltage at Buses 18 and 25 are less affected, which is in good correlation with the lower sensitivities to the critical generator GEN-9. Furthermore, Fig. 8 suggests that the load buses where GEN-16 is dominant experience a slight increase of their voltage magnitudes corresponding to the negative sensitivity and the decreasing rotor angle of GEN-16. This is in good agreement with the voltage evolutions shown in Fig. 6.

Contribution of individual generators

Another use of the load voltage sensitivities is to determine the contribution of each generator to an observed voltage sag at a

Please cite this article in press as: Weckesser T et al. Derivation and application of sensitivities to assess transient voltage sags caused by rotor swings. Int J Electr Power Energ Syst (2015), http://dx.doi.org/10.1016/j.ijepes.2015.02.013

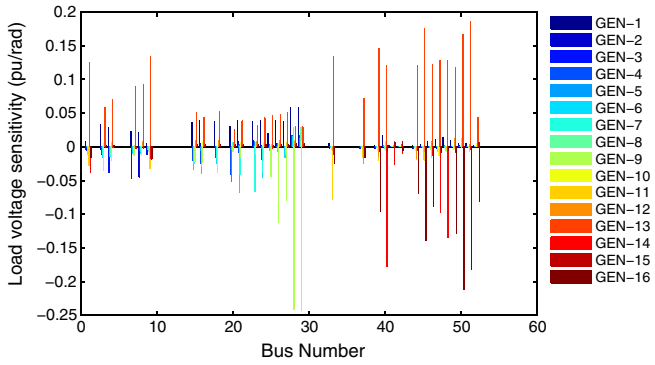

Fig. 7. Load voltage sensitivities to a 1° change in rotor angle of the individual generators.

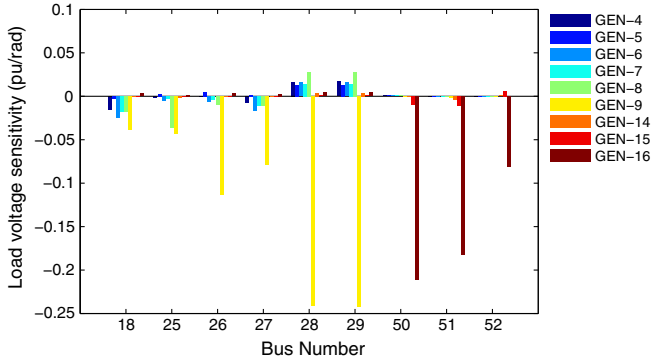

Fig. 8. Load voltage sensitivities for a subset of loads and generators to a 1° change in rotor angle.

particular bus, as described in Section "Contribution of individual generators to a voltage sag", more precisely by Eq. (7). For the same test scenario, the contributions $\Delta V^*_{i,k}$ of each generator to the voltage sags are presented in Fig. 9.

As for the load voltage sensitivities, the individual contributions of the generators show that each generator strongly impacts load buses in a certain vicinity and can have either a positive or a negative effect on the voltage magnitude. Moreover, it can be seen that, at an individual load bus, either a positive or a negative contribution can be dominant (see for instance Buses 28, 29, 50 and 51), or the contributions of various generators compensate each other to a large extent (see for instance Bus 37).

Application to generator re-dispatch

The above individual generator contributions also point out effective locations for preventive control aimed at mitigating the voltage sags.

In the scenario under concern, GEN-9 has been identified as the major source of the voltage sags. Consequently, a reduction of its rotor angle excursion due to the fault could significantly improve the post-fault voltage evolutions. This can be achieved by reducing the critical generator's pre-fault active power and re-dispatching the power difference to appropriate non-critical generators.

The results of such a re-dispatch are presented next. The power output of GEN-9 was reduced by merely 50 MW (from 850 to 800 MW) while the power output of GEN-8 was increased to cover the difference. These two generators were chosen, because GEN-9 has a large contribution to the severe voltage sags at Buses 26–29, while the sensitivities shown in Fig. 8 suggest that a rotor angle increase of GEN-8 tends to increase the voltage magnitudes at the most critical Buses 28 and 29. Alternatively, any other generator with a negligible sensitivity could have been chosen to compensate the power reduction of the critical generator. In this test scenario the critical group of machines, which is the group that will loose synchronism in case of a fault cleared a little after the critical clearing time, consists of solely GEN-9.

Fig. 10 shows a comparison of the rotor angle responses of GEN-8 and GEN-9, before and after the re-dispatch, respectively. It can be observed that, due to the active power re-dispatch, the large rotor angle excursion is significantly reduced for GEN-9. Furthermore, the duration of the first swing is almost halved. The beneficial effect on the voltage evolutions is evident in Fig. 11, showing the voltage evolutions at the load Buses 25–29. The depth of the voltage sag at each load bus is reduced dramatically and the duration of the swing is halved.

The individual generator contributions updated after the power re-dispatch are shown in Fig. 12. It can be observed that all the negative contributions are significantly lower in magnitude. At the same time, the load voltage sensitivities have been little affected by the small power re-dispatch. Consequently, the voltage improvement results essentially from the decreased rotor angle excursion of the critical generator.

The above example has demonstrated the usefulness of load voltage sensitivities and individual generator contributions to identify the source of voltage sags and appropriate locations for preventive control. It should be noted that, at this stage, those indexes do not provide information on the required amount of preventive control.

Derivation of generator power sensitivities

Motivation

A depressed voltage, falling below a certain critical level, may trigger consecutive events such as load disconnection by internal protections, or possibly under-voltage load shedding in a system provided with this integrity protection scheme. The subsequent reduction of power consumption at some load buses may lower the maximum of the $P(\delta)$-curves of some generators. This leads to a reduction of the available deceleration area, which is detrimental for stability if those generators belong to the critical group, and beneficial if they belong to the non-critical one [11].

In order to investigate the effect of load variations on generator active powers, a second type of sensitivities is considered, based on the same model as in Section "Modelling for discussion of the mechanism causing the voltage sags and for sensitivity analysis". The increase of load consumption is obtained from an extra load admittance Δy added at the bus of concern, and the goal is to determine the effect on the generator active powers. It was found that these sensitivities provide the most accurate results when calculated directly after fault clearance, at time t_c^+.

Derivation of generator power sensitivities

The first step consists in estimating the bus voltages after increasing the load admittance at the k-th bus by a small value Δy. To this purpose, let us assume that this additional admittance draws a current $\Delta\bar{I}_k$ from the network. The resulting change in bus voltages is given by:

$$\Delta\bar{\mathbf{V}} = -\Delta\bar{I}_k\, \mathbf{Y}^{-1}\boldsymbol{e}_k \tag{8}$$

where $\boldsymbol{e}_k$ is the unit vector with the k-th entry equal to one. The bus voltages after variation of the load admittance are given by:

Please cite this article in press as: Weckesser T et al. Derivation and application of sensitivities to assess transient voltage sags caused by rotor swings. Int J Electr Power Energ Syst (2015), http://dx.doi.org/10.1016/j.ijepes.2015.02.013

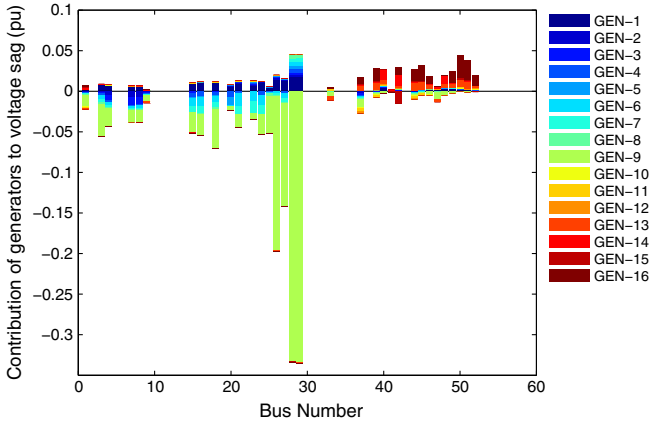

Fig. 9. Contribution of individual generators to voltage depressions.

$$\bar{\mathbf{V}} = \bar{\mathbf{V}}^o + \Delta\bar{\mathbf{V}} = \bar{\mathbf{V}}^o - \Delta\bar{I}_k \, \mathbf{Y}^{-1}\boldsymbol{e}_k \tag{9}$$

where the upper script $^\circ$ denotes a value before the load change. This equation particularized to the k-th bus gives:

$$\overline{V}_k = \overline{V}_k^o - \Delta\bar{I}_k \, \left[\mathbf{Y}^{-1}\boldsymbol{e}_k\right]_k = \overline{V}_k^o - \Delta\bar{I}_k \, \left[\mathbf{Y}^{-1}\right]_{kk} \tag{10}$$

where $\left[\mathbf{Y}^{-1}\right]_{kk}$ is nothing but the Thévenin impedance seen from Bus k. Furthermore, the current $\Delta\bar{I}_k$ relates to the bus voltage $\overline{V}_k$ through:

$$\Delta\bar{I}_k = \Delta y \, \overline{V}_k \tag{11}$$

Combining Eqs. (10) and (11) and solving for $\Delta\bar{I}_k$ yields:

$$\Delta\bar{I}_k = \frac{\overline{V}_k^o}{\left[\mathbf{Y}^{-1}\right]_{kk} + \frac{1}{\Delta y}} \tag{12}$$

Replacing $\Delta\bar{I}_k$ by this expression in Eq. (9) provides the expression of bus voltages resulting from the addition of the admittance Δy at the k-th bus:

$$\bar{\mathbf{V}} = \bar{\mathbf{V}}^o - \frac{\overline{V}_k^o}{\left[\mathbf{Y}^{-1}\right]_{kk} + \frac{1}{\Delta y}} \mathbf{Y}^{-1}\boldsymbol{e}_k \tag{13}$$

The second step consists in determining the variations of generator active powers that result from the change of voltages from $\bar{\mathbf{V}}^o$ to $\bar{\mathbf{V}}$. From the Thévenin equivalent of the j-th generator (Fig. 1(a)), one easily derives the current before the load change:

$$\bar{I}_j^o = (\bar{E}' - \overline{V}_j^o)/jX_j' \tag{14}$$

and after the load change:

$$\bar{I}_j = (\bar{E}' - \overline{V}_j)/jX_j' \tag{15}$$

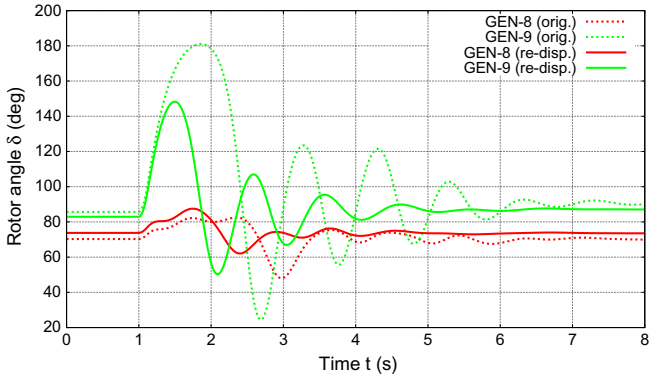

Fig. 10. Rotor angle responses before and after power re-dispatch.

The variation of active power of the j-th generator is merely given by:

$$\Delta P_j = Re\left(\overline{V}_j\bar{I}_j^* - \overline{V}_j^o(\bar{I}_j^o)^*\right) \tag{16}$$

where * denotes the complex conjugate.

Eq. (16) provides the sensitivities of the generator active powers to a change of the load admittance at the k-th bus. The main computational effort involves solving one sparse linear system from the LU factors of $\boldsymbol{Y}$ with the sparse independent term $\boldsymbol{e}_k$, which again is well suited for real-time application, e.g. determination of preventive controls. By repeating the computation for the various load buses of interest, a sensitivity matrix can be assembled column by column. As shown in the sequel, this matrix gives useful information on e.g. the effect of load tripping/shedding on generators during a transient voltage sag.

Results for generator power sensitivities

Investigation of the effect of load variation

In the following an application of the power injection sensitivities is presented, where the sensitivities are used to estimate the effect of under-voltage load tripping.

Fig. 13 shows the generator power sensitivities computed from Eq. (16) for the same scenario as in Section "Results for load voltage sensitivities". The bar graph shows how much a 1 pu increase of the load admittance under constant power factor affects the active powers of generators. It can be seen that increasing load power generally results in increasing generator active powers. However, in some rare cases, depending on the load power factor, the opposite effect can be observed. Moreover, it can be seen that there is a strong coupling between certain loads and certain generators, which was as well observed for the load voltage sensitivities.

Fig. 14 shows a detail of the bar graph of Fig. 13. It can be seen that the power injection of GEN-9, which experiences a large rotor angle excursion and was found to have high impact on the voltages at Buses 28 and 29, is as well sensitive to the load power consumed at these buses.

All in all, the relations between, on the one hand, voltage magnitudes at load buses and rotor angles and, on the other hand, active power of generators and load consumptions yield a more complete picture of the system response observed. Namely, the fault causes GEN-9 to have its rotor angles significantly increased. This, in turn, causes the voltage magnitudes at load Buses 28 and 29 to drop significantly, with the consequence that the voltage-sensitive load power is reduced. Eventually, the reduction of the power consumed by these loads further reduces the active powers of the generator, which results in a lower deceleration and, hence, a larger rotor angle excursion.

Effect of load tripping/shedding

Hereafter, the detrimental or beneficial effect of load tripping is discussed, based on the same scenario as before.

Fig. 15 shows the voltage evolution at Bus 28 in three different cases. The red solid curve refers to the original scenario with a pronounced voltage sag. The green dashed curve is the same voltage evolution when 50 MW of load are tripped at the Buses 28 and 29, under constant power factor, 100 ms after the voltage has dropped below the critical value of 0.7 pu. A loss of synchronism results, which can be explained from the sensitivities in Fig. 14. Indeed, reducing the load power at Buses 28 and 29 decreases the active power of GEN-9, which is the critical generator. The blue dotted curve shows the voltage evolution at Bus 28 when load is

Please cite this article in press as: Weckesser T et al. Derivation and application of sensitivities to assess transient voltage sags caused by rotor swings. Int J Electr Power Energ Syst (2015), http://dx.doi.org/10.1016/j.ijepes.2015.02.013

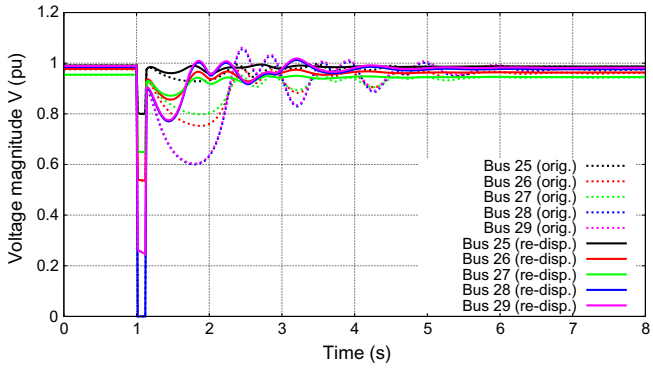

Fig. 11. Voltage magnitude evolutions before and after power re-dispatch.

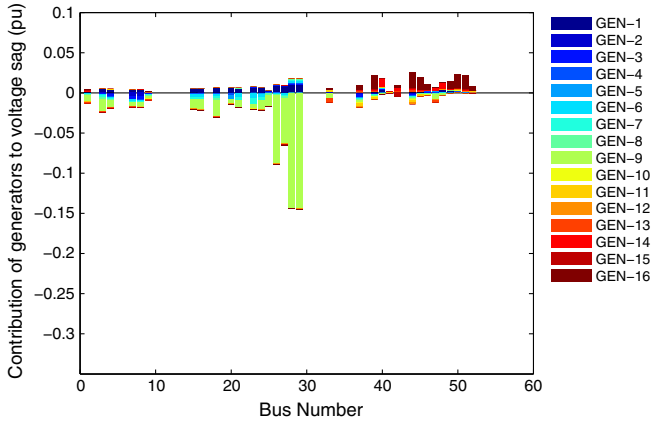

Fig. 12. Contribution of individual generators to voltage depressions after power re-dispatch.

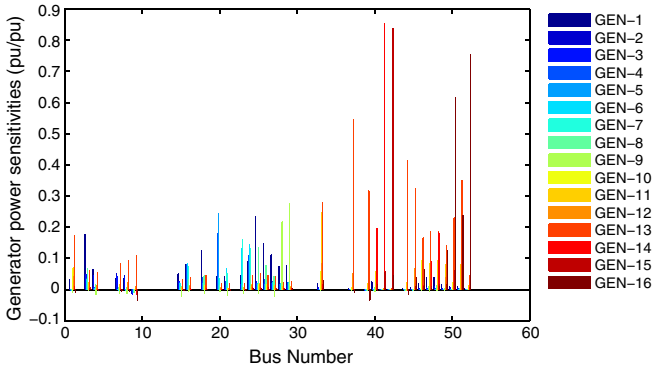

Fig. 13. Generator power sensitivities to a 1 pu increase of the load admittance under constant power factor.

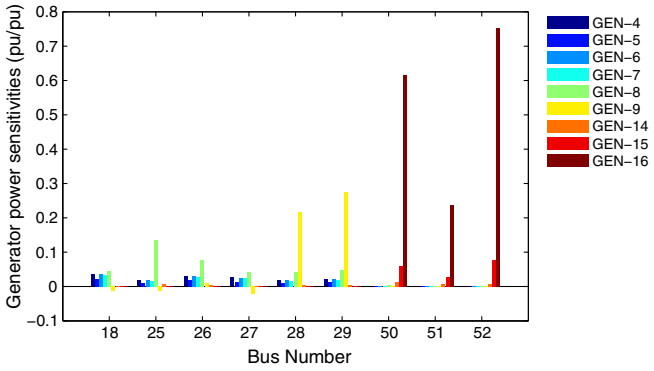

Fig. 14. Excerpt of generator power sensitivities to a 1 pu increase of the load admittance under constant power factor at prior selected buses.

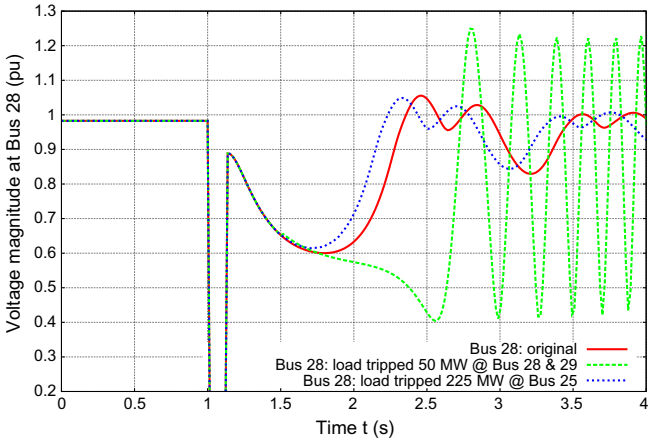

Fig. 15. Effect of load shedding on the voltage magnitude at Bus 28.

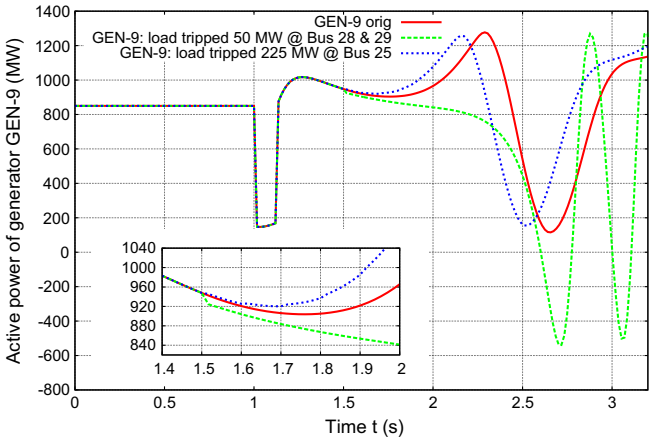

Fig. 16. Effect of load shedding on active power of generator GEN-9.

tripped at Bus 25. Stability is improved, the depth of the voltage sag is reduced and voltage recovery is faster. This is to be expected from the sensitivities in Fig. 14 which indicate that acting at Bus 25 little affects the critical generator GEN-9 but reduces the active power of GEN-8, which belongs to the non-critical group.

This observation could be at the heart of an intelligent load shedding scheme, detecting a voltage sag caused by rotor angle separation and selecting the loads to curtail in order to improve the system response. The case shown with the blue dotted curve in Fig. 15 was obtained by assuming a response-based scheme of this type, acting in several steps in order to apply a proper amount of corrective control. In this very simple example, a first block of 45 MW of load is curtailed when the voltages stay below 0.7 pu for more than 100 ms, followed by one block of 45 MW every 100 ms until all bus voltages recover above 0.7 pu. The power factor is kept constant. In the scenario of concern, this scheme leads to shedding a total of 225 MW. The effect on generator active powers is illustrated in Fig. 16, relative to the critical generator GEN-9. The red solid curve shows the evolution of its active power in the base case with no load shedding. The counterproductive load tripping scenario (50 MW shed at both Buses 28 and 29) is depicted by

Please cite this article in press as: Weckesser T et al. Derivation and application of sensitivities to assess transient voltage sags caused by rotor swings. Int J Electr Power Energ Syst (2015), http://dx.doi.org/10.1016/j.ijepes.2015.02.013

the green dashed curve. Load tripping takes place at $t = 1.50$ s. The magnified plot in Fig. 16 shows that this slightly reduces the power injected by the generator. This decreases the deceleration power (i.e. the difference between the active and mechanical power) and eventually results in a loss of synchronism. In the stabilizing load tripping scenario, shown by the blue dotted curve (225 MW shed at Bus 25), the active power of the same generator is not reduced by the shedding. It is even higher than in the base case. This increase may be explained by a lower relative rotor angle between the critical and non-critical machines as well as a less pronounced voltage drop and, consequently, a higher power consumption.

Conclusion

In this paper, a method is proposed to assess transient voltage sags caused by rotor swings. This can occur when generators experience large relative rotor angle displacements after a fault. The system may be assessed transiently stable since no loss of synchronism takes place, but the voltage sag leads to critically low voltages and, hence, to an unacceptable system response.

The voltage sag assessment uses new sensitivities, derived from the well-known linear algebraic network equations and aimed at complementing detailed time-domain simulations. To this purpose, generators are represented by the "classical" model adjusted to fit some points of the system evolution obtained with the full model. Under these assumptions, two sensitivities were developed.

The first sensitivity provides information on the impact of rotor angle changes on the voltage magnitude of load buses. This sensitivity can be used to detect critical generator–load pairs. Furthermore, it allows computing the contribution of a generator to an observed voltage sag, which gives valuable information to point out a location for preventive control. Presently, the sensitivity must be complemented with information on the amount of preventive measure. The second sensitivity reveals the impact of load consumption variation on the active power injected by generators. Simulations have shown that this sensitivity can be used to determine if under-voltage load tripping/shedding will improve or deteriorate transient stability and, thereby, identify critical locations for under-voltage load shedding.

The simulation results showed that although the sensitivities do not encompass all the existing controls, they provide useful information about the voltage sags caused by rotor swings. Moreover, since the sensitivities are obtained from a very fast computation, they could be used to determine preventive actions in real time. Assuming the availability of fast communication means, the sensitivities could also be used for emergency control. This extension of the work reported in this paper, however, requires a reliable early detection of voltage sags and proper tools to compute the amount and type of control.

References

[1] Weckesser T, Jóhannsson H, Østergaard J, Van Cutsem T. Sensitivity based assessment of transient voltage sags caused by rotor swings. Power systems computation conference 18th, vol. 1. Wroclaw (Poland): IEEE; 2014. p. 1–7.
[2] Bollen MH. Understanding power quality problems, vol. 3 Edition. New York: IEEE press; 2000.
[3] Fouad AA, Sreedhara R. Transient voltage dip analysis using the transient energy function method. In: Proceedings of the twenty-second annual North American power symposium. IEEE Comput Soc Press; 1990. p. 264–73. http://dx.doi.org/10.1109/NAPS.1990.151379.
[4] Dominguez F, Debs AS, Anasis J. Transient voltage dip in power systems: computation and sensitivity analysis using the hybrid method. In: Proceedings of the 31st IEEE conference on decision and control, 1992, vol. 1; 1992. p. 576–81. http://dx.doi.org/10.1109/CDC.1992.371665.
[5] Xue Y, Xu T, Liu B, Li Y. Quantitative assessments for transient voltage security. In: Proceedings of the 21st international conference on power industry computer applications. Connecting utilities. PICA 99. To the millennium and beyond (Cat. No.99CH36351); 1999. p. 101–6. http://dx.doi.org/10.1109/PICA.1999.779391.
[6] Tiwari A, Ajjarapu V. Contingency assessment for voltage dip and short term voltage stability analysis. In: 2007 iREP symposium – bulk power system dynamics and control – VII. Revitalizing operational reliability; 2007. p. 1–8. http://dx.doi.org/10.1109/IREP.2007.4410569.
[7] Shoup D, Paserba J, Taylor C. A survey of current practices for transient voltage dip/sag criteria related to power system stability. In: IEEE PES power systems conference and exposition, 2004; 2004. p. 1499–506. http://dx.doi.org/10.1109/PSCE.2004.1397688.
[8] Kundur P. Power system stability and control. McGraw-Hill Inc; 1994.
[9] Rogers G. Power system oscillations. Springer; 2000.
[10] Molina D, Liang J, Harley RG, Venayagamoorthy GK. Virtual generators: simplified online power system representations for wide-area damping control. In: IEEE power and energy society general meeting; 2012. p. 1–8. http://dx.doi.org/10.1109/PESGM.2012.6345608.
[11] Pavella M, Ernst D, Ruizvega D, Ruiz-Vega D. Transient stability of power systems: a unified approach to assessment and control. Kluwer Academic Publishers; 2000.

Please cite this article in press as: Weckesser T et al. Derivation and application of sensitivities to assess transient voltage sags caused by rotor swings. Int J Electr Power Energ Syst (2015), http://dx.doi.org/10.1016/j.ijepes.2015.02.013

Appendix G

Early Prediction of Transient Voltage Sags caused by Rotor Swings

---

This paper has been presented at the 2014 IEEE Power & Energy Society General Meeting (IEEE PES GM) in National Harbor, MD - Washington, DC Metro Area and has been published as part of the conference proceedings.

Early Prediction of Transient Voltage Sags caused by Rotor Swings

Tilman Weckesser Hjörtur Jóhannsson Thierry Van Cutsem

***Abstract*—The paper investigates various methods to predict voltage sags at load buses caused by large generator rotor swings and following a transient disturbance. Three different prediction methods are proposed, which all use real-time measurements from PMUs. One of the methods uses a slightly extended version of the E-SIME method. The other two methods use measurements and process them by recursive least square estimation. It is shown that the prediction method employing E-SIME allows the earliest detection of a critical voltage sag with satisfactory accuracy.**

***Index Terms*—power system stability, rotor swings, transient stability, voltage sag prediction**

I. Introduction

THE primary cause for voltage sags/dips is the occurrence of a fault. In the literature on power quality voltage sags/dips is a topic vastly addressed [1]. A rarely addressed reason for voltage sags is angular separation of generators or rotor angle swing resulting from a fault. Certain fault scenarios cause large rotor angle displacements, which result in transiently low voltages for which the system response should be considered unacceptable. However, from a rotor angle stability viewpoint, such a scenario may be assessed transiently stable, since the generators remain in synchronism.

Voltages falling below a critical level can cause subsequent events such as unintentional load tripping, which may further deteriorate the system condition. An early and accurate detection of an unacceptable voltage sag can be used to trigger appropriate control actions and avoid such detrimental events.

The prediction of this type of voltage sag using the Transient Energy Function was described in the early reference [2]. In [3] sensitivities relative to voltage dips were derived using this method. The sensitivities relate the voltage sag depths to certain parameters such as terminal voltages and power generation. However, approaches using the transient energy function always suffer from restrictions placed on the power system model. In [4] the authors treated the transient voltage dip acceptability problem using a two-dimensional table of critical voltage level and critical voltage dip duration. The paper also analyzed the issue of transient voltage stability of dynamic loads such as induction machines. In the recent publication [5], the authors developed a method for contingency filtering and ranking with respect to voltage dips using sensitivities. A survey of current practices for transient voltage sag criteria related to power system stability was presented in [6].

T. Weckesser and H. Jóhannsson are with the Technical University of Denmark, Kgs. Lyngby, Denmark, email: {jtgw}{hjjo}@elektro.dtu.dk

T. Van Cutsem is with the Fund for Scientific Research (FNRS) at the University of Liège, Belgium, email: t.vancutsem@ulg.ac.be

Research supported by the Danish Council for Strategic Research (DSF).

In the present paper voltage sags are investigated with focus on system dynamics rather than power quality. The aim is to derive a method, which in real-time allows early and accurate prediction of voltage sags caused by angular separation. To this purpose, different approaches have been implemented and their performance is assessed. In order to avoid limitations due to the model or data, the proposed methods utilize synchronized phasor measurements.

II. Voltage Sag Prediction

In this section three approaches are described, which intend to early predict an imminent voltage sag. These approaches will later be compared and benchmarked against time-domain simulation. It should be noted that all the proposed methods use wide-area measurements, which introduce a delay due to the communication time needed to collect the measurements.

A. Modelling for voltage sag prediction

For voltage sag prediction, the generators are modelled using the so-called "classical" model [7]. This corresponds to a representation of each generator by an e.m.f. $\bar{E}'$ of constant magnitude behind the transient reactance X'_d while loads are converted to constant shunt admittances. The reason for using this very simple model is threefold. First, the time frame of concern is short, in the order of one second after fault clearing. Second, the model is only used to get a fast estimation of the voltage sag. Third, the method utilizes real-time measurements from phasor measurement units (PMUs) to fit the parameters of the classical model to the current operating point. To simplify matters the Norton equivalent, i.e. a current source $\bar{E}'/(jX'_d)$ in parallel with the admittance $1/(jX'_d)$, is chosen to represent each generator. Under these assumptions, the following well-known algebraic equations can be used:

$$\bar{\boldsymbol{I}} = \boldsymbol{Y}\bar{\boldsymbol{V}} \tag{1}$$

where the vector of complex current injections is $\bar{\boldsymbol{I}}$, the vector of complex bus voltages is $\bar{\boldsymbol{V}}$, and $\boldsymbol{Y}$ is the "augmented" bus admittance matrix, which is obtained by adding the transient reactances of the generators and shunt admittances of the loads to the admittance matrix of the network.

The number of buses is n and the number of generators is m. The bus entries are sorted so that the buses where generators are connected have the indices from $n-m+1$ to n. Hence,

Eq. (1) can be written as:

$$\begin{bmatrix} 0 \\ \vdots \\ 0 \\ \bar{E}'_1/(jX'_{d,1}) \\ \vdots \\ \bar{E}'_m/(jX'_{d,m}) \end{bmatrix} = \boldsymbol{Y} \begin{bmatrix} \bar{V}_1 \\ \vdots \\ \bar{V}_{n-m} \\ \bar{V}_{n-m+1} \\ \vdots \\ \bar{V}_n \end{bmatrix} \tag{2}$$

where the zero sub-vector has dimension $n-m$ and $\bar{V}_i$ is the complex voltage at the i-th bus.

B. Voltage Sag Prediction using PMU Voltage Measurements

The first method to predict the depth of a voltage sag consists in acquiring bus voltage measurements in the post-fault configuration and computing a quadratic approximation of each voltage evolution. To this purpose a Recursive Least Square (RLS) estimator with exponential forgetting factor [8] is used together with the linear regression model.

$$\mathbf{V}_i = \mathbf{\Theta}_i^T \mathbf{x}_i \tag{3}$$

where $\mathbf{x}_i$ is the regressor $[t_i^2,\, t_i,\, 1]^T$ at a discrete time, $\mathbf{V}_i$ is the observation, which is a vector of the measured bus voltages at time t_i, and $\mathbf{\Theta}_i$ is the corresponding parameter matrix determined at t_i:

$$\mathbf{\Theta}_i = \begin{pmatrix} a_1 & \dots & a_l \\ b_1 & \dots & b_l \\ c_1 & \dots & c_l \end{pmatrix} \tag{4}$$

The first three sets of voltage magnitudes are used to compute a first estimate of the parameter matrix, which holds all the parameters of the quadratic approximations of all l load bus voltages. This is achieved through linear least square approximation. Additionally, the covariance matrix is computed, which is used in the RLS estimator and needs to be updated at each step. The covariance matrix $\mathbf{R}$ is initialized as:

$$\mathbf{R}_i = \mathbf{X}^T \mathbf{X} \tag{5}$$

where $\mathbf{X}$ is the regression matrix holding the regression vectors $\mathbf{x}_k^T,\ k = i-2, i-1, i$. The parameter matrix $\mathbf{\Theta}$ is updated by the RLS estimator as follows:

$$\mathbf{\Theta}_i = \mathbf{\Theta}_{i-1} + \mathbf{R}_i^{-1} \mathbf{x}_i (\mathbf{V}_i - \mathbf{x}_i^T \mathbf{\Theta}_{i-1}) \tag{6}$$

The inverse of the covariance matrix is updated as follows:

$$\mathbf{R}_i^{-1} = \lambda^{-1} [\mathbf{R}_{i-1}^{-1} - \mathbf{R}_{i-1}^{-1} \mathbf{x}_i (\lambda + \mathbf{x}_i^T \mathbf{R}_{i-1}^{-1} \mathbf{x}_i)^{-1} \mathbf{x}_i^T \mathbf{R}_{i-1}^{-1}] \tag{7}$$

Consequently, only one time at the beginning the inverse of the covariance matrix has to be determined and, thereafter, it solely is updated using (7), which does not involve inverting a matrix.

In [9] a typical range for the forgetting factor is stated as $\lambda = 0.95 \dots 0.995$. λ equal to one implies that all measurements are "remembered" and considered in the computation of the parameters. Due to the strong non-linear equations describing the dynamics of the power system, it was chosen to use a factor at the lower limit of the common range ($\lambda = 0.95$).

The RLS estimator determines from the voltage magnitude measurement for each load bus k a function $V_k(t)$.

$$V_k(t) = a_k t^2 + b_k t + c_k \tag{8}$$

This approximated function of the voltage is then used to predict the depth of the voltage sag through an assessment of its extreme values.

C. Voltage Sag Prediction using the phase angle of E'

Since the voltage sag in this study originates from a deviation of the rotor angles of a group of generators, the second proposed method uses an RLS estimator to predict the individual rotor angle evolution. Thus, the rotor angle of the k-th generator is obtained as:

$$\delta_k(t) = a_k t^2 + b_k t + c_k \tag{9}$$

In order to do so, the method computes from each acquired set of synchronized bus voltage and current measurements the matching operating point for each generator, when represented by the classical model. The phase angle δ of the computed e.m.f. $\bar{E}'$ corresponds to the rotor angle of the machine and its evolution may be predicted with an RLS estimator, as introduced in the previous section. For the period, where the rotor angle evolution is sufficiently described by the quadratic approximation of Eq. (9) and under the assumption of constant magnitude of the e.m.f.'s, the load bus voltages can be computed by solving:

$$\begin{bmatrix} 0 \\ \vdots \\ 0 \\ \bar{E}'_1\, e^{j\Delta\delta_1}/(jX'_{d,1}) \\ \vdots \\ \bar{E}'_m\, e^{j\Delta\delta_m}/(jX'_{d,m}) \end{bmatrix} = \boldsymbol{Y} \begin{bmatrix} \bar{V}_1^{\dagger} \\ \vdots \\ \bar{V}_{n-m}^{\dagger} \\ \bar{V}_{n-m+1}^{\dagger} \\ \vdots \\ \bar{V}_n^{\dagger} \end{bmatrix} \tag{10}$$

where $\Delta\delta$ corresponds to changes in rotor angle from the current state to a state some time ahead. In this work the rotor angle prediction was performed over the next 300 ms.

D. Voltage Sag Prediction using E-SIME

1) E-SIME Method: The SIngle Machine Equivalent (SIME) Method is a transient stability assessment method based on the Equal-Area Criterion (EAC). A detailed description of the method can be found in [10]. A recent discussion of the achievements and prospects of Emergency-SIME (E-SIME) is available in [11]. The methodology of SIME relies on the possibility of representing the post-fault dynamics of a multi-machine power system by a suitable One-Machine Infinite Bus (OMIB) equivalent. The transient stability of the OMIB can then be assessed applying EAC.

In E-SIME real-time measurements are collected in the post-fault configuration at regular time steps t_i. These measurements are used to formulate an OMIB equivalent, which represents the dynamics between a group of "Critical" Machines (CMs) and a group of "Non-critical" Machines (NMs). The OMIB is characterized by its rotor angle δ, speed ω,

inertia coefficient M and acceleration power P_a, which is the difference between mechanical and electrical power. These parameters and variables can be computed from machine parameters and appropriate aggregation of the CMs and NMs.

Subsequently, the EAC allows to compute a transient stability margin η, which is negative for an unstable and positive for a stable case [10]:

$$\eta = -\int_{\delta_i}^{\delta_u} P_a d\delta - 1/2M\omega_i^2 \tag{11}$$

where δ_i and ω_i correspond to $\delta(t_i)$ and $\omega(t_i)$ and δ_u is the angle where the following instability conditions are met:

$$P_a(\delta_u) = 0 \text{ and } \dot{P}_a(\delta_u) > 0 \tag{12}$$

In E-SIME the angle δ_u is estimated through a prediction of the $P_a(\delta)$-curve of the OMIB. To this purpose, three successive data sets of the OMIB, consisting of P_a and δ, are used to compute a quadratic approximate of the curve:

$$P_a(\delta) = a\delta^2 + b\delta + c \tag{13}$$

of which the parameters a, b and c are computed from the three data sets and, subsequently, are refined using a weighted least square technique.

The implementation of E-SIME comprises the following steps. *Step 1:* Collect the first three post-fault measurement sets of the multi-machine system. *Step 2:* Using Taylor series expansion, predict the rotor angles of the individual machines some time ahead (e.g. 100 ms). *Step 3:* Identify the CMs by ranking the machines according to the predicted rotor angles and searching for the maximum angular gap between two successive machines. The machines above the gap form the candidate CMs and the ones below the candidate NMs. The two groups are aggregated into two equivalent machines and, thereafter, the "candidate" OMIB can be determined. *Step 4:* The parameters of the OMIB from (at least) three successive data sets are utilized to estimate its $P_a(\delta)$-curve with Eq. (13). *Step 5:* Then the angle δ_u can be computed, if Eq. (13) meets the conditions (12). If not, a new set of data is acquired and the procedure is repeated from *Step 2*. If the conditions are met, the stability margin is computed utilizing Eq. (11). Then a new set of data is acquired and *Steps 2* to *5* are repeated to refine the computed δ_u and η. The procedure is terminated when the margin converged to a constant value or the return angle is reached, where:

$$P_a(\delta_r) < 0 \text{ and } \omega_r = 0 \tag{14}$$

2) Prediction using E-SIME: In the following, a method is derived, which uses E-SIME to predict and early detect a voltage sag. The idea is that E-SIME uses real-time data to predict the rotor angle evolution in each time step of the post-fault configuration. If the system is found stable, the method predicts the return angle of the critical cluster. This angle together with the up-to-date bus voltage measurements are then used to predict the expected minimum load bus voltage.

Just after fault clearance, the admittance matrix as described in Section II-A is computed and the assessment with E-SIME is executed. If the computed stability margin is positive, the return angle δ_r is computed by solving:

$$0 = \int_{\delta_i}^{\delta_r} P_a(\delta) d\delta - 1/2M\omega_i^2 \tag{15}$$

where P_a is approximated by the quadratic function in Eq. (13). From the current rotor angle δ_i of the candidate OMIB and the predicted angle δ_r, the maximum angular deviation of the CMs relative to the NMs can be estimated by

$$\Delta\delta_r = \delta_r - \delta_i \tag{16}$$

Since it is assumed that the voltage sag origins from the rotor swing of the generators, it is expected that the voltage sag minimum will be reached when the group of CMs and the group of NMs have reached there maximum angular separation [2], which occurs at the return angle. The operating point of the synchronous machine represented by the classical model is computed by utilizing the most recent bus voltage PMU measurements and solving Eq. (2). Hence, the minimum bus voltages are computed by assuming constant magnitude of the e.m.f.'s, but a rotation of $\bar{E}'$ of the CMs by $\Delta\delta_r$. Then the bus voltages at δ_r can be computed by solving Eq. (2).

III. Results for Voltage Sag Prediction

A. Test system and test case

1) Test system: In order to validate the proposed prediction methods and to assess their accuracy, the well-known New England & New York system [12] is used. The system is composed of 68 buses and 16 generators. In the time-domain simulations the 33 loads are modelled as constant impedances. The generators are all equipped with a simple excitation and voltage regulation system, as well as a thermal turbine/governor model. Additionally, all generators, but GEN-7 and GEN-14, are equipped with power system stabilizers. The machines are modelled with four rotor windings.

2) Test case: In the test scenario a three-phase short-circuit on the transmission line connecting buses 16 and 21 occurs at time $t = 1$ s. This fault is very close to bus 21 and is cleared after 150 ms through the opening of the breakers at both ends of the faulted transmission line. This scenario was also proposed in [12].

Due to the fault some generators accelerate relative to the others. This leads to a large angular separation of the rotors. The response of a selection of generators is shown in Fig. 1. The selection consists of the five generators with the largest increase of rotor angle (GEN-1, GEN-4, GEN-5, GEN-6 and GEN-7), the three generators with the largest decrease (GEN-14, GEN-15 and GEN-16) and one which is barely affected (GEN-13). The rotor angle evolution shows that certain generators are affected to a higher degree than others; for instance GEN-6 and GEN-7. Yet, synchronism is maintained, a new stable equilibrium is reached and the scenario can be assessed to be transiently stable. The voltage magnitudes at a selection of load buses over time are presented in Fig. 2. This selection includes the five buses which experience the deepest voltage sag (buses 15, 16, 21, 23 and 24),

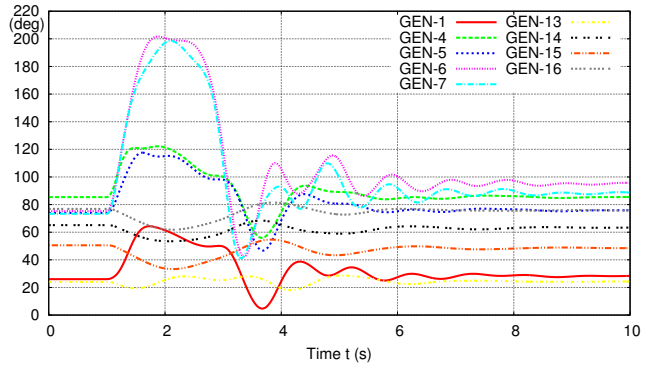

Fig. 1. Evolution of generator rotor angles (with respect to center of inertia)

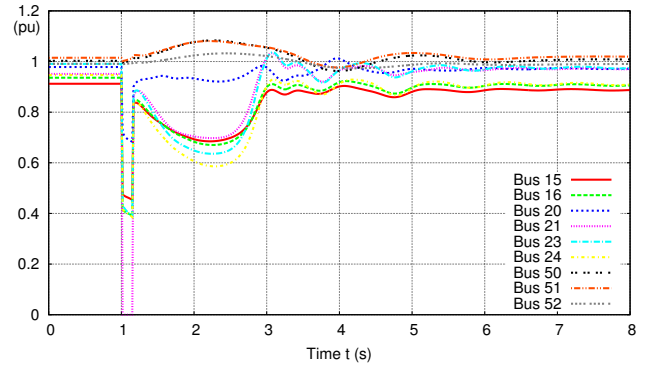

Fig. 2. Evolution of voltage magnitudes at load buses

the three buses whose voltage magnitude are slightly increased (buses 50, 51 and 52), and one bus barely affected by the post-fault dynamics (bus 20). In the fault-on period voltage magnitudes in the vicinity of the fault location experience a dramatic drop and immediately recover after fault clearance. However, in the subsequent evolution a voltage sag can be observed at certain buses with voltage dropping below the critical value of 0.7 pu, which is unacceptably low and long lasting. An early and accurate detection of these voltage sags is very valuable for a secure operation of the power systems.

B. Detection of critical load buses

In this section the different prediction methods are evaluated with respect to their ability to early and consistently predict the crossing of a critical voltage level (here taken as 0.7 pu). Figure 3 shows on the abscissa the simulated time and on the ordinate the loads. A data point at a certain time and for a certain load indicates that the particular method predicted, at that time instant, that the voltage at this load bus will drop below the critical level during the voltage swing.

The black crosses depict the results when using directly PMU voltage measurements and an RLS estimator (see Section II-B), the blue circles show the results using the phase angle of the e.m.f.'s and an RLS estimator (see Section II-C) and the green $\times$'s relate to the approach using SIME (see Section II-D). Consequently, the graph allows to assess how early a critically low voltage at a certain load can be predicted and how consistent this prediction is. Furthermore, the graph

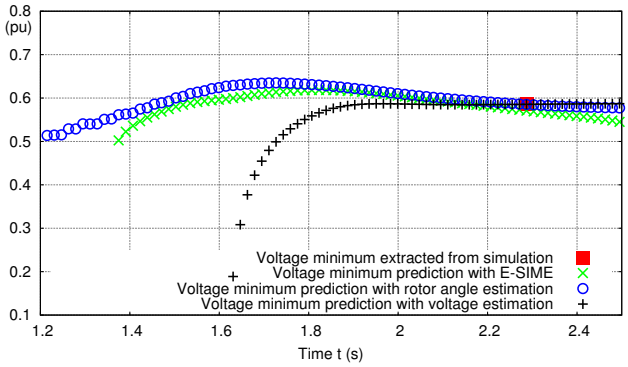

Fig. 4. Prediction of voltage minimum at bus 24 (load 14)

discloses if a method predicts critically low voltages only at those buses, where the voltage actually drops below the critical value. Finally, the red squares indicate the time instants at which the voltage of a particular load drops below the critical value in the time-domain simulation. This is the case, in the analysed scenario, for loads 8, 9, 12, 13 and 14, which correspond to buses 15, 16, 21, 23 and 24.

Figure 3 indicates that the method utilizing real-time voltage measurements (black crosses) needs to acquire a large number of measurements to correctly predict the critically low voltage sags, which leads to some detections taking place after the critical level has been crossed (e.g. loads 13 and 14). Furthermore, at some point the method unduly predicts low voltage for some non-critical loads (e.g. loads $2-5$). The second method, which uses the phase angle of the e.m.f.'s for the prediction (blue circles), is more consistent in the prediction of the critical loads. It allows an early identification, while only for a short initial period some loads are unduly flagged as critical (e.g. loads $3-5$). However, for some loads, the identification of critically low voltages is interrupted before the respective voltage falls below the critical level (e.g. loads 8, 9 and 12). The results depicted by the green $\times$'s and utilizing E-SIME are very satisfactory. Generally, only the critical loads are flagged and the identification is well before the voltage at the particular bus falls below the critical level.

C. Earliness and Accuracy of the Prediction

In this section, the methods are assessed with respect to their ability to early and accurately detect the actual minimum of the voltage sag observed at a particular bus. The results are presented for the bus experiencing the lowest voltage sag (bus 24, Fig. 4) and the bus where the voltage marginally drops below the critical level (bus 21, Fig. 5). In both graphs the red squares indicate the time and value of the voltage minimum at the particular bus provided by time-domain simulation.

The prediction method which uses the bus voltages directly (black crosses) detects late that both voltages will fall below the critical value. Furthermore, the first predicted values are very pessimistic, although the predicted voltage minimum, subsequently, converges to the accurate value in both cases. The second method, which predicts the voltage sag from the phase angle of the e.m.f.'s (blue circles), early indicates a

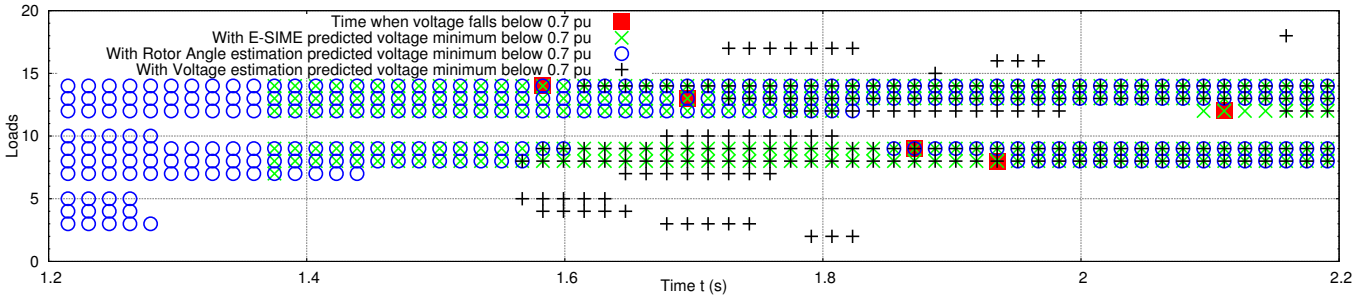

Fig. 3. Early detection of load bus voltages falling below the critical value of 0.7 pu

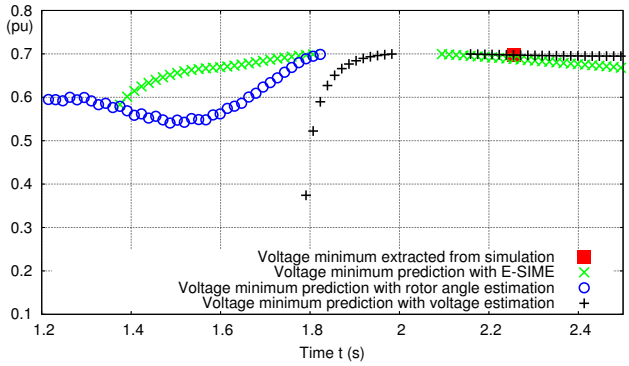

Fig. 5. Prediction of voltage minimum at bus 21 (load 12)

voltage below the critical value at both buses. The maximum deviation to the actual minimum is smaller compared to the first method. However, the prediction for bus 24 is not as accurate as with the first method, when getting close to the time where the actual voltage minimum occurs. Moreover, at bus 21 the prediction is interrupted, because the voltage is no longer identified to be critical. This occurs before the actual voltage has reached its minimum and, thereafter, the method fails to again detect the shortfall of the critical voltage magnitude. The third method, which uses E-SIME for the prediction of the depth of the voltage dip (green $\times$'s), detects the crossing of the critical voltage around 200 ms later than the second method, but still significantly earlier than the first method. The prediction accuracy is comparable to the second approach, but not as good as the first method. In the prediction of the minimum voltage in the marginally critical case at bus 21, the prediction is interrupted at some point, as it is for the other methods, but is resumed before the other methods do.

IV. Conclusion

In this paper three approaches were described to predict critically low voltages during a transient voltage sag caused by large rotor swings of certain generators. Voltages below a critical level can lead to further events in the system such as unintentional load tripping, which again can cause deterioration of the system condition. An early and accurate prediction of critical voltage sags is a basic requirement to execute corrective control actions. The three approaches have been assessed with respect to their abilities to correctly and early predict the crossing of a critical voltage level and the minimum of the corresponding voltage.

The results show that each of the methods can predict the voltage sags to a certain extent. While the method utilizing the phase angle of the e.m.f.'s and the method applying E-SIME allow an early detection of critical buses and low voltages, the method using voltage measurements directly allows a more accurate prediction of the voltage minimum. All in all the prediction method employing E-SIME seems to be promising. It allows early and consistent identification of critical buses and the prediction of the voltage sag minimum is sufficiently accurate. Furthermore, the approach poses an acceptable computing time and is suitable for an online application. Together with indicators providing insight on type, size and location for control actions, the method could be part of a closed-loop emergency control. For such an application the time delay, due to gathering of measurements, becomes crucial.

References

[1] M. H. Bollen, *Understanding power quality problems*, vol. 3 ed. New York: IEEE press, 2000.

[2] A. A. Fouad and R. Sreedhara, "Transient Voltage Dip Analysis using the Transient Energy Function Method," in *Proceedings of the Twenty-Second Annual North American Power Symposium*. IEEE Comput. Soc. Press, 1990, pp. 264–273.

[3] F. Dominguez, A. S. Debs, and J. Anasis, "Transient voltage dip in power systems: computation and sensitivity analysis using the hybrid method," in *Decision and Control, 1992., Proceedings of the 31st IEEE Conference on*, 1992, pp. 576–581 vol.1.

[4] Y. Xue, T. Xu, B. Liu, and Y. Li, "Quantitative assessments for transient voltage security," *Proceedings of the 21st International Conference on Power Industry Computer Applications. Connecting Utilities. PICA 99. To the Millennium and Beyond*, pp. 101–106, 1999.

[5] A. Tiwari and V. Ajjarapu, "Contingency assessment for voltage dip and short term voltage stability analysis," *2007 iREP Symposium - Bulk Power System Dynamics and Control*, pp. 1–8, Aug. 2007.

[6] D. Shoup, J. Paserba, and C. Taylor, "A survey of current practices for transient voltage dip/sag criteria related to power system stability," *IEEE PES Power Systems Conference and Exposition*, 2004.

[7] P. Kundur, *Power System Stability and Control*, N. J. Balu and M. G. Lauby, Eds. McGraw-Hill Inc., 1994.

[8] M. I. Jordan, "Notes on recursive least squares," 1998.

[9] B. Lindoff, "On the Optimal Choice of the Forgetting Factor in the Recursive Least Squares Estimator," 1997.

[10] M. Pavella, D. Ernst, D. Ruizvega, and D. Ruiz-Vega, *Transient Stability of Power Systems: A Unified Approach to Assessment and Control*. Kluwer Academic Publishers, 2000.

[11] M. Glavic, D. Ernst, D. Ruiz-Vega, L. Wehenkel, and M. Pavella, "E-SIME - A Method for Transient Stability Closed-Loop Emergency Control : Achievements and Prospects Fundamentals of E-SIME," in *2007 iREP Symposium - Bulk Power System Dynamics and Control*, 2007.

[12] G. Rogers, *Power System Oscillations*. Springer, 2000.

Appendix H

Real-Time Remedial Action Against Aperiodic Small Signal Rotor Angle Instability

---

This paper will appear in a future issue of IEEE Transaction on Power Systems.

Real-Time Remedial Action Against Aperiodic Small Signal Rotor Angle Instability

Tilman Weckesser, *Member, IEEE*, Hjörtur Jóhannsson, *Member, IEEE*, and Jacob Østergaard, *Senior Member, IEEE*

***Abstract*—This paper presents a method that in real-time determines remedial actions, which restore stable operation with respect to aperiodic small signal rotor angle stability (ASSRAS) when insecure or unstable operation has been detected. An ASSRAS assessment method is used to monitor the stability boundary for each generator in real-time. The ASSRAS boundary represents the condition when a generator reaches the maximum steady state active power injection. The proposed control method exploits analytically derived expressions for the ASSRAS boundary and other characteristic curves in the injection impedance plane to determine an active power redispatch among selected generators to restore stable and secure operation. Since the method is purely based on analytically derived expression, the computation of the remedial actions is fast and well suited for real-time operation. The method was tested on the IEEE 14-bus and the Nordic32 test systems where results show that the method can efficiently determine the required active power redispatch to avoid an imminent instability.**

***Index Terms*—Power system control, power system generation redispatch, power system stability, remedial action schemes.**

I. Introduction

MODERN societies are highly dependent on a stable and secure operation of the power system. A continuously increasing share of power production based on renewable energy sources (RES) can be observed in numerous countries, where, e.g., in Denmark the government's energy strategy states that 50% of the electricity consumption is to be supplied by wind power by 2020 [1]. The foreseen challenges associated with these goals are great as the future power system has to be securely operated and delivering energy at competitive prices.

The fluctuating nature of RES such as wind and solar radiation may cause rapid changes in future generation patterns, leading to rapid fluctuations of the power system's operating point. Existing offline and computationally demanding approaches for assessing stability and determination of remedial or preventive actions may become insufficient. Hence, a need for real-time approaches will arise for the future system [2].

Efforts have been made to meet the real-time requirements for the assessment of the future system. A method for online assessment of voltage stability is presented in [3] and [4]. The method does not rely on a dynamic model to predict the system response, instead basic assumptions and simplifications are applied in the modeling process resulting in reduced computational burden.

Manuscript received July 04, 2014; revised September 23, 2014 and January 05, 2015; accepted February 11, 2015. This work was supported by the Danish Council for Strategic Research (DSF) . Paper no. TPWRS-00914-2014.

The authors are with the Center for Electric Power and Energy, Department of Electrical Engineering, Technical University of Denmark, 2800 Lyngby, Denmark (e-mail: jtgw@elektro.dtu.dk).

Color versions of one or more of the figures in this paper are available online at http://ieeexplore.ieee.org.

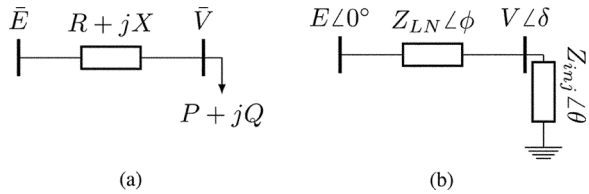

Fig. 1. In [13], for this two-bus system, critical and characteristic curves were expressed in terms of the injection impedance. (a) Two-bus system. (b) Equivalent two-bus system with injection impedance.

In [5] an element wise approach is proposed for stability assessment where each individual assessment method analyzes a particular instability mechanism. [5] describes such a method to monitor the aperiodic small signal rotor angle stability (ASSRAS) of the individual generators and to determine their respective stability margin. This stability mechanism refers to the ability of each individual generator to produce sufficient steady state electromechanical torque. If this torque balance is upset, an aperiodic increase in rotor angle and a subsequent loss of synchronism can be observed.

The authors of [6] emphasize that efficient remedial action schemes (RAS) are an enabler for connecting more RES based generation. The real-world implementation of a centralized remedial action scheme (CRAS) system was described in [6]. The system executes corrective actions such as load or generation reduction to ensure reliable and safe system operation after fault occurrence. The automatic system-wide RAS arming system currently used in the power grid of British Columbia was described in [7]. The RAS arming patterns are determined periodically employing a transient stability analysis tool, which ensures security of the system. To achieve real-time performance, the system relies on a large case database build from extensive off-line planning studies.

A new methodology for determining the security region for operation of transmission systems is described in [8]. The calculation of the boundaries is done offline and can be used to identify efficient controls and remedial actions. The authors of [9] propose an adaptive damping control scheme, which uses online measurements to adapt the controller parameters to changing operating conditions. The initial parameters are determined offline using a set of nominal operating conditions. In [10] the authors compare two different approaches for damping inter-area oscillations and come to the conclusion that wide-area control methods are more effective than local controls. The previous two paper determine controls for periodic small signal rotor angle stability, while the following method and the one proposed in this paper address ASSRAS.

Digital Object Identifier 10.1109/TPWRS.2015.2404872

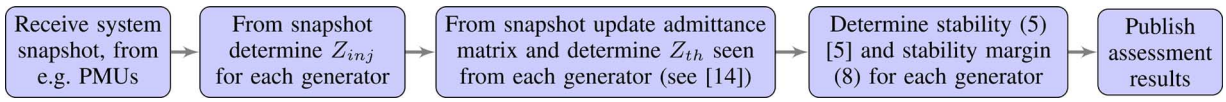

Fig. 2. Function blocks of the ASSRAS assessment method [5].

In [11] the authors developed a method, which determines the necessary countermeasures to be applied to a number of loads to restore stability and security of the system with respect to the ASSRAS boundary. The method therefore alters the consumption pattern of load buses, which were identified to be the most effective locations for applying countermeasures.

This paper presents a new method to restore ASSRAS for which a patent has been submitted [12]. The investigated instability mechanism is a quasi steady state phenomena. Consequently, the assessment method as well as the developed remedial action method require that the system is in quasi steady state. Most of the prior mentioned methods rely on extensive offline studies to determine the corrective control actions. In contrast to that, the proposed method is derived analytically and only requires online measurements of the current system condition. With these information, the method can fast and accurately determine the required control actions. The structure of the paper is as follows. In Section II, the ASSRAS assessment method is briefly described. The data provided by the assessment method are utilized in the developed remedial action method to compute corrective active power redispatch solutions, which is described in Section III. The method's capability to avoid an imminent collapse in voltage is presented in Section IV, where the results from two test systems are presented. Finally, in Section V the presented method and results are discussed.

II. Background

A. Algebraic Expressions for Critical Transmission Limits

Reference [13] describes the mapping of some characteristic curves from a PQV-surface of a two-bus system into the injection impedance plane (see Fig. 1). For such a system the relationship of the voltage magnitudes in both ends (E and V) and the active & reactive power (P and Q) becomes

$$V^4+V^2(2(RP+XQ)-E^2)+(R^2+X^2)(P^2+Q^2)=0 \quad (1)$$

where R and X are the resistance and reactance of the line. In [13] it is shown, by manipulation of (1), that the condition for maximum deliverable power to the receiving end, under the assumption of constant E and V, is represented by a circle in the injection impedance plane, which is in polar coordinates:

$$Z_{inj}=\frac{-Z_{LN}\sin(\theta)}{\sin\phi}. \quad (2)$$

Here, $Z_{inj}\angle\theta$ represents the complex injection impedance and $Z_{LN}\angle\phi$ the impedance of the line where $Z_{LN}=\sqrt{R^2+X^2}$. Furthermore in [13], it was shown that lines of constant voltage magnitude V and voltage angle δ (the angle between E and V) map as circles in the injection impedance plane. For later use the equations describing these characteristic curves are stated at this point. The curves of constant voltage magnitude satisfy

$$Z_{inj}=r_0\cdot\cos(\theta-\varphi)\pm\sqrt{r^2+r_0^2\cdot\sin^2(\theta-\varphi)} \quad (3)$$

where

$$r=\frac{EV\sqrt{R^2+X^2}}{V^2-E^2};\ r_0=\frac{V^2\sqrt{R^2+X^2}}{V^2-E^2};\ \tan\varphi=\frac{-X}{-R}.$$

From [13], the curve for constant voltage angle δ is given by

$$Z_{inj}=-\left(\frac{Z_{LN}}{\sin\delta}\right)\cdot\sin(\delta+\phi-\theta). \quad (4)$$

B. Method for Real-Time Assessment of ASSRAS

In [5] a method is presented to quickly assess the ASSRAS of all system generators. In Fig. 2, a block diagram of the employed method is shown to visualize the different steps carried out to assess stability. The algebraically derived expression for maximum injection of active power in (2) is exploited to formulate an algebraic assessment criterion which enables stability assessment in linear time [14]. The ASSRAS boundary of a generator is given by

$$Z_{inj,i}=\frac{-(Z_{th,i}\sin(\theta))}{(\sin\phi_{th,i})} \quad (5)$$

where $Z_{inj,i}\angle\theta=\overline{Z}_{inj,i}$ is the complex injection impedance seen from the i^{th} generator's node of constant steady state voltage magnitude and $Z_{th,i}\angle\phi_{th,i}$ is the complex Thévenin network impedance seen from the same node. In [15] it was shown that the Thévenin equivalent parameters seen from each generator can be directly computed from the network admittance matrix and a system snapshot. The authors of [14] presented a test case with 7917 buses and 1325 voltage control nodes and demonstrated that all the Thévenin equivalent parameters could be computed within 2.5 ms.

Equation (5) appears as a circle in the injection impedance plane and the generator's ASSRAS is determined from its value of $\overline{Z}_{inj,i}$. A value of $\overline{Z}_{inj,i}$ outside the circle represents stable operation while a value inside represents unstable operation. An unstable operation is characterized by the condition when a small increase of the steady state rotor angle δ of a given generator reduces its active power output. While during stable operation, an increase in δ increases the generator's active power output. The assessment method determines whether a steady state equilibrium point exists between the mechanical power applied to a given generator and its active power output. If a disturbance causes a loss of the generator's steady state equilibrium point, the generator will begin to lose synchronism in a process that may take tens of seconds and up to a few minutes to evolve [5], [15] . In order to track the stability condition of a generator in real-time, system snapshots need to be available at a sampling rate equivalent to the repetition rate of measurements provided by PMUs or from a fast state estimator. The sampling rate of the snapshots should be sufficient to trace the movement of the operating points and a higher rate allows to choose lower security limits.

As the cause of aperiodic small signal rotor angle instability is the lack of existence of an equilibrium point between the me-

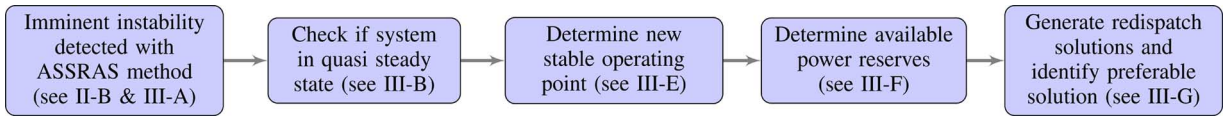

Fig. 3. Function blocks of the proposed remedial action method.

chanical and electrical power of a given generator, an intuitive choice of a counter action is to lower mechanical power applied to the critical machine to restore an equilibrium.

1) Stability Margin: In [5] the authors showed that the distance of the operating point (OP) of a generator to the stability boundary is a measure of the distance to instability and that it can be expressed in terms of various variables. When representing a generator by a voltage source $V\angle\delta$ and the remaining grid by a Thevenin equivalent corresponding to a voltage source with magnitude E_{th} and an impedance $Z_{th}\angle\phi_{th}$, then its power injection P_{inj} is

$$P_{inj} = \left(\frac{E_{th}V}{Z_{th}}\right)\cos(\delta+\phi_{th}) - \left(\frac{V^2}{Z_{th}}\right)\cos(\phi_{th}). \quad (6)$$

Under the assumption of constant voltage magnitudes at nodes of power injection and freezing of all other phase angles, the power injection of a particular generator becomes a function of solely the phase angle δ and is maximal at the angle $\delta = 180° - \phi_{th}$, which represents the ASSRAS boundary. Consequently, the maximum power injection $\hat{P}_{inj}$ can be expressed as

$$\hat{P}_{inj} = \frac{-E_{th}V}{Z_{th}} - \left(\frac{V^2}{Z_{th}}\right)\cos(\phi_{th}). \quad (7)$$

This allows to define a stability margin in percentage of the maximum power injection $\%\Delta P_{inj}$:

$$\%\Delta P_{inj} = \frac{\cos(\delta+\phi_{th})+1}{1+\frac{V}{E_{th}}\cos\phi_{th}} \cdot 100\%. \quad (8)$$

C. Relative Electrical Distance

In [16], the authors describe an approach to determine the relative electrical distance between load buses and generator buses. For that purpose the authors utilize the network admittance and the linear algebraic network equations:

$$\begin{bmatrix}\mathbf{I}_G\\ \mathbf{I}_L\end{bmatrix} = \begin{bmatrix}\mathbf{Y}_{GG} & \mathbf{Y}_{GL}\\ \mathbf{Y}_{LG} & \mathbf{Y}_{LL}\end{bmatrix}\begin{bmatrix}\mathbf{V}_G\\ \mathbf{V}_L\end{bmatrix} \quad (9)$$

where the complex current and voltage vectors at the generator and load buses are represented by $\mathbf{I}_G, \mathbf{I}_L, \mathbf{V}_G$, and $\mathbf{V}_L$. The sub-matrices $\mathbf{Y}_{GG}$, $\mathbf{Y}_{GL}$, $\mathbf{Y}_{LG}$, and $\mathbf{Y}_{LL}$ are the corresponding parts of the network admittance matrix.

The authors showed that the sub-matrices can be used to determine the relative electrical distance of the load buses to the generator buses in the system, which can be computed as follows:

$$[R_{LG}] = 1 - abs[F_{LG}] = 1 - abs([\mathbf{Y}_{LL}]^{-1}[\mathbf{Y}_{LG}]). \quad (10)$$

The values in each column of the resulting matrix contain a measure of the relative electrical distance between a load bus and the respective generator.

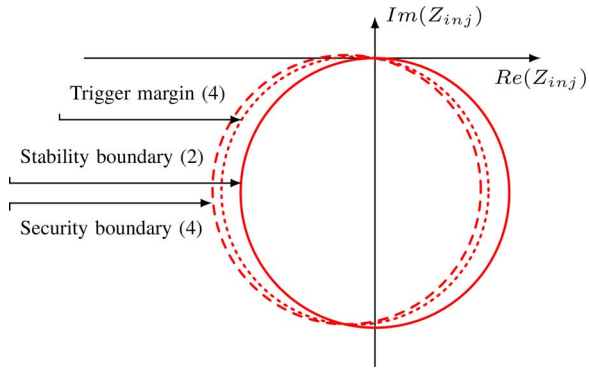

Fig. 4. Injection impedance plane displaying the aperiodic small signal rotor angle stability boundary (solid circle), the security boundary (dashed circle) and the circle corresponding to the trigger margin (dotted circle).

III. Method for Real-Time Determination of Remedial Actions

This section describes a method capable of determining a generator redispatch solution to circumvent ASSRA instability in real-time. Fig. 3 shows the function blocks of the proposed method.

A. Trigger and Security Margins

It is preferable that the remedial actions are executed before the system becomes unstable. Hence, a trigger margin is introduced that corresponds to a percentage of the maximum power injection and represents the stability margin threshold below which the remedial action method is executed. To find a new set point and to limit how much the remaining generators can contribute to the remedial action, a second threshold is introduced, called security margin m_{sec}, which defines the security boundary. In this approach, it was assumed that the voltage at the node of power injection remains constant during the remedial action. This assumption is valid, because the node of power injection is chosen to be at the terminal of the generator or behind the synchronous reactance depending on the respective excitation system of the generator. Due to the constant voltage magnitude the power injection of the generator is solely determined by its voltage angle, see (6). Consequently, the curve corresponding to the trigger and the security margin are represented by a curve of constant voltage angle in the injection impedance plane—see (4) and Fig. 4.

The selection of appropriate margin thresholds is a trade-off between level of system security and additional constraints on the generator's capacity. Since the requirement of a greater margin directly affects the maximum power that a generator can provide to the system and, hence, may lead to an economical loss. Therefore, a balance between required margins for secure system operation and economically efficient operation of the generators has to be found. The margins may be different in each individual power system and it is suggested that the system operators choose them based on their experience and

from offline studies of a selection of aperiodic small signal rotor angle stable and unstable contingencies.

The assessment method analyses the ASSRAS of the system during quasi steady state conditions. However, a crossing of the stability boundary is acceptable in dynamic transition periods from one to another steady state equilibrium point. Consequently, the remedial action method should only be executed, when the system is in quasi steady state and the generator's stability margin has fallen below the trigger margin.

B. Quasi Steady State and Error Estimation

Since the method is based on the assumption of constant voltage magnitude at the nodes of power injection, the voltage magnitudes at these nodes can be used to determine the steadiness of the system. It is assumed that the system is in quasi steady state, when the maximum power injection at a node of constant voltage magnitude can be determined with satisfactory accuracy. Therefore, at a node with assumed constant voltage magnitude the measured voltage magnitudes provided by a PMU are stored for a certain period. Under the assumption that the Thevenin voltage has constant voltage magnitude, the maximum power injection at the node can be computed as a function of the measured voltage magnitudes $V(t_n)$ using (7). When extracting the maximum $V_{\max}$ and minimum $V_{\min}$ of the voltage magnitude in the period of concern, the corresponding maximum error of the computed maximum power injection $\Delta\%P_{inj,err}$ can be determined:

$$\Delta\%P_{inj,err} = \frac{\hat{P}_{inj}(V_{\max}) - \hat{P}_{inj}(V_{\min})}{\hat{P}_{inj}(V(t_n))} 100\%. \qquad (11)$$

In this paper, the acceptable error was chosen to be 0.5%.

C. $N-1$ Operating Point

The discussed assessment method assumes either the voltage magnitude at the terminal of the machine to be constant or at the internal node behind the synchronous reactance X_s. If saliency is neglected, X_s is equal to the reactance in the d-axis X_d and q-axis X_q. Hence, under the assumption that the complex voltage $\bar{E}_t$ and the complex current $\bar{I}_t$ at the terminal of the machine are monitored, then the internal voltage $\bar{E}_q$ can be computed as follows:

$$\bar{E}_q = \bar{E}_t + jX_d\bar{I}_t. \qquad (12)$$

For a salient machine the assumption of constant voltage behind X_d introduces an error, which was investigated in [15]. The results showed that the assumption leads to very small deviations and slightly more conservative assessment results. A machine equipped with an automatic voltage regulator (AVR) will keep the voltage magnitude at the terminal constant, unless the excitation exceeds its limit and the over excitation limiter (OEL) is activated. The activation will cause that the field current is kept constant at a limit value and, hence, the voltage at the terminal can no longer be assumed constant. However, under such conditions the voltage magnitude at the internal node behind X_d can be assumed constant. During AVR operation with constant voltage magnitude at the terminal, the stability of the $N-1$ OP, which assumes constant voltage magnitude at the internal node, can be monitored simultaneously with the actual OP. This allows to provide information on the stability condition of the system in case of activation of an OEL of a machine. Furthermore, it allows to determine control actions guaranteeing secure operation in case of activation of an OEL. If remedial actions are considered for $N-1$ OPs, the trigger and security margins may be chosen lower than for actual OPs, since a stability boundary crossing of an $N-1$ OP only corresponds to an insecure, but not unstable situation.

TABLE I
LOCATION OF NODE OF CONSTANT VOLTAGE MAGNITUDE DURING REMEDIAL ACTION IN DIFFERENT GENERATOR CONFIGURATION AND OPERATION CONDITIONS

Excitation system	OEL	Actual OP	$N-1$ OP
Manually	–	behind X_d	–
AVR with OEL	inactive	at terminal	at terminal
	active	behind X_d	-

D. Assumption of Constant Voltage Magnitude

In this section it is described at which node the voltage magnitude is assumed to be constant during the remedial action. Table I shows where the voltage magnitude is assumed to be constant depending on the generator's excitation system, the state of the OEL and the type of the OP, whose stability margin fell below the trigger margin or rather is imminent to experiencing instability.

In the simple case that the machine is manually excited, the voltage magnitude is assumed to be constant behind X_d and may be computed with (12). In the more complex case, where the machine is equipped with an AVR the location of the node of constant voltage during the remedial action is dependent on the state of the OEL. If the OEL is inactive and, hence, the AVR keeps the voltage magnitude at the machine terminal constant, then the voltage magnitude during the remedial action is assumed to be constant at the terminal independent on the type of OP that is imminent unstable/insecure. If the OEL is activated, the node of constant voltage magnitude moves behind X_d and, consequently, this is also the node, where the voltage magnitude is assumed to be constant throughout the control action.

E. Computation of new Stable and Secure Operating Point

1) Imminent Unstable Node is Actual Operating Point: In the case that the margin of the actual OP of a generator fell below the trigger margin, the power output of the generator has to be reduced to move the OP back into the region of secure operation. Since the desired security margin m_{sec} is known as a percentage of the maximum power injection and under the assumption that the voltage magnitude ratio V/E_{th} remains constant throughout the remedial action, (8) can be used to compute the voltage angle at the new secure OP:

$$\delta^* = \arccos\left[\frac{m_{\text{sec}}}{100\%}\left(1 + \frac{V}{E_{th}}\cos(\phi_{th})\right) - 1\right] - \phi_{th}. \quad (13)$$

Subsequently, with the new voltage angle δ^*, the new active power injection at the secure OP can be determined utilizing (6). Then the necessary power reduction can be determined as the difference between power injection at the current voltage angle δ and the new secure voltage angle δ^*. Fig. 5 depicts the determination of the new secure OP in the injection impedance plane.

The injection impedance Z_{inj} (blue dot) of the respective generator crossed the trigger boundary, which executed the

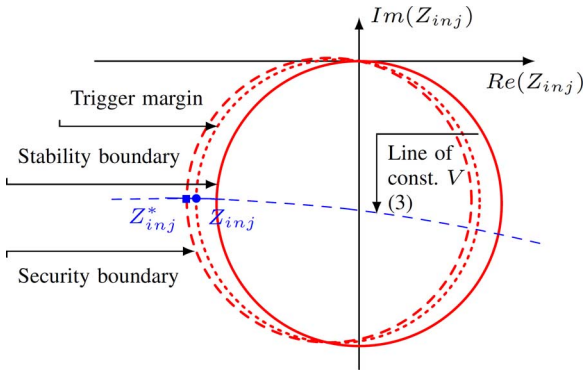

Fig. 5. Graphical representation of the computation of a new secure operating point for the case of imminent instability due to an actual operating point.

method. Following, the new angle δ^* was computed using (13). The new injection impedance Z^*_{inj} of the generator is then found by determining the intersection of the curve of constant voltage magnitude and the line of constant voltage angle corresponding to δ^*.

2) Imminent Unstable Node is $N-1$ Operating Point: In order to operate the system in a secure manner, it is desirable that the $N-1$ OP of a machine is also in the stable and secure operating region. The computation of the needed power reduction differs from the calculations in Section III-E1, since the voltage magnitude at the internal node, which is used to compute the $N-1$ OP, cannot be assumed to be constant throughout the process. It is assumed that also in this case the AVR of the generator keeps the voltage magnitude at the terminal constant and, hence, the corresponding characteristic curve of constant voltage magnitude can be utilized.

In the injection impedance plane, the distance between the injection impedance of the $N-1$ OP and the injection impedance of the actual OP is purely imaginary and equal to X_d. This allows to map characteristic curves of the actual to the $N-1$ OP (see Fig. 6).

The new secure OP of the $N-1$ OP can be found as the intersection of the circle representing the security boundary of the $N-1$ OP with the circle corresponding to the curve of constant voltage magnitude of the actual operating point mapped to the $N-1$ OP (see Fig. 6).

The equation for curves of constant voltage magnitude as described in (3) can be rewritten as

$$\overline{Z}_{inj,const.|V|} = r_0 \cdot e^{j\phi_{th}} + r \cdot e^{j\theta} \tag{14}$$

where r is the radius of the circle, the distance from the origin to the centre of the circle is r_0 and the angle between real axis and a line through the origin and centre of the circle is ϕ_{th}.

This circle of constant voltage magnitude can be mapped to the $N-1$ OP by subtracting jX_d:

$$\overline{Z}_{inj,const.|V|,T} = r_0 \cdot e^{j\phi_{th}} + r \cdot e^{j\theta} - jX_d. \tag{15}$$

Curves of constant voltage angle in the injection impedance are described by (4) and this shows that all the circles of constant voltage angle intercept the origin. Consequently, the term in front of the sine corresponds to the diameter of the circle. This allows to determine the radius of the circle as well as the angle between real axis and the line through origin and centre of the

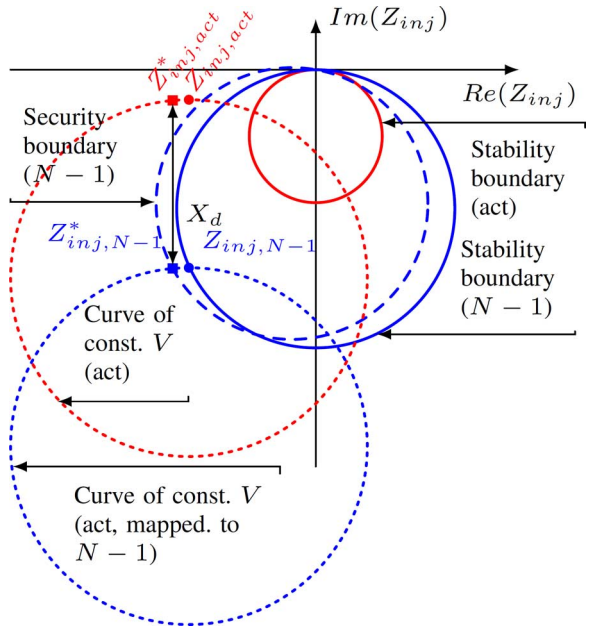

Fig. 6. Graphical representation of the computation of a new secure operating point for the case of imminent instability due to an $N-1$ operating point.

circle. The equation can be rewritten and expressed in terms of the Thevenin parameters as follows:

$$\overline{Z}_{inj,const.\delta} = \frac{Z_{th}}{2\sin\delta}\left(e^{j(\delta+\phi_{th}\pm\pi/2)} + e^{j\theta}\right). \tag{16}$$

Knowing the desired stability margin m_{sec} and after computation of the current voltage magnitude at the internal node of the machine, the new secure voltage angle of the $N-1$ OP can be determined utilizing (13). Subsequently, the circle corresponding to the curve of constant voltage angle can be computed using (16). The intersection of the circle of constant voltage angle described by (16) and the mapped circle of constant voltage magnitude of the actual OP described by (15) gives the new secure $N-1$ OP in terms of the injection impedance $Z^*_{inj,N-1}$. The corresponding new actual OP can be computed from the new actual injection impedance $Z^*_{inj,act}$, which can be computed by adding the synchronous reactance to $Z^*_{inj,N-1}$ (see Fig. 6). Since the voltage magnitude in the actual OP was assumed to be constant, the active power injection in the new and secure OP can be computed and the necessary active power reduction can be determined.

F. Computation of Available Power Reserves

After the required power reduction was calculated the available power resources of the remaining generators have to be determined to eventually propose a power redispatch solution. The available resources are calculated, while respecting the following constraints. The "new" power injection should not

- exceed the $\hat{P}_{inj}$ plus the respective security margin;
- exceed nominal power of the generator plus a sec. margin;
- move the corresponding $N-1$ OP into an insecure or unstable position. Hence, also for the $N-1$ OP a security margin should be maintained.

The power reserve with respect to the nominal power of the generator can directly be computed knowing the security margin and the machine parameter.

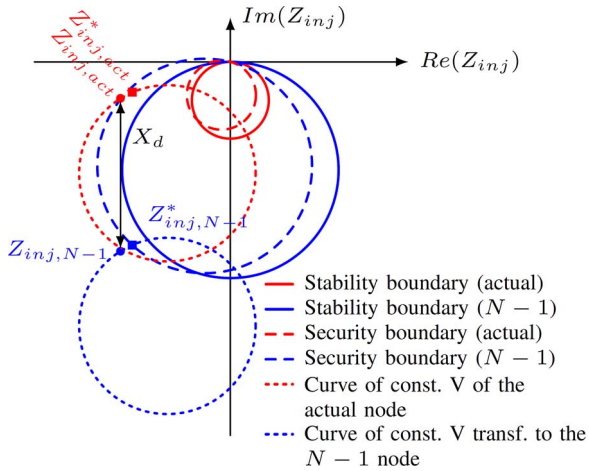

Fig. 7. Determining the power reserves of the actual operating point with respect to the maximum power injection of the corresponding $N-1$ OP.

In the following, the power reserve computation for an actual OP and for an actual OP with respect to its $N-1$ OP are presented.

1) Power Reserve of an Actual Operating Point: The available power reserve $\Delta P_{inj,res}$ of a generator with respect to its maximum power injection can simply be computed from the difference between the current stability margin $\%\Delta P_{inj}$ (8) and the pre-determined security margin m_{sec}, since both are expressed as percentages of $\hat{P}_{inj}$ (7):

$$\Delta P_{inj,res} = \frac{(\%\Delta P_{inj} - m_{\text{sec}})}{100\%} \cdot P_{inj,\max}. \qquad (17)$$

2) Power Reserve of an Actual Operating Point With Respect to Corresponding $N-1$ Operating Point: In order to compute the power reserve an approach similar to the one in Section III-E2 was taken. For that purpose the characteristic curves derived in [13] were exploited (see Fig. 7).

The first step in determining the available power reserve is to calculate the phase angle corresponding to the security margin of the $N-1$ OP utilizing (13). Then the respective curve of constant phase angle (blue dashed curve in Fig. 7) can be computed with (16).

Because of the preventive action the voltage magnitude of the $N-1$ OP may change, but the voltage magnitude at the actual OP is assumed to remain constant. Consequently, the curve of constant voltage magnitude can be used to determine the available power reserve. The curve of constant voltage magnitude at the actual OP (red dotted curve in Fig. 7) is computed employing (15). Then this curve is transferred to the $N-1$ OP by adding jX_d (blue dotted curve). The injection impedance that respects the security margin of the $N-1$ OP can be found as the intersection of the blue dotted and blue dashed circle. This impedance is transferred back to the actual OP and the available power reserve can be computed.

G. Determination of Redispatch Solutions

The preventive action comprises the power reduction at a particular generator to restore its stability (see Section III-E) and the increase of power generation of one generator or a group to counterbalance the power reduction. Depending on the determined power reserves of the remaining generators (see Section III-F), a variety of redispatch solutions can be identified employing different criteria for generator selection and for sharing of the required power increase between several generators. Possible generator selection criteria can be size of the individual power reserve, power margin, electrical distance to the generator in distress or consensus in served loads. Criteria for computing a share size for a particular supporting generator may be determined e.g., by the size of the generator or its available power reserve.

In the implementation presented in this paper, the generator or the group of generators to counter balance the power reduction are chosen corresponding to there relative electrical distance to the generator in distress. The idea is to redispatch the reduced power to the electrically close generators. For that purpose indices representing the relative electrical distance are computed with an approach based on the one described in Section II-C and [16]. The approach allows to determine the relative electrical distance of an internal machine node behind the synchronous reactance to an terminal of another machine. In order to utilize the method, the extended and augmented grid admittance matrix was assembled as follows:

$$\mathbf{Y} = \left(\begin{array}{c|c} N \times N & N \times M \\ \hline M \times N & M \times M \end{array}\right) = \begin{bmatrix} \mathbf{Y}_{nn} & \mathbf{Y}_{ng} \\ \mathbf{Y}_{ng}^T & \mathbf{Y}_{gg} \end{bmatrix} \qquad (18)$$

where N is the number of buses and M the number of generators in the system. The matrix is augmented by the load admittances and the synchronous reactances of the generator. Furthermore, it is extended to the internal nodes of the generators. The $N \times N$ sub-matrix $\mathbf{Y}_{nn}$ is the regular grid admittance of the power system augmented by the load admittance and the synchronous reactances of the generators. The $M \times M$ matrix $\mathbf{Y}_{gg}$ is the sub-matrix containing all the entries due to the additional internal nodes, which were included due to the chosen representation of synchronous machines. The $N \times M$ matrix $\mathbf{Y}_{ng}$ is a sub-matrix, which is linking the internal nodes of the generators to the system buses corresponding to the generator terminals, and $\mathbf{Y}_{ng}^T$ is its transpose.

After dividing the grid matrix into the sub-matrices according to [16], the relative electrical distance of the internal nodes to the remaining nodes in the system can be calculated as follows:

$$[R_{ng}] = 1 - abs[F_{ng}] = 1 - abs([\mathbf{Y}_{nn}]^{-1}[\mathbf{Y}_{ng}^T]). \qquad (19)$$

The values in each column of the resulting matrix now contain a measure of the relative electrical distance between an internal node of the respective generator to its own terminal, to the terminals of the other generators and the remaining system nodes. Each entry has an offset due to the electrical distance between internal node and terminal, which can be corrected by subtracting the respective relative electrical distance between internal node and generator terminal from all the remaining entries in the particular column.

In the case that the total available power reserves are not sufficient to perform the required redispatch, an emergency solution is proposed, which aims at moving the OP of the critical generator as far as possible away from the stability boundary and towards the security boundary without jeopardizing stability and security of the remaining generators. For that purpose, the power reserves of the non-critical generators are computed as described in Section III-F and the total reserve $\Delta P_{res,total}$

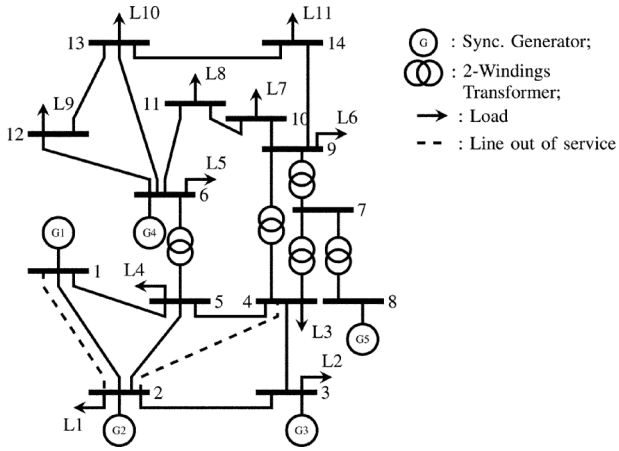

Fig. 8. One-line diagram of the modified IEEE 14-bus test system.

as the sum of all reserves is computed, where NC is the set of non-critical generators:

$$\Delta P_{res,total} = \sum_{NC} \Delta P_{inj,res}. \tag{20}$$

As stated before, in this case the total reserves are less than the needed power reduction computed in Section III-E. However, in order to stabilize the critical generator, its power injection is reduced by $\Delta P_{res,total}$, which can be counterbalanced by the remaining generators without putting them at risk.

IV. Results

A. Scenario 1: $N-1$ OP Crosses Stability Boundary

1) Test System: A modified version of the IEEE 14-bus test system [17] was used. Modifications of the original system were amongst others the following. The three condensers in the system were replaced by generators to allow an active power redispatch. Bus 8 was considered to be an infinite bus and the generator connected to it represents a strong external grid. The synchronous machines G2-G4 are manually excited. The generators G1 and G5 are equipped with automatic voltage regulator (AVR), over excitation limiter (OEL) and power system stabilizer (PSS). A one-line diagram of the test system can be found in Fig. 8.

2) Unstable Scenario: In this scenario the system was highly loaded and in stressed conditions. To provoke instability, a sequence of contingencies were applied (see Fig. 9). The results of the time domain simulation were used to generate synthetic PMU measurements, which were fed to the assessment method. After the first and second disturbance, each corresponding to a loss of a transmission line, the system seems to reach a new quasi steady state (see Fig. 9). However, at the new OP the excitation voltage of G1 is too high and the OEL is activated after a pre-set delay. This last disturbance led to a loss of synchronism of the respective generator and, furthermore, to a collapse in voltage in the system.

The stability assessment results, when applying the ASSRAS method [5], are shown in Fig. 10. The figure shows a magnified detail of the normalized injection impedance plane. Here, the actual OP of a generator is depicted by a blue circle and the $N-1$ OP is indicated by a blue filled square. The color of the large circle, which represents the stability boundary, indicates

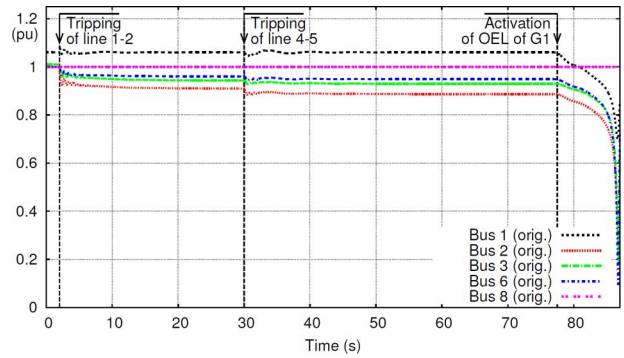

Fig. 9. IEEE 14-bus: Instability scenario: Generator bus voltages.

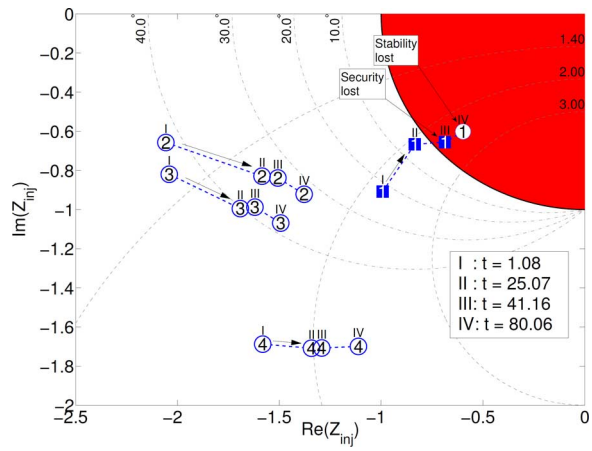

Fig. 10. IEEE 14-bus: Stability assessment results: Pre-fault (1.08 s), after first disturbance loss of line 1–2 (25.07 s), after second disturbance loss of line 4–5 (41.16 s), after third disturbance activation of OXL of G1 (80.06 s). Arabic numbers refer to the number of the generator, e.g., "1" refers to G1.

the stability state of the system, where green corresponds to a stable state and red to an unstable state. The state is assessed to be insecure if an OP has crossed the security margin or a $N-1$ OP has crossed the stability boundary, but the OEL is not yet activated.

Fig. 10 shows the stability assessment results at four time instances labelled with the Roman numerals I-IV. In the pre-fault condition (see Fig. 10 I) the system is in steady-state. The first disturbance leads to a considerable reduction of the stability margin of the actual OPs of G2 and G3 and the $N-1$ OP of G1, but the system remains stable and secure (see Fig. 10 II). After the second disturbance and when a new quasi steady state is reached, the method identifies that the $N-1$ OP of G1 crossed the stability boundary (see Fig. 10 III). However, as long as the OEL of the generator is not activated the system remains stable, but is no longer considered secure. Consequently, the third disturbance, which corresponds to the activation of the OEL of G1, leads to an unstable state and, eventually, to a collapse in voltage (see Fig. 10 IV and Fig. 9).

The results show that the assessment method could detect an insecure operation of the system approximately 40 s before the actual collapse in voltage occurred.

3) Scenario With Remedial Action: In the following the same instability scenario is discussed, but this time, when insecure operation is detected, then the remedial action method described in Section III is triggered and a power redispatch is determined

TABLE II
ACTIVE POWER RESERVES AND RE-DISPATCH SOLUTION

Generator:	1	2	3	4
$\Delta P_{reserve}$ $[MW]$:	–	9.7	9.7	4.9
P_{before} $[MW]$:	179.8	64.9	64.9	20.0
Size $[MVA]$:	200.0	75.0	75.0	25.0
$\hat{P}_{inj}$ in $[MW]$:	179.5	76.3	80.9	33.3
ΔP_{REM} $[MW]$:	-22.4	9.0	9.0	4.4
P_{after} $[MW]$:	157.4	73.9	73.9	24.4

and executed to bring the system back into a secure state. Offline simulation of the test system showed, that for an $N-1$ OP, the security and trigger margin can be chosen low with 0.5% and 0.1% of $\hat{P}_{inj}$.

The stability margin of the $N-1$ OP of G1 had fallen below the trigger margin and the system reached a quasi steady state (see Section III-B) at the time instance shown in Fig. 10 III. Consequently, the remedial action method was executed and a redispatch as shown in Table II was determined. It should be noted, that generator G5 was not considered for the redispatch, since it represents the connection to a strong external grid.

The method determined that the active power of G1 needs to be reduced by 22.4 MW to bring the system back into a secure state. The computation of the power reserves of the remaining generators showed that only all three generators together can balance the needed power reduction. The contribution of each generator was determined from the size of its power reserve with respect to the available total power reserve. Table II shows the complete redispatch solution and that in this case the size of the machine rather than the maximum power injection was the limiting factor. Fig. 11 shows the simulation results, when the proposed redispatch of active power is applied. Fig. 11(a) shows the voltages at the generator buses over time and Fig. 11(b) shows the active power injection of the generators. In both graphs, the simulation results without corrective actions are illustrated with dashed lines and the results with the proposed redispatch with solid lines.

It can be seen that the collapse in voltage was prevented, due to the power redispatch, where the power output of G1 was reduced and the power injections of G2-G4 were increased. An additional benefit was the prevention of the third disturbance, which was the activation of the OEL of G1.

Fig. 12 shows the stability condition of the system at the time when insecure operation was detected (see Fig. 10 III and Fig. 12 III) and when a new quasi steady state was reached after the corrective redispatch (Fig. 12 V). The labels at the OPs show the stability margin of the corresponding generator.

The stability margins of the generators G2-G4 were reduced considerably and the stability margin of the $N-1$ OP of G1 was increased to a secure margin ($\geq 0.5\%$). Finally, the graph shows that all generators are secure and stable.

B. Scenario 2: Actual OP Crosses Stability Boundary

1) Test System: The Nordic32 system [18] was chosen for the second test case. The system topology was modified as described in [5]. Moreover, in the presented case the initial condition from [18] were altered. The modifications are as follows: 1) Generator G22 is set out-of-service and its load is shared by G7, G8, G20, and G21. 2) Generator G7 is manually excited.

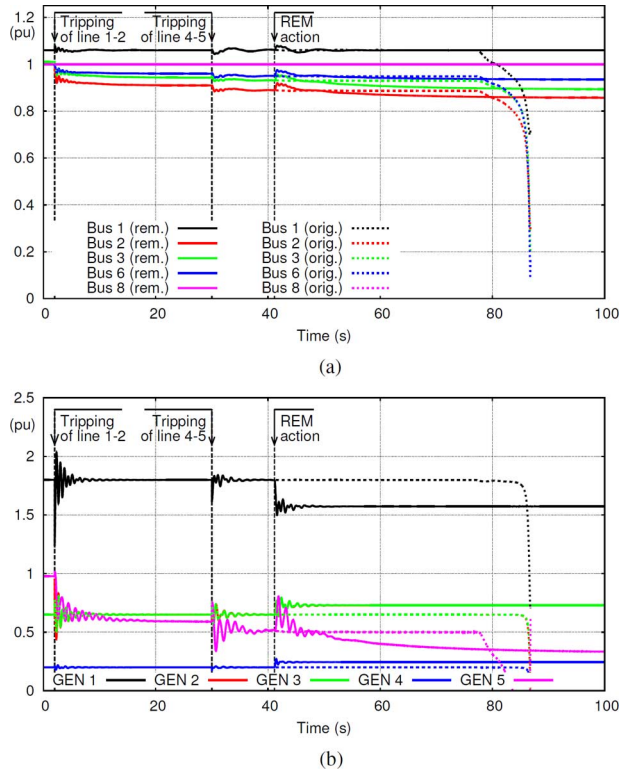

Fig. 11. IEEE 14-bus: Results of the instable scenario, when applying the remedial action method. (a) Stabilized scenario: Generator bus voltages with preventive actions. (b) Stabilized scenario: Generator power injection with preventive actions.

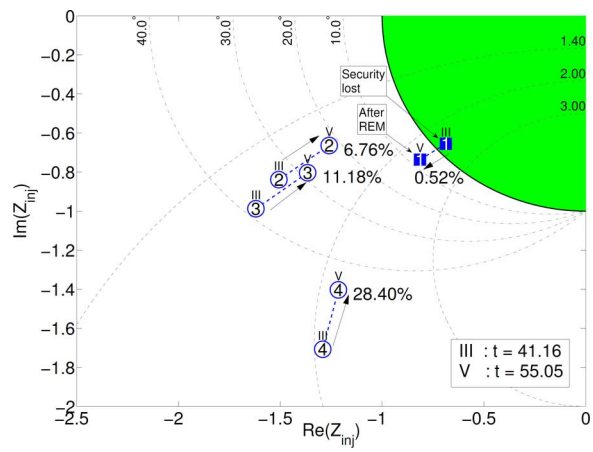

Fig. 12. IEEE 14-bus: Stability condition before and after preventive action, the percentages indicate the stability margin after the preventive action. The Arabic numbers refer to the number of the generator, e.g., "1" refers to G1.

3) One line connecting 2031 and 2032 is disconnected. 4) Load alternations: at 41 increased by 20 MW, at 2031 increased by 10 MWand at 2032 decreased by 10 MW.

In the presented case, the system is in a very stressed condition, where the excitation voltage of various generators is close to the respective limit.

2) Unstable Scenario: In order to provoke instability and a collapse in voltage, the line connecting bus 4021 and 4042 was tripped at $t = 5$ s. The disturbance leads to electromechanical oscillations, which damp out, but lead to activation of various OELs before a collapse in voltage can be observed (see

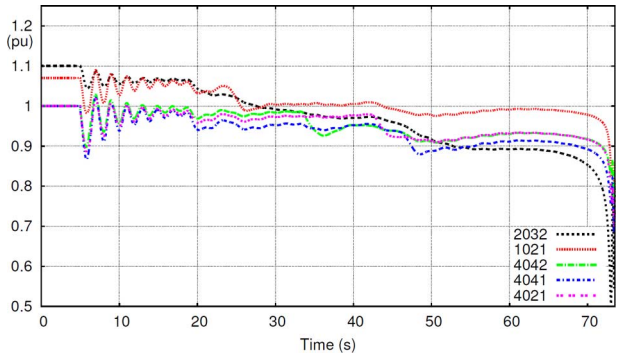

Fig. 13. Voltage magnitude at a selection of buses.

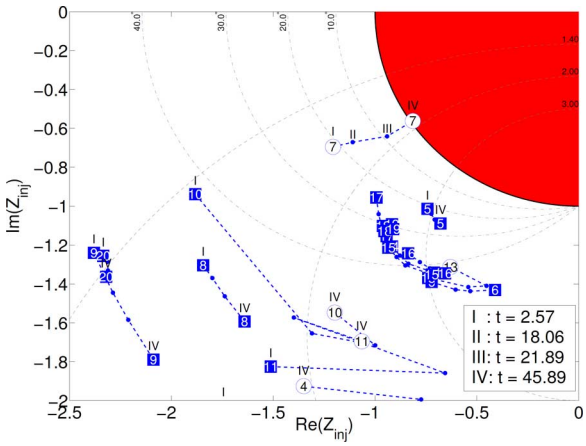

Fig. 14. Nordic32: Stability assessment results: Pre-fault (2.5 s), after first disturbance loss of line 4021–4042 (18.06 s), after second disturbance activation of OEL of G11 (21.89 s), G7 crosses stability boundary (45.89 s). Arabic numbers refer to the number of the generator, e.g., "1" refers to G1.

Fig. 13). The OELs are activated successively beginning with G11 at 18.28 s, G4 at 23.70 s, G13 at 33.11 s, G10 at 42.15 s, G12 at 45.90 s, and G6 at 47.13 s.

The ASSRAS assessment results are shown at a selection of time instances I-IV in Fig. 14. Here only the start and end OPs (I and IV) are depicted by big markers, which indicate the type of the OP, while the intermediate OPs at II and III are solely represented by small blue dots.

In the pre-fault condition seen in Fig. 14 I all the generators are stable and secure. It can be observed that the most critical generator is the manually excited generator G7 since its actual OP is relatively close to the stability boundary with a margin of 5.73%. The remaining displayed OPs are $N-1$ OPs and, consequently, are less critical. However, these will become the actual OPs, when the OEL of the respective generator is activated. The loss of the transmission line connecting bus 4021 and 4042 reduced the stability margin of G7 to 3.68% (II) and its OP moved closer to the boundary. Afterwards, the OEL of G11 was activated at 18.28 s and, hence, the prior $N-1$ OP G11 now became the actual OP. This second disturbance led to a further reduction of the stability margin of the critical machine G7 to 0.98% (III). The subsequent activations of the OEL's of G4, G10, and G13 caused further depression of the stability margin of G7 and the generator eventually crossed the stability boundary at 44.98 s, as shown in Fig. 14 IV. Afterwards, the generator started to drift

TABLE III
ACTIVE POWER RE-DISPATCH SOLUTIONS

Time s	Critical Gen.	Margin $\%\Delta P_{inj}$	Necessary ΔP	Supp. Gen.	Margin after red.
21.89	G7	0.98%	8.25 MW	G11	1.53%
27.05	G7	0.81%	9.44 MW	G11	1.05%
49.46	G7	0.83%	9.09 MW	G11	2.14%

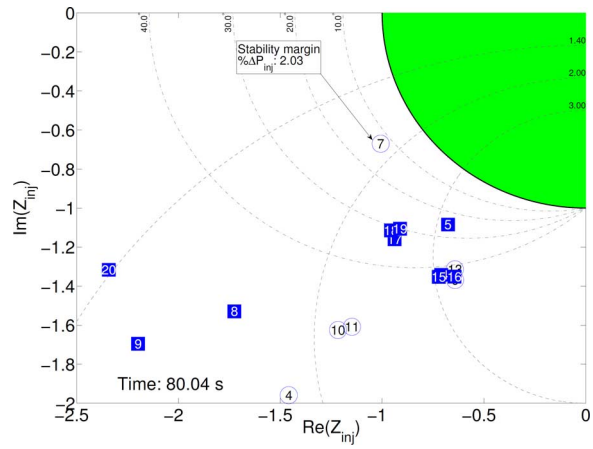

Fig. 15. Stability condition ca. 30 s after the last corrective redispatch. The Arabic numbers refer to the number of the generator, e.g., "1" refers to G1.

away from the remaining generators, which eventually causes a collapse of the voltages at $\approx$ 73 s (see Fig. 13).

The results show that the assessment method detects the imminent instability approximately 28 s before the collapse.

3) Scenario With Remedial Action: In this section, the same instability scenario as prior is investigated, but this time the remedial action method is executed, when a generator's stability margin falls below the trigger margin. Offline simulation of the test system showed, that the margin thresholds for actual OPs has to be chosen more conservative with 2% for the security margin and 1% for the trigger margin.

In the prior described scenario, the stability margin of generator G7 fell below the trigger margin at 21.89 s (see Fig. 14 III). The developed method determined the necessary remedial action to bring the system back into a secure state to be an active power reduction of G7 by 8.25 MW. Furthermore, the method computed the available power reserves of the remaining generators. G11 was chosen to counterbalance the power reduction with an equal increase, because of its electrical proximity and its sufficient power reserve. Due to the OEL activation of G4, the margin of G7 again fell below the trigger threshold, which in return executed the remedial action method and caused a second corrective power redispatch. The plurality of OEL activations caused G7 to cross the threshold a third time. Details on the three corrective actions can be found in Table III.

The table shows the time, when a corrective action is applied, the critical generator, whose power injection is reduced, as well as its stability margin and the needed power reduction. Furthermore, it shows the supporting generator, which will counterbalance the power reduction, and the stability margin of the critical generator after the corrective action. During the first two corrective actions, the system is in a state, where ULTC transformers and OELs are acting. Consequently, the assumption of

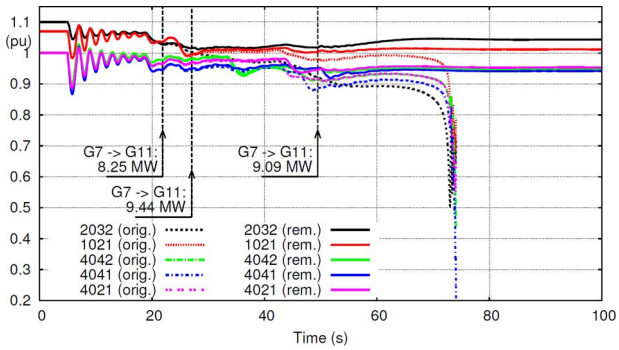

Fig. 16. Voltage magnitude at a selection of buses with corrective redispatch.

quasi steady state conditions introduces an error and may explain, why the remedial action do not lead to a stability margin greater or equal to the chosen security margin. The last corrective redispatch succeeds to bring the system back into a secure state. Fig. 15 depicts the system after the last redispatch and after a new quasi steady state was reached. It can be seen that all OPs are in the secure and stable region.

Fig. 16 displays the voltage magnitudes at a selection of buses over time. The dashed lines are the voltages in the unstable case and the solid lines are the voltages in the case with corrective control actions. The graph shows that the corrective actions prevented the system collapse and led to a stabilization of the voltages.

V. Discussion

In this paper a new patented method was presented that determines remedial actions to prevent a blackout. A real-time ASSRAS assessment method is used to identify insecure or unstable system operation. The presented method utilizes these information to compute corrective power redispatch solutions. The method is based on algebraically derived expressions, which makes it very well suited for real-time application. The control actions move the OP of the critical generator back into the secure region, while ensuring that none of the supporting generators enters an insecure state.

The method's capability of avoiding a collapse in voltage and an imminent blackout was demonstrated with simulation results from two scenarios and two test systems (IEEE 14-bus and Nordic32). In both cases, the determined corrective redispatches stabilized the system and restored the stability margin of the critical machine to a secure level. This demonstrates accuracy and effectiveness of the proposed methodology.

In future work, the proposed approach could be further developed, e.g., taking into account additional constraints, such as the limits of the OELs, when determining the available active power reserves.

References

[1] Danish energy agency, Energy Policy in Denmark Tech. Rep Danish energy agency, Amaliegade 44, 1256, Copenhagen, Denmark, 2012.
[2] F. Li, W. Qiao, H. Sun, H. Wan, J. Wang, Y. Xia, Z. Xu, and P. Zhang, "Smart transmission grid: Vision and framework," *IEEE Trans. Smart Grid*, vol. 1, no. 2, pp. 168–177, Sep. 2010.
[3] M. Glavic and T. Van Cutsem, "Wide-area detection of voltage instability from synchronized phasor measurements. Part I: principle," *IEEE Trans. Power Syst.*, vol. 24, no. 3, pp. 1408–1416, Aug. 2009.
[4] M. Glavic and T. Van Cutsem, "Wide-area detection of voltage instability from synchronized phasor measurements. Part II: Simulation results," *IEEE Trans. Power Syst.*, vol. 24, no. 3, pp. 1417–1425, Aug. 2009.
[5] H. Jóhannsson, A. H. Nielsen, and J. Østergaard, "Wide-area assessment of aperiodic small signal rotor angle stability in real-time," *IEEE Trans. Power Syst.*, vol. 28, no. 4, pp. 4545–4557, Nov. 2013.
[6] J. Wen, W.-H. E. Liu, P. L. Arons, and S. K. Pandey, "Evolution pathway towards wide area monitoring and protection: A real-world implementation of centralized RAS system," *IEEE Trans. Smart Grid*, vol. 5, no. 3, pp. 1506–1513, May 2014.
[7] Z. Yao, V. R. Vinnakota, Q. Zhu, C. Nichols, G. Dwernychuk, and T. Inga-Rojas, "Forewarned is forearmed: An automated system for remedial action schemes," *IEEE Power Energy Mag.*, vol. 12, no. 3, pp. 77–86, May 2014.
[8] Y. Makarov, S. Lu, X. Guo, J. Gronquist, P. Du, T. Nguyen, and J. Burns, Wide Area Security Region, Tech. Rep., Pacific Northwest National Laboratory, Richland, WA, USA, 2010.
[9] J. Ma, T. Wang, S. Wang, X. Gao, X. Zhu, Z. Wang, and J. Thorp, "Application of dual youla parameterization based adaptive wide-area damping control for power system oscillations," *IEEE Trans. Power Syst.*, vol. 29, no. 4, pp. 1602–1610, Jul. 2014.
[10] A. Heniche and I. Kamwa, "Assessment of two methods to select wide-area signals for power system damping control," *IEEE Trans. Power Syst.*, vol. 23, no. 2, pp. 572–581, May 2008.
[11] E. Dmitrova, A. Nielsen, H. Jóhannsson, and K. Johannsson, Early Prevention Method for Power Systems Instability Tech. Univ. Denmark, Dept. Elect. Eng., 2013.
[12] T. Weckesser and H. Jóhannsson, "Method of determining remedial control actions for a power system in an insecure state," 2013, WO2013098184; G05D5/00; H02J3/24; H02J3/46.
[13] H. Jóhannsson, J. Østergaard, and A. H. Nielsen, "Identification of critical transmission limits in injection impedance plane," *Int. J. Elect. Power Energy Syst.*, vol. 43, no. 1, pp. 433–443, Dec. 2012.
[14] S. Sommer and H. Jóhannsson, *Real-Time Thevenin Impedance Computation*, IEEE, p. 6497824, 2013.
[15] H. Jóhannsson, "Development of early warning methods for electric power systems," Ph.D. dissertation, Tech. Univ. Denmark (DTU), Lyngby, Denmark, 2011.
[16] K. Visakha, D. Thukaram, and L. Jenkins, "Transmission charges of power contracts based on relative electrical distances in open access," *Elect. Power Syst. Res.*, vol. 70, no. 2, pp. 153–161, 2004.
[17] Power system test case archive, Univ. Washington, Aug. 2012 [Online]. Available: http://www.ee.washington.edu/research/pstca/
[18] M. Stubbe, Long-term dynamics-phase II (report of CIGRE task force 38.02.08), 1995, CIGRE, Tech. Rep.

Tilman Weckesser (M'12) received the M.Sc. degree in sustainable energy engineering from the Technical University of Denmark (DTU), Lyngby, Denmark, in 2011. He is currently pursuing the Ph.D. degree at the Centre for Electric Power and Energy (CEE), Department of Electrical Engineering, DTU.

His research interests are in the field of power system dynamics and stability with a focus on the development of fast stability assessment methods.

Hjörtur Jóhannsson (M'10) received the M.Sc. and the Ph.D. degrees in electrical engineering from the Technical University of Denmark (DTU), Lyngby, Denmark, in 2007 and 2011, respectively.

He is currently a research consultant at CEE, DTU Electrical Engineering. His research interests concern the development of methods that provide an early warning for instability in electric power systems, and power systems dynamics, stability, and control.

Jacob Østergaard (M'95-SM'09) received the M.Sc. degree in electrical engineering from the Technical University of Denmark (DTU), Lyngby, Denmark, in 1995.

He was with the Research Institute of Danish Electric Utilities for 10 years. Since 2005, he has been Professor and Head of CEE at DTU Electrical Engineering. His research interests cover smart grids with focus on system integration of renewable energy and distributed energy resources, control architecture for future power system, and flexible demand.

Appendix I

Test systems

I.1 New England & New York system

The employed test system is the New England & New York system described in [65]. It consists of 68 buses and 16 generators. The loads are modelled as constant impedances in the time-domain simulation.

The rotor dynamics of the generators are represented by a sixth order model. Moreover, the generators are all equipped with a simple excitation and voltage regulation system, as well as a thermal turbine/governor model. In addition, all generators, but GEN-7 and GEN-14, are equipped with a power system stabilizer. Figure I.1 shows a one-line diagram of the system.

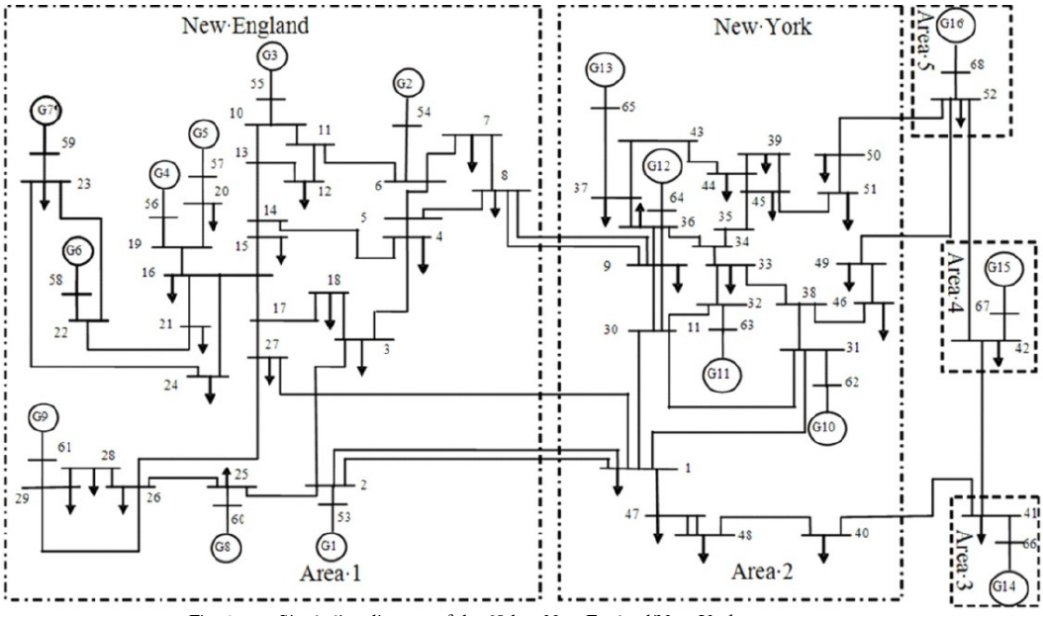

Figure I.1: One-line diagram of the New England and New York system [87].

The initial state of the system was as well adopted [65].

I.2 Nordic32

The system is a simplified representation of the Swedish transmission grid and has been used extensively to test and evaluate the efficiency of stability assessment methods, e.g. [9] and [11]. A one-line diagram is depicted in Fig. I.2.

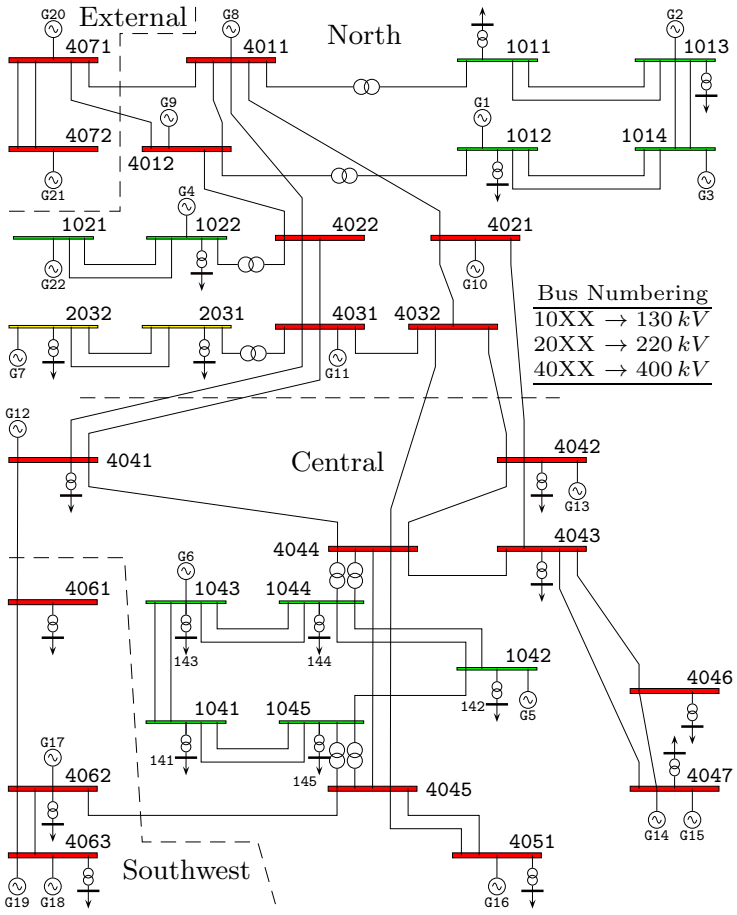

Figure I.2: Oneline diagram of the Nordic32 system, figure adopted from [9]

The topology of the system was slightly modified as described in [9], where ULTC-transformers were introduced at the buses $1041-1045$ to serve the connected loads. This resulted in the introduction of the additional buses $141-145$. Moreover, to further stress the system the initial condition from [84] were altered as follows:

1. Generator $G22$ is out-of-service and its production is shared between $G7$, $G8$, $G20$ and $G21$.
2. Generator $G7$ is manually excited.
3. One line connecting 2031 and 2032 is disconnected.
4. Changes to loads: at bus 41 the load is increased by 20 MW, at bus 2031 it is increased by 10 MW and at bus 2032 the load is decreased by 10 MW.

This resulted in very stressed system conditions were various of the generators' excitation voltages are close to their respective limits.

www.elektro.dtu.dk

Department of Electrical Engineering
Centre for Electric Power and Energy (CEE)
Technical University of Denmark
Elektrovej building 325
DK-2800 Kgs. Lyngby
Denmark
Tel: (+45) 45 25 38 00
Fax: (+45) 45 93 16 34
Email: info@elektro.dtu.dk